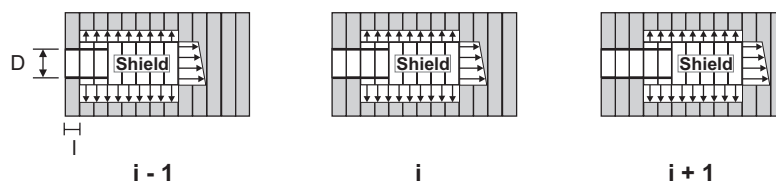
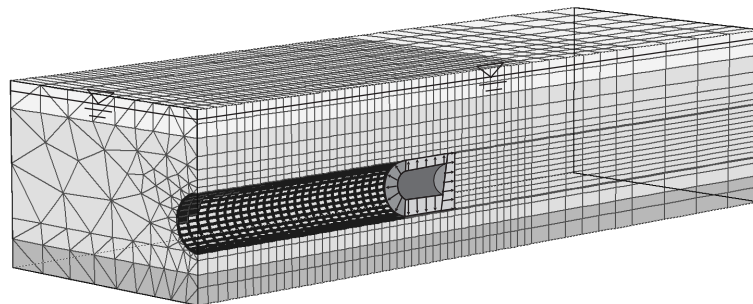


Universität Stuttgart

## Tunnel induced settlements and structural forces in linings

Sven Möller



2006 Mitteilung 54  
des Instituts für Geotechnik  
Herausgeber P. A. Vermeer





**Herausgeber:**

Prof. Dr.-Ing. P. A. Vermeer  
Institut für Geotechnik  
Universität Stuttgart  
Pfaffenwaldring 35  
70569 Stuttgart  
Telefon 0711/685-62436  
Telefax 0711/685-62439  
e-mail: pieter.vermeer@igs.uni-stuttgart.de

ISBN-10: 3-921837-54-5

ISBN-13: 978-3-921837-54-2

Gegen Vervielfältigung und Übersetzung bestehen keine Einwände, es wird lediglich um Quellenangabe gebeten.

Herausgegeben 2006 im Eigenverlag des Instituts für Geotechnik

# **Tunnel induced settlements and structural forces in linings**

Von der Fakultät für Bau- und Umweltingenieurwissenschaften  
der Universität Stuttgart  
zur Erlangung der Würde eines Doktors der Ingenieurwissenschaften (Dr.-Ing.)  
genehmigte Abhandlung,

vorgelegt von  
**SVEN CHRISTIAN MÖLLER**  
geboren in Berlin

Hauptberichter: Prof. Dr.-Ing. P. A. Vermeer  
Mitberichter: Prof. A. J. Whittle B.Sc Sc.D  
Prof. Dr.-Ing. G. Anagnostou

Institut für Geotechnik der Universität Stuttgart  
Tag der mündlichen Prüfung: 26. 06. 2006



## Preface by doctoral thesis supervisor

Over the past decades considerable advances have been made in techniques of tunnel construction in soft ground; both in conventional open face tunnelling and closed face shield tunnelling. These developments were pushed by increasing mobility and growing transport within the society. In any tunnelling project adequate stability during construction is clearly of prime importance and this was the motivation of a previous doctoral study by RUSE (2004)\* on tunnel heading stability. Besides stability, settlements and other ground movements have to be considered. In the urban environment these tend to be of particular significance, because of their influence on existing buildings. This important subject of ground movements associated with tunnelling is addressed in this study by Sven Möller. In addition to ground movements attention is focussed on structural forces in linings.

The dissertation study begins with a detailed review of methods of analyses, including both conventional open face and closed face shield tunnelling. It covers the complete range of elementary methods, *2D* finite element analysis and *3D* simulations. No doubt, the review might have been restricted to FE-analyses, but being not familiar myself with the structural design of linings, I requested Sven Möller to consider such elementary methods as well. As a consequence constitutive modelling had to obtain less attention, but this topic is fully covered in another doctoral study (BENZ, 2006)\* that is to be printed before the end of this year.

The thesis focuses on the use of non-linear finite element analyses to compute the ground deformation and the forces induced in the tunnel lining. No doubt, the conclusions on overconsolidation, initial horizontal stresses and the pressure method for *2D* and *3D* analyses of shield tunnelling are of significant importance; both for advanced engineering and further research on the numerical simulation of tunnelling.

Pieter A. Vermeer

\*) for references the reader is referred to the list at the end of this dissertation study



## Acknowledgments

The research presented in this thesis is a result of the work carried out in the years 2001-2006 at the Institute of Geotechnical Engineering, University of Stuttgart. No doubt, this result could only be achieved by the support of a number of people to whom I would like to express my gratitude.

To my supervisor Professor Pieter Vermeer: I experienced the freedom I needed to be creative while at the same time I was always helped to continue research in case of difficulties. Most grateful I am to him knowing that the last years will be of great profit for my further way. I am really looking forward to continue this valuable working relationship.

To my colleagues: Thank you for being such a good team. I have always enjoyed working and having a good time with you.

To my wife Anna: I know that a man can only be as strong as the woman behind the man. Thank you for all your energy and patience.

To my parents: Thank you Mom for correcting my English. After reading my thesis I hope you are not afraid of driving through tunnels. Believe me when I say, most of them are safe. Thank you Dad for supporting me and my family throughout my entire studies.

Stuttgart, May 2006

Sven Möller





# Contents

<b>1</b>	<b>Introduction</b>	<b>1</b>
<b>2</b>	<b>Modern tunnelling methods</b>	<b>3</b>
2.1	Open face tunnelling . . . . .	3
2.1.1	Conventional open face tunnelling method . . . . .	4
2.1.2	Open face shield tunnelling . . . . .	5
2.1.3	Tunnel boring machine without shield . . . . .	7
2.2	Closed face tunnelling . . . . .	7
2.2.1	Closed face shield tunnelling . . . . .	7
<b>3</b>	<b>Elementary computational methods for tunnels</b>	<b>11</b>
3.1	Tunnels in rock versus soil . . . . .	11
3.2	Tunnels in soil and soft rock . . . . .	12
3.3	Deformations due to closed shield tunnelling . . . . .	12
3.4	Deformations in open face tunnelling . . . . .	13
3.5	Lining forces . . . . .	14
3.6	The empirical assessment of settlements . . . . .	15
3.6.1	Transverse surface settlement . . . . .	15
3.6.2	Width of settlement trough . . . . .	16
3.6.3	Depth of settlement trough . . . . .	19
3.6.4	Horizontal displacements . . . . .	21
3.6.5	Longitudinal surface settlement . . . . .	22
3.7	The ground response curve for loads on linings . . . . .	24
3.8	Structural design models for tunnels . . . . .	27
3.8.1	On the use of analytical solutions of continuum models for lining forces . . . . .	28
3.8.2	The bedded-beam model . . . . .	31
3.8.3	Ground pressures on tunnel linings . . . . .	35
<b>4</b>	<b>Finite element modelling of tunnels</b>	<b>41</b>
4.1	Basic terms and modelling aspects of FEM tunnel analysis . . . . .	42
4.1.1	Finite Elements as used in this thesis . . . . .	43
4.1.2	Boundary conditions . . . . .	43
4.1.3	Steady-state settlement trough . . . . .	44
4.1.4	Zigzagging and steady-state of structural forces . . . . .	45
4.1.5	Tolerated error . . . . .	47

4.2	On FE-mesh dimensions . . . . .	47
4.2.1	2D mesh dimensions . . . . .	48
4.2.2	3D mesh dimensions . . . . .	49
4.2.3	Concluding remarks on mesh dimensions . . . . .	50
4.3	The influence of the mesh coarseness . . . . .	50
4.3.1	3D mesh coarseness . . . . .	50
4.4	On the initial stress . . . . .	54
4.4.1	The horizontal initial stress . . . . .	55
4.4.2	The role of $K_0$ . . . . .	57
4.5	Review of 3D FEM installation procedures . . . . .	69
4.5.1	Step-by-step installation for conventional tunnelling . . . . .	70
4.5.2	Installation for closed shield tunnelling . . . . .	70
4.5.2.1	Slurry versus earth pressure balance shield . . . . .	72
4.5.2.2	Step-by-step pressure method . . . . .	72
4.6	Review of 2D FEM installation procedures . . . . .	74
4.6.1	Installation procedures for conventional tunnelling . . . . .	76
4.6.1.1	Core support method ( $\alpha$ -method) . . . . .	76
4.6.1.2	Lining reduction method ( $\delta$ -method) . . . . .	77
4.6.1.3	Stress reduction method ( $\beta$ -method) . . . . .	77
4.6.2	Installation procedures for closed shield tunnelling . . . . .	78
4.6.2.1	The gap method . . . . .	79
4.6.2.2	The stress reduction method . . . . .	80
4.6.2.3	Contraction method . . . . .	81
4.7	Improved installation procedure for shield tunnels: The grout pressure method . . . . .	81
4.8	Evaluation of unloading factors for use in the stress reduction method . . . . .	84
4.8.1	Three-dimensional FE-analyses . . . . .	85
4.8.2	2D- versus 3D-analyses . . . . .	85
4.8.3	On ground and lining stiffnesses . . . . .	86
4.8.4	Linear elastic analyses . . . . .	87
4.8.5	Elasto-plastic analyses . . . . .	89
4.8.6	Case study of a subway tunnel . . . . .	91
4.8.7	Conclusions on unloading factors . . . . .	91
4.8.8	A fast 3D analysis for unloading factors of settlement . . . . .	92
<b>5</b>	<b>Tunnel case studies</b>	<b>97</b>
5.1	Steinhaldenfeld conventionally driven tunnel . . . . .	97
5.1.1	3D FE-analyses . . . . .	98
5.1.2	2D FE-analyses . . . . .	103
5.2	Second Heinenoord slurry shield tunnel . . . . .	107
5.2.1	3D FE-analyses . . . . .	108
5.2.2	2D FE-analyses . . . . .	115

<b>6</b>	<b>Conclusions</b>	<b>127</b>
6.1	On elementary design methods . . . . .	127
6.2	On the FEM . . . . .	128
6.3	Recommendations for further research . . . . .	130
<b>A</b>	<b>On constitutive models as used in this thesis</b>	<b>131</b>
A.1	The Mohr-Coulomb Model . . . . .	131
A.2	The Hardening-Soil Model . . . . .	133
A.3	The HS-Small Model . . . . .	138
	<b>Bibliography</b>	<b>141</b>



# Zusammenfassung

Bei der Planung von Untertagebauten stellen Berechnungen von Baugrundverformungen und Schnittkräften in der Tunnelschale eine wichtige Entscheidungsgrundlage für die Wahl einer konstruktiven Lösung oder eines geeigneten Bauverfahrens dar. Numerische Methoden und leistungsfähige Computeranlagen haben derzeit einen Entwicklungsstand erreicht, welcher es ermöglicht, die Kräfteinteraktion zwischen Baugrund und Tunnelschale in einer realistischen Weise zu simulieren. Die Vorhersage von Oberflächensetzungen und Schnittkräften ist dabei zweifelsohne maßgeblich von der gewählten modellhaften Beschreibung des Baugrundverhaltens, d.h. des Stoffgesetzes abhängig. Eine weitaus wichtigere Rolle, wie in vorliegender Arbeit gezeigt wird, spielt jedoch die Berücksichtigung der jeweiligen Tunnelvortriebsmethode. In Abhängigkeit davon welches Verfahren es zu berücksichtigen gilt, ob konventioneller Vortrieb oder geschlossener Schildvortrieb, müssen unterschiedliche statische Systeme und Randbedingungen berücksichtigt werden. In vorliegender Arbeit wird die Wahl von geeigneten statischen Systemen und Randbedingungen untersucht, um aussagekräftige Ergebnisse für die Prognose von Setzungen und Schnittkräften zu erlangen.

Schaut man sich die gängigen Berechnungsverfahren der heutigen Tunnelbaupraxis näher an, so findet man u. a. noch eine Vielzahl von vereinfachten Berechnungsmodellen vor, welche die statischen Besonderheiten unterschiedlicher Tunnelvortriebsverfahren nur geringfügig oder gar nicht berücksichtigen. Hier sind noch einfache, meist zweidimensionale Methoden zur Berechnung von Oberflächensetzungen und Schnittkräften weitverbreitet, darunter empirische Verfahren, Verfahren der Gebirgskennlinie, elastische oder elastoplastische analytische Lösungen des kreisrunden Tunnels und gebettete Stabwerksverfahren.

Mit der rasanten Entwicklung der Computerleistungsfähigkeit wurde diese vereinfachte Herangehensweise erstmalig durchbrochen, indem die Berücksichtigung von komplexeren Zusammenhängen durch numerische Verfahren möglich wurde. Weitaus realistischere, auch zeitaufwändige dreidimensionale Simulationen, sowie nichtlineares Stoffverhalten und komplizierte geometrische Gegebenheiten wie Baugrundsichtungen oder von der Kreisform abweichende Tunnelquerschnitte sind hier gegenwärtiger Stand der Berechnungstechnik. Darüber hinaus können statische Besonderheiten in Bezug auf die Tunnelvortriebsmethode ohne weitere Umstände untersucht werden.

Die vorliegende Arbeit verschafft einen Überblick sowohl über gängige vereinfachte Tunnelberechnungsmethoden als auch über tunnelstatische Berechnungen mit Hilfe von drei- und zweidimensionalen Finite-Element-Simulationen. Ein Hauptaugenmerk wird dabei auf die Wahl und den Einfluss von statischen Systemen und Randbedingungen zur Berücksichtigung unterschiedlicher Tunnelvortriebsmethoden gelegt. Darüber hinaus wird auch die Auswirkung unterschiedlicher Stoffgesetze zur Modellierung des Baugrundverhaltens untersucht. In diesem Zusammenhang werden folgende Kapitel berücksichtigt:

**Kapitel 2** Dieses Kapitel verschafft dem Leser einen Überblick über gängige moderne Tunnelvortriebsmethoden. Dabei wird unterschieden zwischen Methoden bei denen eine ungestützte Ortsbrust zur Ausführung gelangt und solchen, bei denen die Ortsbrust durch ein Stützmedium verschlossen ist.

**Kapitel 3** Innerhalb diese Kapitels werden die gängigen vereinfachten Berechnungsmethoden für Setzungen und Schnittkräfte auf der Grundlage einer Literaturrecherche dargestellt. Beginnend mit der empirischen Berechnungsmethode für die Vorhersage von Oberflächensetzungen und Baugrundverformungen, wird anschließend das Konzept der Gebirgskennlinie nach FENNER/PACHER, zur Darstellung der Interaktion zwischen Baugrundverformung und Belastung der Tunnelschale erläutert. Darauf folgend werden statische Berechnungsmodelle zur Bestimmung von Schnittkräften der Tunnelschale behandelt. Hierbei werden sowohl die Ansätze der geschlossenen analytischen Lösungen vorgestellt als auch die Herangehensweise von gebetteten Stabzugsverfahren erläutert. Im Hinblick auf die vereinfachten Berechnungsmodelle werden in einem Unterkapitel die Größe und Verteilung der jeweiligen Baugrundlasten auf die Tunnelschale untersucht, d.h., es werden die Ansätze zur Berücksichtigung der Tunnelvortriebsmethode untersucht.

**Kapitel 4** Dieses Kapitel behandelt die Simulation von Tunnelvortrieben mit Hilfe der Finite-Element-Methode. Um ein besseres Verständnis für das weitere Studium dieser Arbeit zu fördern, werden zunächst einige grundlegende Begriffe sowie Modellierungsaspekte von zwei- und dreidimensionalen Finite-Element-Tunnelsimulationen aufgegriffen und erläutert. Die Finite-Element-Methode ist durch eine Reihe von Faktoren beeinflusst, welche bei Nichtbeachtung zu einem erheblichen Genauigkeitsverlust der Berechnungsergebnisse führen können. Aus diesem Grunde werden zunächst die Bedeutung und der Einfluss des tolerierten Gleichgewichtsfehlers und die Bestimmung von ausreichenden Finite-Element-Netzabmessungen sowie Netzfeinheiten für die Berechnung von zwei- und dreidimensionalen Setzungs- und Schnittkraftverläufen untersucht. Die Auswirkung der Größe und Verteilung der Ausgangsbaugrundspannungen auf die Ergebnisse von Oberflächensetzungen und Schnittkräften wird in einem gesonderte Unterkapitel untersucht. Ein Schwerpunkt dieses Kapitels liegt auf der Berücksichtigung unterschiedlicher Tunnelvortriebsmethoden bei der numerischen Simulation von Setzungen und Schnittkräften. In diesem Zuge werden sowohl zwei-, als auch dreidimensionale numerische Tunnelsimulationen anhand einer Literaturstudie zusammengefasst. Zur Berechnung von geschlossenen Schildvortrieben wird sowohl ein verbessertes drei- als auch ein zweidimensionales Verfahren vorgeschlagen, welche die Simulation des Ortsbruststützdruckes oder/und der Zementmörtelverpressdrücke vorsieht. Eine gängige zweidimensionale Berechnungsmethode wird genauer untersucht, indem Ergebnisse von systematischen Parameterstudien sowie Empfehlungen zur Größe des sogenannten Vorentlastungsfaktors gezeigt werden.

**Kapitel 5** Die Bedeutung und der Einfluss der numerischen Tunnelsimulationsmethode und die Auswirkung unterschiedlicher Stoffgesetze auf Setzungen und Schnittkräfte, wird in diesem Kapitel anhand von Vergleichen mit Messungen zweier Tunnelfallstudien aufgezeigt. Für einen konventionell aufgefahrenen Tunnel und einen geschlossenen Schildvortrieb werden sowohl drei- als auch zweidimensionale Finite-Element-Berechnungen durchgeführt, um den vorwiegenden Einfluss der der numerischen Simulationsmethoden hervorzuheben. Darüber hinaus wird gezeigt, dass die Wahl eines geeigneten Stoffgesetzes von erheblicher Bedeutung zur Berechnung von Baugrundverformungen ist. In vorliegender Arbeit werden dabei das weit verbreitete Stoffgesetz nach Mohr-Coulomb sowie das nichtlineare elastoplastische Hardening-Soil -Modell und die Erweiterung des letzteren, das Hardening-Soil-Small-Modell, zur Erfassung der Steifigkeit unter kleinen Dehnungen, untersucht. Es wird aufgezeigt, dass die Berücksichtigung der Steifigkeit unter kleinen Dehnungen zu einer realistischeren Simulation von Baugrundverformungen im Tunnelbau beiträgt. Insbesondere in Bezug auf die Simulation der Steigung der Setzungsmulde wird gezeigt, dass die Berücksichtigung der Steifigkeit unter kleinen Dehnungen eine wesentlich steilere Mulde und damit eine bessere Annäherung an Messungen ergibt.

**Kapitel 6** Im letzten Kapitel werden die Ergebnisse dieser Arbeit noch einmal zusammengefasst und mit den wichtigsten Schlussfolgerungen bedacht. Anschließend wird ein Ausblick auf fortführende Forschungsmöglichkeiten gegeben.





## Abstract

The design of tunnels requires a proper estimate of surface settlements and lining forces. In engineering practice different design methods tend to be used, varying from simple empirical and analytical formulations to advanced finite element analyses. Depending on the tunnelling method, e.g. conventional or closed shield tunnelling, different procedures are applied for the modelling of the excavation and support sequence. Such procedures have a significant effect on predicted/computed deformations and lining forces. The method of analysis needs to take into consideration the effects of the installation on the ground-lining interaction.

This thesis focuses on shallow tunnelling in soil. It begins with a summary of modern tunnelling methods, distinguishing between installation procedures of open face and closed face tunnelling. Subsequently elementary methods of analysis for both settlements and lining forces are reviewed, placing emphasis on installation procedures. Hereafter the focus is on the use of three- and two-dimensional finite element analyses. Besides the influence of some basic modelling aspects of finite element analyses, the importance of adequately modelling the excavation and support sequence, in particular the appropriate boundary conditions to be specified at the tunnel face and wall are examined. After a review on the aspects of such installation procedures, results for different installation procedures and different constitutive models are presented on the basis of two case studies. It is shown that installation procedures are most important to be considered in order to arrive at proper predictions for tunnelling settlements, horizontal ground movements and lining forces.



# Chapter 1

## Introduction

Tunnel design requires a proper estimate of both ground deformations and pressures on the tunnel lining. Depending on the method of excavation and support, tunnelling may induce considerably different magnitudes of deformation to the surrounding ground, resulting as well in different ground pressures on tunnel linings. For the design of the tunnel lining and for the prediction of surface settlements, the excavation and support sequence needs to be taken into consideration, in order to come to a reliable conclusion whether or not the design is adequate. In the present thesis the use of appropriate 3D and 2D FE-simulation methods for both conventionally driven open face tunnels and closed face shield tunnels will be analyzed to demonstrate their significant influence on the prediction of surface settlements and lining forces. Moreover, the influence of different constitutive models will be evaluated, to show improved predictions of surface settlements and horizontal ground movements when accounting for the small-strain stiffness.

Tunnel engineers traditionally use a number of elementary methods of analysis, which comprise a large variety of empirical, simple (mostly elastic or elastoplastic) analytical or bedded beam models for the assessment of surface settlements and lining forces. On reviewing the literature on the aspects of elementary design methods with respect to installation procedures, one gets the impression that peculiarities of support and excavation of different tunnelling methods are hardly accounted for. Nevertheless, elementary methods of analysis are still frequently used in engineering practice and they can not be omitted as they reflect both tunnelling tradition and design experience.

However, with the rise of computer capacity, complex numerical methods came into the realm of design practice and tunnelling can thus be simulated more realistically. Both non-linear ground behavior and complex geometries, such as ground layering or non-circular tunnel cross sections can easily be accounted for. Moreover, the effects of tunnel support installation may be incorporated, in order to arrive at appropriate loads on the lining and realistically estimate associated surface settlements.

The transition from elementary methods of analysis to advanced numerical analysis should not be abrupt and a sufficient validation in terms of measurements and engineering experience should be gained before bidding farewell to a well proven approach. The present thesis is intended to contribute to the effective application of numerical analysis of tunnelling settlements and lining forces. In order to do so the following chapters will be considered:

**Chapter 2** This chapter gives a condensed overview on modern tunnelling methods, making distinction between installation procedures of open face and closed face tun-

nelling methods. Starting with a description of conventional tunnelling, the principles of shield tunnelling and other mechanized tunnelling methods are explained.

**Chapter 3** A literature review is given which presents common elementary computational methods for the assessment of tunnelling settlements and lining forces. Starting with the empirical method for the prediction of both surface and subsurface ground deformations, the concept of the so-called ground response curve for the estimate of loads on linings is presented in a subsequent section. Hereafter structural design models for tunnels, including both analytical closed form solutions and the approach of bedded beam computations is reviewed. A special section is dedicated to the effect of installation procedures for these structural models in terms of magnitudes and distributions of ground pressures on tunnel linings.

**Chapter 4** This chapter deals with the finite element modelling of tunnels. In order to provide a better understanding it starts by introducing some basic terms and modelling aspects of two- and three-dimensional FEM tunnel analyses. Factors which may significantly decrease the accuracy of the method when not considered properly, including amongst others the influence of the tolerated equilibrium error, mesh dimensions and the mesh coarseness, are discussed. The importance of the magnitude and orientation of initial stresses is considered in a separate section. Special attention is given to the numerical modelling of the tunnel excavation and support sequence. Both two- and three-dimensional models of open and closed face tunnels are studied, giving a detailed literature overview. For closed shield tunnelling an improved numerical excavation and support procedure is proposed, being named the grout pressure method. The two-dimensional modelling of open face tunnels is studied in detail carrying out a parametric study on the magnitude of the so-called unloading or  $\beta$ -factor.

**Chapter 5** The importance of the numerical modelling of the excavation and support sequence and the influence of constitutive models is evaluated in this chapter, considering measured surface settlements and horizontal ground deformations of two tunnel case studies. Both two- and three-dimensional FE-analyses are carried out to demonstrate the predominant importance of the excavation and support sequence. Besides the influence of the constitutive model is significant. The well known Mohr-Coulomb Model, the non-linear elastoplastic Hardening Soil Model and an extension of the latter, which includes the small-strain stiffness and is named the Hardening Soil Small Model, are all considered to demonstrate the importance of the small-strain stiffness for the simulation of ground deformations. In particular it will be shown that the small-strain stiffness significantly improves the steepness of the settlement trough.

**Chapter 6** In this chapter the work of the present thesis is summarized, arriving at conclusions and giving recommendations for future research.

# Chapter 2

## Modern tunnelling methods

### Introduction

There is a basic distinction between simple *cut-and-cover* construction methods for shallow tunnels, where a trench is excavated and roofed over, and underground construction methods, which are tunnelling methods to undermine without removing the overburden ground. Whereas the first category of tunnels is reduced more or less to a general type of excavation problem, the second category is related to what is usually understood as tunnelling in the sense of classical mining techniques (trenchless tunnelling methods). In this thesis attention will only be paid to the latter type of tunnels. Moreover, the focus is on shallow tunnels in soil, where depending on the method of construction it will be generally distinguished between open face tunnelling and closed face tunnelling.

### 2.1 Open face tunnelling

Whereas closed shield tunnelling with a pressurized slurry, earth pressure balance control or compressed air continuously apply face support and they will be classified as closed face tunnelling, open face construction of tunnels involves tunnelling methods without applying permanent support to the excavated tunnel heading. In the context of this thesis numerical simulations of open face tunnelling will be associated with conventional tunnelling, although e.g. shield tunnelling without a pressurized face support or tunnel boring machines without a shield can also be classified as open face tunnelling methods. No doubt, conventional tunnelling is very flexible as it provides a large variability of supporting means and therefore in weak and unstable grounds the face may be stabilized e.g. by the installation of anchors or nails after every excavation sequence. Moreover, in the special case of applying compressed air, conventional tunnelling may also be considered as closed face tunnelling, but this will not be considered in the present thesis.

In this thesis open face and closed face tunnelling methods will be distinguished to arrive at principles for numerical simulations. The author is aware of the fact that there are many more tunnelling methods than the ones named above which might be summarized under open face and closed face tunnelling. However, for the sake of convenience the focus in this thesis will be on some basic tunnelling methods. In the following open face tunnelling methods will be briefly reviewed.

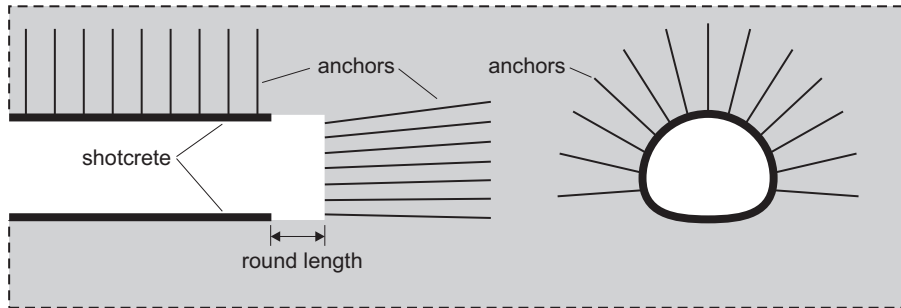


Figure 2.1: Principals of conventional tunnelling to control ground stability and ground deformation: Systematic use of shotcrete and anchors

### 2.1.1 Conventional open face tunnelling method

The discontinuous excavation and support sequence of conventionally driven tunnels involves the use of shotcrete (sprayed concrete) and the systematic installation of anchors (or a number of further supporting means) to support the ground <sup>1</sup>. Whereas in the beginnings of conventional tunnelling the method was specific to strong and stable grounds, nowadays it is also applied to soft grounds <sup>2</sup>. The flexibility of the method to account for the smaller stability and higher deformability of such grounds has been further and further developed. The use of versatile supporting means to increase the stability of softer grounds is also associated with a reduction of ground deformations. This is of utmost importance for the control of tunnel induced deformations to nearby existing structures. Last but not least the efficient interplay of the observational method and the controllability of tunnel induced deformations has made the method suitable also for urban tunnelling.

Fig. 2.1 illustrates an important means to increase the stability of tunnels by applying face and radial anchors. Besides the systematic use of shotcrete and anchors, the fast ring closure of the shotcrete lining at the excavation bottom is important to stop ongoing ground deformation. When approaching softer grounds or larger tunnel diameters, the face can be stabilized by an inclination of approximately  $60^{\circ}$ - $70^{\circ}$ . The round length displayed in Fig. 2.1 is usually in the order of  $0.5m$ - $1.5m$  (KOLYMBAS, 1998). Reducing the round length significantly contributes to the reduction of surface settlements.

Depending on ground quality, the excavation of the ground mass can be carried out by a variety of different excavation means. In softer grounds the material may be removed using special designed tunnel excavators. In jointed rock roadheader machines can be used and for weak to strong rock the drill and blast method applies. When approaching changing ground conditions the excavation means may be easily exchanged. This makes conventional tunnelling a very flexible method when compared to mechanized

<sup>1</sup>The conventional tunnelling method is often referred to as NATM (New Austrian Tunnelling Method) or sprayed concrete method.

<sup>2</sup>In this thesis the term *soft* ground is meant with respect to tunnelling. In order to address soft ground from a geotechnical point of view, the term *soft soil* will be used.

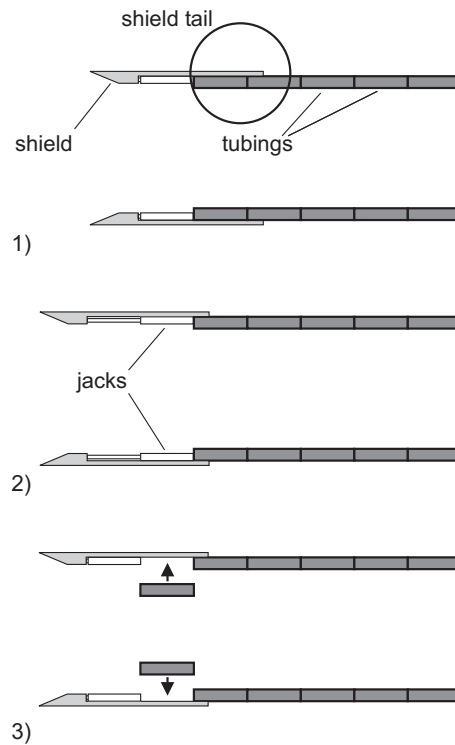


Figure 2.2: Working stages of shield tunnelling

tunnelling methods (e.g. earth pressure balance machine, slurry machine or tunnel boring machine).

Until a final lining is placed, the primary shotcrete lining has to guarantee the stability of the ground alone. The sealing of the ground with shotcrete after each excavation is a stepwise procedure. In a first immediate action the ground is covered with a thin shotcrete layer to protect against rock fall. In a following step a lattice girder is applied and finally the full shotcrete lining is sprayed. Accompanied by deformation measurements the shotcrete lining will be thickened and if necessary supplemented with steel arches.

### 2.1.2 Open face shield tunnelling

Shield tunnelling was first introduced by the famous engineer BRUNEL, who under-passed the river Thames in London in the years 1825-1841 using a rectangular shield construction. The tunnel was hand-excavated and the tunnel lining was a bricklayer construction. A later tunnel underneath the Thames in 1869 used a circular shield and the tunnel lining consisted of cast iron segments. Because of the statically favorable shape of a circular tunnel, the rectangular shield was not further developed and the circular shield with the installation of a lining built up from tubing segments became the archetype of modern shield tunnelling.



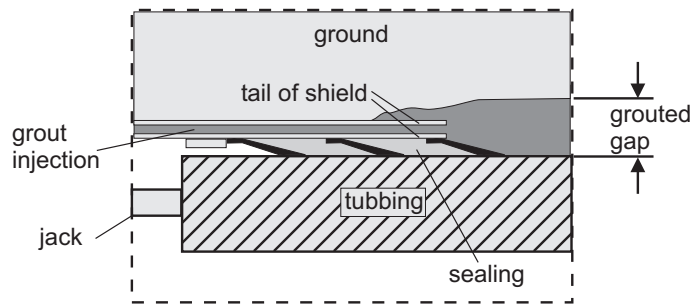


Figure 2.3: Shield tail with grouting of the ground-lining gap

Tunnelling with a shield in particular is well suited for softer grounds which need continuous radial support. The shield is mostly a cylindrical construction out of steel. The shield has to be designed to be able to take all ground and working loads with relatively small deformations. It is usually made of thicker steel plates at its front, to transfer the relatively high axial working forces of the jacks from the lining to the ground. At the shield tail, the steel is not as thick as at the shield front because only radial ground loading has to be accounted for. The inner shield diameter is somewhat larger than the outer diameter of the lining, enabling the installation of tubbings (precast concrete lining segments) in cases where tunnels have to undergo curvatures. Fig. 2.2 shows the principal working stages of shield tunnelling. Jacks installed in the shield push the shield away from the installed lining into the soil. Depending on the length of the tubing segments, the equal length of one sequence of tunnel advance is usually in between 0.8m-2.0m.

After each sequential tunnel advance of one segment length, the jacks are released, giving space for a new tubing ring to be built. As shown in Fig. 2.2 tubbings are installed inside the tail of the shield, which keeps the ground from deforming or falling into the excavated tunnel. Fig. 2.3 shows a detailed view of the shield tail. Inside the shield tail, grout<sup>3</sup> is pumped into the gap between ground and tunnel lining, to limit further radial ground deformation. To prevent the continuous grouting to flow into the shield, between shield tail and tubing ring a sealing is installed. The sealing consists of steel brushes filled with grease. During tunnel advance this sealing is sliding over the tubbings.

An unstable tunnel face can be improved e.g. by applying steel plates which are connected to hydraulic jacks, giving a certain face pressure. Alternatively the soil at the face may be given its natural inclination, letting it roll into the shield, but ground deformation will be significantly larger. Underneath the ground water table open face tunnelling is problematic and therefore the ground water table should be lowered. When tunnelling underneath the ground water table or with larger tunnel diameters it is more efficient to apply closed face tunnelling methods, where a shield is combined with a cutting wheel. Closed face tunnelling methods are to be considered in the following section.

<sup>3</sup>For shield tunnelling in rock also gravel is used to fill the ground-lining gap.

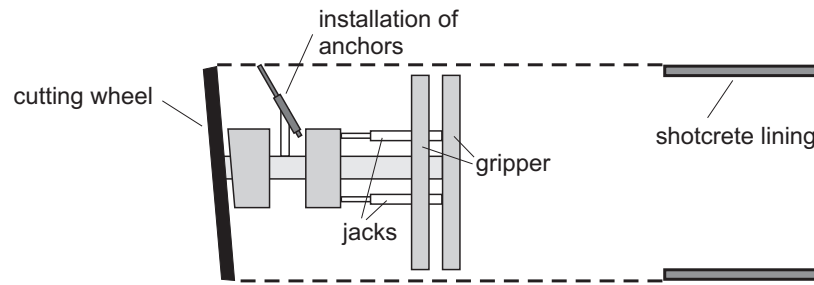


Figure 2.4: Tunnel boring machine without shield

### 2.1.3 Tunnel boring machine without shield

The principles of a tunnel boring machine (TBM) without a shield are shown in Fig. 2.4. A TBM without a shield is generally applied to rocklike materials. The cutting wheel is pressed against the tunnel face by jacks, but jacking forces are not transferred to the tunnel lining. Instead so-called grippers are used, which apply a force at the tunnel walls to clamp the machine to the rock mass. Because the ground is stable enough a lining is usually installed only after some distance behind the TBM. Here shotcrete is used to protect against rockfall and if necessary a lattice girder is included. In addition to the shotcrete lining, invert tubing stones are often used to install railway tracks. Directly behind the cutting wheel the ground is open and anchors can be drilled in case of unstable rock blocks. As the machine is not closed with a shield and unexpected rockfall constitutes a considerably danger, it is of great importance to investigate the ground conditions to be approached. In deep rock this can be achieved by drilling exploratory boreholes from the tunnel face. Often boreholes are drilled for lengths of up to 50m. A particular aim of such investigations is to avoid unexpected water influx.

## 2.2 Closed face tunnelling

Closed face tunnelling methods involve a continuous face support to the tunnel face. In contrast to open face tunnelling these methods in principle are aimed at a reduction of ground deformations. This is of particular importance for shallow urban tunnelling. The relatively small ground deformations which can be achieved in closed face tunnelling often lead to higher ground loads on the tunnel lining, but in shallow urban tunnelling loads on tunnel linings are generally relatively small and they tend to be of minor importance for tunnel design. Instead settlements are an important topic of consideration.

### 2.2.1 Closed face shield tunnelling

The principles of shielded tunnels have been explained in the previous Section 2.1.2. For larger tunnel diameters the use of such a shield can be combined with mechanized tun-

nelling, where the ground is excavated by a cutting wheel. In machinized tunnelling methods face support can be applied in various different ways. Depending on ground conditions, in principal three different types of tunnel face support are most commonly used: Shield tunnelling with mechanical support, with compressed air, with earth pressure balance or with a slurry pressure, as shown in Fig. 2.5.

**Mechanical support** Shield tunnelling with mechanical support provides a pressure to the face by the cutting wheel itself. As shown in Fig. 2.5a, in addition to the cutting wheel, steel plates may be installed in between the free spaces of the cutting arms, to slide along the tunnel face while rotating the boring machine. This method is somewhat similar to a shielded tunnel in combination with pressurized steel plates at the tunnel face, described in the previous section, and the transition to closed face tunnelling is thus not so sharp. Although the pressure applied in mechanical support is more or less continuous, the method is only suitable for predominantly stable cohesive grounds above the ground water table. For shield tunnelling underneath the ground water table shields with compressed air, earth pressure balance or slurry shields can be used.

**Compressed air** As shown in Fig. 2.5b compressed air is used to stabilize the tunnel face. The method is mainly applied to tunnels driven underneath the ground water table to avoid water influx. To apply an effective pressure to the soil skeleton the surface of the tunnel face needs to have a small permeability. In soils with permeabilities of  $k < 10^{-6}$  the pores are small enough to prevent the air of flowing into the soil body (BABENDERERDE and HOLZHÄUSER, 2000). In soils with high permeabilities the face can be sealed with a filter cake. If erosion takes place there is the danger of a blowout. For this reason one tends to use EPB or slurry shields.

**Earth pressure balance** Earth pressure balance (EPB) shields are most commonly used in soft grounds. As shown in Fig. 2.5c, the excavated soil is used to apply a support pressure to the tunnel face. Various additives are often used to ensure appropriate muck properties. This is of particular importance for the screw conveyer, which is extracting the soil from the chamber behind the tunnel face. The screw conveyer is controlling the pressure at the tunnel face by its advance rate. For tunnelling underneath the ground water table, the length of the screw conveyer has to be designed for the hydrostatical water pressure. It should be long enough in order to reduce the water pressure to atmospheric pressure.

**Slurry support** Slurry shields stabilize the tunnel face by applying a pressurized bentonite slurry, as illustrated in Fig. 2.5d. During operation soil is mixed into the slurry and at the end the soil is removed from the slurry in a separation plant. For the slurry pressure it is important that a more or less impermeable mud layer is formed, the so-called filter cake, which is sealing the tunnel face. It ensures that the slurry does not totally flow into the ground, keeping a certain pressure on the tunnel face. To control the slurry pressure a chamber with air pressure is connected to the slurry, as shown in Fig.

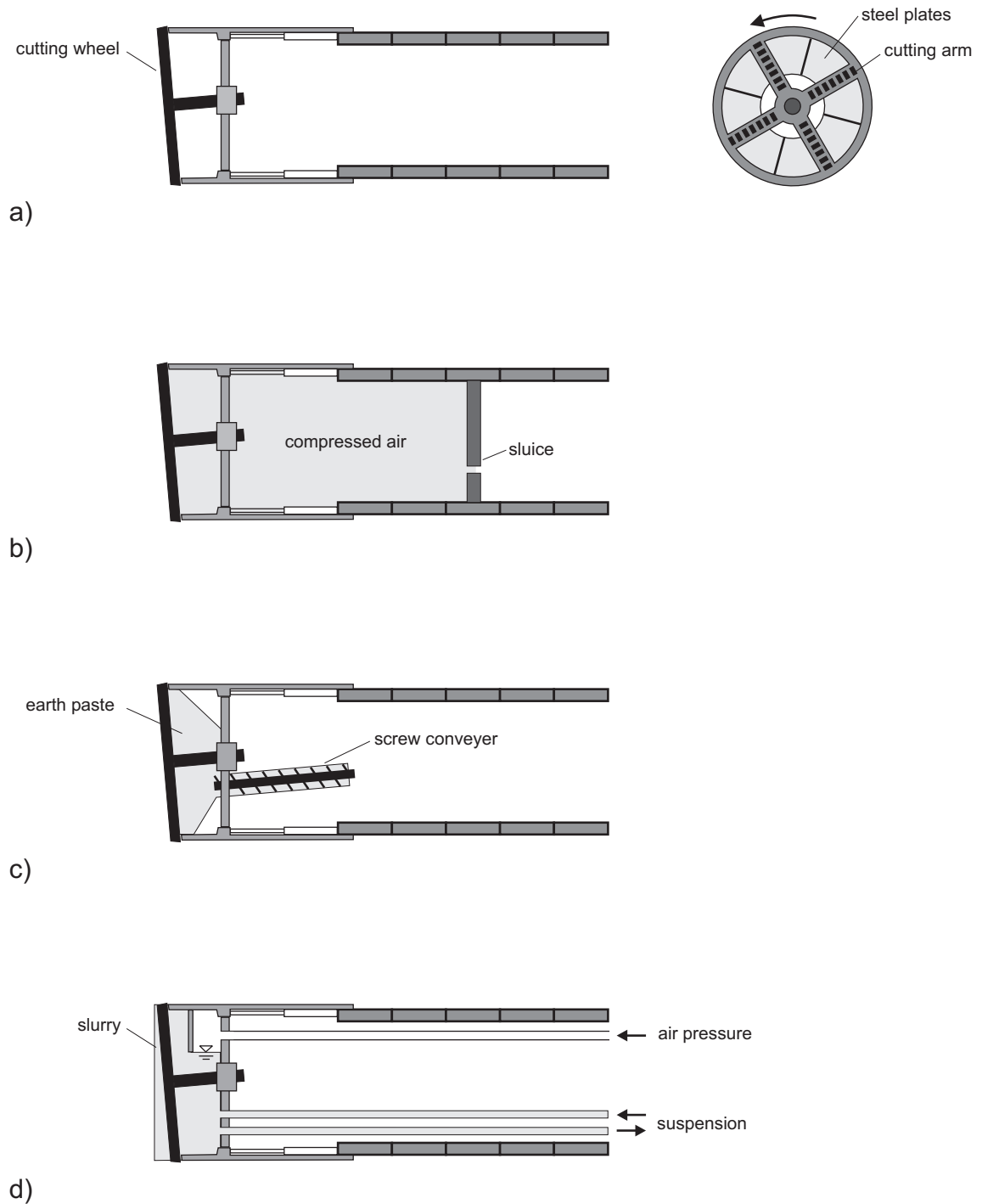


Figure 2.5: Shield tunnelling with a) mechanical support, b) compressed air, c) earth pressure balance and d) slurry support

2.5d. In contrast to mechanical and EPB-shields, in slurry shields the excavated soil is pumped away together with the slurry. Bigger stones need therefore to be crushed by a special stone crusher before they enter the slurry chamber. Slurry shields are well suited for almost all types of soil. In particular they can be well applied to sandy soils.

# Chapter 3

## Elementary computational methods for tunnels

### Introduction

When the tunnelling engineer designs a tunnel structure, he guarantees that the structure is safe with respect to structural collapse and ground deformations during its projected lifetime. Depending on ground conditions and tunnelling method he must choose an appropriate method of analysis and derive, or even invent, a structural model, i.e. a structural idealization. By applying equilibrium and compatibility conditions to the model, the engineer has to arrive at those criteria that are factors in deciding whether or not the design is safe. Different structural design methods and design models have been developed and they are used for different excavation and support sequences, for the preliminary and the final tunnel lining, or for different ground behavior, e.g. in discontinuous rock or homogeneous soil.

There is no other section of geomechanics where structural design methods have proven so controversial and debated as it is the case for tunnel constructions. Therefore a condensed overview of relevant computational methods for settlements and lining forces will be given in the following. Papers that applied a broader approach to all the complex aspects of tunnelling, including different structural design methods, have been published e.g. by CRAIG and MUIR WOOD (1978) or EINSTEIN (1979-1980).

### 3.1 Tunnels in rock versus soil

In tunnelling literature the terminologies *hard rock* and *soft ground* are often adopted. Hard rock is understood as a stiff and strong ground that is able to carry itself without support by a tunnel lining and tunnelling in soft ground <sup>1</sup> is understood to involve more or less immediate tunnel support as, e.g., in driving a closed shield tunnel or by applying shotcrete with the short-time closure of the full lining ring. The present thesis, however, shall be understood as a contribution to tunnelling from the background of geotechnical engineering, and therefore the terminologies hard rock and soft ground are more properly expressed as tunnelling in rock and soil.

The transition between rock and soil is not abrupt, and there are many kinds of rock like materials, which may be called either soft rock or hard soil. In such a case the rock

---

<sup>1</sup>Please note that the term *soft ground* is meant to be soft with respect to tunnelling. It should not be mistaken with the term *soft soil*, as used to express a *really* soft material from a geotechnical point of view.

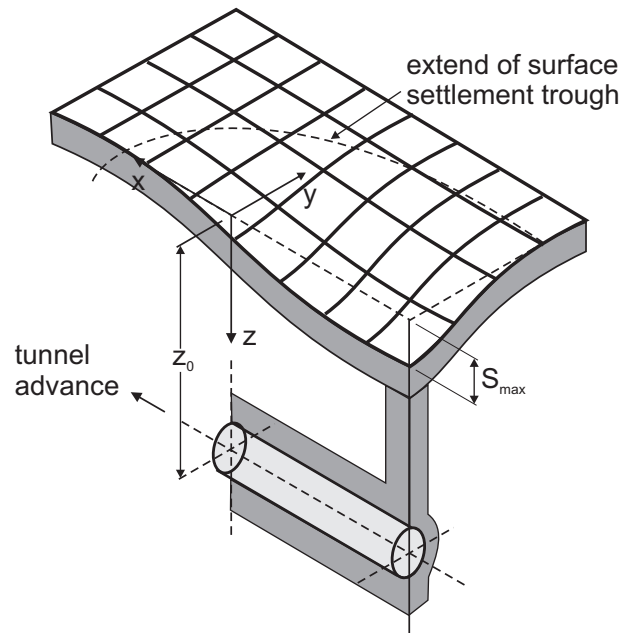


Figure 3.1: Tunnel induced settlement trough after ATTEWELL et al. (1986)

mass may be modelled in the same way as soil. In the present thesis the focus is on tunnelling in soil and soft rock rather than on tunnelling in hard rock, although some of the structural design approaches may be generally applicable. In order to address geomaterials uniformly, regardless of whether it concerns soil or rock, in the present thesis the word *ground* will be used.

### 3.2 Tunnels in soil and soft rock

When a tunnel in soil is planned, ground movements are an important topic to be considered for tunnel design. Depending on the method of tunnel construction different support measures are taken to guarantee stability and to limit deformation. Urban tunnelling is aimed at reducing ground deformations to a minimum, but in deep tunnelling tolerable deformations may be significantly larger. No matter what tunnelling method the ground will be loaded or unloaded and deformations will inevitably take place, leading to a settlement trough as shown in Fig. 3.1. This thesis focuses on deformations due to open face conventional tunnelling and closed face shield tunnelling, as indicated in Fig. 3.2.

### 3.3 Deformations due to closed shield tunnelling

MAIR and TAYLOR (1997) summarized the following primary components of ground deformation associated with closed shield tunnelling:

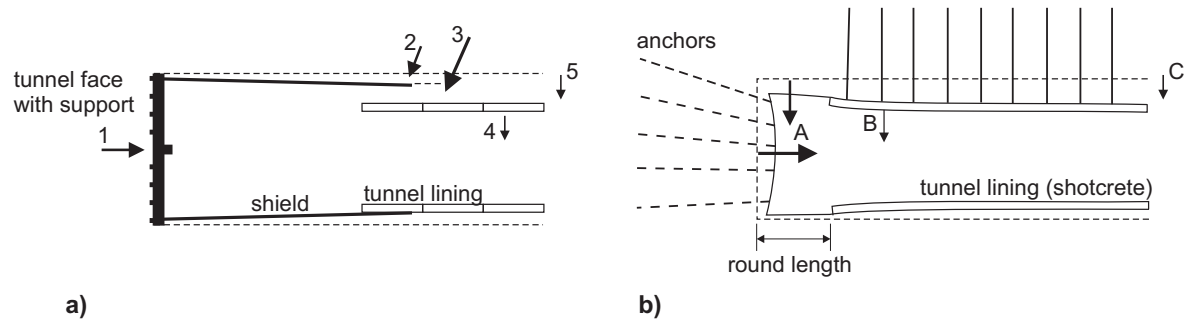


Figure 3.2: Principal components of ground deformation: a) Closed shield tunnelling (after MAIR and TAYLOR (1997)), b) open face tunnelling

1. Movement of the ground towards the face, due to stress relief.
2. Radial ground movement towards the shield, due to over-cutting and ploughing.
3. Radial ground movement into the tail void, due to a gap between shield and lining.
4. Radial ground movement towards the lining, due to deformation of the lining.
5. Radial ground movement towards the lining due to consolidation.

For shield tunnelling with adequate face support (Fig. 3.2a), the first component of ground deformation will be relatively small, but the second component may be appreciable; in particular for a somewhat conical shield or in case of over-cutting, as well if there are steering problems in maintaining the alignment of the shield. The third component of ground deformation can be minimized by grouting, but this component is strongly influenced by the experience of the crew and the ground pressure control being implemented. This third component is usually the major cause of settlements. Component four tends to be of minor importance in relation to conventional tunnelling. Component five can be of importance for tunnelling in soft soils with low permeabilities. In case of insufficient face pressure the pore water pressure dissipation/consolidation phenomenon may take place in front of the tunnel face.

### 3.4 Deformations in open face tunnelling

For open face tunnels (Fig. 3.2b) the following main causes of settlements can be specified:

- A** Movement of the ground towards the non-supported tunnel heading.
- B** Radial ground movement towards the deforming lining.
- C** Radial ground movement towards the lining due to consolidation.



Ground movement (A) towards an unsupported tunnel heading is obvious. No doubt, this component of settlements can be reduced by, e.g., reducing the unsupported round length, or by the use of face anchors, but heading deformations remain significant. The radial ground movement (B) towards the lining is relatively large, as an initially ductile shotcrete lining is used for temporary support. Various different additives are often used to accelerate the hardening of the concrete and thus its stiffening, to allow for an increase of the tunnel excavation rate. When tunnelling in grounds with low permeabilities some consolidation after tunnel construction may take place. In cases where the finished tunnel will act as a drain, or where other reasons impose consolidation to the surrounding ground, delayed radial movements of type (C) may occur. In grounds with high permeabilities, the pore water pressure dissipation/consolidation phenomenon also tends to take place in front of the tunnel face and ground movements may occur quickly during construction.

For tunnelling in the urban environment, deformations are a major design topic, as existing structures might be damaged by differential settlements. When interaction problems of tunnels with existing structures need to be accounted for, a green field settlement trough (Fig. 3.1) is often assumed as it implies a conservative approach. Independent of the tunnelling method the shape of the green field settlements is well matched by a Gaussian function, as considered in Section 3.6.

### 3.5 Lining forces

The lining, whether it be temporary or permanent, must withstand ground pressures with a sufficient margin of safety. The assessment of the water pressure is straight forward, but effective stresses on the lining depend again significantly on installation procedures. MAIR and TAYLOR (1997) report that this stress may amount up to 50% of the overburden stress. In urban shield tunnelling ground deformation is minimized by face support and grouting, but this increases loads on linings so that effective stresses may get more close to the overburden stress. CRAIG and MUIR WOOD (1978) stated that monitoring of stresses in shield tunnel linings has shown that the average stresses generally increase during the first few months up to 50% - 70% of the equivalent overburden stress. Higher stress concentrations have been recorded in the early measurements, but these may be partly associated with moment stress, as reported by CRAIG and MUIR WOOD.

In the period of planning a tunnel structure the engineer has to rely on a method of analysis, from which he may derive criteria whether the design is suitable, safe and economical. Relevant methods for the assessment of bending moments and normal forces are to be considered.

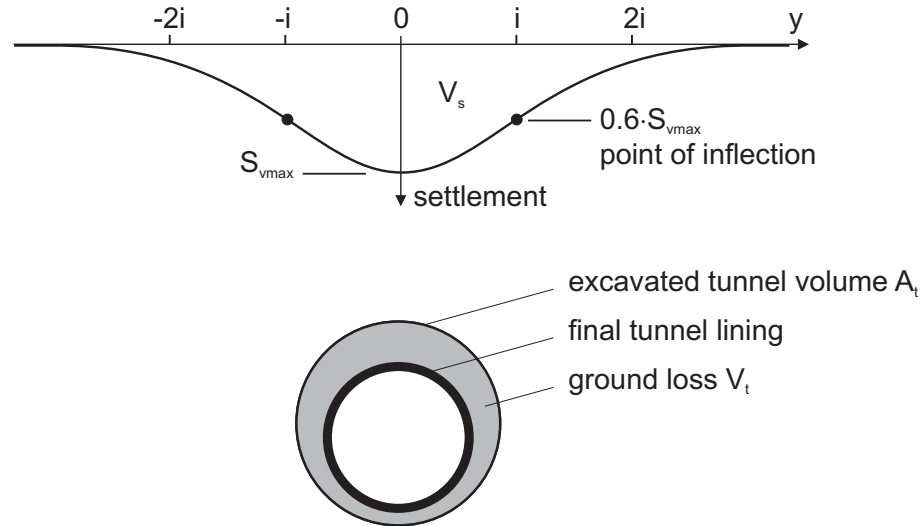


Figure 3.3: Gaussian curve for transverse settlement trough and ground loss  $V_t$

## 3.6 The empirical assessment of settlements

### 3.6.1 Transverse surface settlement

The most common empirical method to predict ground movements is based on a Gaussian distribution, which is often referred to as the empirical method. SCHMIDT (1969) and PECK (1969) were the first to show that the transverse settlement trough, taking place after construction of a tunnel, in many cases can be well described by the Gaussian function:

$$S_v(y) = S_{vmax} \cdot e^{-\frac{y^2}{2i^2}}, \quad (3.1)$$

where  $S_{vmax}$  is the settlement above the tunnel axis,  $y$  is the horizontal distance from the tunnel axis and  $i$  is the horizontal distance from the tunnel axis to the point of inflection of the settlement trough, as shown in Fig. 3.3. The volume of the settlement trough (per unit length of tunnel)  $V_s$  is obtained by integrating Equation 3.1. This yields

$$V_s = \int S_v(y) \cdot dx = \sqrt{2\pi} \cdot i \cdot S_{vmax}. \quad (3.2)$$

In addition to the settlement volume  $V_s$  one has to consider the ground loss  $V_t$ . This is the volume of the ground that has deformed into the tunnel after the tunnel has been constructed, as illustrated in Fig. 3.3. For tunnelling in undrained ground, the settlement volume is more or less equal to the ground loss, but the settlement volume tends to be somewhat smaller for drained excavations. Indeed, dilation and swelling due to unloading may result in soil expansion, such that  $V_s < V_t$  (CORDING and HANSMIRE, 1975). However, differences tend to remain small and it can be assumed that  $V_s \approx V_t$ . As the ground loss depends more or less linearly on the tunnel volume, it is convenient to

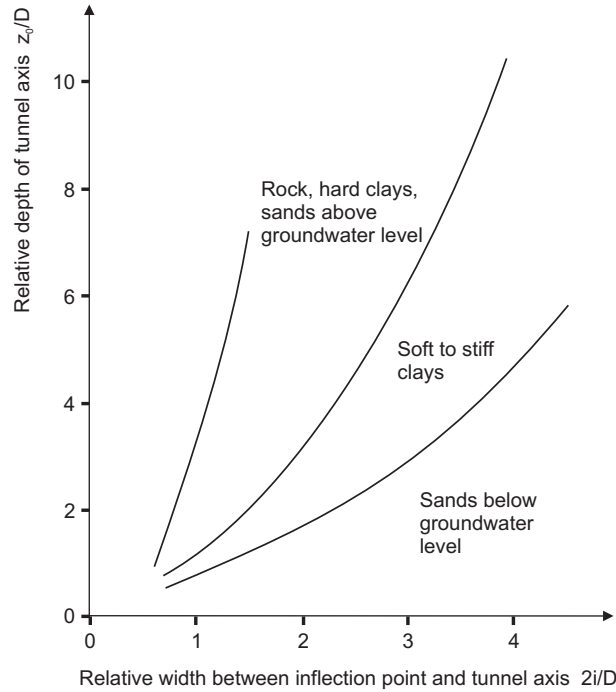


Figure 3.4: Relation between settlement trough width and tunnel depth for different grounds (PECK, 1969)

consider the ground loss ratio

$$GLR = \frac{V_t}{A_t} \approx \frac{V_s}{A_t}, \quad (3.3)$$

where  $A_t$  is the tunnel volume per unit of length. It follows from Equations 3.1 - 3.3 that

$$S_{vmax} \approx \frac{A_t}{i \cdot \sqrt{2\pi}} \cdot GLR \quad (3.4)$$

and

$$S_v(y) \approx \frac{A_t}{i \cdot \sqrt{2\pi}} \cdot GLR \cdot e^{-\frac{y^2}{2i^2}}. \quad (3.5)$$

Assuming the Gaussian curve to assess the distribution of transverse surface settlements, one needs information on two input parameters, namely the distance to the point of inflection  $i$  for the width of the settlement trough and the ground loss ratio  $GLR$  for the depth of the settlement trough.

### 3.6.2 Width of settlement trough

**Homogenous ground:** The distance from the tunnel axis to the inflection point  $i$ , which is determining the width of the settlement trough, has been subject to many investigations. PECK (1969) suggested a relationship to tunnel depth  $z_0$  and tunnel diameter  $D$ ,

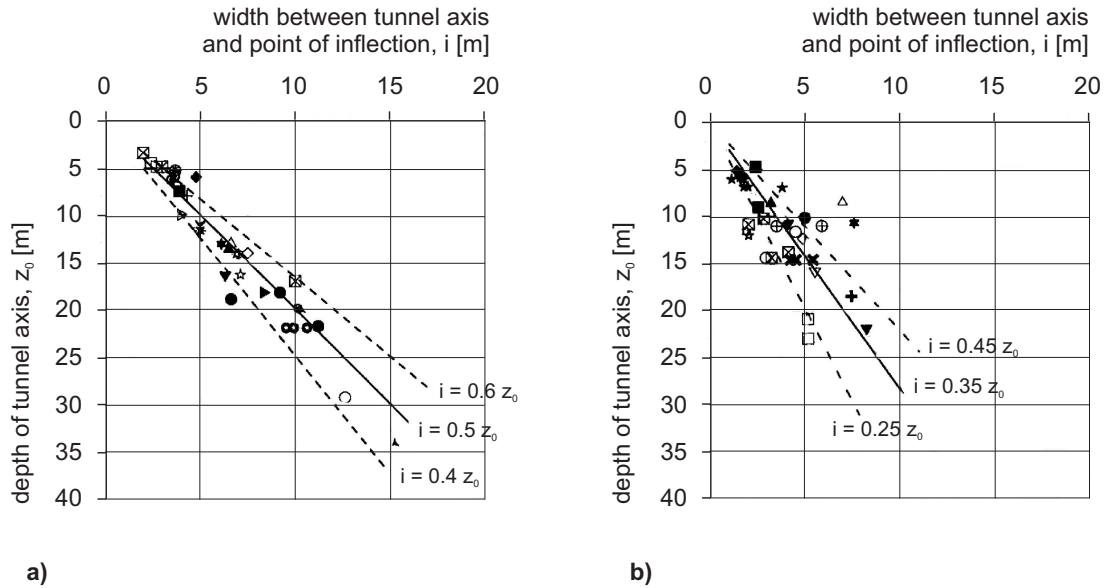


Figure 3.5: Observed width of surface settlement trough as a function of tunnel depth: a) In clays, b) in sands and gravels (MAIR and TAYLOR, 1997)

depending on ground conditions, as shown in Fig. 3.4. After the suggestion by PECK many other authors have come up with similar relationships, e.g. CORDING and HANSMIRE (1975) or CLOUGH and SCHMIDT (1981). O'REILLY and NEW (1982) presented results from multiple linear regression analyses performed on field data, confirming the strong correlation of  $i$  with tunnel depth, but showing no significant correlation of  $i$  with tunnel diameter (except for very shallow tunnels, with a cover to diameter ratio less than one) or method of construction. They stated, that for most practical purposes the regression lines may be simplified to the form

$$i = K \cdot z_0, \quad (3.6)$$

where  $K$  is a trough width parameter, with  $K \approx 0.5$  for clayey grounds and  $K \approx 0.25$  for sandy grounds. The approach of Eq. 3.6 has been generally confirmed by RANKIN (1988), who presented a variety of tunnel case histories in clayey, sandy, residual and in mixed grounds. MAIR and TAYLOR (1997) presented a large number of tunnelling data with different linear regressions for tunnels in clays and tunnels in sands and gravels. As shown in Fig. 3.5, the regressions confirm the findings of O'REILLY and NEW (1982) for clayey soils, with a trough width parameter ranging in between 0.4 and 0.6, with a mean value of  $K = 0.5$ . However, for sandy soils they obtain a  $K$  ranging in between 0.25 and 0.45, with a mean value of 0.35, indicating somewhat wider settlement troughs.

**Layered ground:** Often tunnels are constructed in layered ground, including both clayey and sandy ground layers. For tunnels in layered ground NEW and O'REILLY (1991) pro-

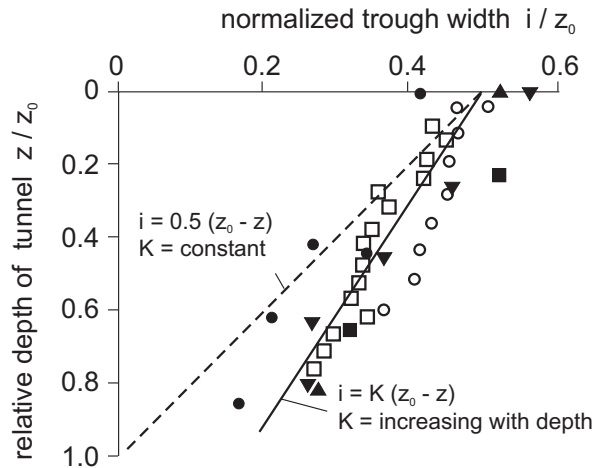


Figure 3.6: Variation of settlement trough width with depth of subsurface settlement profiles above tunnels in clays (MAIR et al., 1993)

posed a relationship for  $i$  of the form

$$i = K_1 \cdot z_1 + K_2 \cdot z_2, \quad (3.7)$$

where  $K_1$  is the trough width parameter for ground layer 1 with thickness  $z_1$  and  $K_2$  is the trough width parameter for ground layer 2 with thickness  $z_2$  respectively. MAIR and TAYLOR (1997) also discussed this formula and they report that it agrees reasonably well with field observations of tunnels in sands overlain by clay layers. However, when sandy layers overlay clays they found Eq. 3.7 to be less evident. Nevertheless, in combination with estimated ground losses it would seem that Eq. 3.7 may be used for a first prediction of surface settlements, both for open and for closed face tunnelling.

**Subsurface settlement** When tunnelling in urban areas, one may have to consider the interaction with deep foundations or existing tunnels. This leads to the need of having information about the development of subsurface settlement profiles. MAIR et al. (1993) analysed subsurface deformations from tunnels in clays as well as centrifuge tests in clay (Fig. 3.6 and Fig. 3.7). They showed that subsurface deformations can also be reasonably approximated by a Gaussian distribution. A possible extension of Eq. 3.6 for subsurface settlement profiles is

$$i = K \cdot (z_0 - z), \quad (3.8)$$

where  $z$  is the depth of the subsurface profile being considered. As shown in Fig. 3.6 MAIR et al. (1993) observed that the value of  $i$  for subsurface settlement profiles is significantly larger than would be predicted with a constant  $K$ . To match the data of Fig. 3.6 and Fig. 3.7 for tunnels in clay, MAIR et al. proposed the expression

$$K = \frac{0.175 + 0.325 \cdot (1 - z/z_0)}{(1 - z/z_0)}. \quad (3.9)$$

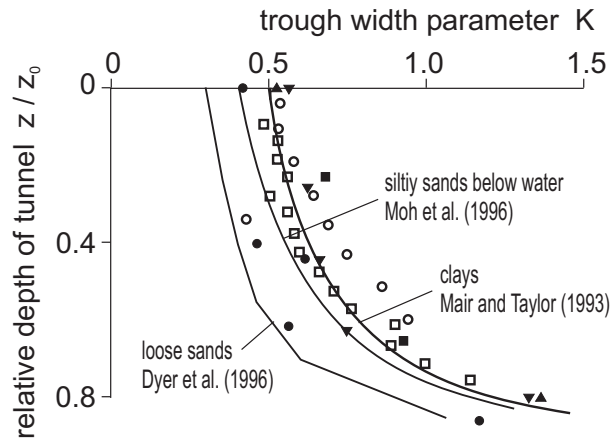


Figure 3.7: Variation of trough width parameter  $K$  with depth of subsurface settlement profiles above tunnels after MAIR and TAYLOR (1997)

Considering subsurface measurements of tunnels MOH et al. (1996) analyzed tunnels in loose sands and DYER et al. (1996) obtained similar relationships for tunnels in silty sands, as shown in Fig. 3.7.

### 3.6.3 Depth of settlement trough

According to CRAIG and MUIR WOOD (1978) it is generally found that the volume of the settlement trough at the surface is approximately equivalent to the volume of the ground lost in the tunnel. The ground loss ratio  $GLR$  in Equation 3.3 is used for an initial estimate of  $S_{vmax}$ .

The method of construction of the tunnel will have a considerable effect on the ground loss ratio. In shield tunnelling the ground loss is predominantly a result of tail void grouting and face pressure. If the ground is stable enough, and the lining can be erected and grouted without the ground falling onto the lining, very little settlement will occur. If the ground falls onto the lining and fills the grouting space, the whole of this movement will be reproduced at the surface.

Depending on equipment, control procedures and experience of the crew,  $GLR$ -values between 0.5% and 2% are realistic in homogeneous ground. In sands a loss of only 0.5% can be achieved, whereas soft clays involve the range from 1% to 2%, as reported by MAIR (1996). Considering data for mixed ground profiles with sands or fills overlaying tertiary clays, MAIR and TAYLOR (1997) reported values between 2% and 4%.

In conventional driven tunnels the  $GLR$  is largely controlled by the round length and the size of the (partial) excavations, whilst ground stiffness and initial stresses also have a significant influence. MAIR (1996) concluded that ground loss ratios in stiff clays are between 1% and 2%, whilst conventional tunnelling in London clay has resulted in even smaller losses varying between 0.5% to 1.5%.

Many authors have proposed various different relationships for ground loss ratios.

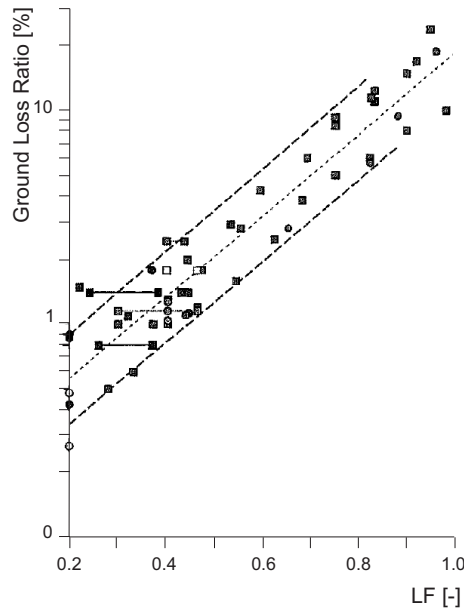


Figure 3.8: *GLR* versus load factor *LF* in overconsolidated clay (MACKLIN, 1999)

Several proposals are related to the stability number  $N$ , defined by BROMS and BENNERMARK (1967) as

$$N = \frac{p_v - p_t}{c_u}, \quad (3.10)$$

for tunnelling under undrained conditions, where  $p_v$  is the total overburden pressure at tunnel axis level,  $p_t$  is the tunnel face support pressure (if present) and  $c_u$  is the undrained shear strength of the ground. Here it should be noted that RUSE (2004) defined the stability number by the equation

$$p_f = p_v - c_u \cdot N_f, \quad (3.11)$$

where  $p_f$  is the minimum face support pressure at failure and  $N_f$  a given function of the tunnel cover over tunnel diameter ratio  $H/D$ . In fact it would be better to refer to  $N$  as the mobilized stability number and it should be obvious that  $N \leq N_f$ .

For tunnels in undrained clays, CLOUGH and SCHMIDT (1981) proposed a relationship between mobilized stability number  $N$  and ground loss ratio based on the closed form solution for the unloading of a circular cavity in a linear elastic-perfectly plastic continuum under axisymmetric conditions. According to CLOUGH and SCHMIDT for  $N$  less than 2 the response is elastic with small ground movements and the tunnel face being stable. For  $N$  between 2 and 4 loads increase and limited plastic yielding occurs, while for  $N$  between 4 and 6 the yielding zone is spreading leading to larger movements. For  $N$  greater than 6 the yielding zone is significant, leading to tunnel face instability with large ground movements. From a mechanical point of view such findings should be generalized by considering the ratio of  $N/N_f$  rather than simply  $N$ , as  $N_f$  is not a constant but is heavily dependent on tunnel depth.

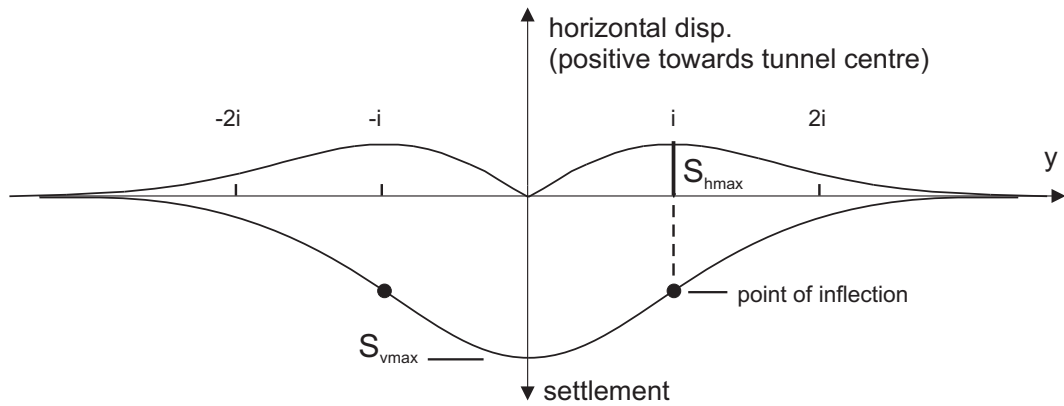


Figure 3.9: Horizontal surface displacements and transverse settlement trough

ATTEWELL et al. (1986) and URIEL and SAGASETA (1989) presented field data of ground loss ratios related to the mobilized stability number, based on CLOUGH and SCHMIDT'S proposal. The results show a very wide scatter, which is probably associated with the use of  $N$  rather than  $N/N_f$ .

Recent work of MACKLIN (1999) on the assessment of Ground Loss Ratio ( $GLR$ ) is shown in Fig.3.8. He related measured  $GLR$ -data from different tunnelling projects in overconsolidated clay to the load factor  $LF = N/N_f$ , which is the inverse of the factor of safety. For  $LF \geq 0.2$  he proposed the linear regression

$$GLR = 0.23 \cdot e^{4.4(LF)}. \quad (3.12)$$

Considering the fact that measured  $GLR$  data in Fig.3.8 show a considerable scatter, MACKLIN emphasizes that for design purposes the range of values Fig.3.8 should be considered, rather than just Eq. 3.12. However, ground movements are affected by a large number of different factors and thus such relations on the assessment of  $GLR$  can be indicative only. It would seem that Fig.3.8 ideas has not yet found its way into engineering practice, but the idea of estimating settlements in relation to a factor of safety or load factor would seem to be sound.

### 3.6.4 Horizontal displacements

When tunnels in urban areas are constructed, damage of buildings can arise from horizontal ground displacements. However, there are relatively few case histories of tunnels where horizontal ground or structure movements have been measured. O'REILLY and NEW (1982) proposed that resultant ground displacement vectors point towards the center of the tunnel. This assumption leads to the distribution of surface horizontal ground displacements given by

$$S_h(y) = \frac{y}{z_0} \cdot S_v(y). \quad (3.13)$$



Using Eqs. 3.1 and 3.5 in Eq. 3.13 the horizontal surface displacement can be written as

$$S_h(y) = \frac{y}{z_0} \cdot S_{vmax} \cdot e^{-\frac{y^2}{2i^2}} \approx \frac{y}{z_0} \cdot \frac{A_t}{i \cdot \sqrt{2\pi}} \cdot GLR \cdot e^{-\frac{y^2}{2i^2}}. \quad (3.14)$$

Fig. 3.9 shows the distribution of the horizontal displacement together with the Gaussian settlement trough. Consistent with field observations by CORDING and HANSMIRE (1975) the theoretical maximum horizontal displacement,  $S_{hmax}$ , occurs at the point of inflection of the settlement trough, where  $S_v(y) = 0.6 \cdot S_{vmax}$ . Hence Eq. 3.13 can be written as

$$S_{hmax} = \frac{i}{z_0} \cdot 0.6 \cdot S_{vmax}. \quad (3.15)$$

Using Eqs. 3.14 and 3.15 the horizontal displacement yields

$$\frac{S_h(y)}{S_{hmax}} = 1.65 \cdot \frac{y}{i} \cdot e^{-\frac{y^2}{2i^2}}. \quad (3.16)$$

When considering tunnel induced horizontal deformations on existing buildings, horizontal strains are important. Horizontal strains may be obtained by differentiating the horizontal displacement with respect to  $y$ .

### 3.6.5 Longitudinal surface settlement

Besides the consideration of the transverse settlement profile, the longitudinal profile also is important. In cases where information on the three-dimensional influence of settlements is required, where buildings might be subjected to twisting and respective torsion forces, longitudinal settlements need to be analyzed.

ATTEWELL and WOODMAN (1982) showed that the longitudinal settlement profile can be derived, by considering a tunnel as a number of point sources in the longitudinal direction and by superimposing the settlement craters caused by each point source. The assumption that the incremental longitudinal settlement trough is a Gaussian curve, leads to the logical extension that the longitudinal settlement trough should follow the shape of a cumulative probability curve. The settlement above the tunnel center line at location  $x$  can be obtained from the equation

$$S_v(x) = S_{vmax} \cdot \frac{1}{i \cdot \sqrt{2\pi}} \cdot \int_{-\infty}^x e^{-\frac{x^2}{2i^2}}, \quad (3.17)$$

where  $x$  is the distance from the tunnel face in the longitudinal direction of the settlement trough, as shown in Fig. 3.1. ATTEWELL and WOODMAN (1982) have validated the assumption of a cumulative probability function reasonably well by an examination of several field study reports.

ATTEWELL et al. (1986) assumed that generally the settlement directly above the tunnel face ( $x = 0$ ) coincides with 50% of the maximum settlement  $S_{vmax}$ , as indicated in Fig. 3.10. This may be more appropriate in case of open face tunnelling. However, for closed

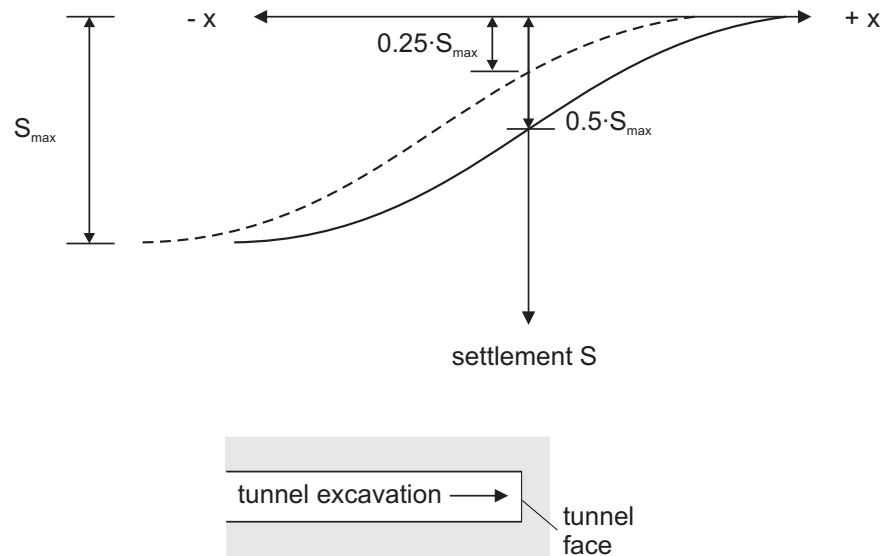


Figure 3.10: Longitudinal settlement trough above tunnel center line after ATTEWELL et al. (1986)

face tunnelling where significant face support is provided, settlements ahead of the tunnel face will reduce significantly. MAIR and TAYLOR (1997) concluded that for closed face tunnelling much lower values of only 25% - 30% are to be obtained, which leads to a translation of the longitudinal settlement profile as indicated by the dashed line in Fig. 3.10. CRAIG and MUIR WOOD (1978) have reviewed shield tunnels in the United Kingdom on this matter. They stated that the percentage of the maximum settlement that occurs ahead of the shield, over the shield and behind the shield varies for different grounds. In general the percentages fall into the ranges given in Table 3.1. CRAIG and MUIR WOOD stated that in most instances 80% - 90% of the maximum settlement will be complete when the face of the tunnel has travelled a distance equivalent to one, to two times the depth of the tunnel past the point of observation. On the centreline of a

Type of ground	Percentage of total settlement completed	
	At face of shield [%]	At passage of tail of shield [%]
Sand above water table	30-50	60-80
Stiff clays	30-60	50-75
Sand below water table	0-25	50-75
Silts and soft clays	0-25	30-50

Table 3.1: Development of settlement profile (CRAIG and MUIR WOOD, 1978)

tunnel the settlements commence at a distance from the face roughly equivalent to half the width of the transverse settlement trough.

### 3.7 The ground response curve for loads on linings

The ground response curve, also referred to as Fenner-Pacher curve or *Convergence-Confinement* curve, is used to illustrate the ground pressure on the lining as a function of deformations. The idea of using ground response curves for tunnel design was initiated by FENNER (1938) and thereupon considered by PACHER (1964), who suggested to measure load-deformation curves in a test gallery. PACHERS basic idea of a cylindrical cavity contraction is shown in Fig. 3.11a. Fig. 3.11b shows different ground response curves for shallow tunnels plotted as normalized effective ground pressure  $p'/p'_0$ , where  $p'_0$  is the initial effective ground pressure, over tunnel crown settlement  $S$  of a tunnel in different grounds. Curve *I* represents a very stable situation of a stiff and strong ground that allows for an unlined tunnel. Curve *II* stands for a moderately stiff and strong ground in which tunnels need some support. Curve *III* shows a relatively flat ground response curve for a really soft ground. In order to obtain a stable situation for such a soft ground, significant support by a lining needs to be provided.

The stress relaxation of the ground, the delayed installation of the lining and the load sharing between ground and lining can be illustrated by the ground response curve. Fig. 3.12 shows a ground response curve which relates the tunnel crown settlement  $S$  to time. In order to provide stability for a relatively soft ground as shown here, a significant part of the load needs to be carried by the lining. For open face tunnelling the crown settlement increases with the round length and the diameter of the excavation, i.e.  $S$  can also be understood as a round length and excavation diameter related measure. The freshly excavated length will be supported after a certain time by the installation of a lining, as indicated by point *A*. Due to further cutting and creep the lining will deform along lining response curve *a* until a quasi final state of stress is reached, as indicated by point *B*. In closed face tunnelling only very little ground deformation is achieved by an earlier support of the ground as indicated by lining response curve *b*. In the latter case a final state of lining and ground is reached at a significantly higher ground pressure, indicating that an earlier installation of lining leads to less ground deformations but higher pressures on the lining. Vice versa a later installation of lining causes more ground deformations while smaller pressures are transferred to the lining.

In present engineering practice analytical or numerical (VERMEER et al., 2002) solutions of ground response curves have been adopted. Various different authors have presented analytical solutions of ground response curves, one of them given by BROWN et al. (1983) together with an overview on further solutions for the axisymmetric tunnel problem. Most of the solutions incorporate a linear elastic or elastic perfectly plastic behavior for both ground and lining. The one-dimensional character of the ground response curve approach needs some simplifications (DUDDECK, 1979) as

- axisymmetric and homogeneous initial stress field ( $K_0 = 1$ ),

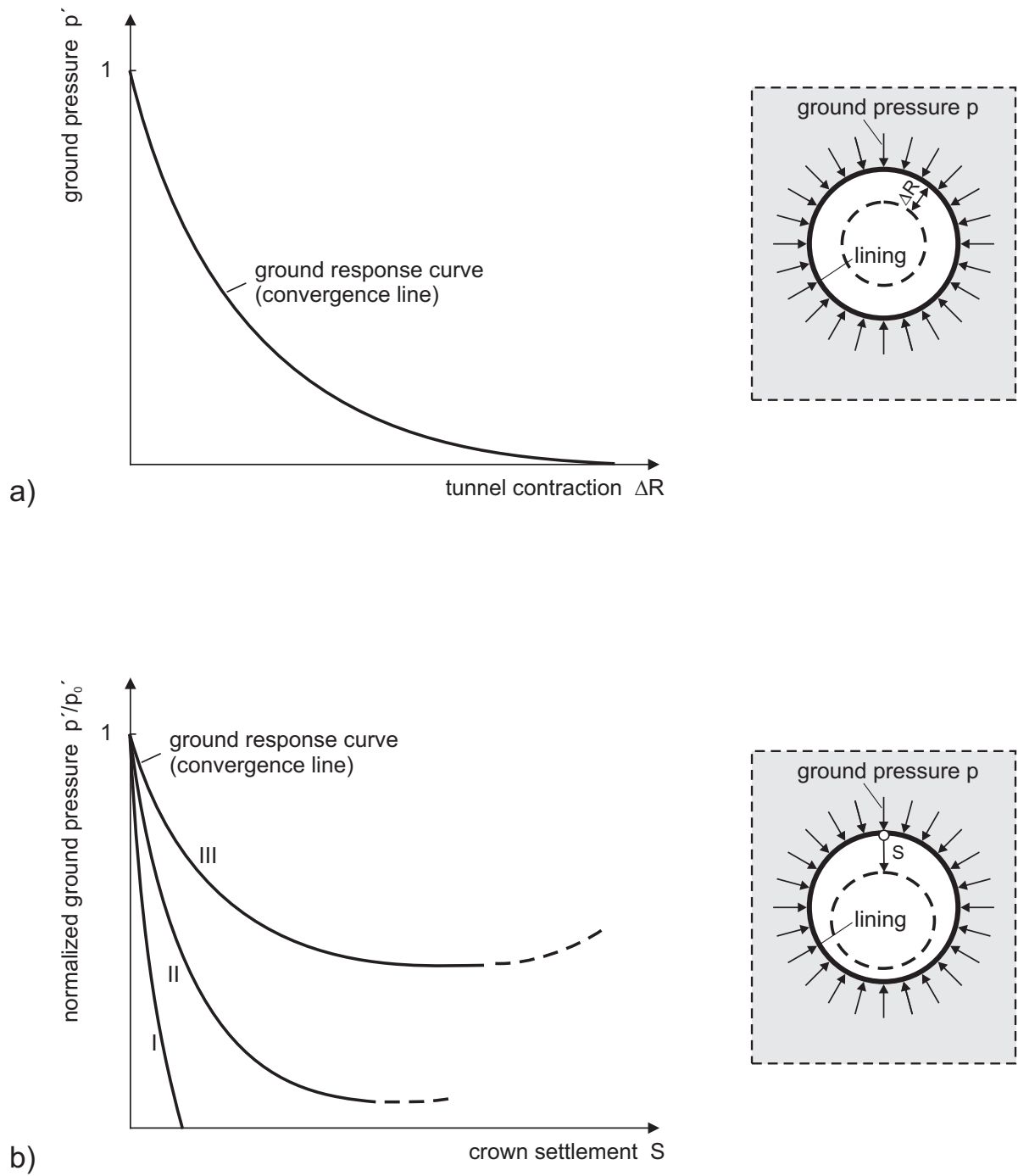


Figure 3.11: Ground response curves after PACHER (1964) for a) deep tunnels, b) shallow tunnels in different grounds

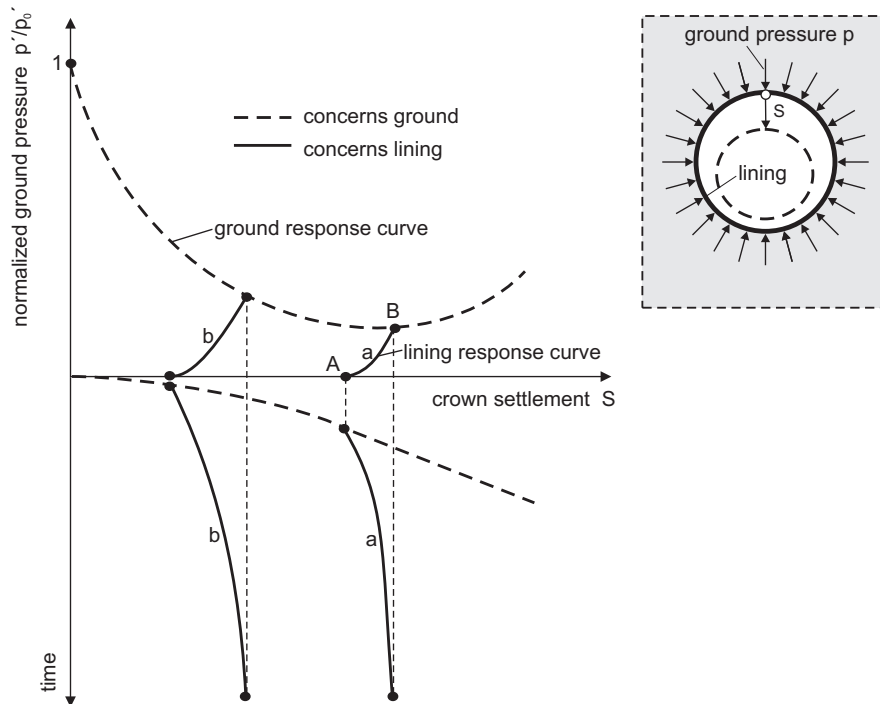


Figure 3.12: Ground response curve: Time dependent interaction between ground and lining after PACHER (1964)

- circular lining with constant lining thickness,
- isotropic behavior of the ground.

In Germany Fenner-Pacher curves were recommended to be used only for preliminary tunnel design (*Empfehlungen für Felsbau unter Tage*, issue 1979). In Austria and Switzerland important tunnel projects like the Arlberg, Gotthard and Tauern tunnels have been successfully designed on the basis of ground response curves and it would seem that they still tend to be used in present engineering practice for deep tunnels in Switzerland, e.g. the Gotthard Base tunnel, and Italy.

Although the quantitative application of ground response curves in engineering practice will be more and more suppressed by the development of numerical methods, their importance for the understanding of basic tunnel design will still remain. They nicely illustrate both the influence of ground stiffness and the influence of ground deformations on lining pressures; the more the ground is allowed to deform the smaller the lining pressures and vice versa. Fig. 3.12 applies both for open and for closed face tunnelling as it also applies to urban tunnelling, where a minimization of ground deformations requires a higher support by the lining. For shallow urban tunnels, little ground deformation will be allowed, but in deep tunnelling significant ground deformation tends to be allowed to reduce pressures on the lining.

## 3.8 Structural design models for tunnels

By designing a tunnel engineers "promise" that the lining will neither suffer structurally nor collapse during its projected lifetime. Thus, models of the reality are necessary for analysis in order to predict the behavior of a tunnel during the excavation and during its lifetime.

Tunnel construction on an international level is carried out using a large variety of different methods of analysis. Published replies in synopsis form to a questionnaire of the ITA (1982) working group on *Structural Design Models for Tunnelling* show significant qualitative as well as quantitative differences in design approaches of several countries. Design methods have been developed on a national level, accompanied with national recommendations.

Structural design models, including a variety of analytical closed form solutions and bedded beam approaches, have been developed for the use in both conventional and shield tunnelling. The different installation procedures of these tunnelling methods significantly influence the magnitude and distribution of loads on tunnel linings and it has been discussed throughout the literature, whether or not it is appropriate to incorporate reduced primary stresses as ground loads. Special attention to loads on tunnel linings is given in Section 3.8.3.

Closed form solutions of continuum models are restricted to a number of simplifications, such as circular cross-sections or homogeneous ground. Solutions of such simplified two-dimensional models have been used worldwide including Austria and Germany (ITA, 1982). The bedded beam approach is most commonly used in German speaking countries, but it seems to be used as well in Belgium, France, Japan and the United States (ITA, 1982). The development of such quasi numerical approaches has reached a state, where also more complex influences like non-circular cross-sections or layered ground can be accounted for.

The excavation of a tunnel changes the primary stress field into a three-dimensional pattern at the tunnelling face. Farther from the face, the stress field eventually will return to an essentially two-dimensional system. Therefore, common structural design models consider only two-dimensional stress-strain fields. Three-dimensional approaches have been proposed e.g. by LOMBARDI (1971) or ERDMANN (1983), but it would seem that such approaches are not widely-used in engineering practice. Instead three-dimensional models tend to be analyzed on the basis of numerical finite element computations.

Because elementary models are easier to apply and they give qualitative insight into the matter, they still are commonly used in engineering practice. But due to fast increasing computer capacities it is not surprising that such models have been more and more replaced by finite element approaches.

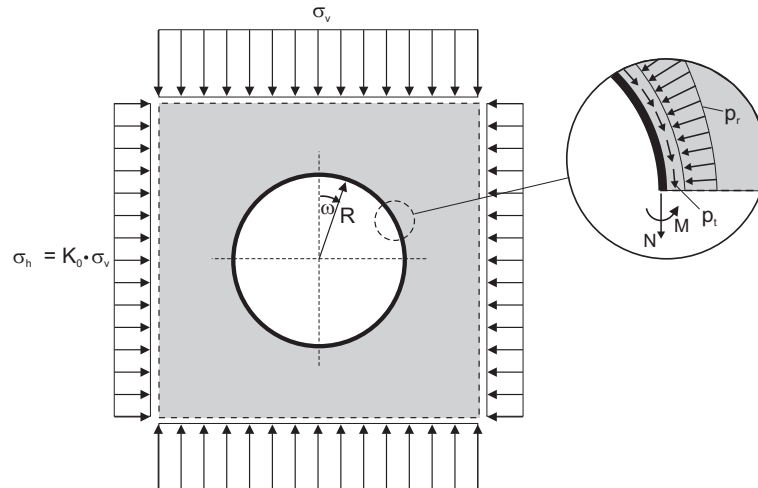


Figure 3.13: Continuum model with stresses at infinity

### 3.8.1 On the use of analytical solutions of continuum models for lining forces

Ground pressures on linings depend heavily on construction procedures and in many cases pressures become extreme during construction rather than after construction. Considering measurements of shield tunnels CRAIG and MUIR WOOD (1978) for instance reported that uneven stresses of a factor of four within one lining segment may occur. Most probably such uneven stresses are associated with twisting of joints or *birdsmouthing* during the erection of the lining. As a consequence bending moments and normal forces are difficult to assess and analyses cannot be expected to give accurate results. This holds in particular for analytical analyses, but closed form solutions have the advantage of giving a direct qualitative insight into the matter. For this reason, attention will be paid to such analytical solutions of continuum models.

Many of the analytical solutions are based on the following simplifications and assumptions, leading to a continuum model as displayed in Fig. 3.13: The circular tunnel with lining radius  $R$  is so deep that the increase of stress due to gravity can be omitted. Hence soil weight is neglected in the sense that there is an initially uniform stress field, with  $\sigma_h = K_0 \cdot \sigma_v$ , where  $\sigma_h$  and  $\sigma_v$  are the horizontal and the vertical stress respectively and  $K_0$  is the coefficient of lateral earth pressure. The lining is either rough (full bonding: both radial  $p_r$  and tangential stresses  $p_t$  are transferred to the lining) or smooth with no bonding at all (no tangential stresses  $p_t$  between lining and ground). Both lining and ground behave linearly elastic.

SCHMID (1926) was probably the first to present an analytical solution for a continuum model. Later analytical solutions for bending moments and normal forces were presented by BULL (1944), ENGELBRETH (1961), SCHULZE and DUDDECK (1964b), WINDELS (1967), MORGAN (1971), PECK et al. (1972), MUIR WOOD (1975), CURTIS (1975), EINSTEIN and SCHWARZ (1979) and AHRENS et al. (1982). Most of these analytical solutions

	Elb-tunnel	Different tunnel linings		
$d$ [cm]	24	20	25	30
$R$ [m]	5.30	3.00	4.00	5.00
$A$ [ $\frac{cm^2}{m}$ ]	286	2000	2500	3000
$I$ [ $\frac{cm^4}{m}$ ]	24418	66670	130210	225000
$\frac{\alpha}{\beta}$	$3.29 \cdot 10^3$	$2.70 \cdot 10^3$	$3.07 \cdot 10^3$	$3.33 \cdot 10^3$

Table 3.2: Characteristics of tunnel linings (ERDMANN, 1983)

use the relative stiffnesses expressed as

$$\alpha = \frac{ER^3}{E_l I_l} \quad (3.18)$$

and

$$\beta = \frac{ER}{E_l A_l}, \quad (3.19)$$

where  $E_l A_l$  and  $E_l I_l$  are the normal stiffness and the flexural rigidity of the lining respectively and  $E$  is the elasticity modulus of the ground. ERDMANN (1983) supplemented the findings of AHRENS et al. (1982) to obtain relatively simple solutions for normal forces  $N$  and bending moments  $M$

$$N = N_0 + N_2 \quad \text{and} \quad M = M_2, \quad (3.20)$$

with

$$N_0 = \frac{\sigma_v + \sigma_h}{2} \cdot R \cdot n_0, \quad (3.21)$$

and

$$\begin{bmatrix} N_2 \\ M_2 \end{bmatrix} = \frac{\sigma_v - \sigma_h}{2} \cdot \begin{bmatrix} R \cdot n_2 \\ R^2 \cdot m_2 \end{bmatrix} \cdot \cos 2\omega. \quad (3.22)$$

Here the subscript 0 implies a constant loading and the subscript 2 indicates a non-constant load that is changing with angle  $\omega$ , as adopted in Fig. 3.13. Values of the coefficients  $n_0$ ,  $n_2$  and  $m_2$  for bending moments and normal forces are shown in Figs. 3.14 - 3.16 respectively, for full bonding, tangential slip and for different Poisson's ratios  $\nu$  of the ground.

The coefficients  $n_0$ ,  $n_2$  and  $m_2$  for bending moments and normal forces shown in Figs. 3.14 - 3.16 are obtained for a relative stiffness ratio of  $\alpha/\beta = 3 \cdot 10^3$ , they increase with decreasing relative stiffnesses  $\alpha$  and  $\beta$  respectively. For tunnels with a radius of 5m one tends to find ratios of  $\alpha/\beta$  between 1000 and 5000, but such variations have little effect on the curves in Figs. 3.14 - 3.16 (ERDMANN, 1983). Typical ratios of tunnel linings are given in Tab. 3.2.



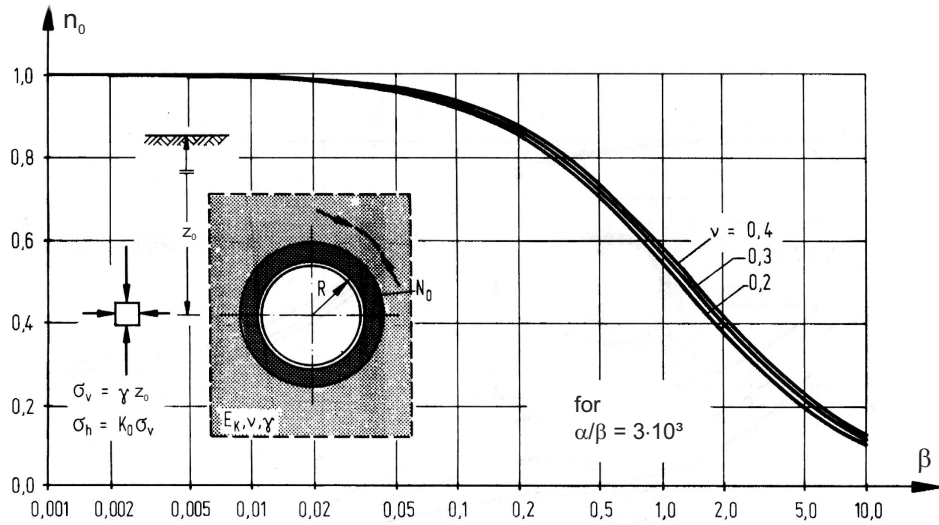


Figure 3.14: Coefficient  $n_0$  for constant part of normal force (ERDMANN, 1983)

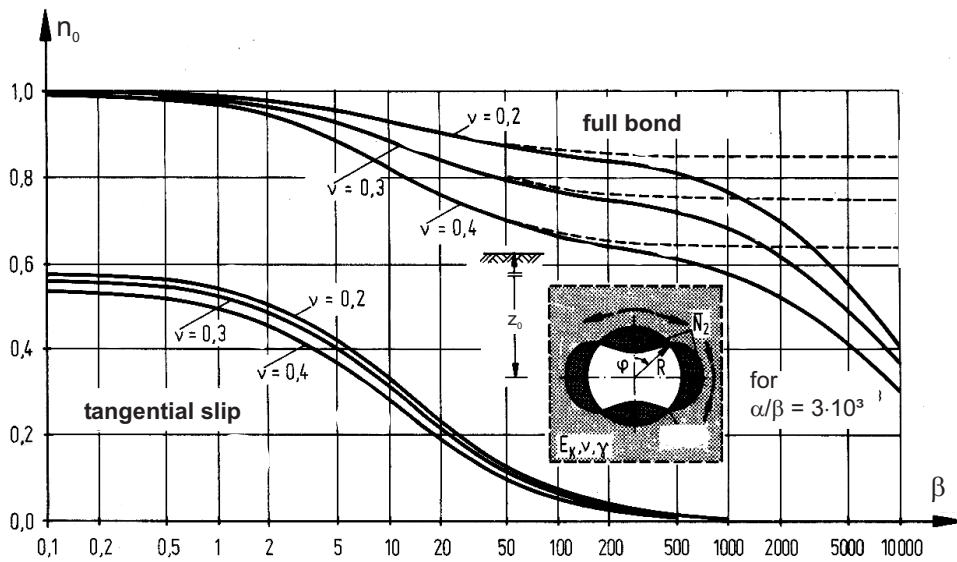


Figure 3.15: Coefficient  $n_2$  for non-constant part of normal force (ERDMANN, 1983)

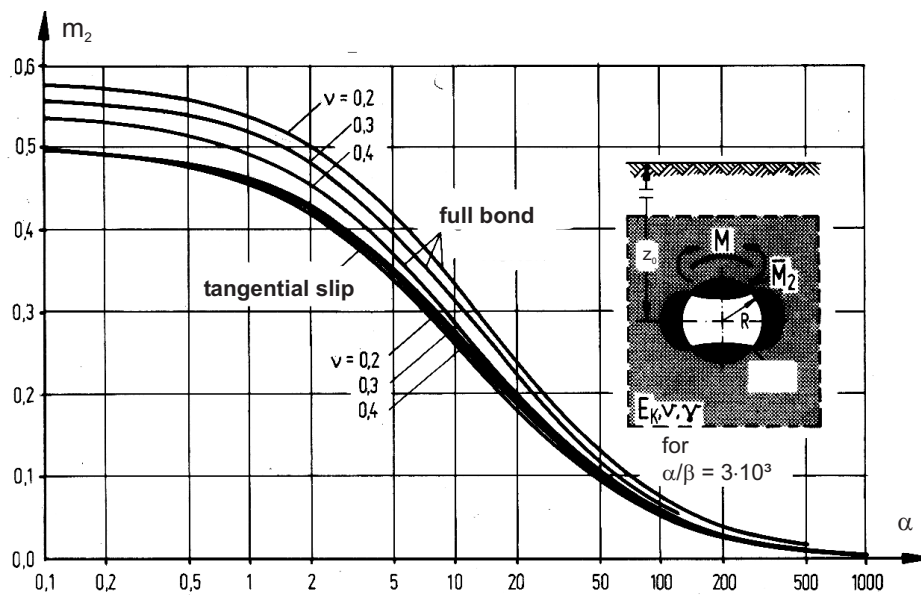


Figure 3.16: Coefficient  $m_2$  for bending moment (ERDMANN, 1983)

Bending moments depend linearly on the deviatoric stress  $(\sigma_v - \sigma_h)/2$ , i.e. on tunnel depth and tunnel installation. To incorporate installation procedures the stress reduction method may directly be applied to the stresses of Eqs. 3.21-3.22 of the analytical solution. Tunnel installation might also be accounted for by a displacement approach, as done by CHOU and BOBET (2002). They considered 28 shield tunnels to find values for the gap between lining and ground ranging from 10mm to 288mm, depending on tunnel radius and installation procedures. Information on the so-called gap might be transferred into a stress reduction and then be applied to analytical solutions, but such an approach would seem to be circumstantial. Instead, analytical solutions can more easily be combined with the stress reduction method.

### 3.8.2 The bedded-beam model

The above continuum approach may be suitable for very deep tunnels in uniform ground, but not for shallow ones in layered ground and neither for non-circular tunnels. In order to overcome these shortcomings the bedded-ring model has been developed, where springs replace the ground reaction and lining loads are applied as external forces. This approach allows to solve for structural forces and deformations of the lining, but it gives no information on settlements.

The following brief overview on contributions to the development of bedded beam approaches is inevitably incomplete, as a number of important contributions have been omitted. BULL (1944) would seem to be the first to have proposed a bedded beam ap-

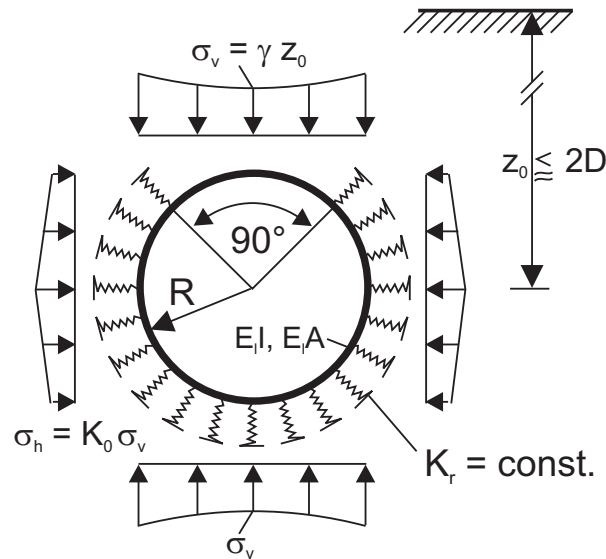


Figure 3.17: Example of a bedded-beam model for shallow shield tunnels in soils (DUDDECK and ERDMANN, 1982)

proach. His approach divides the tunnel ring into 16 equal divisions with the external ground loads combined to give 16 point loads, one acting upon each of the divisions. The ground reaction forces are governed by spring constants. Further contributions were given by ROZSA (1963), SATTLER (1965), WINKLER (1970) and WAGNER et al. (1980).

Models which are still used in present engineering practice have been presented e.g. by DUDDECK (1972). He distinguishes between shallow tunnels with  $z_0 < 2D$  and deep tunnels with  $z_0 \geq 3D$ , where  $D$  denotes the tunnel diameter. For shallow tunnels a model as shown in Fig. 3.17 is proposed. Here bedding is only accounted for in regions, where lining deflection is oriented outwards leading to ground compression. At the tunnel crown, where the lining deforms inwards, tension bedding is not applied. Commonly a non-bedded lining arc length with an angle of  $90^\circ - 120^\circ$  is assumed. At the same time, a ground load, having the magnitude of the full vertical overburden, is assumed to act on the non-bedded tunnel crown.

According to the ITA (1988)-working group on *General Approaches to the Design of Tunnels*, a design model such as that shown in Fig. 3.17 may be particularly well-suited to the design of linings of shallow shield-driven tunnels in soil. For deep tunnels a bedded beam model as presented in Fig. 3.18 may be applied. Using supporting means like anchors the ground is well involved into the tunnel structure to carry a significant part of the load. An idealized ground-lining ring, as shown in Fig. 3.18 is proposed. The thickness of the incorporated ground ring depends on the active anchor length. This ring needs not to be circular and non-circular cross-sections like a horse shoe profile may as well be accounted for.

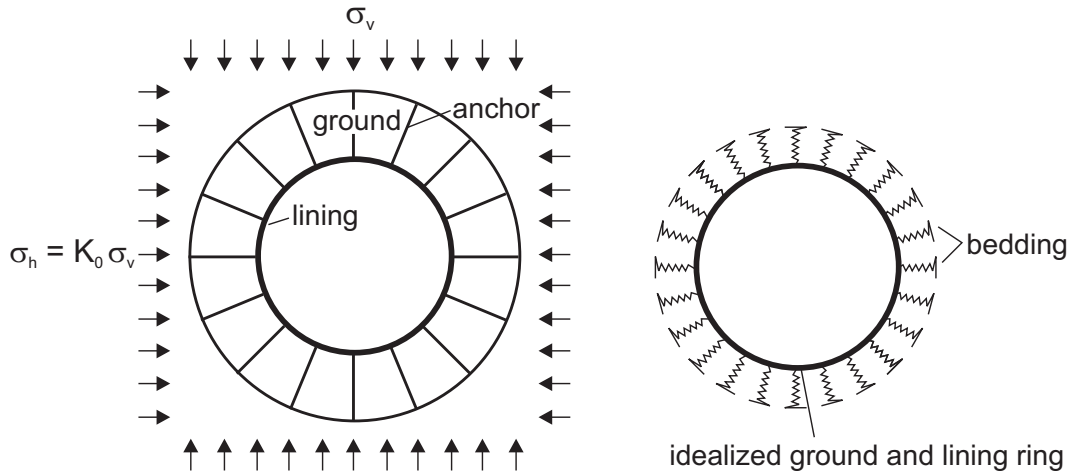


Figure 3.18: Example of a bedded-beam model for deep tunnels (DUDDECK, 1979)

**Spring constants for bedding** Bedded beam approaches consider a ground behavior according to the hypothesis by WINKLER (1867), describing the load-deformation relationship as

$$p = k \cdot S, \quad (3.23)$$

where  $p$  is the ground bedding pressure,  $S$  is the radial displacement of the tunnel and  $k$  is the ground reaction modulus. This approach implies a pointwise consideration of ground behavior (no coupling with neighbor regions).

As shown in Figs. 3.17 and 3.18, in numerical bedded beam approaches the ground bedding is represented by a certain number of springs at regularly distributed locations along the tunnel lining with a certain spring stiffness  $K_{spring}$ . These spring stiffnesses have the correlation

$$K_{spring} = a \cdot b \cdot k, \quad (3.24)$$

where  $a$  is the distance of springs in the transverse cross-section and  $b$  is the distance of springs in the longitudinal cross-section (generally 1.0 per unit length of tunnel). The spring stiffness  $K_{spring}$  has the unit  $[kN/m]$ .

To involve radial bedding in a numerical bedded beam calculation, a radial ground reaction modulus  $k_r$  has to be determined. Tangential shear bedding may be modelled by a separate ground reaction modulus  $k_t$  with tangentially placed springs. For a circular tunnel in elastic ground under axisymmetric loading, the ground reaction (bedding) is only dependent on the radius of the tunnel and the ground elasticity parameters. In this case the analytical solution for the radial ground reaction modulus yields

$$k_r = \frac{1}{1 + \nu} \cdot \frac{E}{R} \quad (3.25)$$

(e.g. KOLYMBAS, 1998), where  $\nu$  is the Poisson's ratio and  $E$  is the Young's modulus of the ground. Using the theory of elasticity it can be deduced that  $E = 2/3 \cdot E_{oed}$  for

$\nu = 1/3$ . Substituting this relation into Eq. 3.25, one obtains  $k_r = 0.5 \cdot E_{oed}/R$ , where  $E_{oed}$  is the constrained modulus, also referred to as oedometer modulus. In practice one often uses the similar relation

$$k_r = \alpha \cdot \frac{E_{oed}}{R}, \quad (3.26)$$

but for tunnels with  $\sigma_h < \sigma_v$   $\alpha$ -values greater than 0.5 are often applied (KATZENBACH, 1981). For engineering practice the factor  $\alpha$  is difficult to assess, as  $k_r$  is not a material constant, but depends as well significantly on the geometry of the structure. In situ tests, such as plate loading tests, although not representative for the final tunnel geometry, are often used to estimate values of  $\alpha$  (ITA, 1982). In German engineering practice, values for  $\alpha$  between 0.66 and 3.0 (MÜLLER-SALZBURG, 1978) have been proposed, often  $\alpha = 1$  is used (DUDDECK, 1980).

**Advantages of bedded beam models** The bedded beam model in particular is attractive to civil engineers because common rules of beam statics and the design codes of reinforced concrete can be directly assigned. The numerical implementation of bedded beam approaches significantly improves the handling of tunnel calculations. Uncertainties such as the vertical and horizontal ground stresses, the spring constants for the bedding of the lining ring or the elasticity parameters of the lining can be assessed at a relatively low cost by varying them in additional calculations. The model can easily be adjusted to measured data to match displacements and structural forces, such that it can be calibrated for the design of further tunnel cross-sections. The model is applicable to tunnels in layered ground and non-circular cross-sections. For non-circular cross-sections with corners and/or curvatures with smaller radius of the lining, bedding may be increased at corner sections. For complex tunnel structures lining properties may vary within a cross-section. Staged tunnel constructions may be accounted for.

**Shortcomings of bedded beam models** The simplification of the continuum problem to a bedded beam model is achieved at its price. Using spring constants, the ground-lining interaction is only modelled insufficiently, as the ground behavior is considered pointwise, neglecting the coupling with neighbor regions. In a numerical bedded beam calculation the ground is represented using only three constants:

- unit weight of the ground  $\gamma$  for vertical loads on the lining,
- coefficient of lateral earth pressure at rest  $K_0$  for horizontal loads on the lining,
- ground reaction modulus  $k$  for reaction forces of the ground.

Besides the unit weight of the ground and the ground reaction modulus, such calculations are very sensitive to a change of  $K_0$ -values (KATZENBACH, 1981). A small variation of only  $K_0 = 0.5 \pm 0.05$  shows a significant deviation of 20% of the tunnel crown bending moment. Regarding this fact it is recommended to use  $K_0 = 0.5$  independently of the ground conditions observed (DGEG, 1973), but it is very peculiar to consider a heavily overconsolidated ground with large  $K_0$ -values as a normally consolidated one with  $K_0 \approx 0.5$ .

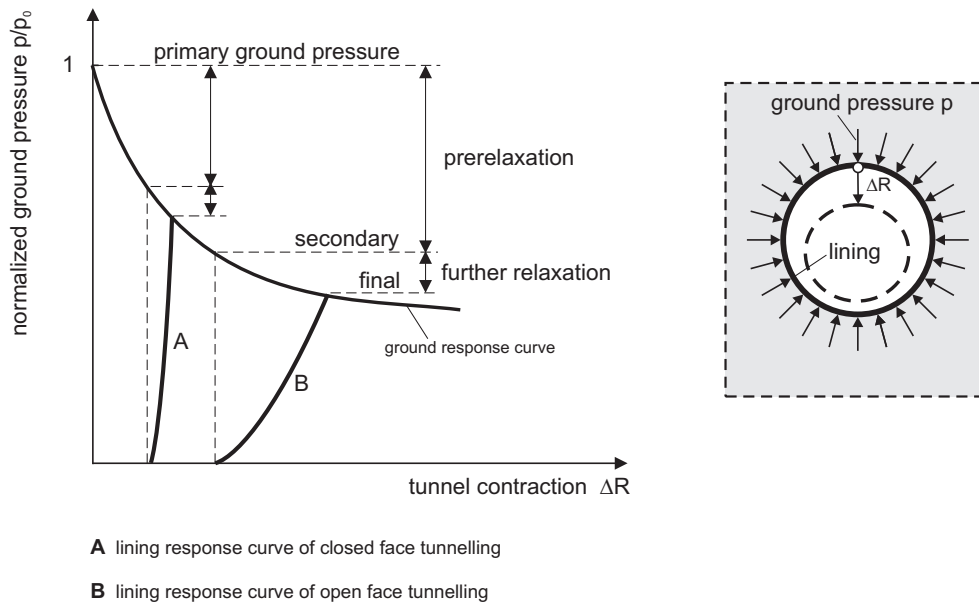


Figure 3.19: Illustration of development of ground pressures on tunnel linings adopting ground response curve

### 3.8.3 Ground pressures on tunnel linings

The deformations resulting from tunnel installation procedures reduce the primary ground pressures and create loads on the lining. The loads correspond to that fractional part of the primary ground pressures which acts on the sustaining lining. The distribution and magnitude of ground pressures on tunnel linings, which will develop during and after the construction of a tunnel, is influenced by a large number of different factors, such as ground and lining stiffnesses, geometry of the tunnel cross-section and installation procedures. In order to arrive at an appropriate estimate of both distributions and magnitudes of ground pressures, the design of a tunnel should take these factors of interaction into account.

Fig. 3.19 illustrates the development of ground pressures on tunnel linings adopting the ground response curve. As shown by this figure, the amount of the ground pressure on the tunnel lining is influenced by a reduction of primary ground pressures before the tunnel lining is installed. Starting from primary ground pressures tunnel excavation induces stress prerelaxation to the ground, reducing primary ground pressures down to a secondary state of stress. Fig. 3.19 shows that the amount of stress prerelaxation is governed by the tunnelling method, i.e. tunnel installation procedures. In the case of closed face tunnelling ground deformations are minimized and therefore the amount of stress prerelaxation is generally relatively small. In open face tunnelling on the contrary, the excavation of an unsupported cut stretch leads to a relatively high ground mobilization and the associated stress prerelaxation is thus relatively large.

In order to guarantee ground stability after tunnel excavation a lining is installed. As demonstrated by Fig. 3.19, lining deformation imposes some further stress relaxation

to the surrounding ground and the secondary ground pressures are reduced down to final pressures on the tunnel lining. For shield tunnelling the use of relatively stiff pre-cast segmental linings (accounting for some stiffness reduction of joints between lining segments) will generally show relatively small lining deformation but in conventional tunnelling lining deformation may become relatively large. Fig. 3.19 shows that the amount of the further stress relaxation resulting from tunnel lining deformation is relatively small compared to the amount of the stress prerelaxation.

In order to assess structural forces in tunnel linings using a suitable structural model, both the amount of stress prerelaxation and the amount of further stress relaxation have to be accounted for. Analytical solutions of continuum models or bedded beam calculations incorporate lining deformations resulting from ground loading and hence the associated further stress relaxation of the ground is automatically accounted for. In contrast the effects of stress prerelaxation, i.e. tunnel installation procedures, are not automatically accounted for and assumptions about its magnitude have to be made.

Besides stress prerelaxation the distribution of primary ground pressures is important to be considered in tunnel analysis. In the following approaches for the distribution of primary ground pressures and the amount of secondary ground pressures resulting from stress prerelaxation will be briefly reviewed.

**Distribution of primary ground pressures** Fig. 3.20 shows a variety of different structural models with different distributions of primary ground pressures on the tunnel lining. The distribution of increasing primary horizontal pressures with depth as indicated by Fig. 3.20a) is used for analyzing shallow tunnels, whereas constant horizontal pressures as shown by Fig. 3.20b) are used for deep tunnels. The reason for reducing horizontal stresses with depth as indicated in Fig. 3.20c) is not made clear in most of the literature.

**Amount of secondary ground pressures** The amount of the secondary ground pressure is influenced by the sum of all stress redistributions which have been caused during tunnel excavation. Before the tunnel lining is installed, ahead of the tunnel face and around the shield machine (or around the unsupported cut-stretch in conventional tunnelling) some stress redistribution inevitably takes place resulting in stress prerelaxation. Depending on tunnel installation procedures, tunnel depth and ground properties, stress prerelaxation may become relatively large and secondary ground pressures may reduce significantly.

DUDDECK and ERDMANN (1982) distinguish between shallow tunnels with  $z_0 \geq 2D$ , moderately deep tunnels with  $2D \leq z_0 \leq 3D$  and deep tunnels with  $z_0 \geq 3D$ . For shallow and moderately deep tunnels they propose that no stress prerelaxation takes place at the crown of the tunnel, applying full primary stresses on top of the tunnel, as indicated in Fig. 3.17. Hence, it is assumed that in the final state (some years after the construction of the tunnel), the ground eventually will return to nearly the same condition as before the tunnelling. Changes in ground water levels, traffic vibrations, etc., may provoke this *readjustment*. Indeed, CRAIG and MUIR WOOD (1978) report that the instrumentation of

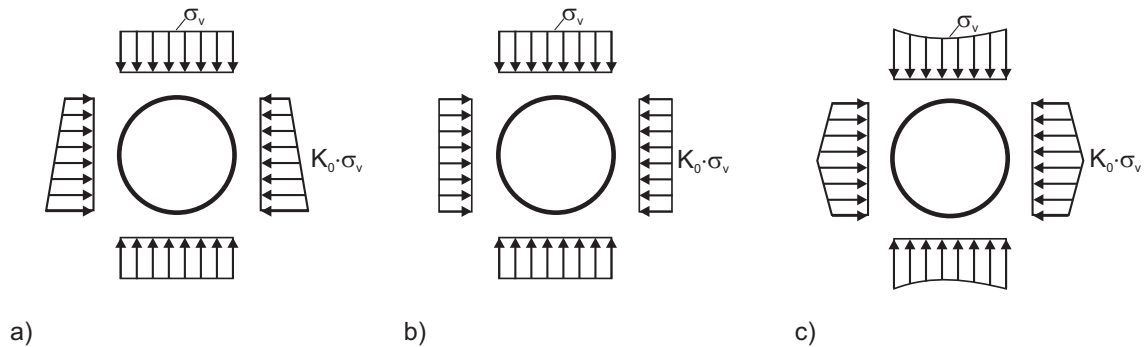


Figure 3.20: Different distributions of ground loads on tunnel linings.

a): HEWETT and JOHANNESSON (1922);

b): WINDELS (1967)

c): SCHULZE and DUDDECK (1964a), HARTMANN (1970), FLECK and SKLIVANOS (1978);

existing shallow tunnels 50 to 75 years old, which have been required to be dismantled during the construction of new works, has shown combined hoop and bending stresses in the lining equivalent to the overburden pressure. For tunnels in sands below the water table they state that measurements have shown combined stresses between 80% and 100% of the equivalent overburden stress, which may develop within the first few months.

For deep tunnels it is obvious that some stress prerelaxation needs to be accounted for to reduce the loads on the lining. DUDDECK and ERDMANN (1982) argue that no matter what tunnel depth, allowance should be made for a tendency towards larger or lower ground stresses, acting on the lining in regard to, at least, cohesion, stiffness of the ground, time to closure of the tunnel ring, excavation procedure, erection method for the lining, time-dependent behavior of the ground and the lining and effects of groundwater. Thus the transition from shallow to deep tunnels is not sharp and the three cases overlap.

To account for installation of closed face tunnelling, MUIR WOOD (1975) proposed to take only 50% of the initial ground stresses into consideration. Indeed, in present two-dimensional numerical analyses of open face tunnelling, a stress reduction factor, being referred to as unloading or beta factor, of around 50% is commonly used, but this value would seem to be rather low for modern closed face tunnelling (see Section 5.2). Because of the relatively high mobilization of the grounds shear strength in open face tunnelling, this method requires a ground with a pronounced cohesion and therefore a significant stress prerelaxation may generally be justified.

The topic of ground pressures on tunnel linings with regard to different structural design models, tunnel depths and ground stiffnesses has also been reviewed by the ITA (1988)-working group on *General Approaches to the Design of Tunnels*. Fig. 3.21 categorizes four different approaches of structural design models:

1. bedded-beam model for very shallow tunnels in soft ground,



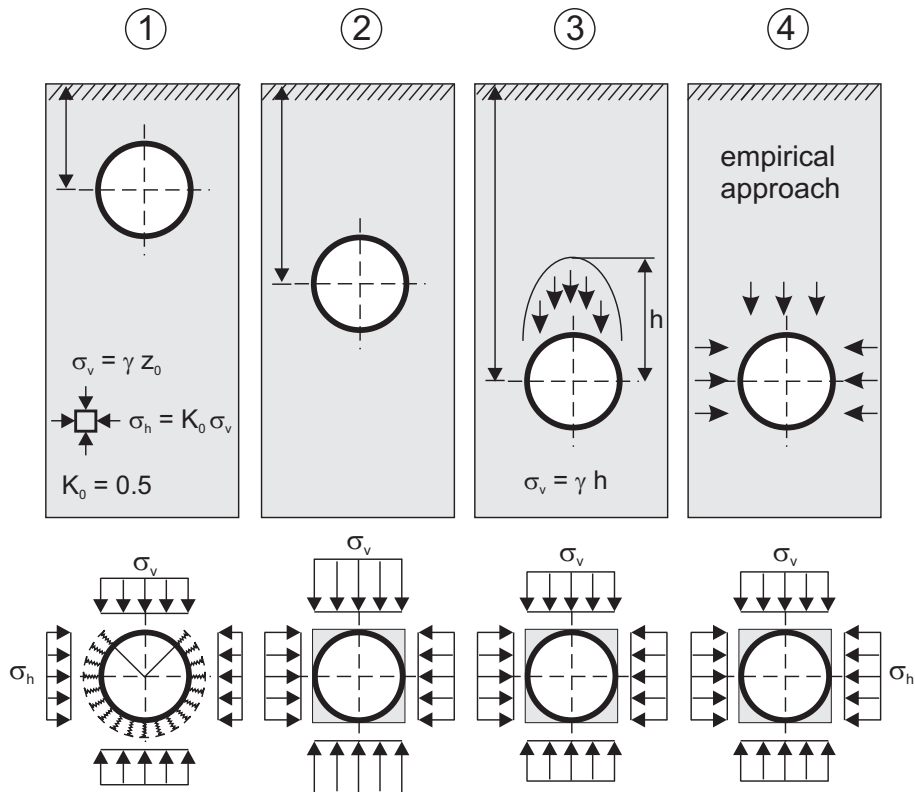


Figure 3.21: Plane-strain design models for different depths and ground stiffnesses (ITA, 1988)

2. continuum model for tunnels at shallow depth and moderately stiff ground,
3. continuum model for deep tunnels in stiff ground,
4. continuum model for deep tunnels, empirical approach for ground pressures.

For tunnels at shallow depth in soil, immediate support must be provided by a relatively stiff lining. Here it is agreed that the three-dimensional stress release at the face of the tunnel during excavation may be neglected. Therefore in cases (1) and (2) of Fig. 3.21 no stress prerelaxation is taken into account incorporating full primary ground pressures.

Case (3) assumes that some stress prerelaxation is caused by deformations that occur before the lining participates. In rock or in highly cohesive soil, the ground may be strong enough to allow a certain unsupported section at the tunnel face. Stress prerelaxation is also assumed for tunnels having a high overburden, and a reduction of the acting crown pressure (as represented in Fig. 3.21 by  $h < z_0$ ) is taken into account. Confirming these recommendations, CRAIG and MUIR WOOD (1978) discuss measurements of tunnels in rock, where readings have been taken of the stresses in the arch ribs prior to the casting of a cast in-situ lining. Their presented results generally show relatively low stresses.

In case (4), the ground stresses acting on the lining are determined by an empirical approach, which may be based on previous experiences with the same ground and the same tunnelling method, on in-situ observations and monitoring of initial tunnel sections, on interpretation of the observed data and on continuous improvements of the design model. Here, some reduction of stresses may generally be incorporated.



## Chapter 4

# Finite element modelling of tunnels

### Introduction

Starting with the 1960ies the last forty years have lead to a significant development and advance in the application of numerical methods to tunnelling. Whereas in the beginning of its development, numerical analysis as a design tool was often criticized, nowadays the increase of computer capacity has caused a revolution within the field of tunnelling. There are no significant tunnelling projects any more, which are carried out without the support of full numerical analyses. No doubt, simlified methods as discussed in the previous section still play an important role and they can not be omitted, as they reflect both tunnelling tradition and experience. But the days are gone in which tunnel design was based on experience, intuition and analytical solutions of simple continuum models alone. Todays tunnelling engineers are provided with a wide range of various modern numerical tools: Finite Element Method, Finite Difference Method, Boundary Element Method, Discrete Element Method, etc. Cumbersome data input and viewing of calculation results may soon be remembered as a thing of the past, as modern user-friendly data pre- and post-processing tools are being developed. Automatic mesh generation and colored output graphs make such calculations even more attractive to the engineer. Thanks to powerful computer capacity and user friendly software, numerical analyses that once took weeks are being performed within a few days and in future within a few hours. The advantages of numerical analysis are obvious. Both complex material behavior and boundary conditions can be taken into account, whilst parameteric studies to improve the design can be easily carried out.

But advantages of numerical analyses are not achieved without their costs. The proper use of numerical tools requires sufficient background knowledge, not only in geotechnical engineering, but also a good basic understanding of the numerical method itself. Unlike analytical solutions, results from numerical analyses often can be hardly verified and only good engineering judgement may estimate whether or not results can be believed as plausible. On the other hand, the need for a high specialization in numerical analysis is often a communication hinderance between designers and analytical modelers. When looking at design practice, the role of numerical analysis seems to be more controversial than ever. Numerical analysis has found itself torn between the temptation to quantify and dimension every single support measure and the fear of being held for nothing but a number crunching exercise. Being so, the success of such calculations is often judged, depending on whether you are a protagonist or an antagonist of numerical

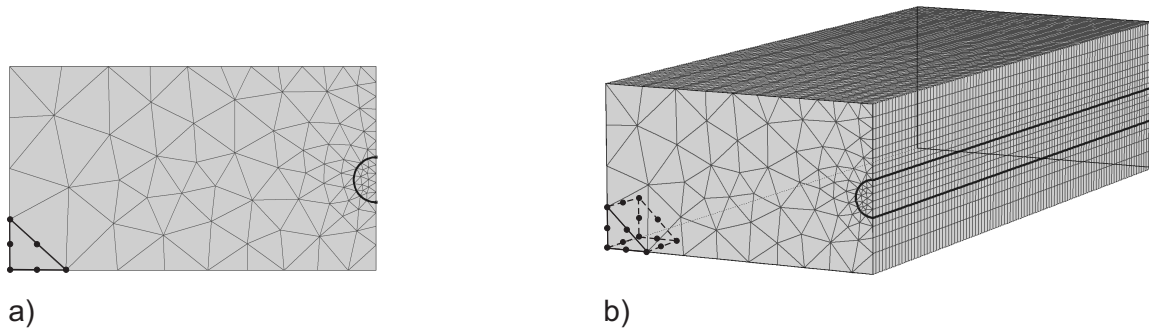


Figure 4.1: Symmetrical half of a) 2D FE-mesh and b) 3D FE-mesh

analysis.

For a condensed overview of numerical methods applicable to geotechnical problems the reader is referred to SCHWEIGER (1995). The most relevant numerical method for tunnelling applications is the Finite Element Method (FEM). The method has been presented throughout the literature and detailed descriptions are available e.g. by ZIENKIEWICZ and TAYLOR (1991) or BATHE (1982). In the following a contribution will be given to the modelling of tunnels with the help of the FEM. The present thesis is intended to discuss some of the points which are of major importance for FE-analysis of tunnelling settlements and lining forces. Besides the consideration of different constitutive models for use in FEM as explained in Appendix A, the influence of the tolerated equilibrium error in numerical analysis, the influence of FE-mesh dimensions and the mesh coarseness as well as the modelling of initial ground stresses will be analyzed in this section. Hereafter the focus will be on both three- and two-dimensional FE-installation procedures for conventional driven tunnels and shield tunnelling. All results presented have been obtained by using the two- and three-dimensional versions of the FE-code PLAXIS.

## 4.1 Basic terms and modelling aspects of FEM tunnel analysis

As for any type of numerical analysis the consideration of constitutive models is an important topic. Because they constitute a very basic factor of FE-analysis, they will not be primarily discussed in the present thesis. Nevertheless, they can not be omitted and the interested reader is referred to Appendix A. The influence of different constitutive models on the results of tunnel analyses has been studied in Section 5. The following sections, however, will focus on some FE-modelling aspects which are of specific importance for numerical tunnel analysis. In order to provide a better comprehension for the present thesis, some basic terms and modelling aspects of FEM tunnel analysis will be introduced.

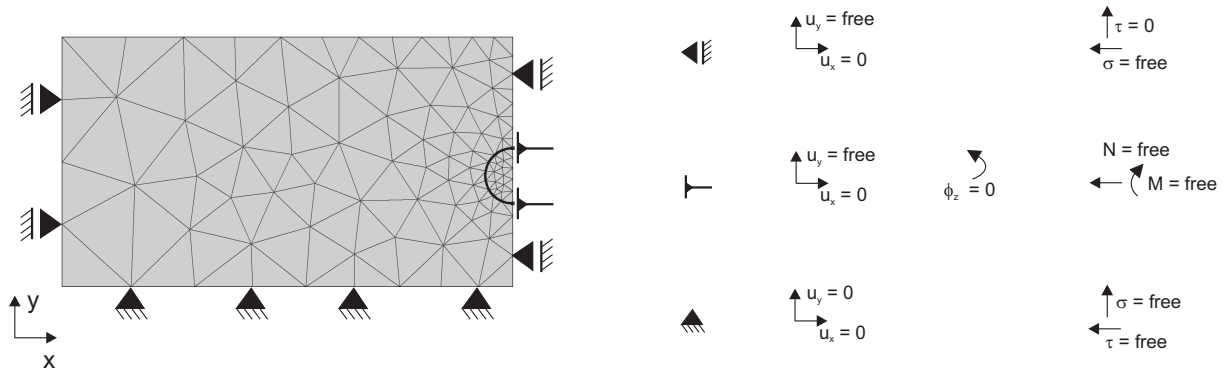


Figure 4.2: Boundary conditions of bottom, surface and vertical boundaries of symmetrical half

### 4.1.1 Finite Elements as used in this thesis

As illustrated in Fig. 4.1, for all two-dimensional analyses six-noded triangular elements with three Gaussian integration points and for all three-dimensional analyses fifteen-noded wedge elements with six Gaussian integration points were used. For more details on the formulation of these elements the reader is referred to BRINKGREVE and VERMEER (2001). In order to save computer capacity, especially with respect to complex three-dimensional FE-meshes, the 2D and 3D meshes of tunnels presented in the present thesis were all modelled half-symmetrical as shown in Fig. 4.1.

### 4.1.2 Boundary conditions

The Finite Element Method is used to solve initial and Boundary Value Problems. The boundary conditions as adopted for the tunnel analyses of the present thesis are as illustrated in Fig. 4.2. For the vertical boundaries at the nodes, the vertical displacement  $u_y$  is left free and the horizontal displacement  $u_h$  is restrained, allowing only for a normal stress  $\sigma$  and no shear stress  $\tau$ . The condition that the vertical shear stress must be zero also satisfies the formulation of the statical symmetry at the right vertical mesh boundary. For the tunnel shell elements, the additional condition applies that the rotation  $\phi_z$  must be zero, allowing also for a bending moment to take place.

The bottom mesh boundary has total fixities restraining both horizontal and vertical displacements. Hence normal stresses as well as shear stresses may occur. The fact that both vertical and horizontal displacements are restrained is related to the specific application of the FEM to geotechnical problems. For deeper ground layers in reality one tends to find a considerable increase of the stiffness, and therefore deformation will hardly occur. Moreover, when approaching stiff and strong rocklike materials at more shallow depth, it is logical not to extend the deformation analysis into such layers. Considering the bottom boundary to represent such a stiff ground layer, it is appropriate to restrain both vertical and horizontal displacements.

The upper horizontal boundary has no fixities at all and is left free to displace.

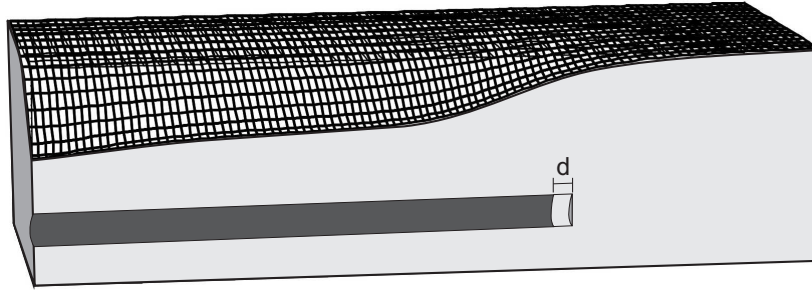


Figure 4.3: 3D settlement trough after 30 steps of excavation

### 4.1.3 Steady-state settlement trough

One of the basic terms used for three-dimensional tunnel analysis is the statement that for a representative prediction of settlements, one should refer to the steady-state of settlements. In order to explain the term steady-state of settlements, a full 3D analysis needs to be considered.

To investigate the development of the settlement trough from a circular tunnel, a block of  $100 \times 55 \times 28m$  was divided into 4300 volume elements. The parameters of the Mohr-Coulomb Model were taken as  $E = 42MPa$ ,  $\nu = 0.25$ ,  $c' = 20kPa$ ,  $\varphi' = 20$ ,  $\psi = 0$  and the coefficient of lateral pressure  $K_0 = 1 - \sin\varphi'$ . The tunnel with a diameter of  $8m$  and a cover of  $16m$  was modelled in a symmetric half with an unsupported excavation length of  $2m$ . The excavation and support was simulated according to the step-by-step procedure described in Section 4.5.1. The shotcrete lining has a normal stiffness of  $E_l A = 6GN$ , a flexural rigidity of  $E_l I = 45MNm^2$  and a Poisson's ratio of  $\nu_l = 0.15$ .

Fig. 4.3 shows the computed settlement trough after 30 excavation phases. The longitudinal shape is somewhat peculiar and obviously there is some disturbance which is related to the boundary conditions at the left model boundary<sup>1</sup>. In fact, a solution with a constant horizontal shape of the centerline settlements is only reached after about  $35m$  away from the left mesh boundary. The reached horizontal settlement shape is what will be referred to as steady-state settlements.

To investigate the reason of the peculiar longitudinal settlement distribution at the left mesh boundary, the initial conditions at the very beginning of the tunnel excavation have been varied. Please note that Fig. 4.3 has been obtained by performing an unsupported excavation for  $d = 2m$  of tunnel for the first computational phase. This type of analysis also leads to the lower curve in Fig. 4.4. In another analysis the first excavation was started with an immediate support by a tunnel lining as indicated by the insert of Fig. 4.4. All further steps were unsupported excavations, as also considered in the analysis of Fig. 4.3. The significant influence of the first excavation phase is demonstrated in Fig. 4.4. Depending on the starting conditions, initial settlements are either below or

<sup>1</sup>The rear mesh boundary can have a physical meaning, e.g. when it represents the launch shaft boundary for the tunnel boring machine

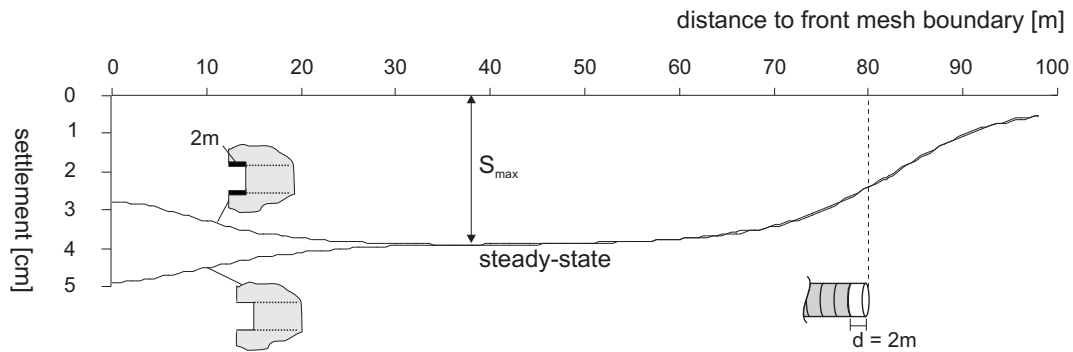


Figure 4.4: Development of steady-state settlement shape

above the steady-state solution. In both cases the disturbance extends over a considerable length of about  $35m$ . Towards the left model boundaries, settlements become too large because of the influence of the vertical fixities which are sliding contact bearings (compare Section 4.1.2). The significant initial disturbance implies that one has to use large mesh dimensions to simulate tunnel excavations over a considerable length with many excavation phases, in order to arrive at a reliable steady-state solution. The use of sufficient FE-mesh dimensions for the steady-state solution will be discussed in Section 4.2.

#### 4.1.4 Zigzagging and steady-state of structural forces

The calculation of the previous Section 4.1.3 may be used to study the distribution of structural forces in the lining. Fig. 4.5 presents normal forces after  $80m$  of step-by-step installation. Within a single shotcrete ring of width  $d = 2m$  there is a sharp drop of the normal force from about  $-1400kN/m$  (compression is considered negative) at the front of the ring down to about  $-200kN/m$  at the back of the ring. At first this zigzagging pattern may seem somewhat peculiar, but in fact it is very logical. The unsupported tunnel heading is arching mainly on the front and not so much on the back of the tunnel segments, leading to a significant increase of structural forces at the front of a lining segment. The average normal force, i.e. the solid line, appears to have a magnitude of about  $-750kN/m$  per meter of tunnel length. At the tunnel heading the normal force has not yet reached the average value of about  $-750kN/m$ . Instead a lower value of about  $-600kN/m$  is obtained, which due to further cutting and destroying of the 3D arching will increase up to the final value of  $-750kN/m$ . Hence, similarly to the shape of the settlement trough there is also a steady-state of structural forces. Beyond the steady state part on the extreme left in Fig. 4.5 the lining is more heavily loaded up to  $-850kN/m$ . Again this is a numerical effect that relates to the use of smooth roller boundaries at the sides of the mesh block. As for settlements one needs to excavate a considerable tunnel length to move away from these boundary effects in order to arrive at the steady-state solution.



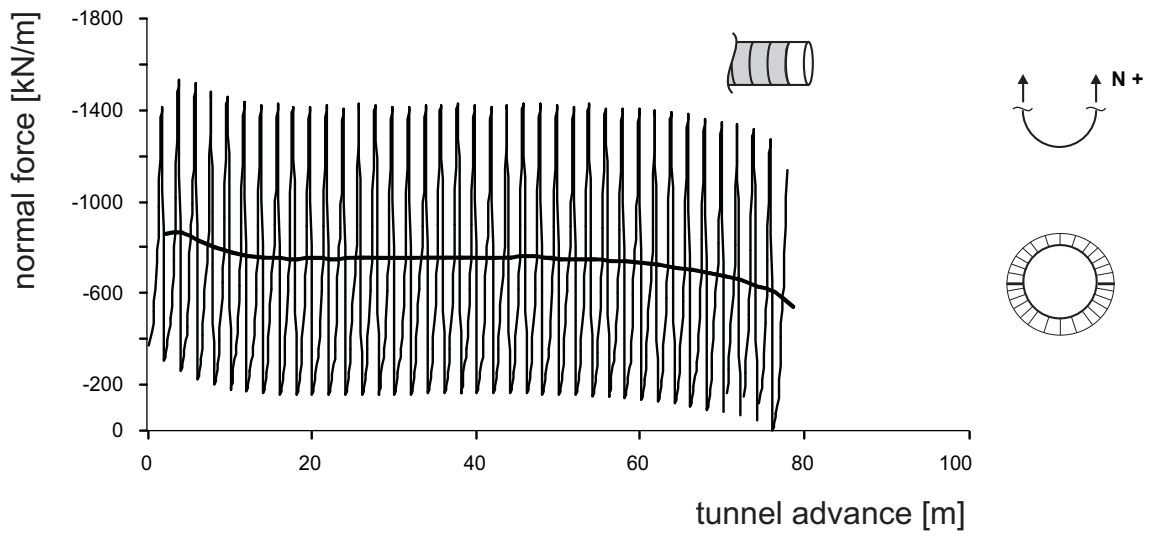


Figure 4.5: Zigzagging of normal forces in the direction of the tunnel axis

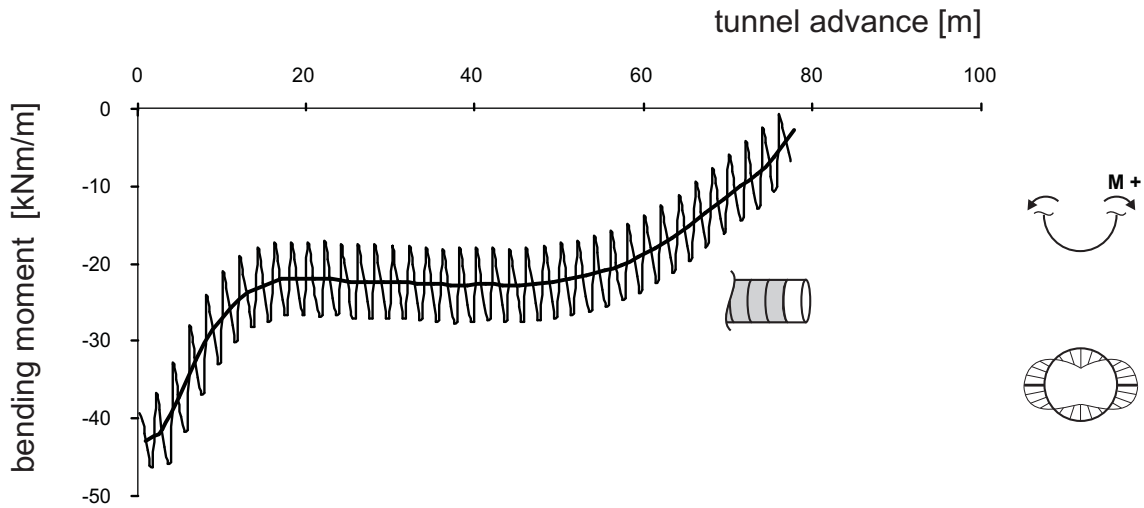


Figure 4.6: Zigzagging of bending moments in the direction of the tunnel axis

Just like the normal forces the bending moments show a zigzagging pattern that matches the step-by-step installation with  $d = 2m$ . For convenience, the focus is on the average value as indicated by the solid line. Near the tunnel heading, vanishing small bending moments of about  $-3kNm/m$  are found. However with the advance of the tunnel face, the bending moment in Fig. 4.6 reaches an average steady-state value of about  $-22kNm/m$ . Again on the left in Fig. 4.6, the lining is more heavily loaded up to  $-43kNm/m$ , indicating the significant disturbance of the mesh boundary.

#### 4.1.5 Tolerated error

When using elastoplastic constitutive models (compare Appendix A) in a FE-deformation analysis, the equations to be solved become non-linear. In order to solve such non-linear equations an iterative solution procedure is needed. After each iteration the equilibrium error is computed. The criterion whether the equilibrium error remains within acceptable bounds is linked to the definition of the tolerated error. When adopting a high value of the tolerated error, the convergence of the iterative procedure may become faster, but at the same time the accuracy of computational results is reduced. On the contrary, when the tolerated error is chosen too low, computer times may become excessive.

The influence of the tolerated error on the results of FE-tunnel analysis has been investigated. It was found that surface settlements require a relatively tight tolerated error in order to give accurate solutions. On the contrary it was observed that structural forces are less affected by the accuracy check, requiring only a relatively relaxed tolerated error. For more details on the influence of the tolerated error the reader is referred to MÖLLER (2006).

## 4.2 On FE-mesh dimensions

The influence of the particular boundary conditions chosen in the present thesis has already been highlighted for results of 3D analyses of surface settlements (Section 4.1.3) and structural forces (Section 4.1.4). Both longitudinal distributions of surface settlements and structural forces require a large number of excavation phases to arrive at a representative steady-state solution, being no more influenced by the mesh boundaries. Similar to the influence of boundary conditions on the development of longitudinal surface settlements, the transverse settlement trough may as well be affected by the model boundaries. When involving too small mesh widths, such that the computed transverse settlement trough does not fit into the selected geometry, the results will be significantly affected by the displacement boundary conditions. Because the vertical boundaries are left free to displace in the vertical direction, the choice of insufficient mesh widths will cause too large settlements. To avoid the influence of boundary conditions on the results of FE-analysis sufficient mesh dimensions have to be considered.

For the choice of sufficient mesh dimensions MEISSNER (1996) states that the stresses at the model boundaries should not be influenced by the tunnel excavation, recommending to use  $(4 - 5) \times D$  from the tunnel center line to the vertical mesh boundaries and  $(2 -$

$3) \times D$  from the tunnel center point to the bottom boundary. BLIEHM (2001) considers a different criterion relating the choice of mesh dimensions to the magnitude of strains. According to his recommendation the dimensions should be chosen such that the strains perpendicular to the mesh boundaries do not exceed 0.005% after construction of the tunnel.

In the present thesis, two different criteria for the vertical and the bottom boundaries respectively were used. For the bottom boundary the magnitude of stress rotation was considered, which is a criterion almost independent of the constitutive model being used. The dimension of the bottom boundary were taken such that the maximum rotation of primary stresses at the bottom boundary did not exceed  $2.5^\circ$  after construction of the tunnel. For the dimension of the vertical boundaries, however, the magnitude of surface settlements was considered, which is directly influenced by the constitutive model being used<sup>2</sup>. The dimension of the mesh width and mesh length were taken such that the maximum settlement at the boundary did not exceed 1% of the maximum centerline settlement. In the following a condensed overview on the results of both  $2D$  and  $3D$  mesh variations will be presented. For more details on the analyses of sufficient mesh dimensions the reader is referred to MÖLLER (2006).

#### 4.2.1 2D mesh dimensions

For the two-dimensional parametric studies different diameters  $D$  and cover to diameter ratios  $H/D$  have been considered in order to arrive at the appropriate dimensions of the mesh height  $h$  between the tunnel invert and the bottom boundary and the minimum mesh width  $w$  between the vertical boundaries. Analyses were carried out for a total of 16 variations. First of all the appropriate dimensions for the bottom boundary have been evaluated. Hereafter the bottom boundary was fixed and the minimum dimensions for the width of the vertical boundaries have been considered.

**Bottom boundary** The results obtained for the bottom boundary  $h$  can be summarized as:

$$h = (1.3 - 2.2) \times D \quad \text{for } D = 4m - 12m, \quad (4.1)$$

comparing well to the recommendations of  $(2 - 3) \times D$  from the tunnel center point to the bottom boundary, i.e.  $h = (1.5 - 2.5) \times D$ , as given by MEISSNER (1996).

**Mesh width** After the evaluation of the bottom mesh dimension these results were incorporated into the mesh variations for the evaluation of sufficient mesh widths  $w$ . The results obtained for the mesh width  $w$  can be well approximated by the equation

$$w = 2D \left( 1 + \frac{H}{D} \right). \quad (4.2)$$

---

<sup>2</sup>For the present studies the elastoplastic HS-Model (see Appendix A.2) has been used

The strong correlation with the ratio  $H/D$  is logical: the deeper the tunnel the wider the surface settlement trough and vice versa. Compared to the recommendations of  $w = (4-5) \times D$  by MEISSNER (1996), the present criterion leads to considerably wider FE-meshes for ratios  $H/D \geq 1.5$ . The indication of Eq. 4.2 that surface settlement troughs will become very wide for very deep tunnels may need a further consideration. The criterion that the boundary settlement should not exceed 1% of the maximum center line settlement may not be required for relatively wide settlement troughs of relatively deep tunnels, as here the magnitudes of resulting surface settlements will generally be relatively small. Therefore an upper bound of the mesh width  $w$  when approaching relatively deep tunnels might be considered.

### 4.2.2 3D mesh dimensions

For the three-dimensional parametric studies different round lengths  $d$ , diameters  $D$  and cover to diameter ratios  $H/D$  have been considered in order to analyze dimensions of the bottom boundary  $h$ , the mesh width  $w$  and the mesh length  $l$ . Analyses were carried out for a total of 18 variations. First of all the appropriate dimensions for the bottom boundary have been evaluated. Hereafter the bottom boundary was fixed and the minimum dimensions for the width  $w$  and the length  $l$  of the vertical boundaries have been considered.

**Bottom boundary** The results of the analyses for the bottom boundary  $h$  of 3D analyses can be expressed as:

$$h = (1.1 - 1.45) \times D \quad \text{for } D = 4m - 12m, \quad (4.3)$$

which is somewhat less than the recommendations of  $h = (1.5 - 2.5) \times D$  given by MEISSNER (1996) and also below the criterion 4.1 for 2D analyses.

**Mesh width** The results for the three-dimensional mesh width are almost the same as for the two-dimensional analyses, being again well described by the equation

$$w = 2D \left( 1 + \frac{H}{D} \right). \quad (4.4)$$

**Mesh length** The results of the mesh length  $l$  which were obtained are almost independent of the round length. But as for the analyses of the mesh width they show a strong correlation to the cover to diameter ratio, which can be well approximated by the equation

$$l = D \left( 13 + \frac{11}{3} \cdot \frac{H}{D} \right). \quad (4.5)$$

### 4.2.3 Concluding remarks on mesh dimensions

The results of sufficient mesh dimensions for the use in  $2D$  and  $3D$  analyses have been obtained using a particular constitutive model with a particular set of ground parameters adopting installation procedures of conventional driven tunnels. No doubt, all these factors are of influence concerning the presented results of mesh dimensions. Moreover, there are some further factors, e.g. the coefficient of lateral earth pressure at rest or the geometry of the tunnel cross-section, which have to be taken into consideration regarding the topic of mesh dimensions. However, the present studies have been carried out without going into more detail about the influences of such factors and they may be used as a general reference. Indeed, such a reference is supportive, but different tunnel analyses require by all means an additional check whether or not the chosen mesh dimensions are sufficient.

## 4.3 The influence of the mesh coarseness

If properly formulated and implemented, the FE-solution converges to the true solution when the number of degrees of freedom is increased. In such  $3D$  analyses the consume of computer resources can increase rapidly and one would thus like to reduce the number of nodes to a minimum keeping computational results within a certain margin of accuracy. Therefore parametric studies of the mesh coarseness are required.

For  $2D$  surface settlements it was observed MÖLLER (2006) that they require a relatively fine local mesh coarseness, whereas  $2D$  structural forces are little affected, requiring only a relatively coarse local mesh. On the contrary it will be shown that  $3D$  structural forces are most sensitive to a variation of the number of nodes per round length, requiring relatively fine  $3D$  meshes with a high number of elements.

In the following some results of the parametric studies on the  $3D$  mesh coarseness will be highlighted. For a more detailed description of results from  $2D$  and  $3D$  mesh coarseness studies of surface settlements and structural forces the reader is referred to MÖLLER (2006).

### 4.3.1 3D mesh coarseness

In order to study the influence of the mesh coarseness of three-dimensional analyses, the number of element slices per round length was varied according to Fig. 4.7. Following  $2D$  parametric studies (MÖLLER, 2006) the crosssectional mesh coarseness shown in the upper left of Fig. 4.7 was chosen and kept constant throughout the three-dimensional mesh variations. As shown in Fig. 4.7, only the mesh coarseness along tunnel longitudinal direction was varied.

The three-dimensional tunnel installation process was modelled using the step-by-step installation method for conventionally driven open face tunnels (see Section 4.5.1) with a constant round length of  $d = 2m$ , as displayed in Fig. 4.7. The HS Model (see AppendixA.2) has been used to model ground behavior with parameters listed in Tab.

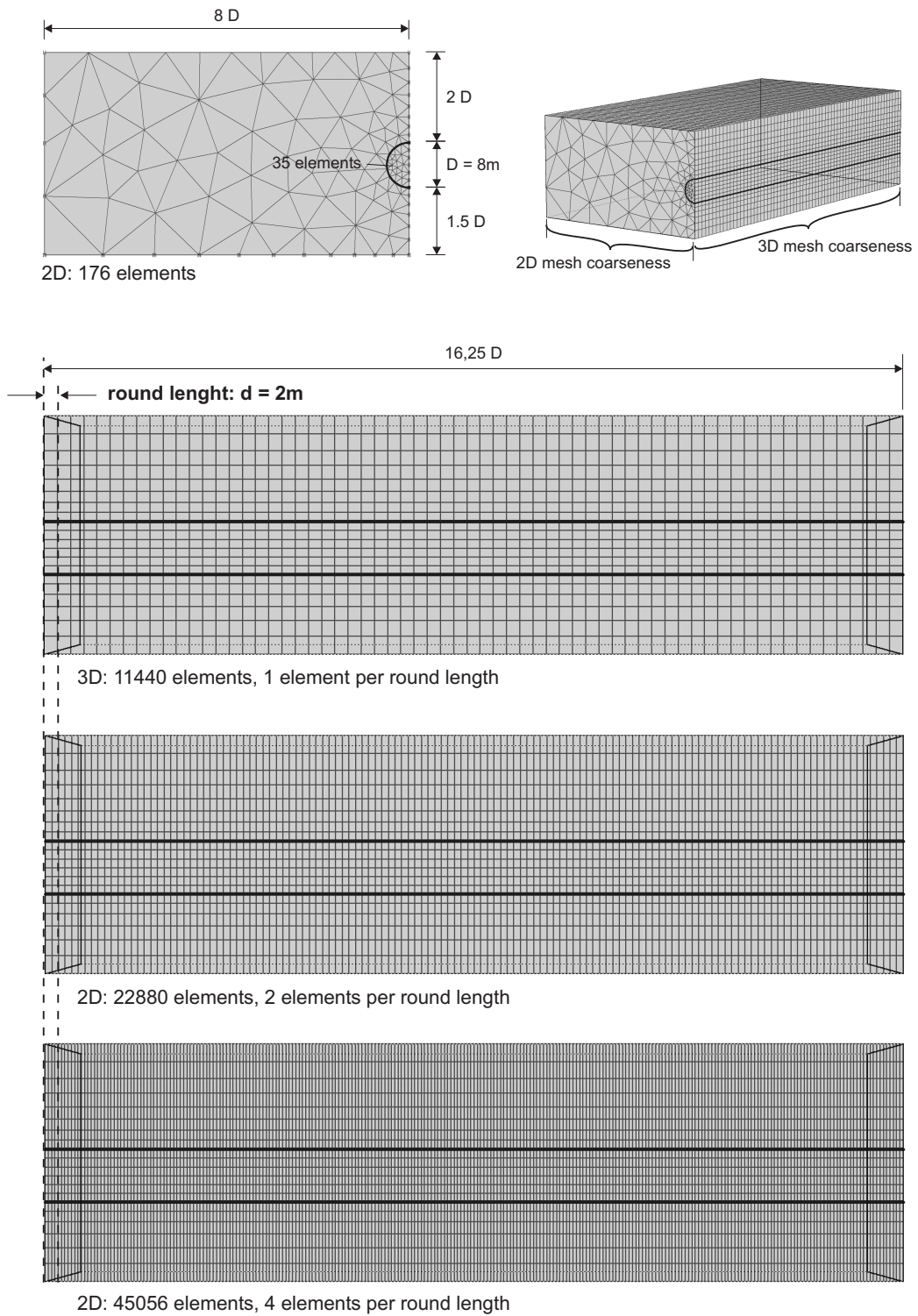


Figure 4.7: Number of elements and mesh dimensions of 3D meshes

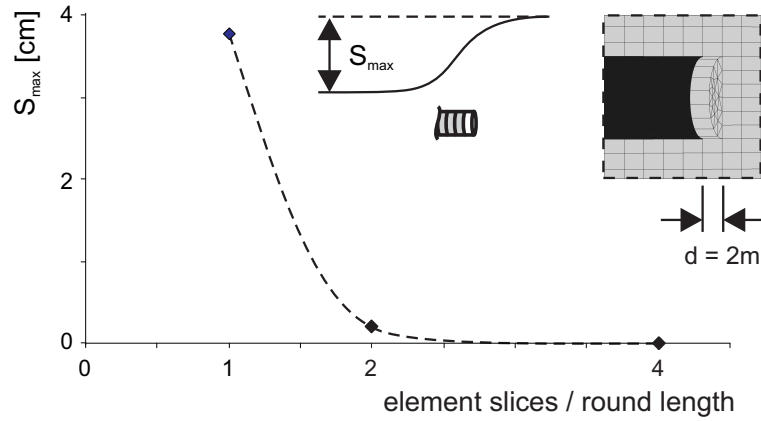


Figure 4.8: Influence of 3D mesh coarseness on surface settlements

$\gamma$ [kN/m <sup>3</sup> ]	$\nu_{ur}$ [-]	$E_{oed}^{ref}$ [MPa]	$E_{50}^{ref}$ [MPa]	$E_{ur}^{ref}$ [MPa]	$m$ [-]	$c'$ [kPa]	$\varphi'$ [°]	$K_0$ [-]	$OCR$ [-]
20	0.2	5	10	60	1.0	20	25	0.5	1.0

Table 4.1: Ground parameters of the HS Model (see Appendix A.2) as used to study mesh coarseness

4.1. The lining was modelled weightless and linearly elastic using  $E_l A = 3.75GN$ ,  $E_l I = 19.53MNm^2$  and  $\nu_l = 0.15$ .

**Surface settlements** Fig. 4.8 shows that the analysis with one element per round length slightly underestimates the settlement, giving a maximum surface settlement of  $S_{max} = 3.7cm$ . The mesh refinements with two and four elements per round length result in a settlement increase of around 10% giving  $S_{max} = 4.1cm$ . Fig. 4.8 is clearly indicating that the mesh dependency is becoming vanishingly small beyond a number of two elements per round length.

**Structural forces** Fig. 4.9 presents results of normal forces for different mesh coarseness for a local tunnel stretch of two round lengths, showing the zigzagging pattern which results from step-by-step installation (compare Section 4.1.4), with high forces at the front and lower forces at the rear of a lining ring. As indicated by the curves of Fig. 4.9, each lining shell element contributes two Gaussian integration points. Whereas the coarse mesh results in two Gaussian integration points per round length, the finer meshes comprise six and eight Gaussian integration points respectively.

The finer meshes of 2 and 4 elements per round length appear to give considerably larger maximum normal forces at the front of a lining ring than the coarse mesh with a single element per round length. Compared to the coarsest mesh, the increase of the

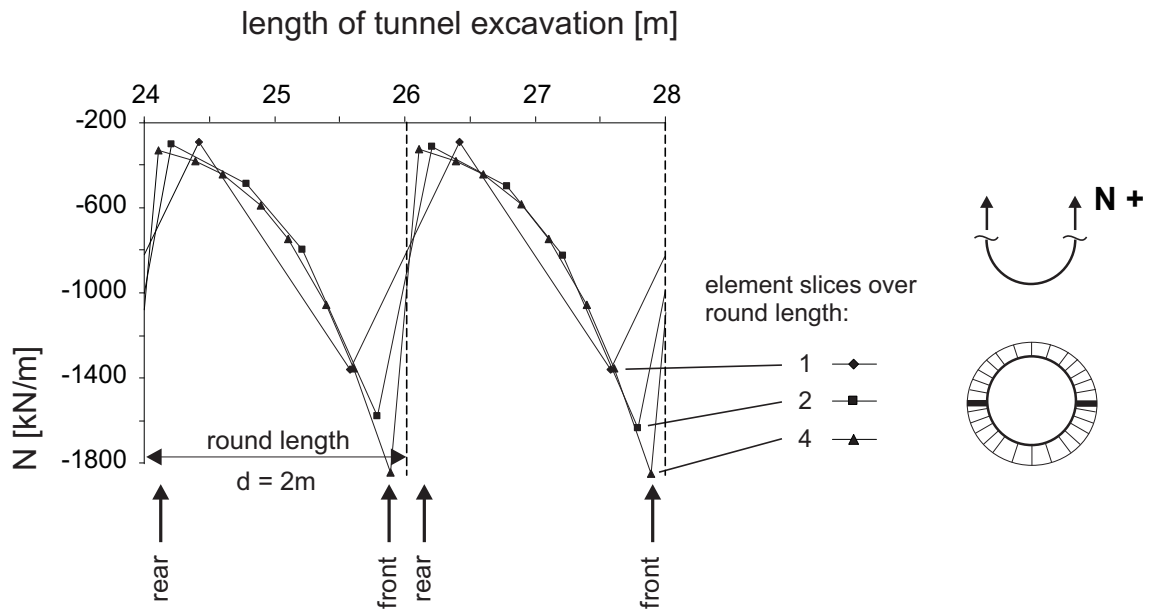


Figure 4.9: Influence of 3D mesh coarseness on distribution of normal forces. Normal forces are shown in the Gaussian integration points of the shell elements, being used for the lining.

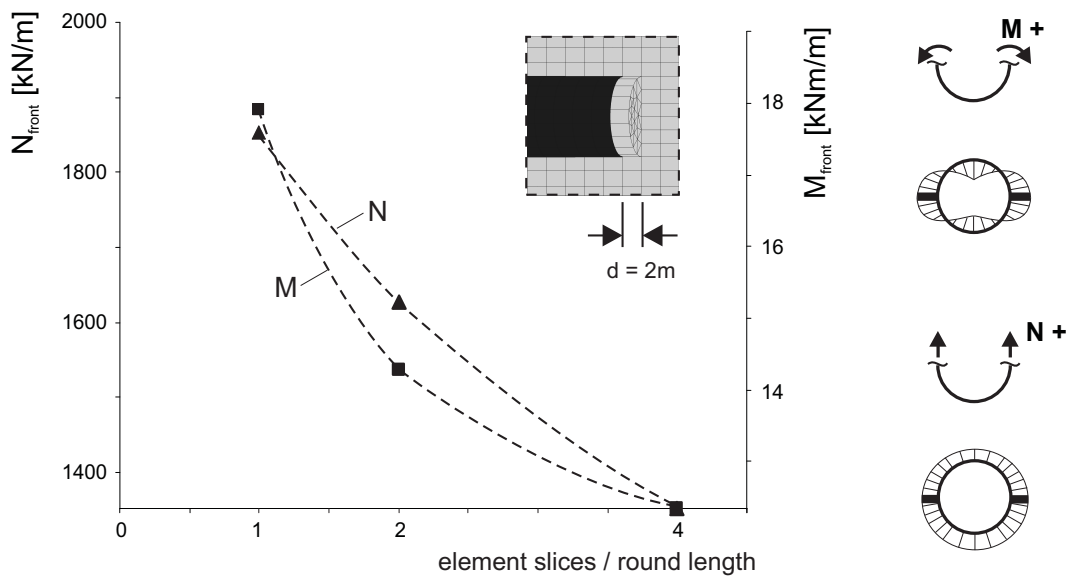


Figure 4.10: Influence of 3D mesh coarseness on magnitudes of bending moments and normal forces at the front of a lining ring. Differences occur because the finer meshes give information in Gauss points that are closer to the joints between adjacent round lengths.



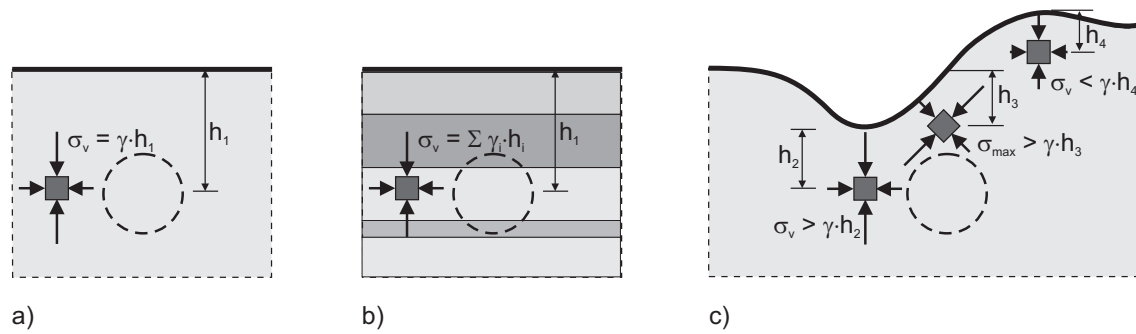


Figure 4.11: Magnitude and orientation of initial stresses

normal force is 26%, as indicated in Fig. 4.10. Fig. 4.9 shows that the results for the coarse meshes produce more or less the correct forces in the integration points considered, but one would have to extrapolate from these data the extremes at the joint between two adjacent round lengths. For the bending moment a similar trend is observed, giving an increase of 28% towards the joint between two adjacent round lengths.

## 4.4 On the initial stress

When comparing tunnel analysis to problems of structural engineering, one main difference is the fact that a significant part of the structure, the ground is not in a stress free situation before the tunnel is built. In tunnelling the ground is already subjected to relatively high initial stresses whereas in structural engineering, stresses for which the structure has to be designed are only developing as a result of (external) loads. In structural engineering a stress free situation may be considered as a starting point and the final stresses may be obtained as a result of numerical analysis. On the contrary, in tunnelling (and also in geotechnical engineering problems in general), initial stresses of considerable magnitude have to be considered as a starting point. As will be shown in this section, surface settlements and structural forces to be obtained from numerical analyses are by a large portion determined by the anisotropy of the initial stress field.

In order to account for the relatively high influence of initial ground stresses, a reasonable estimate of both their magnitude and orientation is needed. The natural initial stress distribution in the ground is mostly unknown and it is influenced by quite a number of factors. Tectonic movements, thermic effects, creep or weathering are only a few such factors and it often is very difficult to evaluate or even measure initial stresses. Thus, for assessing initial stresses some reasonable assumptions and/or approximations are needed.

**$K_0$ -procedure** Fig. 4.11 shows magnitudes and possible orientations of initial stresses. The ground shown in Fig. 4.11a is homogeneous with a horizontal ground surface. In such a case, the effective initial ground stresses around a tunnel may be assumed to

follow the relation

$$\sigma'_v = \sigma_v - u = \gamma \cdot h - u \quad (4.6)$$

$$\sigma'_h = K_0 \cdot \sigma'_v, \quad (4.7)$$

where  $\sigma'_v$  is the effective vertical stress in depth  $h$ ,  $\sigma_v$  is the corresponding total stress,  $u$  is the pore water pressure,  $\gamma$  is the unit ground weight,  $\sigma'_h$  is the effective horizontal stress and  $K_0$  is the coefficient of lateral earth pressure at rest. The use of Eqs. 4.6 and 4.7 is often referred to as  $K_0$ -procedure. It is not a *real* numerical calculation phase because it is used to prescribe initial stresses as a starting point for numerical analysis, i.e., no deformations are computed.

For tunnels in ground water the effective stresses  $\sigma'_v$  have to be considered for a deformation analysis by subtracting the pore water pressures  $u$  from the total stresses. For tunnels which are constructed above the ground water table and are governed by drained ground behavior, the pore water pressures are zero and the effective stresses equal the total ones.

Many geological profiles will have a horizontally layered ground as shown in Fig. 4.11b. Here Eq. 4.6 may be modified adopting a summation of vertical stresses of the respective ground layers  $i$  to arrive at the equation

$$\sigma'_v = \sum_i \gamma_i \cdot \Delta h_i - u_i. \quad (4.8)$$

**Gravity loading** Fig. 4.11c shows magnitudes and orientations of initial stresses in a ground with non-horizontal ground surface. In such a case, initial stresses around a tunnel can not be described by the  $K_0$ -procedure, as they may differ considerably within different regions around the tunnel. Indeed, the vertical stress in depth  $h_2$  may be significantly larger than assumed by Eq. 4.6, whereas the vertical stress in depth  $h_4$  may be significantly smaller. The maximum stress at depth  $h_3$  is not even coinciding with the vertical direction and can be considerably larger than  $\gamma \cdot h_3$  (see also MÜLLER-SALZBURG (1978)).

The numerical procedure commonly adopted to compute initial stresses for non-horizontal ground situations may be referred to as the gravity loading method. Starting from zero stresses in this method, initial stresses are computed by applying the ground self weight  $\gamma$  in a calculation phase.

#### 4.4.1 The horizontal initial stress

When adopting gravity loading to assess the magnitude of the initial stress in numerical analysis, the resulting  $K_0$ -value is related to the constitutive model being used. For homogeneous ground with horizontal ground surface and the Mohr-Coulomb Model (see Appendix A.1),  $K_0$  can be derived from linear elasticity, giving  $K_0 = \nu/(1 - \nu)$ , where  $\nu$  is the Poisson's ratio of the ground. However, this formula correlates  $K_0$ -values to the Poisson's ratio of the ground which gives a relation that does not hold true for

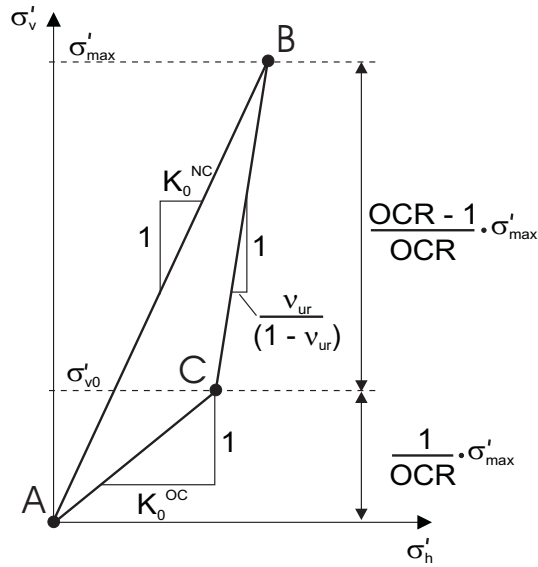


Figure 4.12: Relationship between  $K_0^{OC}$  and  $OCR$  for overconsolidated grounds (BRINKGREVE and VERMEER, 2001)

many grounds. Therefore, instead of computing initial stresses as a result of gravity loading, in most cases it is more appropriate to prescribe a certain  $K_0$ -value using the  $K_0$ -procedure. When adopting Eqs. 4.6-4.7 for the  $K_0$ -procedure, the coefficient of lateral pressure, which is determining the magnitude of horizontal initial stresses, is used as an input parameter. An estimate of the appropriate  $K_0$ -value depends on the material and its geological stress history.

**Normally consolidated ground** A normally consolidated ground is a ground which has never been subjected to a higher loading than the actual initial stress presently acting. For a normally consolidated ground usually the empirical correlation  $K_0^{NC} = 1 - \sin \varphi'$  is adopted to assess the coefficient of lateral pressure. Here the superscript  $NC$  stands for *normally consolidated* grounds and  $\varphi'$  is the effective friction angle of the ground.

**Overconsolidated ground** An overconsolidated ground may be a ground which has been unloaded from a higher state of stress to a lower state of stress or a ground that has been subjected to intensive creep (BJERRUM, 1967). In overconsolidated ground the coefficient of lateral pressure is usually higher than in normally consolidated ground. SCHMIDT (1966) proposed the equation for overconsolidated grounds

$$K_0^{OC} = K_0^{NC} \cdot OCR^{\sin \varphi'}, \quad K_0^{NC} = 1 - \sin \varphi', \quad (4.9)$$

where the superscript  $OC$  stands for *overconsolidated*.  $OCR$  is the Overconsolidation Ratio, which is defined as  $OCR = \sigma'_{max} / \sigma'_{v0}$  where  $\sigma'_{max}$  is the preconsolidation stress and  $\sigma'_{v0}$  is the effective vertical initial ground stress, presently acting in the ground. Considering a friction angle of  $\varphi' = 30^\circ$ , as an average value for many grounds, VERMEER

(2000) simplifies Eq.4.9 to obtain

$$K_0^{OC} = (1 - \sin \varphi') \cdot \sqrt{OCR}. \quad (4.10)$$

Another approach for assessing  $K_0^{OC}$ -values is shown in Fig. 4.12. Here the initial state of stress of overconsolidated grounds is achieved by considering the stress history of overconsolidated grounds. As shown in Fig. 4.12, it is assumed that the loading up to the maximum effective vertical stress  $\sigma'_{max}$  was a one-dimensional compression with  $\sigma'_h = K_0^{NC} \cdot \sigma'_v$ . Starting from point *A* the stress ratio of the vertical and the horizontal stresses up to point *B* is taken according to Eq. 4.7 and  $K_0$  for normally consolidated grounds. From point *B* to point *C* the ground is unloaded from  $\sigma'_{max}$  down to  $\sigma'_{v0}$  according to the magnitude of *OCR*. While unloading it is assumed that the ground behaves linearly elastic, using Eq. 4.7 and  $K_0 = \nu/(1 - \nu)$  with a Poisson's ratio  $\nu_{ur}$  for unloading-reloading (the indices *ur* stand for unloading-reloading). The resulting inclination from point *A* to point *B* can then be described by the coefficient

$$K_0^{OC} = \frac{\sigma'_h}{\sigma'_v} = (1 - \sin \varphi') \cdot OCR - (OCR - 1) \cdot \frac{\nu_{ur}}{1 - \nu_{ur}}. \quad (4.11)$$

Fig. 4.13 shows a comparison between Eqs. 4.9, 4.10 and 4.11 for the formulation of  $K_0^{OC}$  considering *OCR* and different friction angles. The maximum  $K_0^{OC}$ -value is governed by the Mohr-Coulomb failure criterion (Eqs. A.1-A.3), which is incorporated in all constitutive models explained in Appendix A. While Eqs. 4.9 and 4.10 give a non-linear relation, the graph of Eq. 4.11 is a straight line. For a Poisson's ratio of  $\nu_{ur} = 0.2$  and a friction angle of  $\varphi = 35^\circ$  resulting  $K_0^{OC}$ -values of all three equations compare well to each other. However, for a friction angle of  $\varphi = 25^\circ$  and larger *OCR* the resulting  $K_0^{OC}$ -values of Eq. 4.11 are somewhat larger than the ones predicted by Eq. 4.10. Eq. 4.11 appears to give values that lie in between the results of Eq. 4.11 and Eq. 4.10. Even such slight variations of the coefficient of lateral pressure are of considerable importance for tunnelling settlements and lining forces as will be shown in the following section.

#### 4.4.2 The role of $K_0$

The previous sections dealt with the magnitude and orientation of initial stresses. Initial stresses in numerical analysis may either be computed by using the  $K_0$ -procedure or by the gravity loading method. When adopting the  $K_0$ -procedure for the computation of geostatic initial stresses, the coefficient of lateral pressure  $K_0$  is of utmost importance. It determines the magnitude of the horizontal stresses and it will be shown that both surface settlements and structural forces in linings are heavily influenced by a change of this parameter.

Several authors have studied the influence of  $K_0$  in 2D and/or 3D numerical tunnel analysis on surface settlements, e.g. GUNN (1993), ADDENBROOKE et al. (1997), LEE and NG (2002) or FRANZIUS et al. (2005), to find that the settlement trough becomes wider and less deep with increasing  $K_0$ -value. Studies on lining forces were a.o. carried out

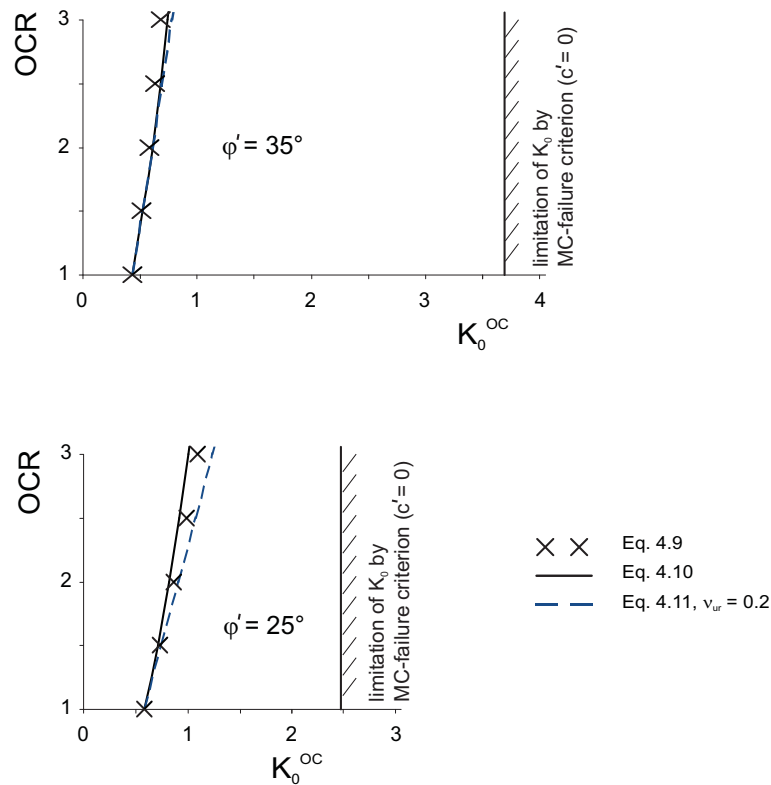


Figure 4.13: Formulation of  $K_0^{OC}$ : comparison between Eqs. 4.9, 4.10 and 4.11

by GUILLOUX et al. (1998) and GUEDES and SANTOS PEREIRA (2002). Many computations performed involve two-dimensional analyses. Several authors have noticed that the settlement trough obtained from such analyses is too wide and too flat compared to measured data in particular when large  $K_0$ -values are used for the initial stresses.

GUNN (1993) modelled tunnel construction in London Clay, involving  $K_0 = 1$ , and different soil models. First of all he used the elastic perfectly plastic Tresca model and secondly a non-linear elastic perfectly plastic Tresca model, which accounts for the small-strain stiffness of soils. He carried out two-dimensional computations and compared his results to the Gaussian distribution curve. Although the ground loss ratios, which he obtained from his numerical analyses, were quite close to common values for tunnels in London Clay, he obtained much wider settlement curves by a factor of two, when compared to a Gaussian curve with the same ground loss ratio. It would seem, however, that such wide predicted settlement troughs have also been caused by the use of elasticity models, which tend to cause too large swelling in the ground layers underneath the tunnel resulting in too large settlement troughs (compare Section 5).

ADDENBROOKE et al. (1997) presented a series of two-dimensional FE analyses on the construction of the Jubilee Line Extension at St James's Park in London. They used linear-elastic and non-linear-elastic soil models with a Mohr-Coulomb yield surface. Inserting  $K_0 = 1.5$  into their analyses they concluded that the computed surface settlement

trough is too wide when using appropriate soil parameters for London Clay.

It has been suggested that 3D effects could account for this discrepancy. Tunnel construction clearly is a three-dimensional problem and one would thus expect that 3D FE-analysis improves the surface settlement predictions, when compared to 2D modelling.

LEE and NG (2002) adopted a linear-elastic perfectly-plastic soil model to compare results of 3D analysis to the results of ADDENBROOKE et al. (1997). Besides a variation of the soils anisotropy they also carried out a variation of  $K_0$ . Although the tunnel diameter and the tunnel depth were different in the two studies, LEE and NG arrive at the conclusion that the shape of the surface settlement curve improves in the three-dimensional FE-analysis.

This statement, however, is in contrast to findings of other authors. GUEDES and SANTOS PEREIRA (2002) presented results of two- and three-dimensional FE-analyses, adopting an elastic soil model and a linearly with depth increasing Young's modulus. Comparing results of the transverse surface settlement trough they show that for  $K_0 = 0.5$  and  $K_0 = 1.0$  both 2D and 3D analyses give almost the same settlement shape. In the present thesis similar results will be shown. For lining forces they showed that with increasing  $K_0$ -values the normal forces in the lining were also increasing, whereas bending moments obviously decreased for a variation from  $K_0 = 0.5$  up to  $K_0 = 1.0$ , to approach a value being very close to zero. The two-dimensional analyses they performed showed a slight deviation from the three-dimensional ones for normal forces and good agreement to 3D results of bending moments. Again a similar trend will be shown in the present thesis.

DOLEŽALOVÁ (2002) compared results of numerical analyses to measurements of the Mrazovka Exploratory Gallery in Prague, using the Mohr-Coulomb Model and a non-linear elastoplastic model. Considering different  $K_0$ -values of 0.5, 1.0 and 1.5 she concluded that only the results of  $K_0 = 0.5$  were satisfactory when compared to the shape of the measured surface settlement trough. She stated that these findings were practically independent of the type of analysis, observing no difference between 2D and 3D computations.

FRANZIUS et al. (2005) carried out two- and three-dimensional FE-analysis for the Jubilee Line Extension at St James's Park, adopting both isotropic and anisotropic non-linear-elastic perfectly plastic soil models, including a formulation for the small-strain stiffness and Mohr-Coulomb's failure criterion. Comparing their results of surface settlements to field data, neither the 2D analyses nor the 3D analyses were steep enough to match the measurements. The difference observed between 2D and 3D computations of the transverse settlement trough was negligible.

In the present studies the non-linear elastoplastic Hardening Soil Model (see Appendix A.2) was applied, to investigate the influence of  $K_0$  on surface settlements and lining forces both for 2D and 3D analyses of conventional driven open face tunnels. Whereas the 2D analyses were carried out using the stress reduction method (see Section 4.6.1.3) the 3D analyses were performed according to the installation scheme of the step-by-step method (see Section 4.5.1) with a round length of  $d = 1.5m$ .

It will be shown that the shape of the transverse settlement trough of a 2D analysis compares well to the one of a 3D analysis, at least when using appropriate unloading

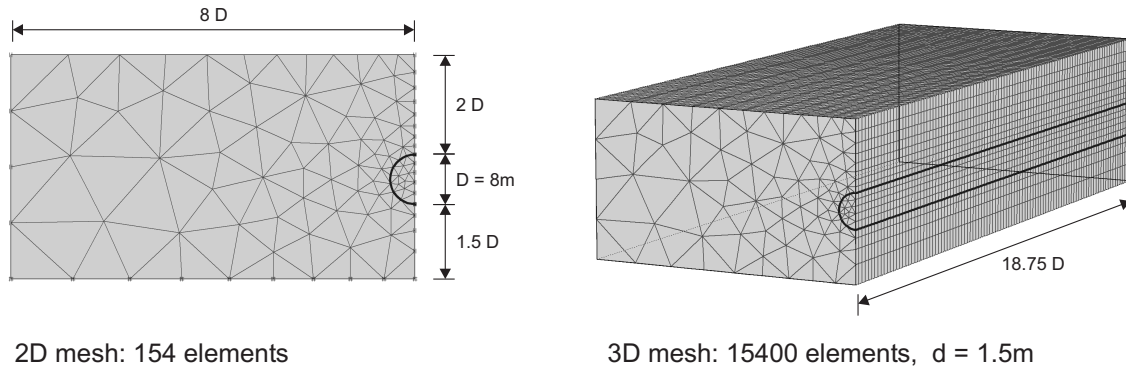


Figure 4.14: 2D and 3D FE-meshes as used to study  $K_0$

$\gamma$ [kN/m <sup>3</sup> ]	$\nu_{ur}$ [-]	$E_{oed}^{ref}$ [MPa]	$E_{50}^{ref}$ [MPa]	$E_{ur}^{ref}$ [MPa]	$m$ [-]	$c'$ [kPa]	$\varphi'$ [°]	$K_0$ [-]	OCR [-]
20	0.2	5	10	60	1.0	20	25	variable	1.0

Table 4.2: Ground parameters of the HS Model (see Appendix A.2) as used to study  $K_0$

factors (compare Section 4.8). Moreover, it will be shown that the settlement shape of the two-dimensional analyses depends significantly on the magnitude of the unloading factor for  $K_0 > 1$ . The results of the analyses will show (when choosing a common unloading factor of 0.5) a considerable difference between the two- and the three-dimensional analyses. Beyond the consideration of surface settlements the influence of  $K_0$  on structural forces will be analyzed.

In order to study the influence of  $K_0$  on the results of tunnel analysis, the two-dimensional and three-dimensional FE-mesh dimensions as shown in Fig. 4.14 have been considered. The ground parameters of the HS Model have been taken as presented in Table 4.2 and the weightless circular lining was modelled linearly elastic using  $E_l A = 3.75GN$ ,  $E_l I = 19.53MNm^2$  and  $\nu_l = 0.15$ .

**Shape of settlement trough** Fig. 4.15 shows results of three-dimensional analyses after 76.5m of step-by-step tunnel excavation. The different longitudinal surface settlement curves have been obtained for  $K_0 = 0.5, 1.0, 1.25, 1.5$  and  $2.0$  respectively. A tremendous influence of  $K_0$  on the magnitude of the maximum steady-state settlement is observed. The analysis with  $K_0 = 0.5$  shows the largest settlement of 2.3cm and considerably smaller settlements of 1.6cm and 0.3cm are obtained from  $K_0 = 1.0$  and 1.25. The analyses with  $K_0 = 1.5$  and 2.0 give heaves of 0.3cm and 1.6cm instead of settlements.

Fig. 4.16 shows the normalized longitudinal settlement curves to demonstrate the influence of  $K_0$  on the shape. As indicated by the vertical axis they have been normalized by the maximum centerline settlement  $S_{max}$ . The graphs show that  $K_0 = 0.5$  and 1.0 give

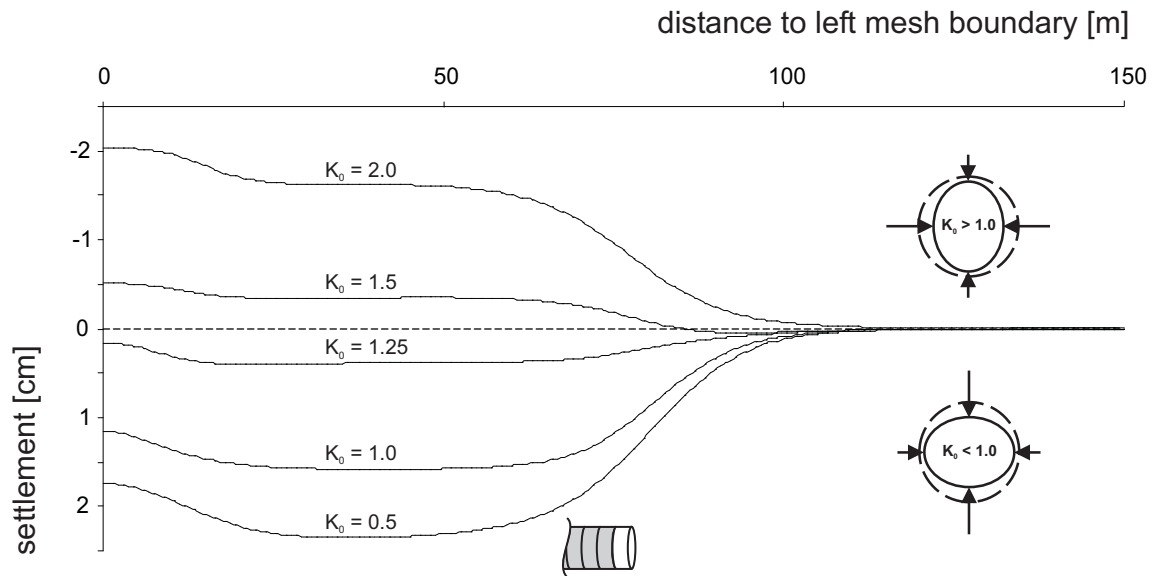


Figure 4.15: Surface settlement above tunnel axis for different  $K_0$ -values

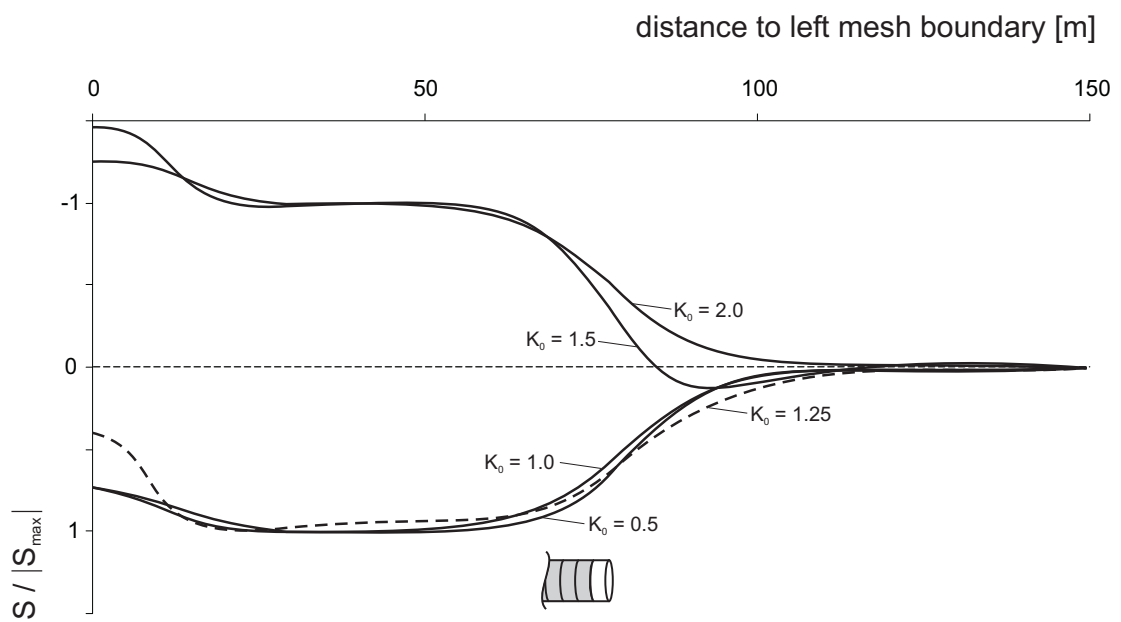


Figure 4.16: Normalized longitudinal surface settlement above tunnel axis



the steepest settlement curves, showing relatively little influence of  $K_0$ . However,  $K_0 > 1.0$  significantly decreases the steepness, as demonstrated by the curve for  $K_0 = 1.25$ . Even for the heave curves this effect is further continued, giving a less steep curve for  $K_0 = 2.0$  than for 1.5.

At first the effect of heave instead of settlements may seem somewhat peculiar and it may be doubted, whether or not it is realistic. Indeed, additional computations with the HS-Small Model (for model formulation see Appendix A.3) confirmed the phenomenon. Using  $G_0^{ref} = 100\text{Mpa}$  and  $\gamma_{0.7} = 2 \cdot 10^{-4}$  in addition to the parameters from Tab. 4.2, the small-strain analysis still yields surface heave. But this time the maximum centerline heave was significantly smaller, giving only 0.7cm instead of 1.6cm. In the present analyses  $OCR = 1$  for normally consolidated grounds was considered and another analysis was carried out to investigate the influence of  $OCR$  on the mechanism of surface heave. Increasing  $OCR$  up to a value of five, it appeared to have almost no influence at all. This is reasonable because the ground around the tunnel is unloading and the mechanical mechanism is predominantly a function of the soils elasticity rather than a function of plasticity associated with material hardening. However, to the authors knowledge in practice so far no surface heave has been measured according to tunnels in grounds with large  $K_0$ -values and the effect of heave is a topic of further research.

From a mechanical point of view surface heave is logical. With  $K_0$  larger than one the major principal stress is no longer in the vertical direction but in the horizontal one. As indicated in the insert of Fig. 4.15 for  $K_0 < 1.0$ , the tunnel will be mainly horizontally ovalized, whereas for  $K_0 > 1.0$  it changes to a vertical ovalization. Fig. 4.17 shows displacements from two-dimensional analyses for  $K_0 = 0.5$  and 2.0. In the first case the total displacements indicate that the ground moves into the crown of the tunnel pushing some ground away sideways at the tunnel wall. This type of mechanism is what is causing a surface settlement trough. In the latter case the total displacements show that the ground is moving inwards towards the tunnel wall, leading also to some ground heave above the tunnel crown with related surface heave. Considering these mechanisms it also becomes clear why the transition from small  $K_0$ -values to larger ones is causing less deep and wider settlement troughs.

Fig. 4.18 shows transverse settlement troughs from 3D and 2D analyses for different  $K_0$ -values. The trough becomes shallower and wider with increasing horizontal initial stress. For  $K_0 = 1.5$  and 2.0 again surface heave is observed but the transverse heave curves show that heave is primarily concentrated over the tunnel center line. For  $K_0 = 1.5$  only the center part of the curve is giving heave and at some distance from the center line settlement is observed again.

The two-dimensional analyses shown in Fig. 4.18 have been carried out with different unloading factors (see Section 4.6.1.3), as also indicated in this figure, in order to match the maximum settlement of the three-dimensional analyses. The conclusion given by LEE and NG (2002) that larger  $K_0$ -values would give steeper three-dimensional settlement curves when compared to the ones of two-dimensional analysis, is not confirmed by the present studies. On the contrary, a slightly steeper 3D-curve is only observed for the smallest  $K_0$ -value of 0.5. For  $K_0 = 1.0$  and 1.25, the three-dimensional analyses are

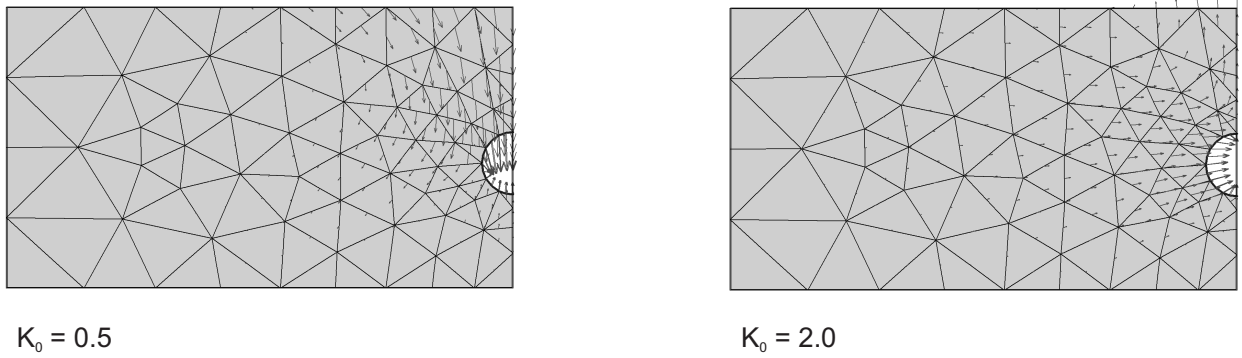


Figure 4.17: Displacements for different  $K_0$ -values

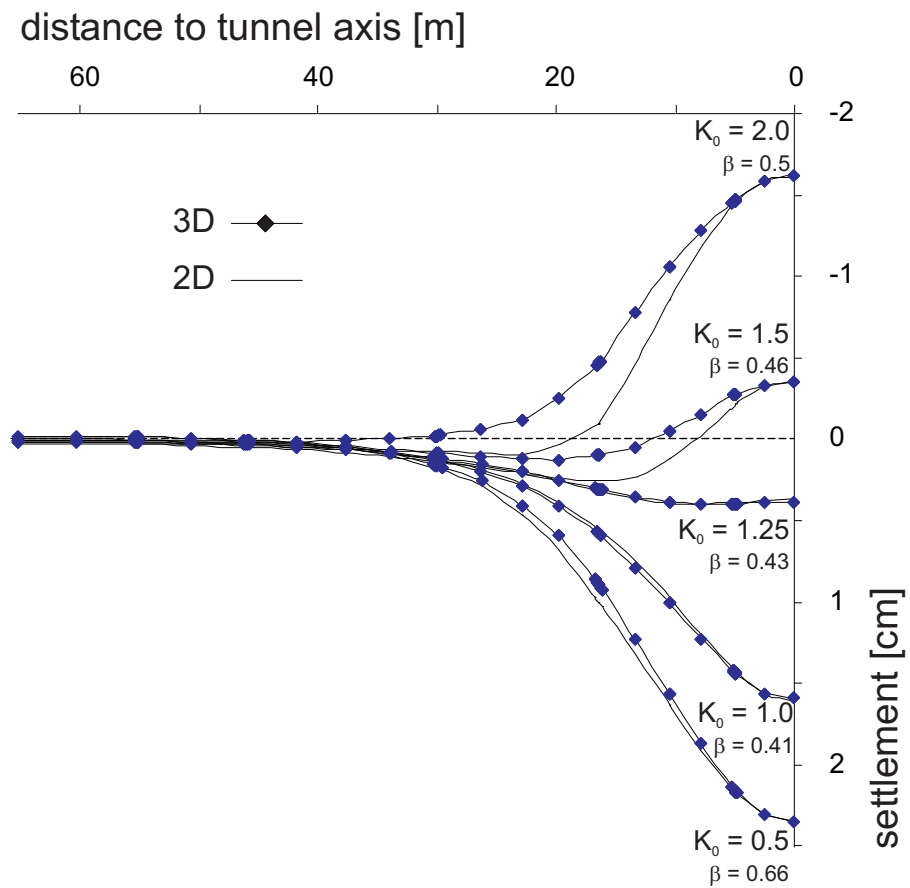


Figure 4.18: Transverse settlement troughs from 2D and 3D steady state analyses for different  $K_0$ -values

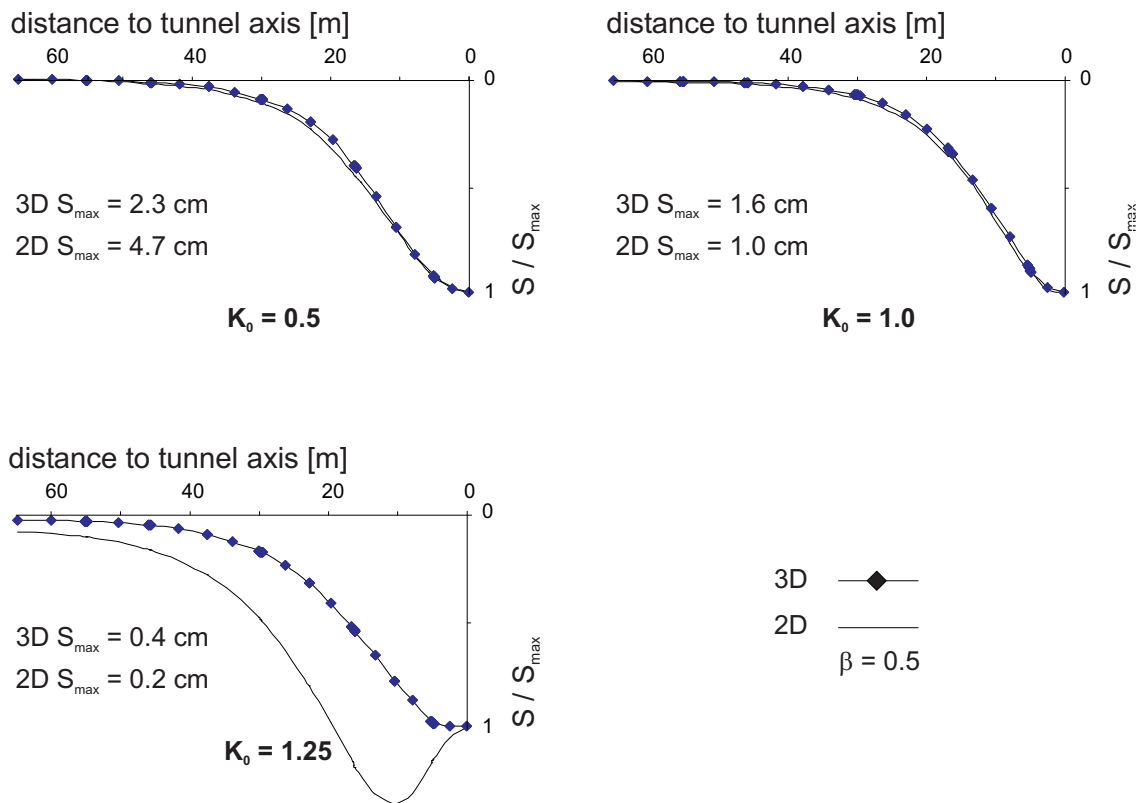


Figure 4.19: Normalized transverse settlement troughs of 3D and 2D analyses

well matched by the two-dimensional ones. For  $K_0 = 1.5$  and  $2.0$ , the heave curves of the two-dimensional analyses become significantly steeper than those from the three-dimensional ones.

Fig. 4.19 shows results of normalized settlement troughs of both 3D and 2D analyses, using a constant unloading factor of 0.5. The analyses with  $K_0 = 0.5$  and  $1.0$  give three-dimensional curves which are slightly steeper than the two-dimensional ones, but still are well matched. For  $K_0 = 1.25$  the shape of the 2D curve does not match the results of the 3D analysis at all and obviously for  $K_0 > 1.0$  and  $\beta = 0.5$  the two-dimensional analysis is no longer predicting a Gaussian shape. Instead, a similar shape as observed for the heave curves in Fig. 4.18 is computed. Apart from the fact that a constant unloading factor of 0.5 does not match the magnitude of the maximum three-dimensional settlement value, the present data show that the shape of the two-dimensional settlement analysis is affected by the magnitude of the unloading factor as well.

**Structural forces** In the following results of structural forces from shallow tunnels will be shown, knowing that they are of relatively low magnitudes and thus of minor importance. Nevertheless, results will be discussed in detail to point out the mechanical effect of  $K_0$  on tunnel linings. Fig. 4.20 shows results of bending moments from three-

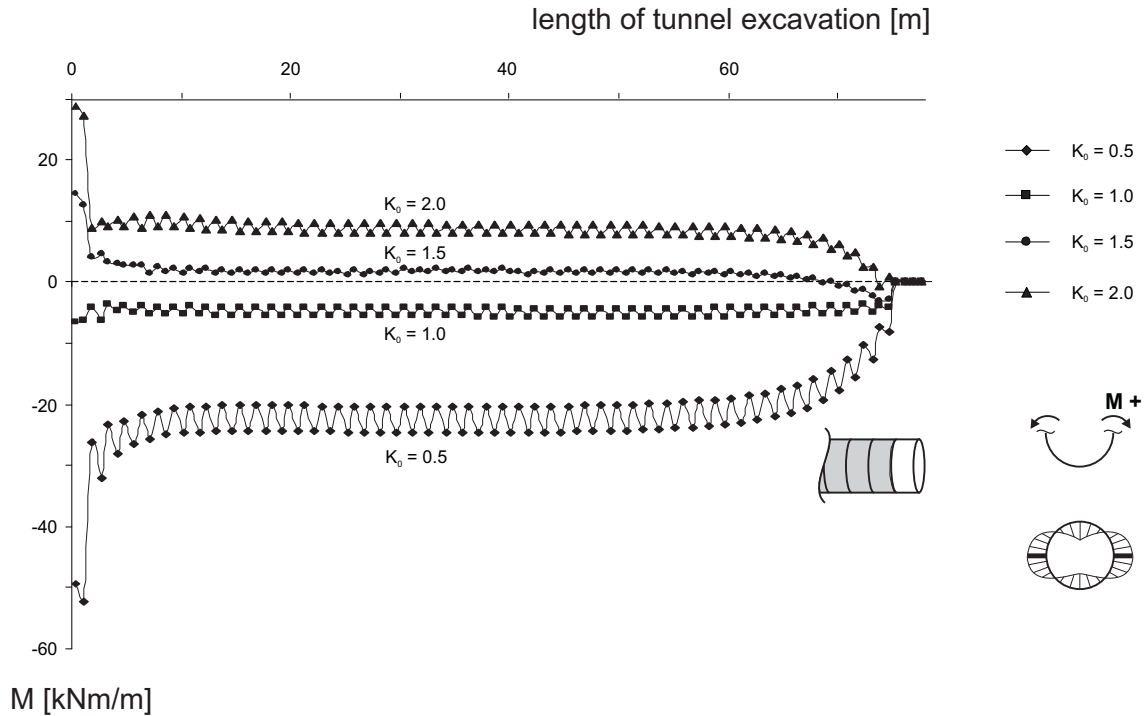


Figure 4.20: Bending moments from 3D analyses for different  $K_0$ -values

dimensional analyses after 76.5m of tunnel excavation, considering different  $K_0$ -values of 0.5, 1.0, 1.5 and 2.0. As shown in this figure, the magnitude of the bending moment which was evaluated at the tunnel wall, is strongly dependent on the magnitude of  $K_0$ . For  $K_0 = 0.5$  the lining is deflecting outward, as has already been discussed in the previous section on surface settlements, and a negative bending moment of around  $-25kNm/m$  at the tunnel wall is observed. For  $K_0 = 1.0$  the lining is obviously not much deflecting and the bending moment has decreased down to a vanishing small value of around  $-5kNm/m$ . This is in good qualitative agreement with the results presented by GUEDES and SANTOS PEREIRA (2002). Similar results are observed for  $K_0 = 1.5$ , but this time the lining is starting to deflect inwards, as indicated by the really small positive bending moment of around  $2kNm/m$ . For an increased  $K_0$  of 2.0 the positive bending moment is becoming larger, having a magnitude of around  $10kNm/m$ . For all values of  $K_0$  the previously described zigzagging is observed. The graphes make it clear that zigzagging of bending moments is strongly correlated to their magnitudes. The highest zigzagging is observed for the highest bending moment from the analysis with  $K_0 = 0.5$ .

Fig. 4.21 shows results of normal forces, taken at the tunnel wall after 76.5m of tunnel excavation. For normal forces a somewhat different behavior than for bending moments is observed. The smaller values at the rear of a lining ring (upper rows of data points) show a continuously decreasing behavior with increasing  $K_0$ . For  $K_0 = 0.5$  the normal force is about  $-500kN/m$  and for  $K_0$ -values of 1.0, 1.5 and 2.0 the normal force has dropped down to a value of around  $-270kN/m$ . The larger values at the front of a lining

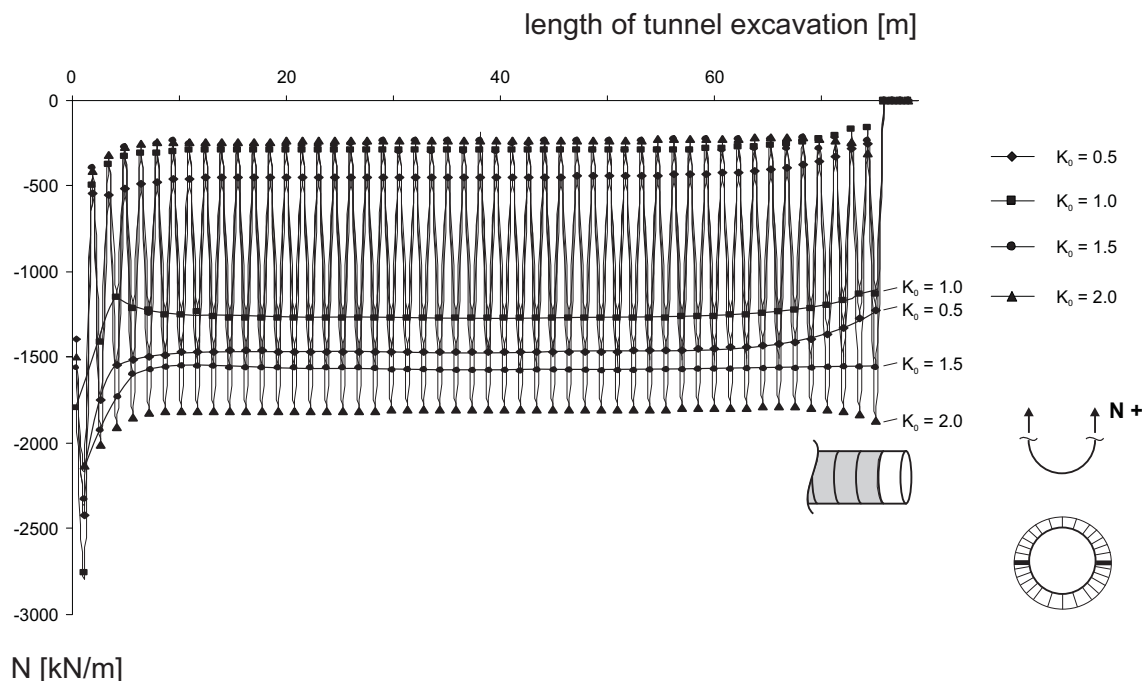


Figure 4.21: Normal forces from 3D analyses for different  $K_0$ -values

ring(lower rows of data points) of the normal force show a different behavior than the rear ones. For  $K_0 = 0.5$  the normal force is about  $-1500\text{kN/m}$ , decreasing to a value of  $-1250\text{kN/m}$  for  $K_0$  increasing to 1.0. When further increasing the  $K_0$ -value, however, the normal force is not dropping further but is increasing to  $-1625\text{kN/m}$  and  $-1875\text{kN/m}$  for  $K_0 = 1.5$  and 2.0 respectively.

Figs. 4.22 and 4.23 show a comparison of structural forces from three-dimensional and two-dimensional analyses for different  $K_0$ -values. The 3D results relate to two adjacent steady-state tunnel cross-sections, one in the front of a lining ring and one in the rear of the same lining ring. The two-dimensional results were taken from the earlier analyses of surface settlements, adopting the same unloading factors as presented in Fig. 4.18.

As reported earlier, the zigzagging of 3D bending moments along the tunnel longitudinal axis is small, as shown by the generally small differences between front and rear values of the three-dimensional bending moment. For  $K_0 = 0.5$  the lining is deflecting inwards at the tunnel crown and invert, giving a positive bending moment of about  $10\text{kNm/m}$ . At the tunnel wall it is deflecting outwards as indicated by the negative bending moment of about  $-25\text{kNm/m}$ . For  $K_0 = 1.0$  the 3D bending moments obviously decrease to a relatively small negative value of around  $-6\text{kNm/m}$ . For  $K_0 = 1.5$  the 3D bending moment at the tunnel wall is almost zero and the values at the crown and invert increase to about  $-15\text{kNm/m}$ , indicating that the crown and invert are deflecting outwards now. For  $K_0 = 2.0$  the tendency observed for  $K_0 = 1.5$  is further increased, giving a 3D bending moment of about  $-30\text{kNm/m}$  at the tunnel crown and invert.

The two-dimensional bending moments match the three-dimensional ones quite well

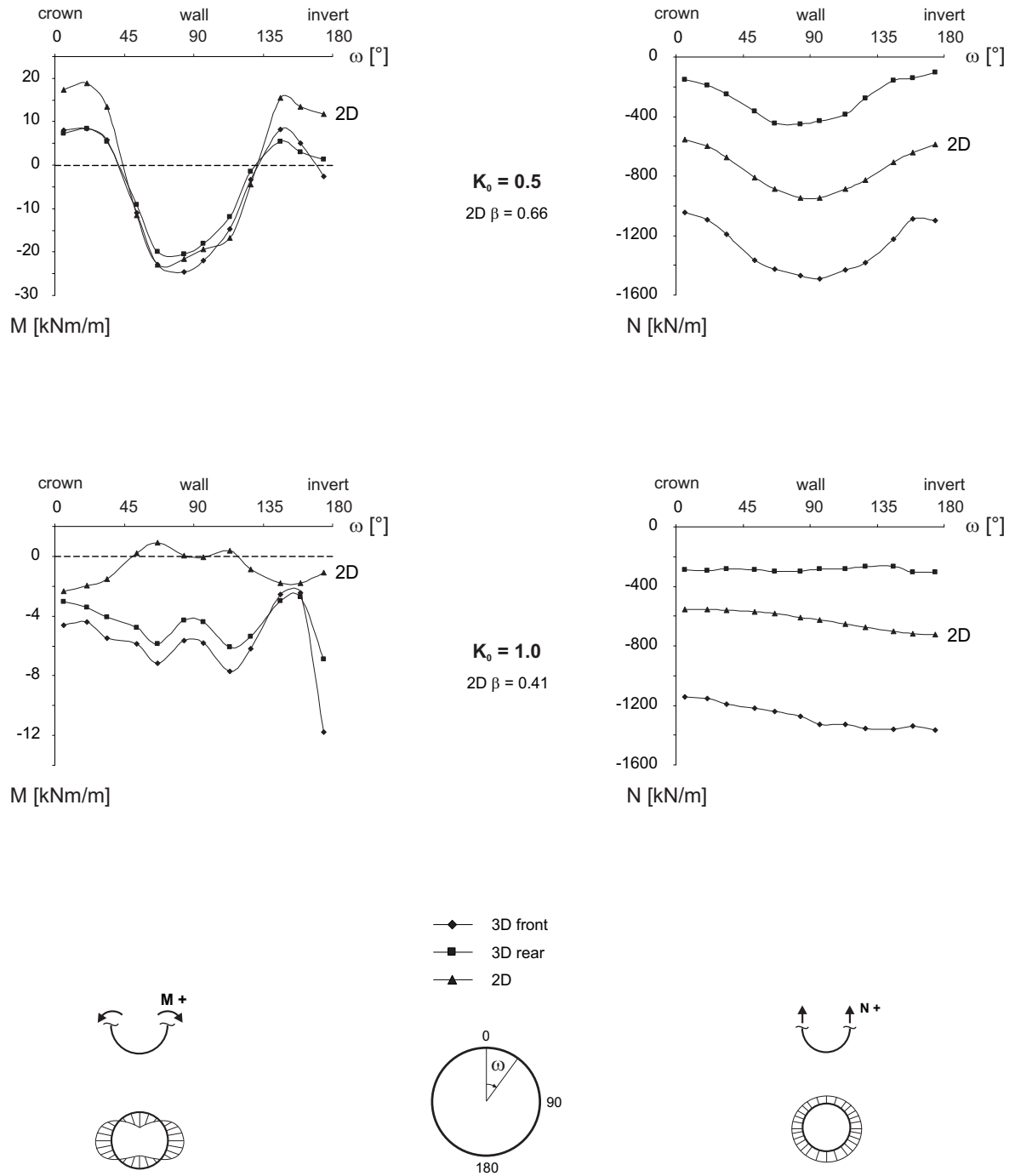


Figure 4.22: Comparison of bending moments and normal forces from 3D and 2D analyses for  $K_0 = 0.5$  and  $1.0$ . Unloading factor  $\beta$  in 2D-analysis is chosen such that it matches the maximum settlement from a 3D analysis.

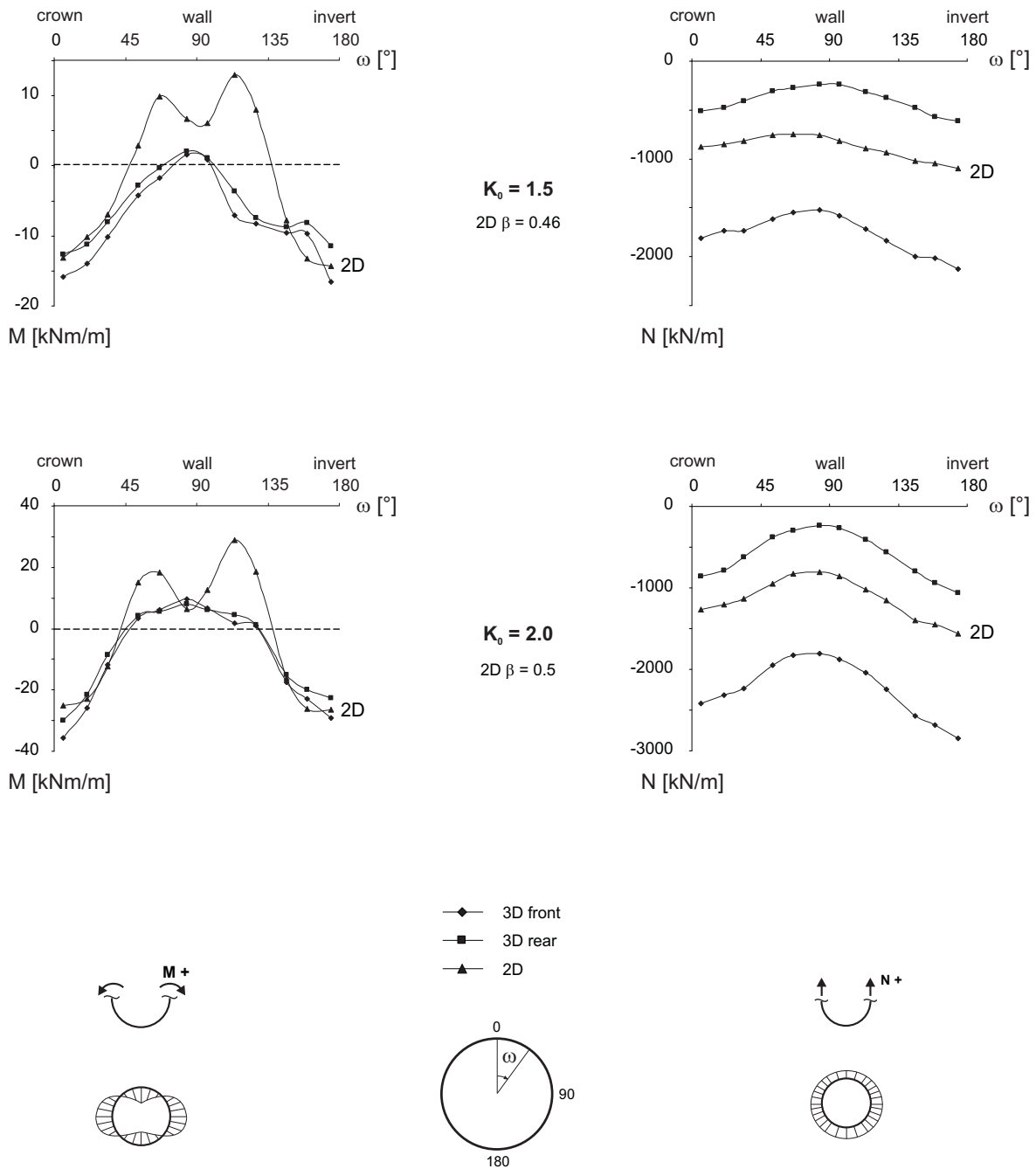


Figure 4.23: Comparison of bending moments and normal forces from 3D and 2D analyses for  $K_0 = 1.5$  and 2.0. Unloading factor  $\beta$  in 2D-analysis is chosen such that it matches the maximum settlement from a 3D analysis.

for  $K_0 = 0.5$ . For the other  $K_0$ -values of 1.0, 1.5 and 2.0, results from three-dimensional analyses are only matched at the crown and at the invert. Around the region of the tunnel wall, the two-dimensional analyses tend to predict considerably smaller negative bending moments or even are giving positive values. The fact that 3D bending moments are well matched by two-dimensional analysis as reported by GUEDES and SANTOS PEREIRA (2002) is thus only observed for a small value of  $K_0 = 0.5$ . For higher values of  $K_0$ , however, the good agreement between 3D and 2D results of bending moments is not observed. However, bending moments are typically low and thus not as important as normal forces.

The three-dimensional normal forces generally show a large difference of around  $1000kN/m$  between front and rear values, as has already been demonstrated previously by the zigzagging pattern of Fig. 4.21. For  $K_0 = 0.5$  the wall is giving the maximum normal forces of about  $-1600kN/m$  at the front and  $-400kN/m$  at the rear of a lining ring. At the crown and the invert the normal forces are about  $-1000kN/m$  and  $-200kN/m$  at the front and the rear respectively. For  $K_0 = 1.0$  the normal force along the cross-section is becoming almost constant, giving about  $-1200kN/m$  at the front and  $-300kN/m$  at the rear of a lining ring. When further increasing  $K_0$ , the normal force both at the front and the rear is mainly increasing at the tunnel crown and invert, reaching finally values of about  $-2500kN/m$  and  $-1000kN/m$  for  $K_0 = 2.0$ .

The two-dimensional normal forces are well in between the upper and lower bounds of the three-dimensional results, showing always a very similar shape. Whereas the 2D solution for  $K_0 = 0.5$  is almost exactly in the middle between front and rear values, the other analyses for  $K_0 = 1.0, 1.5$  and  $2.0$  tend to predict somewhat too low magnitudes, being more close to the results of the rear values.

## 4.5 Review of 3D FEM installation procedures

Tunnel installation involves a three-dimensional stress-strain-situation and three-dimensional FE-analyses have been adopted in engineering practice. In general 3D-FEM analyses are performed when facing complex geologies and/or geometries as illustrated in Fig. 4.24, e.g. when tunnels are connected to underground stations. However, in order to illustrate the simulation of installation processes and to make comparisons to 2D-analyses (Section 4.8), straight ahead tunnelling with a block-type mesh as indicated in Fig. 4.25 and Fig. 4.26 will be considered.

To analyze structural forces in tunnel linings as well as tunnelling settlements, various different installation procedures have been proposed, to simulate tunnel construction of conventional driven tunnels and shield tunnels. For open face tunnelling the process is discontinuous and this leads to step-by-step numerical procedures, being initiated by HANAFY and EMERY (1980). As for conventional tunnelling for shield tunnelling a step-by-step procedure is applied. For closed shield tunnelling the situation is more complex and different methods tend to be used to simulate tunnel installation. Step-by-step procedures require an FE-mesh with clusters of elements in the form of slices perpendicular to the tunnel axis as shown in Fig. 4.25 and Fig. 4.26. In the following



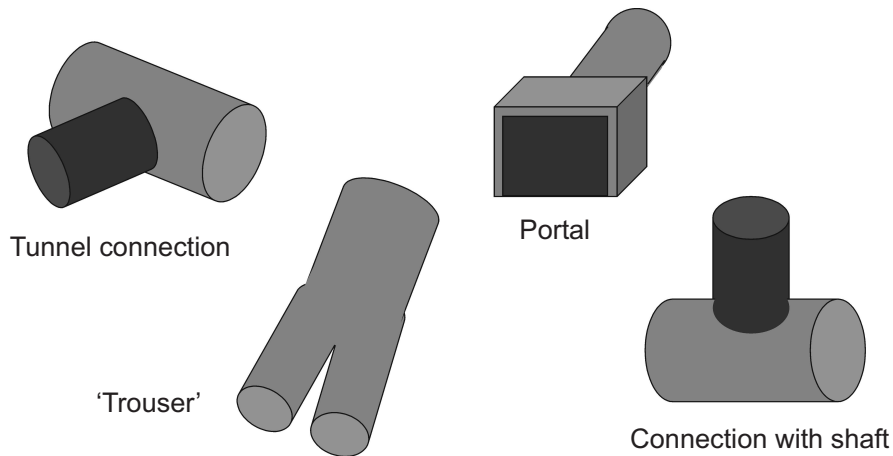


Figure 4.24: Complex three dimensional tunnel geometries

a short overview of 3D FE-installation procedures for both open face and closed face tunnelling will be given.

#### 4.5.1 Step-by-step installation for conventional tunnelling

To simulate the excavation process of open face tunnelling the so-called step-by-step-method is used. It would seem that the first step-by step methods have been introduced by HANAFY and EMERY (1980) followed shortly after by KATZENBACH and BRETH (1981). It thereupon has been considered by WITKE (1984) and SWOBODA et al. (1989). Starting from initial geostatic stresses, the excavation sequence is as indicated in Fig. 4.25. All calculation steps are identical: ground elements inside the tunnel are removed to simulate an unsupported excavation with a particular round length. Each computational phase  $i$  consists thus of an excavation in which one slice of soil elements is switched off. Within the same phase a ring of new lining elements is switched on to support the previous excavation  $i - 1$ . These calculation phases are repeated in steps  $i + 1$  to  $i + n$  until a representative steady-state solution is obtained.

#### 4.5.2 Installation for closed shield tunnelling

In shield tunnelling 3D-simulations have started as a simplified single-step approach (LEE and ROWE, 1991), but the recent trend is to use step-by-step procedures. The simplified stage-by-stage procedure of AUGARDE et al. (1998) might in fact be classified as an *in-between* approach. In the first stage of calculation elements within the tunnel are removed and simultaneously lining elements are activated over the entire length of the tunnel. At the end of this procedure the first stretch of the lining is subjected to a uniform (hoop) shrinkage to develop a prescribed amount of ground loss. Hereafter shrinkage is applied to a subsequent stretch of the lining and so on. On reducing the lining stretches

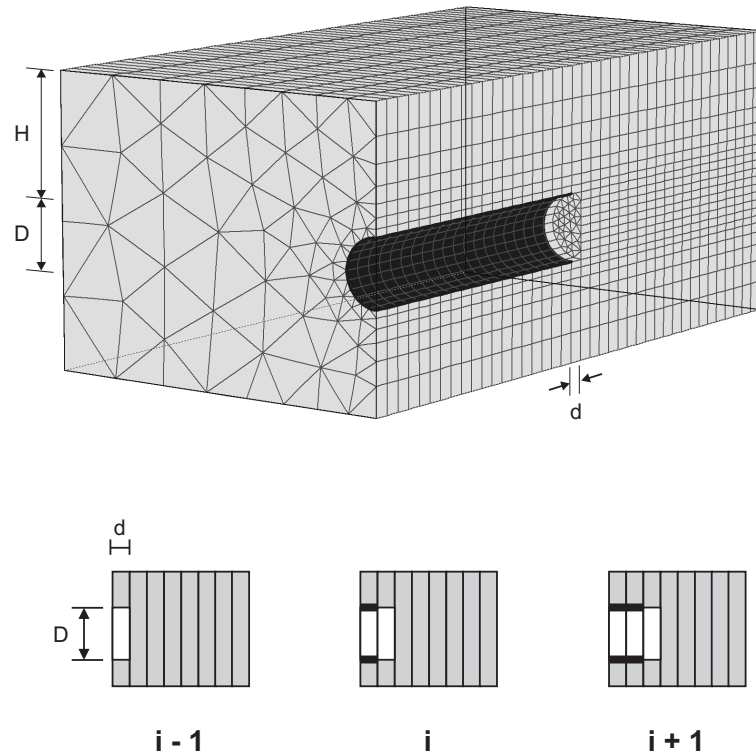


Figure 4.25: Step-by-step installation method for conventional tunnelling

to strokes of the tunnel boring machine this method converges to the real process of shield tunnelling. In fact, closed shield tunnelling is a continuous process with a continuous support pressure and installation of lining segments. However, for the reason of numerical discretization a step-by-step approach needs to be adopted.

It would seem that DIJK and KAALBERG (1998) use a step-by-step approach, but instead of prescribing a contraction of the lining as done by AUGARDE et al., they prescribe a hydrostatic pressure at the tunnel face as well as directly behind the shield, whilst the shield is modelled by elastic shell elements. HOEFSLOOT and VERWEIJ (2005) refine this model by prescribing in the tail void a grout pressure as a function of the distance behind the shield. In addition they model the conicity of the shield by applying a certain contraction, but they report that ground deformations are best matched when modelling only a stress boundary condition. Indeed, the contraction type of approach does not seem to give accurate results, as also reported by DIJK and KAALBERG (1998) and MAIDL et al. (2005). The latter consider the pure pressure type of simulation and they slightly simplify the DIJK and KAALBERG model by prescribing pressures over the entire tunnel heading including the tunnel face, the shield and some lining rings behind the shield. This would seem to be most realistic for high tail and/or face pressures, at least for slurry shields.

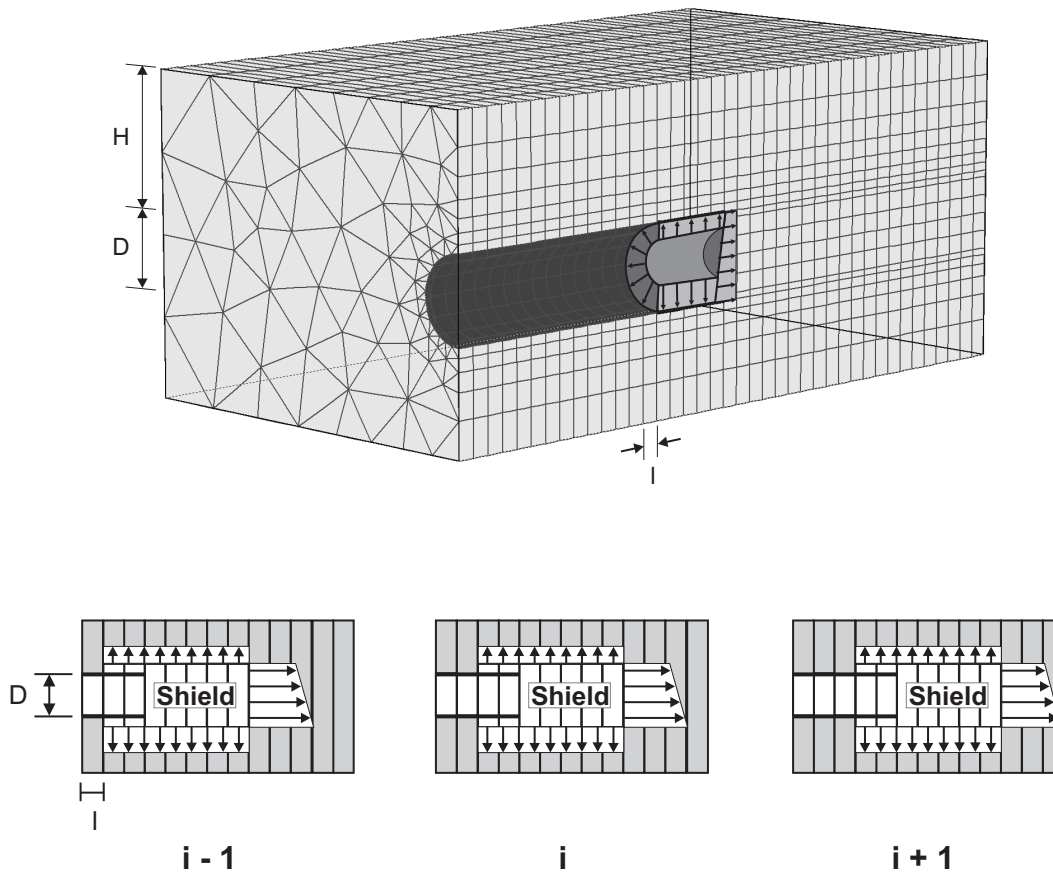


Figure 4.26: Step-by-step pressure method for shield tunnelling

#### 4.5.2.1 Slurry versus earth pressure balance shield

The preceding condensed literature review emphasizes the need for modelling a stress boundary condition in order to match ground deformations. Whereas HOEFSLOOT and VERWEIJ (2005) model a slurry shield tunnel, DIJK and KAALBERG (1998) and MAIDL et al. (2005) advocate a pressure boundary condition regardless of the type of shield machine, i.e. both for earth pressure balance and slurry shields. Although only the simulation of a slurry shield has been considered in detail by comparing results of FE-analyses to measurements (see Section 5.2), it would seem that a pressure boundary condition is also valid to model earth pressure balance shields.

#### 4.5.2.2 Step-by-step pressure method

**Slurry shield** The step-by-step pressure method considered in the present thesis is similar to the pressure method by MAIDL et al. Fig. 4.26 shows details of the step-by-step pressure method. The slurry at the face of the tunnel is simulated by a relatively high axial pressure, the shield is simulated by a somewhat lower radial pressure and the fresh

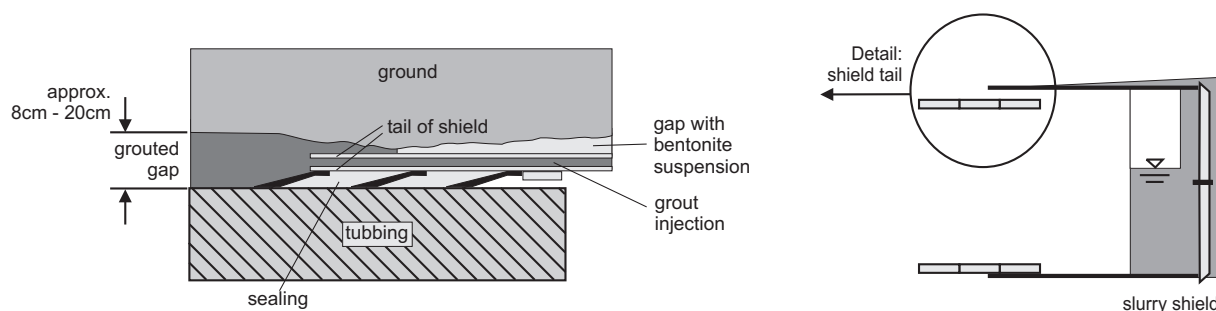


Figure 4.27: Details of the shield tail of slurry shields after BABENDERERDE (2000)

grout in the tail void behind the shield is also simulated by a radial pressure. Hence, instead of modelling the shield by stiff shell elements a pressure controlled boundary condition is applied. This is certainly realistic for modern machines which use injections around the shield to control ground loss, to compensate overcutting and to reduce shield friction (MAIDL et al., 2005).

Moreover, it would also seem realistic for slurry shields where the pressure is so large that slurry will flow from the face to the back of the shield. Fig.4.27 shows details of the ground-shield interaction of slurry shields. Between ground and shield there is a steering gap due to overcutting and conicity of the shield machine. The final tail void amounts up to approximately  $8\text{cm} - 20\text{cm}$ , as reported by BABENDERERDE (2000). The filling with grout in order to compensate this final tail void is achieved by an injection through the shield tail as illustrated in Fig.4.27. This tail void grout is partly flowing back to correspond with the slurry pressure and hence, according to BABENDERERDE, a pressure condition for the entire shield applies.

In the step-by-step pressure method all prescribed pressures increase hydrostatically with depth according to a unit weight of the slurry and the grout respectively. The radial shield pressure is taken equal to the grout pressure. It is applied along the shield and along two lining rings directly behind the shield, as shown in Fig.4.26. Here a ground-lining gap is simulated by deactivating ground elements with a thickness of around  $8 - 20\text{cm}$  (BABENDERERDE, 2000) and a length of approximately  $l = 1.5\text{m}$  according to the width of a lining ring. Within this gap the ground may deform until contact to the lining is made. Hence ground displacements are controlled not to exceed the ground-lining gap. For subsequent lining rings, the grout is assumed to be hardened and the radial pressure is switched off. Each time radial pressures are switched off, volume elements are activated to fill the gap, assuming linear elastic lining properties for the hardened grout.

In reality one may expect a smooth transition from the axial face pressure to the radial shield pressure, rather than a pressure jump, as indicated in Fig. 4.26. Similarly the grout pressure may also be modelled with a smooth transition to the hardened grout (TALMON and BEZUIJEN, 2005). However, in the present analysis the focus is on surface settlements and such abrupt transitions can be accepted, as surface settlements are hardly effected.

In order to model structural forces in linings most accurately one might have to consider a more detailed modelling of shield and grout pressure distributions.

During excavation the shield and the cutting wheel will impose some shear stresses to the ground (KASPAR and MESCHKE, 2004). The present pressure approach slightly simplifies the interaction between ground and shield machine by neglecting such shear stresses, but it would seem that they have little impact on surface settlements.

To simulate excavation for slurry shields, again for numerical reasons the step-by-step pressure approach as indicated in Fig. 4.26 is adopted. Starting from initial geostatic stresses, the following excavation sequence is carried out. In each computational phase  $i$  a tunnel advance of one segment length  $l$  is simulated, in which one slice of ground elements is switched off. At the same time pressure is applied in the new tunnel slice and in five subsequent *shield* slices. Behind the shield the full lining is modelled by shell elements. The first two rings of shell elements are surrounded by a pressurized gap, as explained earlier. Calculation phases are repeated in steps  $i + 1$  to  $i + n$  until a representative steady-state solution is obtained.

**Earth pressure balance shield** For earth pressure balance shields, one might assume a contraction type of boundary condition along the shield to model overcutting and/or a conical shield. Near the tail, however, it is plausible that grout will enter into the shield-soil interface. For high grout pressures the greater part of the shield may even be in contact with grout and a pressure boundary condition may prevail. It is felt, however, that analyses with displacement boundary in the front of the shield and pressure boundary at the rear of the shield make the matter unnecessary complex. For the sake of convenience EPB shields may also be modelled by using a pressure boundary condition, but it is debatable whether or not the same boundary conditions as for slurry shields applies.

## 4.6 Review of 2D FEM installation procedures

A frequently discussed topic is the question whether structural forces in tunnel linings as well as settlements should be computed by a fully three-dimensional analysis, or whether more simple two-dimensional models are sufficient. No doubt, tunnel installation involves a three-dimensional stress-strain-situation and three-dimensional FE analyses have been adopted in engineering practice, but such analyses are still time consuming. For large tunnel projects with several kilometers of excavation and various cross-sections, three-dimensional analyses cannot be used as a design tool and one has to rely on two-dimensional analyses.

In order to simulate tunnel excavation in a two-dimensional FE-analysis, the effect of the missing third dimension has in some way to be included. Fig. 4.28a shows the three-dimensional arch around the unsupported tunnel heading by displaying rotated principal stress directions. This arch is able to carry the vertical ground loads  $p_g$  by transferring them around the unsupported cut stretch.

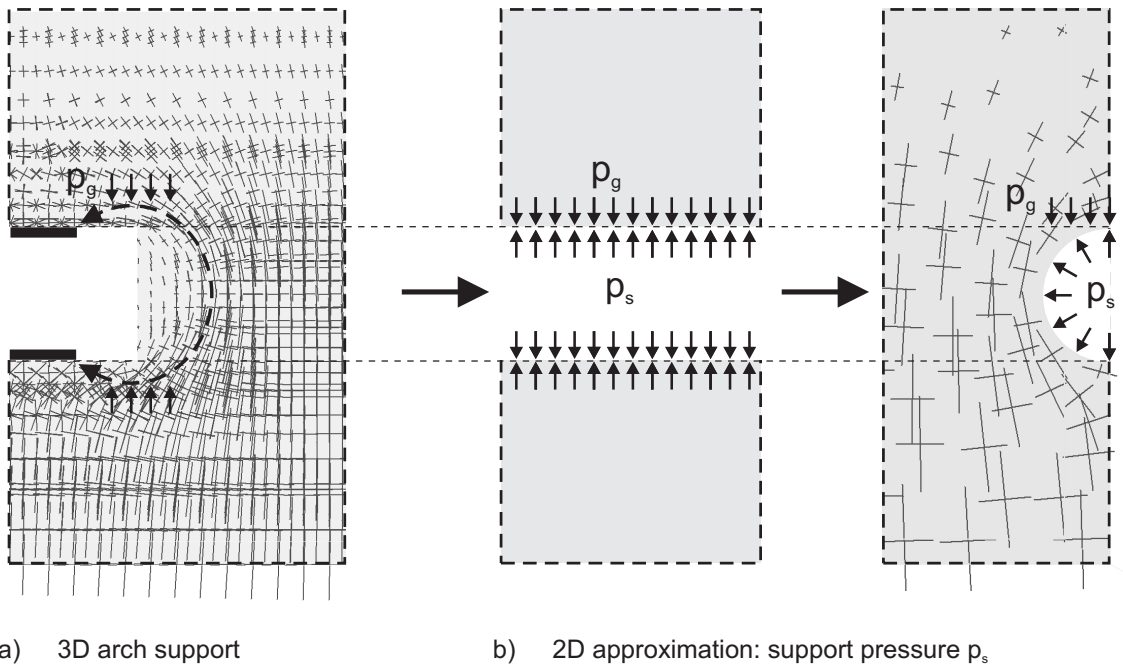


Figure 4.28: 3D arch support and 2D FE-approximation with support pressure

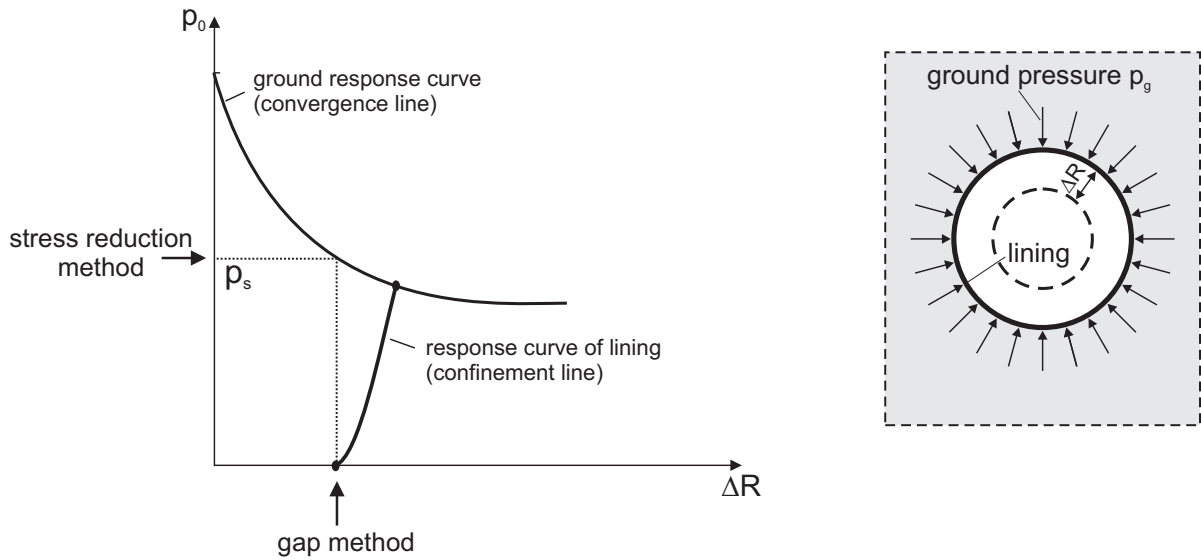


Figure 4.29: 2D FE-approximations: Stress reduction and contraction method adopting ground response curve

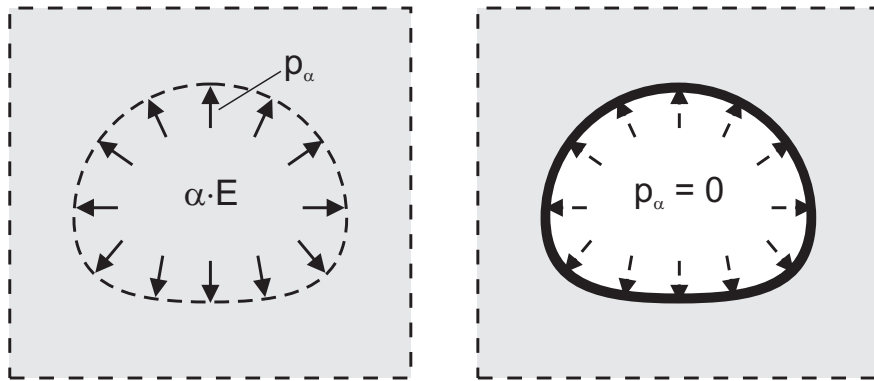


Figure 4.30: Calculation phases of the core support method

As demonstrated by Fig. 4.28b, two-dimensional analyses can not simulate the three-dimensional arching effect. The missing  $3D$  arch is compensated by involving an artificial support pressure  $p_s$ . When reading the literature on  $2D$  approximations for tunnel analyses, this artificial support may not necessarily be incorporated by means of a pressure approach but may as well be accounted for by a displacement approach.

Fig.4.29 illustrates tunnel construction, adopting the ground response curve. As shown in this figure, most  $2D$  approximations can either be classified as a stress reduction method where the initial ground pressure  $p_0$  inside the tunnel is reduced down to a support pressure  $p_s$ , or as a displacement/gap method, where the amount of support is controlled by simply prescribing a certain tunnel contraction  $\Delta R$  or ground loss. In the following both literature on conventional and closed shield tunnelling will be briefly reviewed on the aspects of such  $2D$  approximations.

### 4.6.1 Installation procedures for conventional tunnelling

For the simulation of the excavation and support sequence of conventional tunnelling different  $2D$  approximations are common in engineering practice. The stress reduction type of approach seems to be most popular. However, other methods tend to be used as well and results of different methods have been presented by SCHIKORA and FINK (1982). In the present work these methods will only be briefly reviewed.

#### 4.6.1.1 Core support method ( $\alpha$ -method)

The core support method reduces the stiffness of the tunnel core material by a factor  $\alpha$  and is therefore also referred to as the  $\alpha$ -method. Fig. 4.30 illustrates the two calculation phases of the core support method. In a first calculation phase initial stresses are computed with a gravity loading (see Section 4.4) but with a reduced core stiffness  $\alpha \cdot E$ . In this way a reduced support pressure  $p_\alpha$  is left inside the tunnel and the method can thus be considered the stress reduction type of approach. In a second calculation phase the

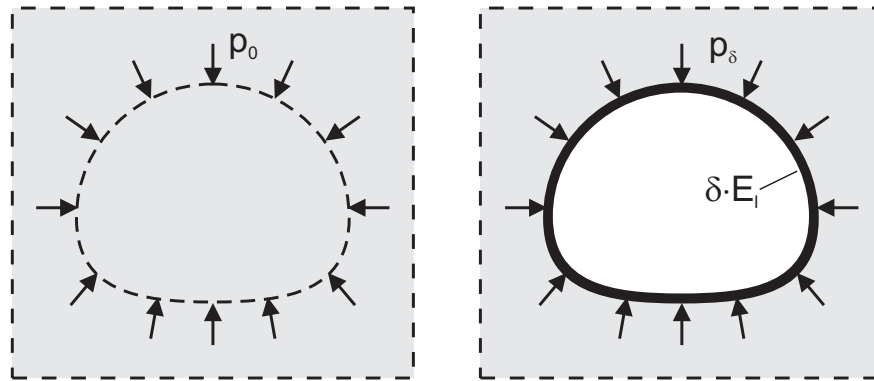


Figure 4.31: Calculation phases of the lining reduction method

soil inside the tunnel is removed and the lining is activated. SCHIKORA and FINK (1982) report realistic values of  $\alpha < 0.2$  for tunnels with  $2 < H/D < 4$ . For partial excavations without immediate closure of the lining ring they recommend values of  $\alpha$  ranging in between 0.3 and 0.5.

#### 4.6.1.2 Lining reduction method ( $\delta$ -method)

The lining reduction method (or  $\delta$ -method) is another approach. Fig.4.31 shows the two calculation phases of the lining reduction method. Starting from initial stresses  $p_0$  the lining is directly activated, but with a reduced stiffness  $\delta \cdot E$ . SCHIKORA and FINK (1982) report that  $\delta < 0.1$  leads to realistic normal forces. This implies an increase of the stiffness ratios  $\alpha$  and  $\beta$  in Figs. 3.14-3.16 and thus a reduction of structural lining forces. However, bending moments decrease faster than normal forces which makes the method not suitable for analyzing normal forces in combination with appropriate bending moments. It can be argued that bending moments are less important than normal forces, but the method seems not to be frequently used in engineering practice.

#### 4.6.1.3 Stress reduction method ( $\beta$ -method)

The most popular method to simulate installation procedures would seem to be the stress reduction method, often referred to as the  $\beta$ - or  $\lambda$ -method. The stress relaxation of the ground due to the delayed installation of the shotcrete lining (compare Fig. 3.12) and the load sharing between ground and lining are nicely addressed by this method.

Starting from initial geostatic stresses the stress reduction method comprises two calculation phases. Fig.4.32 illustrates these two calculation phases by relating them to the so-called ground-response curve (see Section 3.7). Starting from initial stresses, in the first calculation phase tunnel installation is simulated by switching off ground elements inside the tunnel and the initial ground pressure  $p_0$ , which is acting on the inside of the tunnel, is reduced down to  $\beta \cdot p_0$ , with  $0 < \beta < 1$ . Here  $\beta$  is the load reduction factor,



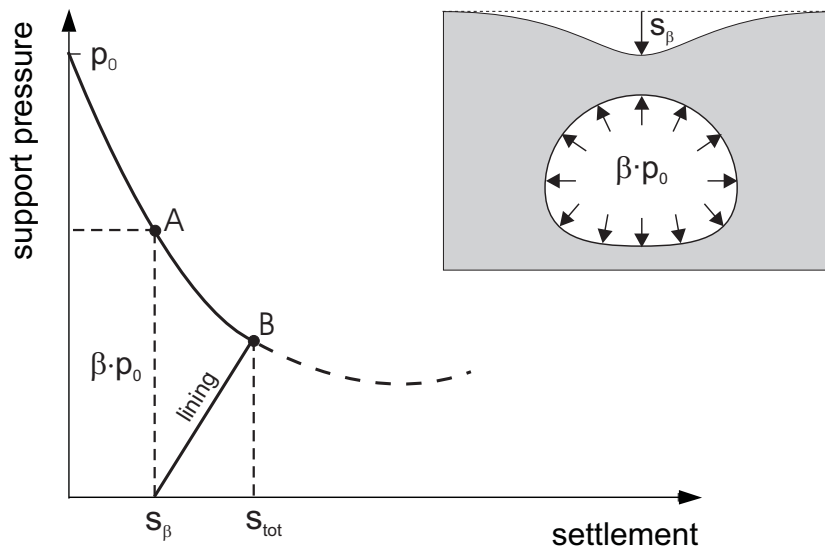


Figure 4.32: Display of stress reduction method adopting ground response curve

often taken around 0.5. In this thesis  $\beta$  will simply be referred to as the unloading factor. To this point only the ground is loaded and settlements of the amount  $S_\beta$  occur, as indicated in Fig. 4.32.

In the second calculation phase the lining is installed and the remaining load  $\beta \cdot p_0$  is divided over the lining and the ground. Final settlements of the amount  $S_{tot}$  occur in this phase due to the combined loading of ground and lining. Structural forces in the lining occur only during this second phase. For stiff linings the remaining load will largely go into the lining. Small  $\beta$ -factors correspond to large round lengths and/or late installation of tunnel lining. In this case ground deformations will be relatively large, whilst structural forces in the lining will be relatively low. Vice versa a larger factor  $\beta$  leads to smaller ground deformations and larger structural forces in the lining. In the later Section 4.8 an extensive parameter study on the unloading factor  $\beta$  will be given. It will be shown that the stress reduction method gives reasonable structural forces and settlements when used in combination with appropriate unloading factors.

#### 4.6.2 Installation procedures for closed shield tunnelling

When using numerical analysis to simulate shield tunnel excavation consideration must be given to the ground in front of the shield machine, which will move both radially and axially towards the tunnel face. This implies that the ground which forms the final cut surface of the tunnelling machine, due to deformation was originally located at some distance farther away from the tunnel. The volume in between the original location and the final cut surface represents a loss of ground before excavation. Additional ground loss will occur when the gap between diameter of cut surface and external diameter of tunnel lining is not compensated with grouting.

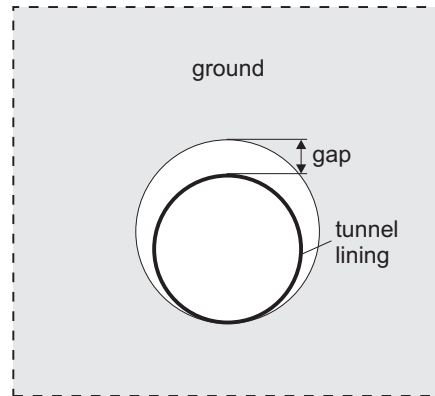


Figure 4.33: Gap method by ROWE et al. (1983)

To simulate shield tunnelling two-dimensional FE-analyses are frequently used and different installation procedures are adopted to simulate ground loss. MUIR WOOD (1975) was probably the first to suggest the stress reduction method for shield tunnelling, but it would seem that his idea was not extended into numerical analysis. Instead different methods, such as the gap approach or stress reduction method have been proposed to simulate ground loss. In the following relevant 2D installation procedures for shield tunnelling will be summarized.

In the subsequent Section 4.7 an improved method for the simulation of shield tunnelling will be introduced, being named the grout pressure method. It combines elements of the gap method with a simulation of grout pressures, as presented by the step-by-step pressure method in Section 4.5.2.2. The lining is considered to be surrounded by a thin grout layer with a known grout pressure, and it will be demonstrated in Section 5.2.2 that this method yields realistic results for both vertical and horizontal displacements.

#### 4.6.2.1 The gap method

It would seem that the first gap method was introduced by ROWE et al. (1983). The latter consider ground loss in terms of a vertical gap between tunnel lining and cut surface, as illustrated in Fig. 4.33. If the invert of the tunnel rests on the underlying soil (allowing for heave), then the gap is the vertical distance between the crown of the tunnel and the original position of the ground cut surface prior to tunnelling.

Starting from initial stresses, the tunnel is excavated in one computational phase, installing as well the tunnel lining with a certain gap at the crown. The ground is unsupported and free to displace until contact to the lining is made. For  $K_0 < 1$ , contact will first occur at the crown and bottom and it will successively move to the sides. During deformation the tunnel cut surface is monitored and once the cut surface comes into contact with the tunnel lining, the interaction between ground and lining is modelled. A description of the ground-structure interaction is given in ROWE et al. (1978).

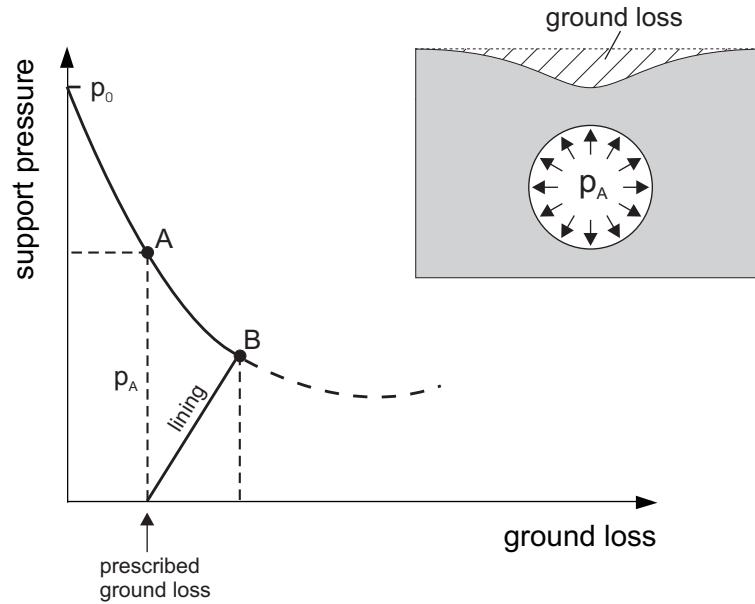


Figure 4.34: Stress reduction method with ground loss control by ADDENBROOKE et al. (1997) adopting ground response curve

#### 4.6.2.2 The stress reduction method

The stress reduction method has also been proposed to model installation of shield tunnelling. As the magnitude of unloading factors are uncertain and shield tunnelling is controlled by the amount of ground loss, unloading factors have been replaced by a control of ground loss (ADDENBROOKE et al., 1997).

Fig.4.34 illustrates the two calculation phases of the stress reduction method with a ground loss control, adopting the ground response curve. Starting from initial stresses, the stresses inside the tunnel are reduced stepwise in a first calculation phase and the resulting ground loss is calculated after each increment. As soon as the prescribed ground loss is reached in point *A* at corresponding pressure  $p_A$ , the lining is activated. Hence, the stress reduction factor  $\beta_g$  is chosen such that it matches a given ground loss.

ADDENBROOKE et al. (1997) assume undrained material behavior, i.e. constant volume deformation, for which the volume of the surface settlement trough is equal to the ground loss. By doing so, they prescribe a ground loss for the monitored volume of the settlement trough.

When the focus is on settlements and no structural forces are analyzed, the calculation can be stopped after reaching the prescribed ground loss. For analyzing structural forces, the load transfer to the lining has to be calculated in a subsequent calculation phase. After placing the lining in a second calculation phase, some further ground loss will take place until final equilibrium is reached in point *B*. But this additional ground loss will be small compared to the ground loss of the first calculation phase, as lining stiffness is considerably higher than ground stiffness.

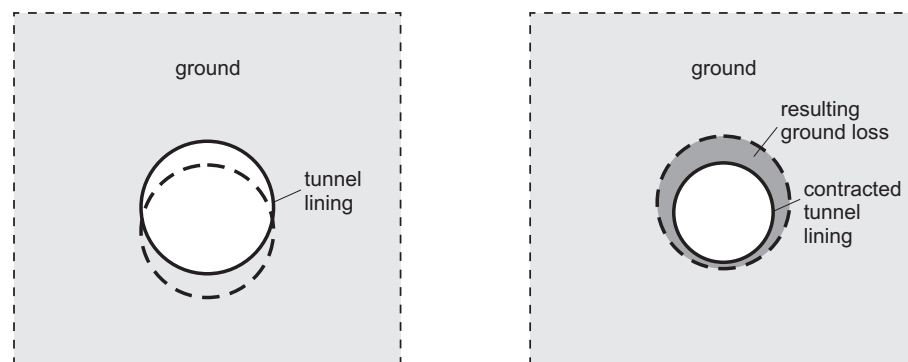


Figure 4.35: Contraction method (VERMEER and BRINKGREVE, 1993)

#### 4.6.2.3 Contraction method

A numerically somewhat different procedure is the contraction method by VERMEER and BRINKGREVE (1993), where the ground loss is simulated by a certain tunnel contraction. Starting from initial stresses this method involves two calculation phases as shown in Fig. 4.35. Within the first phase of calculation tunnel excavation is simulated by removing ground elements inside the tunnel while at the same time the lining is *wished in place*. As the tunnel lining is left free to displace during this phase, there will be some uplift due to the removal of ground weight inside the tunnel. Shell elements to simulate the lining may be combined with the weight of concrete and this will impose some downward force on the tunnel. Nevertheless, lining weight is small compared to the mass of the excavated tunnel cross-section, resulting in tunnel uplift. In the second calculation phase the tunnel lining is stepwise contracted until its contraction matches a prescribed value. As the the lining stiffness tends to be large in comparison to the ground stiffness, this prescribed tunnel contraction imposes more or less a prescribed radial displacement towards the center of the tunnel plus a ground stiffness dependent vertical displacement of the entire tunnel. It will be shown in Section 5.2.2 that this method leads to unrealistic results for both surface settlements and horizontal ground movements.

## 4.7 Improved installation procedure for shield tunnels: The grout pressure method

In the grout pressure method the simulation of ground loss is achieved in a way that combines elements of the gap method and the stress reduction method. As in the gap method, ground deformation is limited by the outer diameter of the tunnel lining and similar to the stress reduction method a pressure boundary condition along the excavated tunnel boundary applies. But unlike the stress reduction method which is reducing the acting initial stresses along this boundary, it will be shown that the grout pressure method replaces the initial stresses by a given grout pressure distribution, which differs

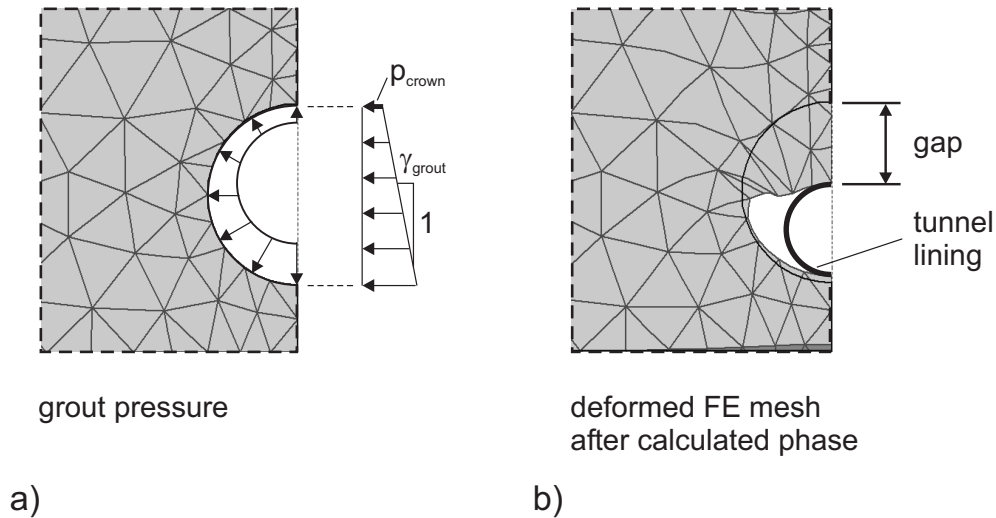


Figure 4.36: Display of the grout pressure method

considerably from the distribution of initial stresses. In the following the grout pressure method will be proposed as an improved installation procedure for shield tunnels.

In the grout pressure method the lining is considered to be surrounded by a thin grout layer with a known grout pressure. The thin grout layer may be modelled with so-called interface elements between the ground and the lining. Within these interface elements the normal grout stress  $\sigma_g$  is assumed to be given, e.g. with an hydrostatical increase with depth as illustrated in Fig. 4.36a, such that the lower pressure  $p_{crown}$  acts at the top of the lining. Before tunnel excavation the interface elements have the initial normal and shear stress

$$\sigma_0 = \sigma_h \cdot \sin^2 \omega + \sigma_v \cdot \cos^2 \omega \quad \text{and} \quad \tau_0 = \frac{\sigma_v - \sigma_h}{2} \cdot \sin 2\omega, \quad (4.12)$$

where  $\omega$  is a rotation angle as illustrated in the insert of Fig. 4.37. The transition of the interface stress  $\sigma$  from  $\sigma_0$  to  $\sigma_g$  can be written as

$$\sigma = (1 - \lambda) \cdot \sigma_0 + \lambda \cdot \sigma_g \quad \text{and} \quad \tau = (1 - \lambda) \cdot \tau_0, \quad (4.13)$$

where  $\lambda$  is a pseudo time parameter, which increases from zero to unity. For  $\lambda = 0$  the interface elements have ground properties and transfer the initial geostatic normal and shear stress  $\sigma_0$  to the lining. Then the geostatic stresses in the interface elements are changed to the normal grout pressure with no shear stresses by increasing  $\lambda$  up to 1. For a linear elastic ground and lining this can be done in a single computational step, but incremental procedures are required when adopting non-linear ground behavior. Depending on the difference between  $\sigma_0$  and  $\sigma_g$  the interface elements will expand or contract. The interface contraction should not exceed a prescribed value. This prescribed value is the difference between the excavation radius and the outer radius of the lining, i.e. the gap as indicated in Fig. 4.36b.

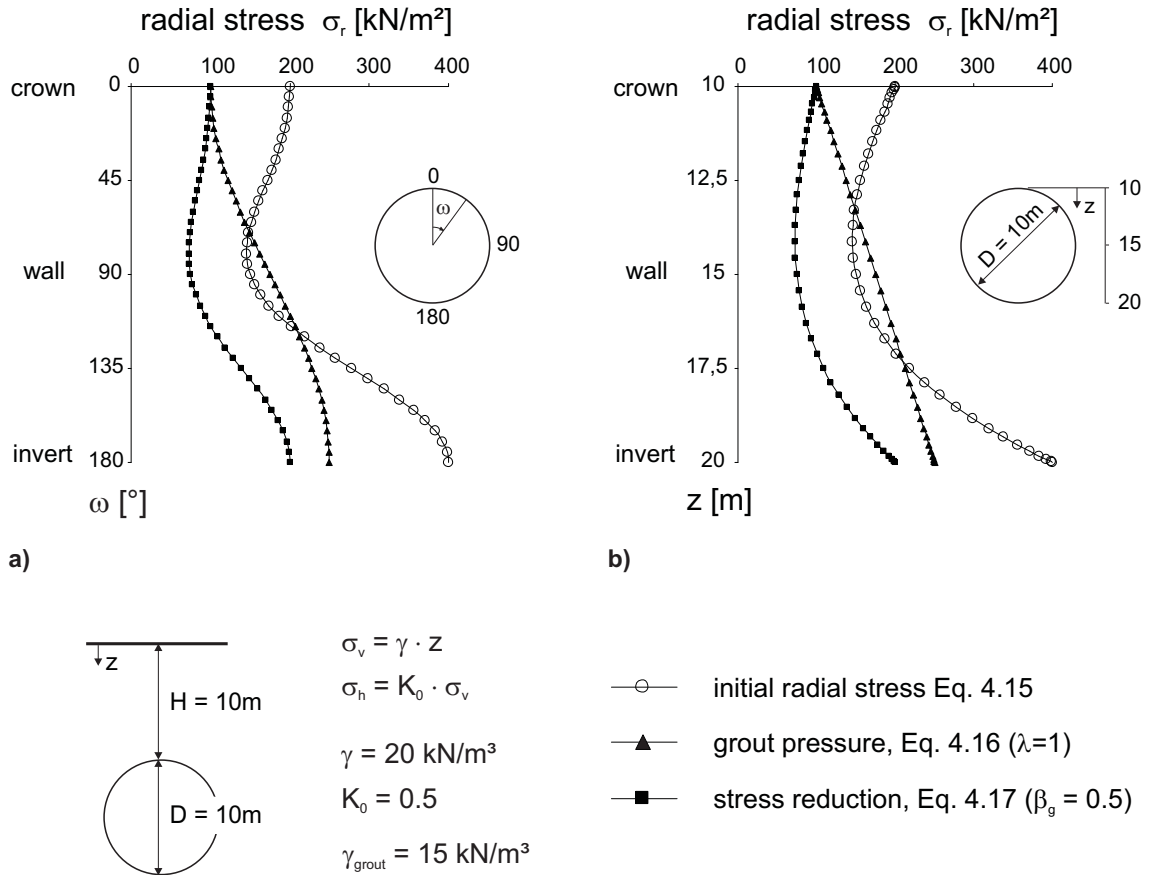


Figure 4.37: Difference in pressure distributions of stress reduction and grout pressure methods. Display of radial stresses: a) as a function of rotation angle  $\omega$ , b) as a function of depth  $z$ .

**Comparison between grout pressure and stress reduction methods** When comparing the stress distribution of the grout pressure method to the one of the stress reduction method, there is a considerable difference. To describe the stress distribution of the stress reduction method, Eq. 4.12 may be extended to

$$\sigma_{\text{radial}} = \beta_g \cdot \sigma_0 \quad \text{and} \quad \tau_{\text{tangential}} = \beta_g \cdot \tau_0, \quad (4.14)$$

where  $\beta_g$  is the unloading factor (compare Section 4.6.2.2) to reach a prescribed ground loss. Hence, the normal and shear stresses have a similar distribution as the initial stresses, but are reduced by a factor  $0 < \beta_g < 1$ . In contrast the grout pressure method considers only normal stresses and no shear stresses (no bonding between ground and lining), which is more realistic for shield tunnelling. Moreover, the grout pressure method results in a considerably different distribution of the radial pressure on the tunnel lining.

Fig. 4.37a) and b) shows the difference of radial stresses of the grout pressure and the stress reduction method, displayed both as a function of the rotation angle  $\omega$  and depth  $z$ .

$z$  respectively. The radial stresses shown here are calculated for a particular tunnel with a diameter of  $D = 10m$  and a cover to diameter ratio of  $H/D = 1$ . The unit weight of the ground is  $\gamma = 20kN/m^3$  and the coefficient of lateral earth pressure was taken as  $K_0 = 0.5$ . In order to compare the two methods, the crown pressure of the grout pressure method was taken the same as the reduced crown stress of the stress reduction method. The unit weight of the grout pressure was taken as  $\gamma_{grout} = 15kN/m^3$ . Fig. 4.37 shows that the radial stresses of the two methods are almost the same at the tunnel invert, but due to  $K_0 = 0.5$  the radial stress of the stress reduction method at the tunnel wall is around two times smaller than the radial stress of the grout pressure method. Moreover, the stress reduction method assumes an uniform reduction of initial stresses, whereas the grout pressure method reduces initial pressures at the tunnel crown and invert, but leads to increased radial stresses at the tunnel wall.

## 4.8 Evaluation of unloading factors for use in the stress reduction method

At present two-dimensional FE-analyses are common in tunnelling practice and a description of installation procedures has been given in the previous sections. Whereas in shield tunnelling different methods tend to be used, in conventional tunnelling the most popular two-dimensional method is the stress reduction method. In order to incorporate effects of 3D tunnel installation into this method, assumptions have to be made about the magnitude of the unloading factor.

To assess the magnitude of unloading factors, several authors have suggested various different values, either based on engineering experience and measurements, theoretical assumptions or derived from the comparison of 2D and 3D computations. For structural forces SCHIKORA and FINK (1982) report values of the unloading factor, being in the range of  $0.35 < \beta < 0.6$  for tunnels with  $2 < H/D < 4$ . BAUDENDISTEL (1979) considered vertical crown displacements of tunnels from three-dimensional linearly elastic analyses to derive unloading factors. He considered unloading factors for partial excavations as well as for fully excavated tunnels. Table 4.3 shows unloading factors after BAUDENDISTEL for a full excavation of a horse shoe profile and different round lengths  $d$ . No doubt, the idea of relating  $\beta$  to  $d$  is correct. LAABMAYR and SWOBODA (1986) derive unloading factors from the percentage of deformation which takes place in the ground in front of the tunnel face and the percentage which is measured behind the face, when the tunnel is completed. For partial excavations they come up with unloading factors of  $0.2 < \beta < 0.5$  for a top heading and  $0.4 < \beta < 0.8$  for a wall heading.

This short literature review makes it obvious that unloading factors vary within a relatively wide bandwidth and it is difficult to come up with some precise numbers. The assessment of unloading factors is awkward, as they are not only dependent on the geometry of the tunnel cross-section, round length or the material behavior, but they depend as well significantly on construction processes.

Nevertheless, an attempt will be made to come up with some information on the un-

$d$	$1.5 \cdot D$	$D$	$0.5 \cdot D$	$0.25 \cdot D$	$0.125 \cdot D$	0
$\beta$	0.0	0.02	0.11	0.23	0.41	0.72

$d$  = round length

$\beta$  = unloading factor

$D$  = excavation diameter

Table 4.3: Unloading factors  $\beta$  for full excavation of a horse shoe profile and different round lengths  $d$  after BAUDENDISTEL (1979)

loading factor, by systematically comparing results of three-dimensional step-by-step analyses to those of two-dimensional stress reduction analyses. But it has to be stated clearly that this information is aimed at giving a qualitative insight into the matter rather than coming up with quantitative numbers of the unloading factor.

In the following analyses are carried out for the design of tunnel linings, i.e. bending moments and normal forces, as well as for settlements due to tunnelling. Finally results of structural forces in tunnel linings and surface settlements will be shown for an underground railroad tunnel in Stuttgart, Germany.

### 4.8.1 Three-dimensional FE-analyses

Until now  $\beta$ -values have been based on engineering judgement and values between 0.2 and 0.8 have been suggested. However, for a true calibration of the procedure,  $\beta$ -values may be obtained by comparing results of 2D-analyses with data from 3D-analyses. In order to do so, first of all the 3D-analyses of conventional driven tunnels have to be considered.

Fig. 4.38 shows a three-dimensional FE-mesh in a half-symmetric condition. Tunnels with a circular cross-section have been analyzed. The mesh of Fig. 4.38 comprises a tunnel diameter of  $D = 7m$  and a round length of  $d = 1.5m$ . It has a total height of  $57m$ , a length of  $120m$  and a width of  $60m$ . Different meshes with diameters of  $9m$  as well as  $11m$ , and round lengths of  $d = 0.5m$  as well as  $1m$  have also been analyzed. All tunnels had a depth of  $H = 21m + 0.5 \cdot D$  and a mesh width of  $60m$ . The minimum mesh length was taken eighty times the round length  $d$ . All meshes were large enough to exclude influences of mesh boundaries. To simulate the excavation and support sequence the *step-by-step*-method (see Section 4.5) has been used.

### 4.8.2 2D- versus 3D-analyses

For a particular tunnel geometry and a particular set of material properties, the finding of the corresponding  $\beta$ -value sometimes requires an iterative procedure. This is best



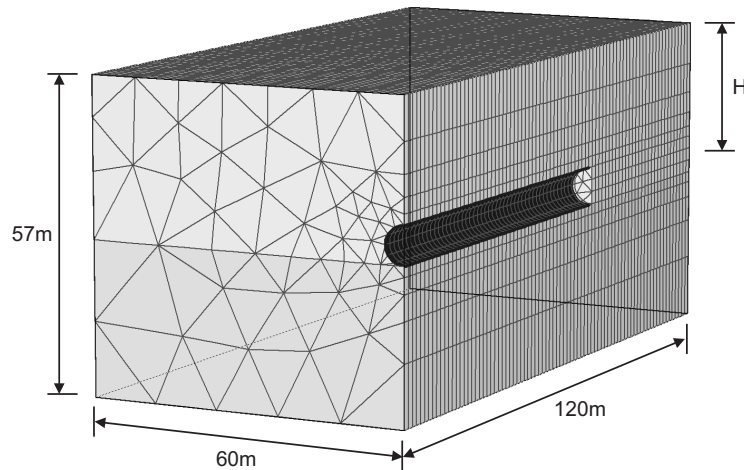


Figure 4.38: Three-dimensional FE-mesh,  $D = 7m$  and  $d = 1.5m$

explained by considering the ground response curve as shown in Fig. 4.32. The complete ground response curve can be computed from a two-dimensional FE-analysis of an unlined tunnel and the settlement  $S_{tot}$  is obtained from a full three-dimensional FE-analysis.

Assuming an elastic tunnel lining, it is straightforward to compute the inclination of line  $B - S_\beta$  in Fig. 4.32 and to find point  $B$  with the corresponding  $\beta$ -value. Indeed, for deep tunnels with  $K_0 = 1$ , there is a more or less axis symmetric state of stress around the tunnel giving a cylindrical compression of the lining. As long as this lining behaves elastically line  $B - S_\beta$  in Fig. 4.32 will be linear. For shallow tunnels in non-linear ground, however, circular tunnel linings deform into ellipses and line  $B - S_\beta$  is no longer linear. In such cases point  $B$  with its corresponding  $\beta$ -value has to be computed iteratively.

The above  $\beta$ -finding procedure applies to settlements. Instead of considering settlements, one may also compute ground response curves for bending moments and/or normal forces in linings. The settlement in Fig.4.32 might for instance be replaced by the maximum bending moment or the maximum normal force, as both of them increase when reducing the support pressure  $\beta \cdot p_0$ . No doubt, all three curves will be somewhat different and one will find three different factors:  $\beta$ -settlement,  $\beta$ -bending moment and  $\beta$ -normal force. In the following results of  $\beta$ -values of bending moments and normal forces will not be plotted as discrete curves but are shown as a band width for structural forces in general.

### 4.8.3 On ground and lining stiffnesses

In tunnelling a large volume of ground is excavated so that the ground underneath the tunnel is unloaded. Moreover, stress decrements decrease with depth so that the ground underneath the tunnel experiences on average only very small stress decrements. In such cases the ground will behave extremely stiff. Rather than using complex material

models, which account for stress and strain-level depending stiffnesses and which distinguish between loading and unloading, computations were carried out for relatively simple material models with a constant Young's modulus  $E$  both for loading and unloading. Such simple models will give appropriate results for structural forces but surface settlements will by no means be computed realistically when not accounting for the unloading stiffness. In order to account to some extent for the unloading and the small strain in the deep ground below the tunnel, a two-layer mesh as shown in Fig. 4.38 was used for all analyses and the deep ground layer was taken much stiffer than the upper layers. For the present case it was appropriate to increase the stiffness by a factor of eight.

The lining shell elements were simulated by using a linearly elastic model. The increase of the shotcrete lining stiffness  $E_l$  with time has been accounted for by using a stepwise increase with excavation phases. In practice time effects of shotcrete such as creep are commonly accounted for by reducing the final lining stiffness to 50% of the stiffness of a 28 days old concrete. In Germany often a concrete C20/25 (German design code DIN 1054-1) is used, which has a 28-days Young's modulus of around  $30,000\text{MN}/\text{m}^2$ . To account for the low stiffness of the very fresh shotcrete, usually the stiffness is once more reduced by a factor of two.

For the three-dimensional analyses an initial stiffness of  $E_{1l} = 7500\text{MN}/\text{m}^2$  in the first lining ring behind the tunnel heading was applied, which was then increased to  $E_{2l} = 15000\text{MN}/\text{m}^2$  for all subsequent lining rings. These Young's moduli were converted into data of the normal stiffness and the flexural rigidity to obtain  $E_{1l}A = 2250\text{MN}$ ,  $E_{2l}A = 4500\text{MN}$  and  $E_{1l}I = 16.875\text{MNm}^2$ ,  $E_{2l}I = 33.75\text{MNm}^2$ . In the two-dimensional analyses no increase of lining stiffness was modelled, considering only the final flexural rigidity  $E_{2l}I$  and final normal stiffness  $E_{2l}A$ .

#### 4.8.4 Linear elastic analyses

First of all a linear elastic constitutive model for the ground behavior has been used to investigate the influences of ground stiffness  $E$ , tunnel diameter  $D$  and round length  $d$  on  $\beta$ . All analyses were carried out for situations without ground water. A unit weight of  $\gamma = 20\text{kN}/\text{m}^3$  and a Poisson's ratio of  $\nu = 0.3$  was taken for all analyses. Moreover, results have been obtained from a tunnel with a depth of  $H = 24.5\text{m}$  and  $K_0 = 0.67$ . Full bonding between lining and ground has been assumed.

Fig. 4.39 shows computed normal forces and bending moments from a 3D analysis after an excavation of  $50 \cdot d$ . The structural force distributions shown in Fig.4.39 approach a steady-state solution after a total excavation length of about  $10 \cdot d$ . In order to compute  $\beta$ -values for the two-dimensional analyses the average steady-state value of these zigzag distributions (thick lines in Fig.4.39a and b) has been considered.

Fig. 4.40 presents results for the unloading factor from linear elastic analyses. The results shown here were obtained from a tunnel with  $D = 7\text{m}$ , but are also valid for  $D = 9\text{m}$  and  $D = 11\text{m}$ . Fig. 4.40 shows the influence of ground stiffness and round length on the unloading factor. Both for structural forces and settlements the unloading

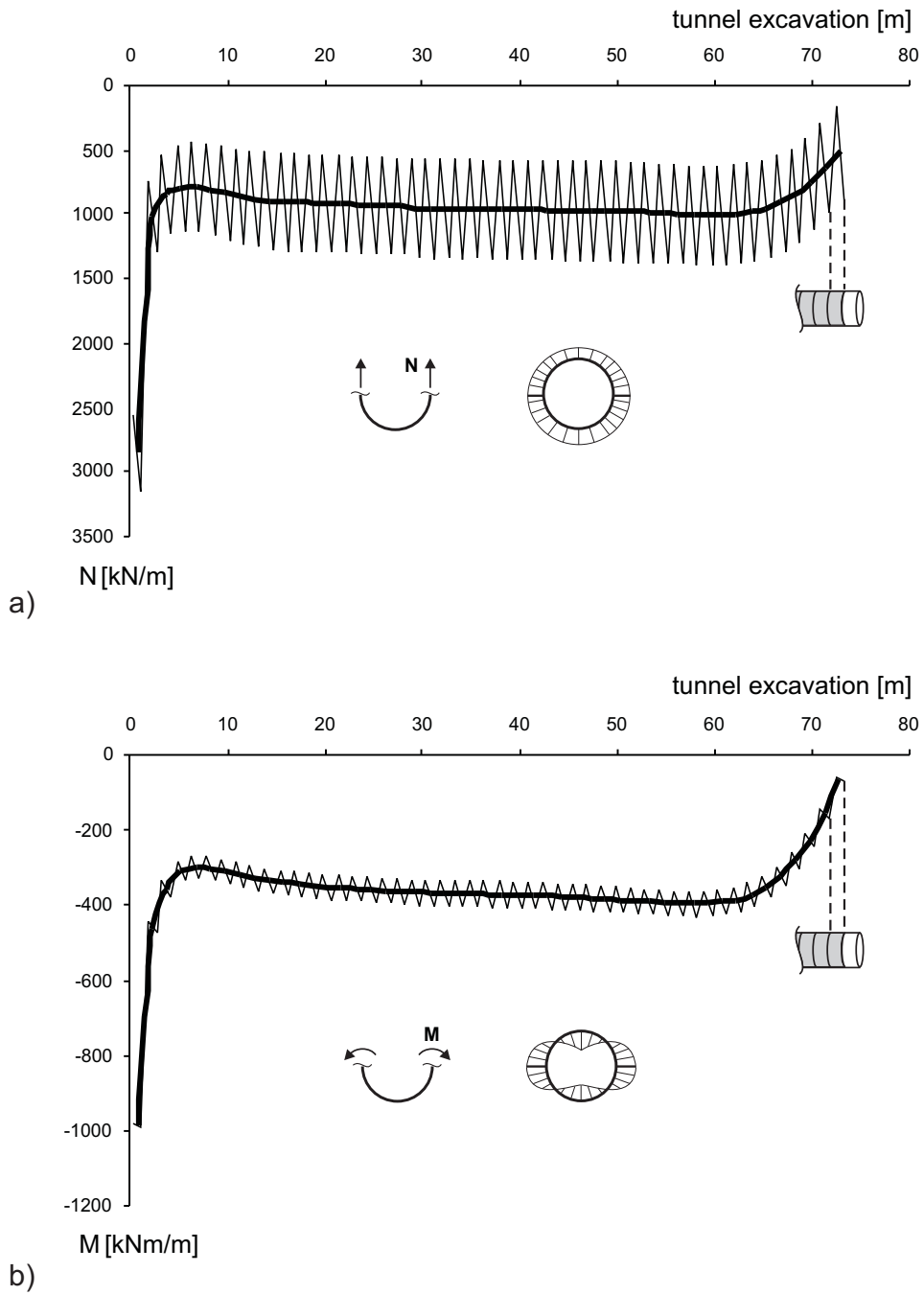


Figure 4.39: Evaluation of three-dimensional lining forces: a) normal forces, b) bending moments

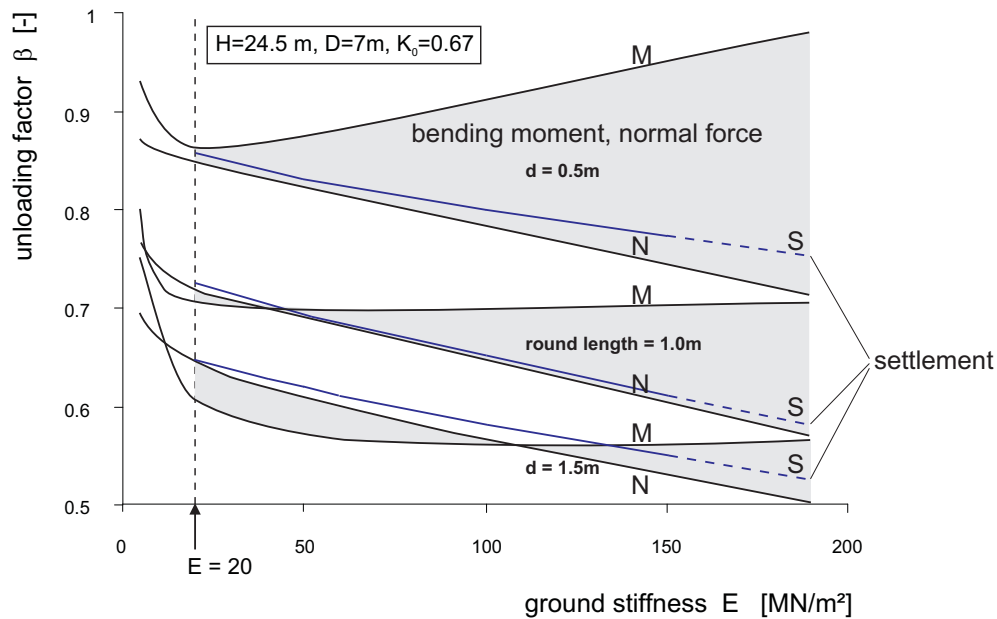


Figure 4.40: Influence of ground stiffness and round length for linear elastic ground

factor is decreasing with increasing round length. This seems logical as a tunnel without a lining, i.e.  $d = \infty$ , has an unloading factor of  $\beta = 0$  (no forces in the lining). Because of different unloading factors for bending moments and normal forces a band width for structural forces is plotted.

With increasing ground stiffness a decrease of unloading factors is observed. The  $\beta$ -values for settlements always remain within the bandwidth for structural forces. The elasticity calculations show the considerable influence of the round length on  $\beta$ . On considering for example a ground stiffness of  $E = 20 \text{ MN/m}^2$ , for a very short round length of  $d = 0.5 \text{ m}$   $\beta = 0.85$  is found, but a much lower value of  $\beta = 0.65$  is found for a long round length of  $d = 1.5 \text{ m}$ .

Elasticity computations give qualitative information on the  $\beta - d$  relationship and possibly quantitative information for tunnels in rock. Indeed, rock has a considerable shear strength and tunnelling will be dominated by the quasi elastic rock properties. On the other hand, soil has a relatively low shear strength and conventional tunnelling will be dominated by plastic deformation rather than quasi elastic deformation. Therefore plastic soil behavior is considered in the following section.

#### 4.8.5 Elasto-plastic analyses

Following the linear elastic evaluations the elasto-plastic Mohr-Coulomb Model (see Appendix A.1) has been used to determine the influences of the shear strength parameters. As for the linear elastic analyses situations without ground water were considered and the ground was modelled with  $\gamma = 20 \text{ kN/m}^3$ ,  $E = 20 \text{ MN/m}^2$  and  $\nu = 0.3$  Dilation

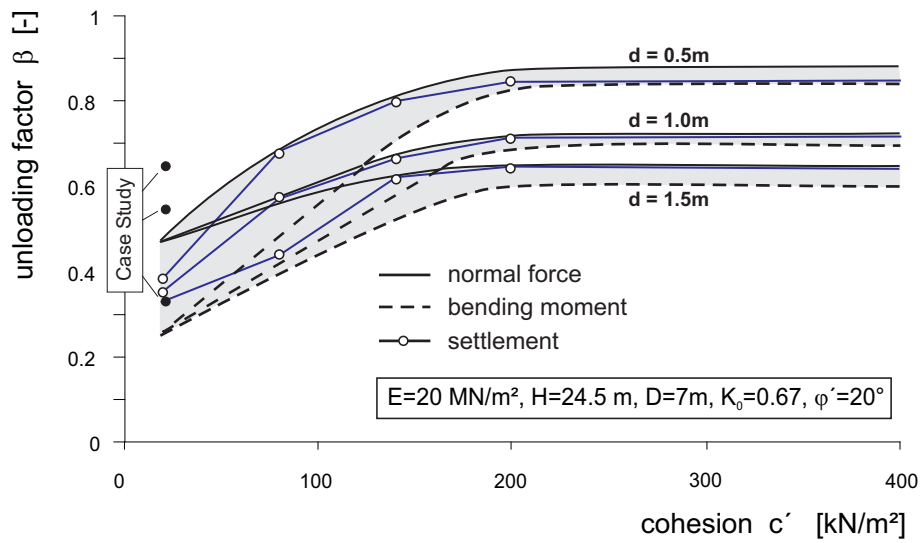


Figure 4.41: Influence of friction angle, cohesion and round length for elasto-plastic ground

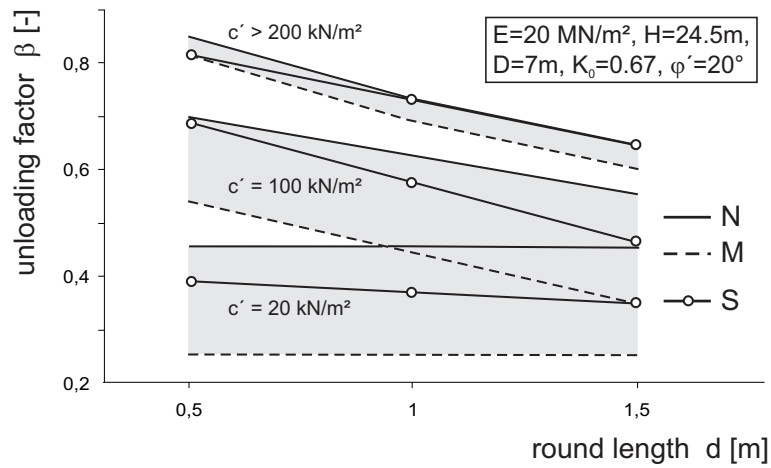


Figure 4.42: Influences of round length and cohesion

was neglected by using a dilatancy angle equal to zero. The coefficient of lateral earth pressure was taken as  $K_0 = 0.67$ .

A variation of the friction angle was carried out by considering  $\varphi' = 20^\circ, 30^\circ$ , and  $40^\circ$ . For this realistic range of friction angles, their influence appeared to be relatively small. Fig.4.41 shows computed unloading factors as a function of the effective cohesion for different round lengths. With increasing cohesion the computed  $\beta$ -values approach a horizontal plateau that corresponds to the linear elastic solution for  $E = 20MN/m^2$  shown in Fig. 4.40, indicating that the analyses with  $c \geq 200kN/m^2$  behave fully elastic. Up to  $c' = 200kN/m^2$  Fig.4.41 shows a significant influence of the cohesion, i.e. for tunnels in soft to hard soils. Here, the  $c - \beta$ -relationship is nearly linear. Beyond an effective cohesion of  $200kN/m^2$ , i.e. for tunnels in rock, the cohesion plays no role at all.

The information of Fig.4.41 is also plotted in Fig.4.42, but this time  $\beta$  is plotted as a function of the round length. Again one observes that the unloading factor decreases when cohesion decreases and when the round length increases.

#### 4.8.6 Case study of a subway tunnel

A subway tunnel, which will be described in detail in Section 5.1, has been taken to evaluate unloading factors for both surface settlements and structural forces in order to compare them to the findings of the present study.

Comparing  $2D$  and  $3D$  elastoplastic analyses of Steinhaldenfeld tunnel, the best fit for a  $2D$  settlement analysis was found for  $\beta = 0.34$  and structural forces were best matched with  $\beta = 0.54$  for the bending moment and  $\beta = 0.64$  for the normal force. Again it becomes obvious that different unloading factors for settlements, bending moments and normal forces have to be used. The  $\beta$ -value for the surface settlement of Steinhaldenfeld tunnel perfectly matches the present study of Fig. 4.41 but unloading factors for structural forces are larger than the results obtained. However, this is demonstrating clearly, that unloading factors can not be transferred directly to different tunnelling projects with different boundary conditions, without reconsidering at least details of FE-installation procedures, ground profiles and tunnel geometry. Most probably unloading factors for the hoarse shoe profile of this particular tunnel can not be compared to previous solutions of unloading factors for circular tunnels, because structural forces are strongly influenced by the shape of the lining cross-section. The simulation of the settlement trough and the analysis of structural forces of Steinhaldenfeld-tunnel will be considered in detail in Section 5.1.

#### 4.8.7 Conclusions on unloading factors

In order to incorporate effects of  $3D$  tunnel installation,  $2D$  FE-analyses are applied in combination with an empirical load reduction factor. This factor represents roughly the portion of the initial ground pressure that is carried by the lining. For assessing this factor, series of  $2D$  and  $3D$  FE-analyses have been performed.

The load reduction factor was found to decrease as a function of ground stiffness.

Moreover, it was found that the reduction factor decreases with decreasing cohesive strength and increasing round length. In contrast to these findings, it was somewhat surprising to find that the soil friction angle has relatively little influence on the load reduction factor, but this is an issue of further research as relatively few variations were carried out.

In the presented studies the coefficient of lateral earth pressure at rest was modelled by the correlation  $K_0 = 1 - \sin \varphi'$ . As has been discussed in Section 4.4.2, larger  $K_0$ -values have a considerable effect on two- and three-dimensional bending moments and thus different unloading factors for higher  $K_0$ -values would have to be considered. Such effects will be more significant for overconsolidated ground, but this has not been considered in these studies.

In the present studies effects of tunnel depth  $H$  and tunnel diameter  $D$  have not been discussed in detail. However, variations that were carried out on the relative tunnel depth  $H/D$  showed that unloading factors slightly decrease with increasing  $H/D$ .

Considering load reduction factors it has been shown that it is not suitable to use one single  $\beta$ -value for bending moments, normal forces and settlements. Instead one needs to use three different values in order to compute both structural forces and settlements precisely.

The load reduction factor for settlements of the Steinhaldenfeld tunnel with a non-circular cross-section in layered ground perfectly matches findings for circular tunnels, whereas load reduction factors of structural forces were found to be somewhat larger. This makes it clear that  $\beta$ -values should be handled with care as they vary with tunnel geometries and/or ground conditions. In particular structural forces will be heavily influenced by the geometry of the tunnel cross-section. Moreover, influences of securing means like anchors etc. or complex ground layering as adopted for the present case study may play an important role, but they have not been evaluated. Indeed, the aim of the present study on  $\beta$ -values was to give a qualitative insight into the matter, rather than coming up with quantitative numbers. For practice, it may be advisable to perform at least a single 3D analysis. For further two-dimensional analyses such a three-dimensional analysis may serve as a reference in order to assess appropriate unloading factors.

For circular tunnels in homogeneous ground with round lengths of 0.5 - 1.5m the settlements are well matched when using  $\beta$ -values between 0.3 and 0.4. For bending moments approximately the same values are found, as long as the ground cohesion is below  $50kN/m^2$ . For a particular non-circular tunnel however, the bending moment was matched with  $\beta = 0.54$  and it would seem that low  $\beta$ -values are not appropriate for bending moments. A conservative approach for structural forces would be to use  $\beta$ -values of at least 0.5 – 0.7 in soil.

#### 4.8.8 A fast 3D analysis for unloading factors of settlement

In the previous section it has been shown that the proper prediction of two-dimensional settlements and lining forces requires the assessment of three different unloading fac-

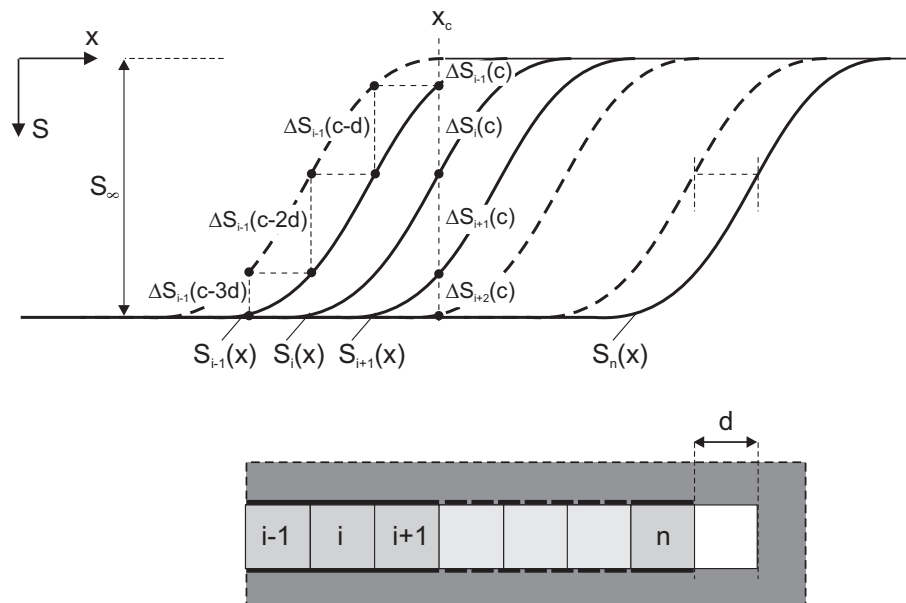


Figure 4.43: Longitudinal settlement curve above advancing tunnel excavation

tors for settlements, bending moments and normal forces respectively. In order to do so, a full three-dimensional analysis is required. Even with the increase of present computer capacities such three-dimensional analyses are still time consuming. When analyzing settlements separately from lining forces, e.g. for an estimate of tunnel induced deformation to existing structures, the unloading factor for surface settlements may be assessed in a fast way. To avoid long lasting computations as are needed to arrive at the steady-state settlement solution in a 3D calculation, a fast way of settlement analysis was developed. Instead of performing the time consuming method of step-by-step installation this analysis requires only two calculation phases. This way of analysis makes it possible to arrive at the three-dimensional steady-state solution in a smart way, at least for settlements.

**The fast settlement analysis** Observations from practice have shown that the distribution of the longitudinal settlement curve has the shape of an s-curve (MAIR and TAYLOR, 1997) as shown in Fig. 4.43. The shape of this curve remains constant but is translated by one round length  $d$  during every excavation. In such a case the position of the settlement curve can be related to the respective excavation step  $i$ , denoting the corresponding surface settlement profile as  $S_i(x)$ , with  $i = 1, 2, 3, \dots, n$ .

If settlements have reached the steady-state,  $S_i$  is not further increasing. Hereafter every additional excavation step leads to the same settlement increment. Considering  $x_c$  as a control point, located at the surface before tunnel excavation, the settlement increments during excavations  $i$  in this point occur in the order  $\Delta S_1(x_c), \Delta S_2(x_c), \dots, \Delta S_{i-1}(x_c), \Delta S_i(x_c), \Delta S_{i+1}(x_c), \dots, \Delta S_n(x_c)$  caused by the translating settlement curve  $S_1(x), S_2(x), \dots, S_{i-1}(x), S_i(x), S_{i+1}(x), \dots, S_n(x)$ .



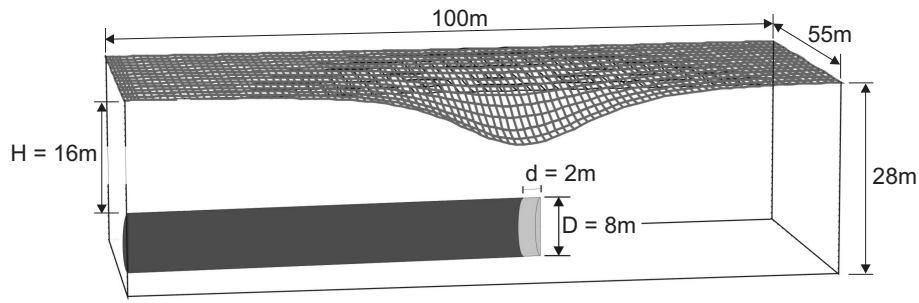


Figure 4.44: Settlement crater from all-in-once installation

Fig. 4.43 illustrates that all respective settlement increments  $1, 2, \dots, i - 1, i, i + 1, \dots, n$  at location  $x_c$  can also be obtained from one single increment  $i - 1$  at translated locations of the order

$$\begin{aligned} \Delta S_i(x_c) &= \Delta S_{i-1}(x_c - d) \\ \Delta S_{i+1}(x_c) &= \Delta S_{i-1}(x_c - 2d) \\ &\vdots \\ \Delta S_{i+n}(x_c) &= \Delta S_{i-1}(x_c - (n + 1) \cdot d). \end{aligned} \quad (4.15)$$

For a general use the settlement at any location  $x$  after a number of  $i$  excavations can be obtained from the settlement increment  $i - 1$  (or any other steady state increment accordingly). This can be expressed as

$$S_i(x) = \sum_{k=1}^i [\Delta S_{i-1}(x - (k + 1) \cdot d)] \quad (4.16)$$

and the final steady state settlement yields

$$S_\infty(x) = \lim_{i \rightarrow \infty} S_i(x). \quad (4.17)$$

For performing the fast 3D analysis the steady-state settlement increment  $i - 1$  may be obtained from a 3D FE-analysis.

**The all-in-once installation** The first phase is used to install a complete tunnel. To this end soil elements are switched off and lining elements are switched on up to the estimated steady-state length of the longitudinal settlement trough. The steady-state length is the length of the tunnel that has to be excavated in order to reach the steady state depth of the settlement trough. The second phase is used to model a single excavation with one unsupported round length  $d$  and all previous displacements are reset to zero. One will now compute a more or less circular settlement crater as indicated in Fig. 4.44. Finally it should be noted that the all-in-once installation does not require such a fine mesh as needed for the step-by-step analysis. When computing the settlement crater after two computational phases as described above, the fine mesh is only needed around

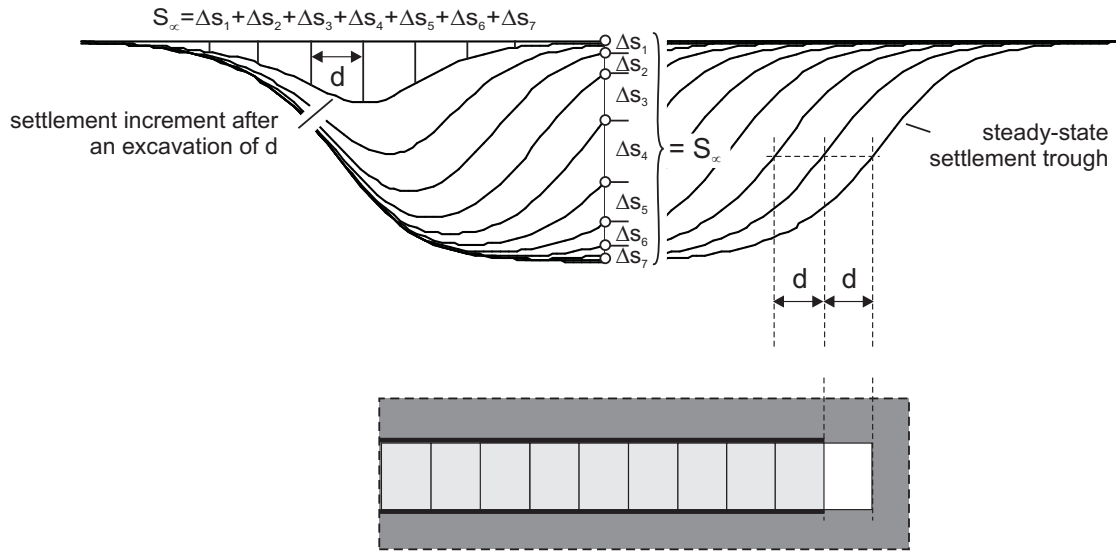


Figure 4.45: Development of longitudinal settlement curve from FE-step-by-step installation

the tunnel heading in the middle of the mesh block. Towards the mesh boundaries the element size can be gradually increased.

In order to obtain results from the all-in-once installation, the circular tunnel as shown in Fig.4.44 was analyzed. To simulate the settlement trough of this tunnel a block of  $100m \times 55m \times 28m$  was divided into 4300 volume elements with a total of 13151 nodes. The parameters for the Mohr-Coulomb Model were taken  $E = 42MPa$ ,  $\nu = 0.25$ ,  $c' = 20kPa$ ,  $\varphi' = 20^\circ$ ,  $\psi = 0$  and  $K_0 = 1 - \sin \varphi'$ . A circular tunnel with a diameter of  $D = 8m$  and a cover of  $H = 16m$  was modelled in a symmetric half with an unsupported excavation length of  $d = 2m$ . The shotcrete lining had a thickness of  $30cm$ , a Young's Modulus of  $E = 20GPa$  and a Poisson's ratio of  $\nu_l = 0$ . The steady state settlement for the circular tunnel computed from the fast 3D analysis was  $S = 3.92cm$  which compares well to the finding of  $S = 3.81cm$  from a full 3D step-by-step installation including a difference of only 2.9%. The step-by-step installation (Section 4.5.1) may be used, to proof Eqs. 4.16 and 4.17.

Fig. 4.45 shows results of steady-state analysis, using the three-dimensional step-by-step installation. Settlement curves have been obtained from a sufficiently large 3D mesh and it has been checked, whether or not steady-state was reached. Independent of the constitutive model being used in the analysis, steady-state should be reached after a certain number of excavations. For higher order constitutive models, which adopt non-linear ground behavior associated with a relatively high portion of plasticity, steady-state might need considerably more excavation phases than e.g. linear elasticity or the Mohr-Coulomb Model.

After reaching steady-state in the present analysis, all displacements were reset to zero. The next excavation phase resulted in a single settlement increment, having the

shape of a settlement crater as shown in Fig.4.45. As indicated in this figure, such a settlement crater may be used to obtain the final settlement value  $S_{\infty}$ . Indeed, adding some several settlement craters by carrying on the step-by-step analysis finally results in the steady-state settlement curve.

# Chapter 5

## Tunnel case studies

### Introduction

This chapter describes two case studies. The first case study considers a conventionally driven tunnel and the second case study analyzes a slurry shield tunnel. The particular importance of installation procedures will be highlighted, whilst constitutive models also play an important role. Conclusions will be given by comparing results of numerical analyses to measured data of both surface settlements and horizontal ground movements.

### 5.1 Steinhaldenfeld conventionally driven tunnel

The Steinhaldenfeld tunnel is located in the north-eastern part of the city of Stuttgart, Germany. With the begin of the tunnel construction in April 2002 an extension of the cities subway system was commenced. The tunnel construction was completed in late 2004 and for the first time operated in early 2005. Fig. 5.1 shows a site plan of Steinhaldenfeld tunnel. The construction of this tunnel was carried out between the old station Hauptfriedhof and the new station Steinhaldenfeld, including two cut and cover parts of each 110m length at the tunnel portals and a conventionally constructed part of 940m length in between. The entire tunnel length is 1060m. Fig. 5.2 shows the top heading cross-section of Steinhaldenfeld tunnel with a zone around the tunnel which was stabilized by anchors. The top heading was excavated over the entire length of

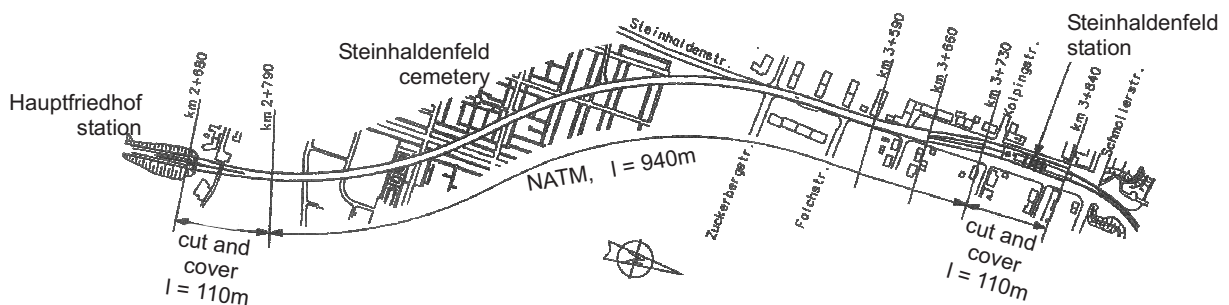


Figure 5.1: Site plan of Steinhaldenfeld tunnel (TIEFBAUAMT STUTTGART)

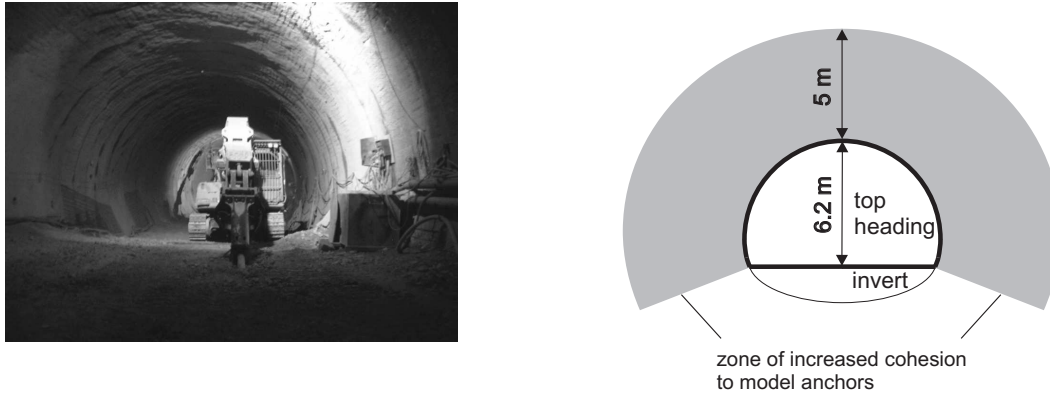


Figure 5.2: Cross-section of Steinhaldenfeld tunnel

940m, followed later by the excavation of the invert. An initial length of 120m will be considered in the numerical analyses for the simulation of the top heading excavation.

### 5.1.1 3D FE-analyses

The three-dimensional FE-analyses of the Steinhaldenfeld tunnel were carried out for a mesh block of 120m length, 40m width and 26m height, as shown in Fig. 5.3. The ground is described with 15-noded wedge elements with a length of 1.2m, being equal to the unsupported round length of the tunnel. The top layer is a manmade fill underlain by two layers of Keuper Marl. This heavily weathered soft rock is underlain by strong limestone, which stiffness is approximately ten times larger than the stiffness of the marl layers on top. Considering its high stiffness the FE-mesh was not extended into the limestone. Mohr-Coulomb parameters as listed in Tab. 5.1 were available from site investigation (MÖLLER et al., 2004; ROGOWSKI, 2004). The Stuttgart Keuper Marl might be classified both as a residual soil or as a (sometimes heavily) weathered soft rock. In such a ground measurements of the initial horizontal stress are extremely difficult to perform; both in case of in situ borehole measurements as well as in case of laboratory tests on (disturbed) samples. Moreover, correlations as presented in Section 4.4.1 came from data of sedimentary clays rather than residual soils. Existing data for Stuttgart Keuper Marl would seem to suggest that horizontal stresses are well above those of a normally consolidated soil, but with  $K_0$  around unity also well below those of a heavily overconsolidated sedimentary clay.

To simulate drained ground behavior in the 3D analyses the HS Model (see Appendix A.2) was considered. Because the HS-Small Model (see Appendix A.3) was not yet operational in 3D, it was only considered in the 2D analyses (Section 5.1.2). Ground parameters of the HS and the HS-Small Models are listed in Tab. 5.2<sup>1</sup>. The Poissons ratio  $\nu_{ur}$  for unloading/reloading and the stiffness exponent  $m$  have been obtained from

<sup>1</sup>For a full description of the HS- and the HS-Small models and their performance in drained and undrained triaxial tests, the reader is referred to BENZ (2006).

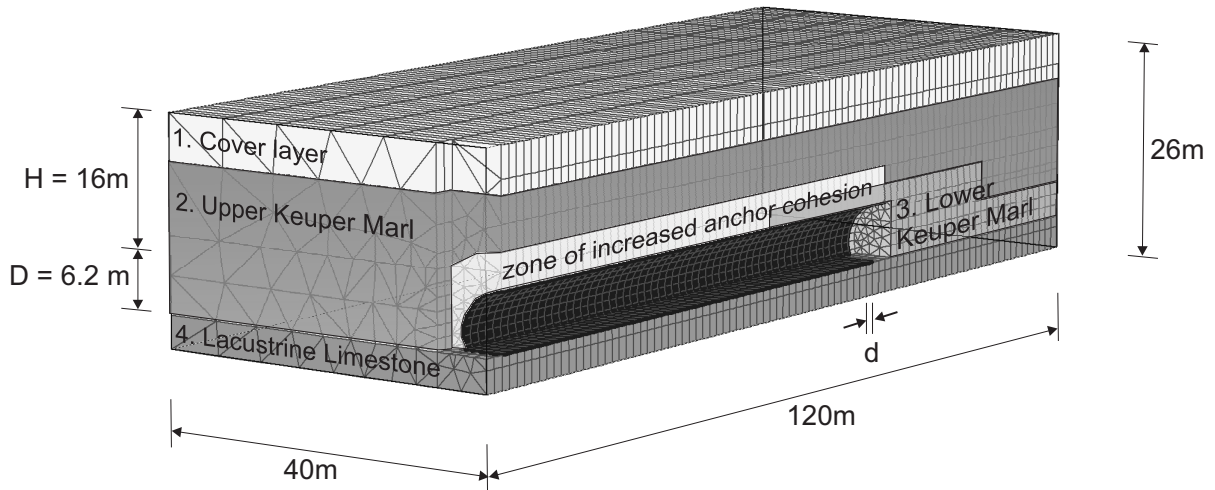


Figure 5.3: Three-dimensional mesh of Steinhaldenfeld tunnel

HORNIG and BUCHMAIER (2005), who performed both triaxial and oedometer laboratory tests on Stuttgart Keuper Marl. The stress dependent Young's modulus  $E_{ur}^{ref}$  for unloading/reloading has been calculated from the Young's modulus in Tab. 5.1<sup>2</sup>, considering the stresses acting in the middle of ground layers and using Eq. A.16 from Appendix A.2. The laboratory tests on weathered Keuper Marl carried through by HORNIG and BUCHMAIER (2005) showed a stiffness ratio of  $E_{ur}^{ref}/E_{oed}^{ref}$  of three and this was used to obtain the stress dependent oedometer modulus  $E_{oed}^{ref}$ . In addition it was assumed that  $E_{50}^{ref} \approx E_{oed}^{ref}$  for hard soils SCHANZ (1998). For the parameters of the HS-Small Model a review of correlations is given by BENZ (2006). For the small strain stiffness in Tab.5.2 the correlation  $E_0[MPa] = 140/e \cdot \sqrt{p'/p_{ref}}$  by BIAREZ and HICHER (1994) has been used, where  $e$  is the void ratio,  $p'$  is the mean effective stress in  $kPa$  and  $p_{ref} = 100kPa$ . Data on the void ratio  $e$  have been obtained from laboratory tests on Stuttgart Keuper Marl by HORNIG and BUCHMAIER (2002). For  $p' = p_{ref}$  the correlation of BIAREZ and HICHER reduces to  $E_0[MPa] = E_0^{ref} = 140/e$ , and  $E_0^{ref}$  can be converted into  $G_0^{ref}$  using linear elasticity with  $G = E/(2 + 2\nu_{ur})$ . For the threshold shear strain  $\gamma_{0.7}$  a correlation chart to the soils plasticity index (BENZ, 2006) has been used.

The tunnel was built above the groundwater level and therefore groundwater was not considered in the FE-analyses. Directly around the tunnel the ground was improved by nails and this was numerically accounted for by an increase of the cohesion of  $25kPa$ . The sprayed concrete lining was modelled linear elastically with an unit weight of  $\gamma = 24kN/m^3$  and a thickness of  $25cm$ . To account for hardening of the lining, the stiffness was increased stepwise, using a Young's modulus for fresh shotcrete of  $E = 7,5GN/m^2$  for the first three lining rings behind the tunnel face and  $E = 15GN/m^2$  for the older shotcrete of the rest of the lining. The lining was modelled by shell elements

<sup>2</sup>Please note that Young's moduli in Tab. 5.1 are for unloading/reloading.

layer	$\gamma$ [kN/m <sup>3</sup> ]	$\nu$ [–]	$E$ [MPa]	$c'$ [kPa]	$\varphi'$ [°]	$K_0$ [–]
1	20	0.37	15	10	25	0.57
2	24	0.2	100	25	25	0.9
3	23	0.35	60	25	25	0.9
4	23	0.2	750	200	35	0.6

Table 5.1: Steinhaldenfeld ground parameters of the MC-Model

layer	$\nu_{ur}$ [–]	$E_{oed}^{ref}$ [MPa]	$E_{50}^{ref}$ [MPa]	$E_{ur}^{ref}$ [MPa]	$G_0^{ref}$ [MPa]	$\gamma_{0.7}$ [%]	$m$ [–]
1	0.2	10	10	30	75	$2 \cdot 10^{-4}$	0.5
2	0.2	33	33	100	250	$2 \cdot 10^{-4}$	0.4
3	0.2	16	16	48	120	$2 \cdot 10^{-4}$	0.4
4	0.2	190	190	575	1438	$2 \cdot 10^{-4}$	0.3

Table 5.2: Additional ground parameters as used for the HS- (see Appendix A.2) and the HS-Small Model (see Appendix A.3).  $G_0^{ref}$  and  $\gamma_{0.7}$  are parameters used in the HS-Small model.

and previous lining data was converted into corresponding values of the flexural rigidity  $E_l I$  and the normal stiffness  $E_l A$ . To simulate the excavation of the hoarse shoe shaped top heading, the step-by-step-excavation was applied (Section 4.5.1) with a round length of  $d = 1.2m$ <sup>3</sup>.

**Structural forces** Fig. 5.4 shows results of bending moments and normal forces at the upper part of the tunnel wall after 57 excavation steps. Normal forces show a zigzagging between about  $1000kN/m$  at the front of a lining ring and  $600kN/m$  at the back of a lining ring. At the tunnel heading the normal force has not yet reached the average value of about  $800kN/m$ . Instead a lower value of about  $300kN/m$  is obtained. This decrease of the normal force towards the tunnel heading is logical, as lining forces build up due to further cutting, while the three-dimensional state of stress gradually changes into a two-dimensional state. The highest normal forces are observed at the entrance of the tunnel. Here arching around the initial excavation could hardly occur as the left side of the mesh was free to displace and a horizontal active earth pressure (earth pressure according to

<sup>3</sup>A numerical  $\varphi$ -c-reduction analysis gave a factor of safety against face instability of around  $\eta = 1.4$ .

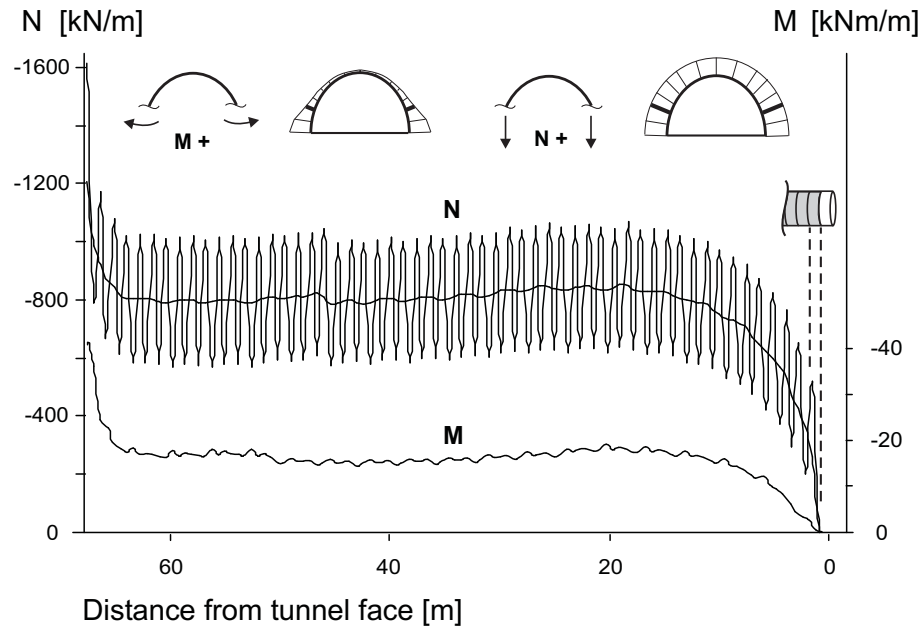


Figure 5.4: 3D bending moments and normal forces of Steinhaldenfeld tunnel

German design code DIN 4085) as shown in Fig. 5.5 was applied to simulate a soldier pile wall.

Just like the normal forces the bending moments in Fig. 5.4 show a zigzagging pattern that matches the step-by-step excavation, but the magnitude of this zigzagging is considerably smaller than for normal forces. This is most probably related to the use of the relatively high  $K_0$ -values, as has been discussed in Section 4.4.2. Near the tunnel heading vanishing small bending moments around zero are found. However, with the advance of the tunnel face the bending moment reaches a relatively small value of about  $15 \text{ kNm/m}$ .

**Surface settlements** Fig. 5.6 shows measured settlements above the tunnel center line as well as computational results. For this particular tunnel, the measurements do not show a horizontal steady-state line, as the ground profile changes significantly along the axis of the tunnel. Moreover, the construction of a soldier-pile wall prior to tunnel excavation has led to large additional settlements, as shown in the left of Fig. 5.6.

The HS Model involves a yield cap which position is controlled by the preconsolidation pressure as explained in Appendix A.2. In addition there is a more or less conical shear yield surface around the space diagonal in principal stress space, as illustrated in Fig. A.3. For a normally consolidated soil with  $OCR = 1$  the model will predict plastic yielding from the onset of loading. For  $OCR > 1$  and  $K_0 > K_0^{NC}$  both the cap and the shear yield surface will be initially positioned some distance away from the initial stress, and the model predicts initially elastic strains. As a consequence  $OCR$  is an important input parameter. Weathered Keuper Marl may have characteristics of a heavily overcon-



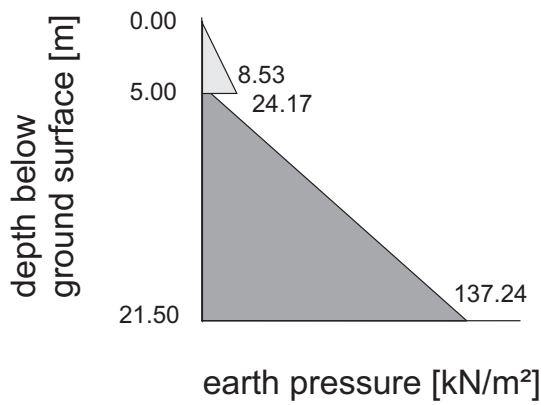


Figure 5.5: Active earth pressure to simulate soldier pile wall

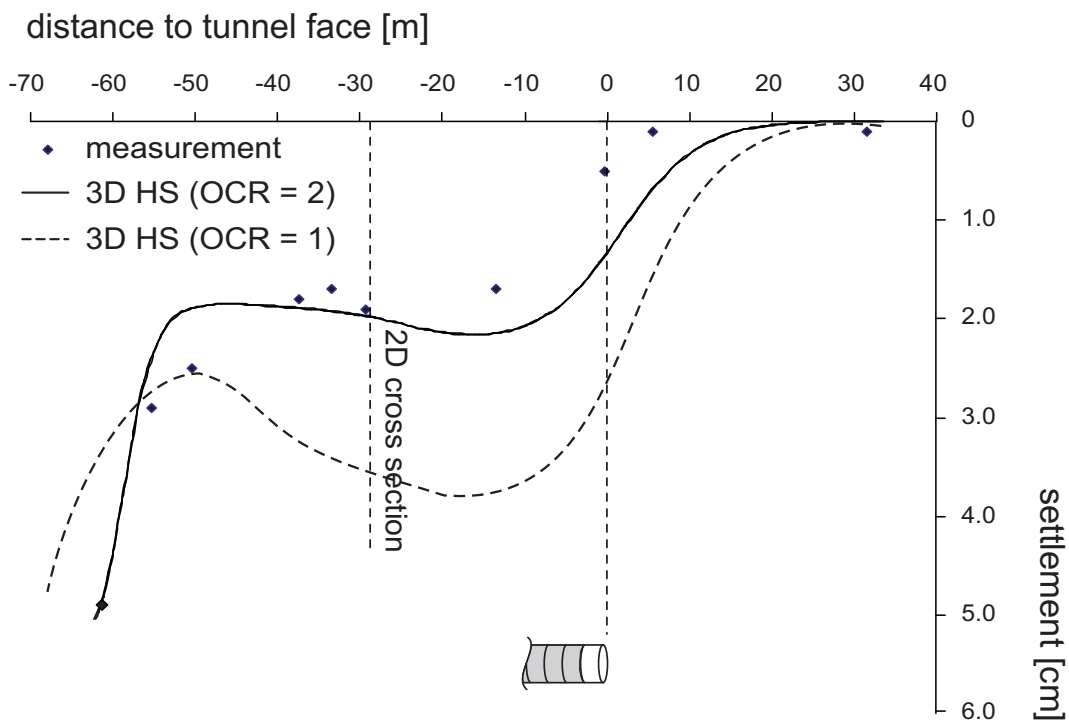


Figure 5.6: 3D longitudinal surface settlements of Steinhaldenfeld tunnel

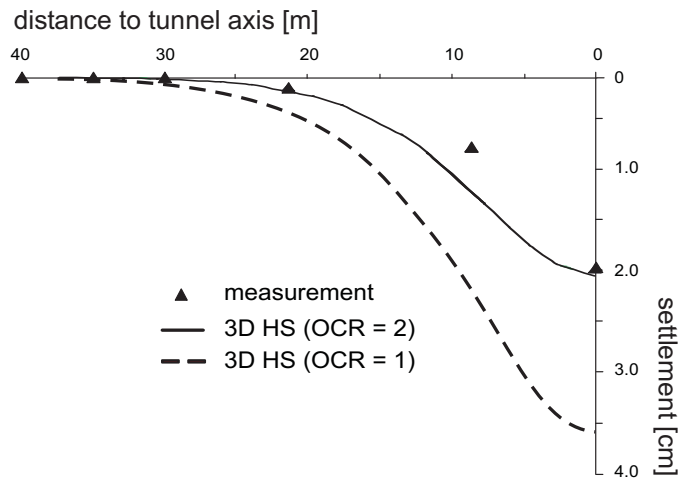


Figure 5.7: 3D transverse surface settlements of Steinhaldenfeld tunnel

solidated soil, but in many aspects it behaves rather like a normally consolidated soil. Indeed, relative to unloading/reloading initial loading gives a soft response and one is tempted to model this behavior by initializing  $OCR$  as unity. However, on the very onset of loading most in situ soils (BENZ, 2006) tend to show a high "small-strain stiffness", being not directly incorporated in the HS Model. This may be modelled by expanding the initial position of the yield surfaces somewhat beyond the existing initial stress. In the present analysis this will be done by using  $OCR = 2$ .

However, to demonstrate the importance of  $OCR$  the settlement analyses shown in Fig. 5.6 were also carried out for a normally consolidated ground ( $OCR = 1$ ). In the HS Model the initially stiffer response of overconsolidated grounds is accounted for by the unloading-reloading Young's modulus  $E_{ur}$ . The softer ground response, associated with material hardening takes place, when stresses exceed the preconsolidation pressure (compare Section A.2).

Fig. 5.6 shows that the analysis for a normally consolidated ground ( $OCR = 1$ ) clearly yields too large settlements but good agreement with measurements is obtained for the overconsolidated ground with  $OCR = 2$ . Fig. 5.7 shows the computed cross-section of the settlement trough. This figure also shows that the settlements of a normally consolidated ground overestimate the measurements, whereas the analysis with  $OCR = 2$  yields basically the correct settlements.

### 5.1.2 2D FE-analyses

Fig. 5.8 shows a two-dimensional FE-mesh of the Steinhaldenfeld tunnel. The mesh consists of 6-noded triangular elements and its dimensions correspond to the cross-section of the three-dimensional FE-mesh in Fig. 5.3. Drained ground behavior was modelled

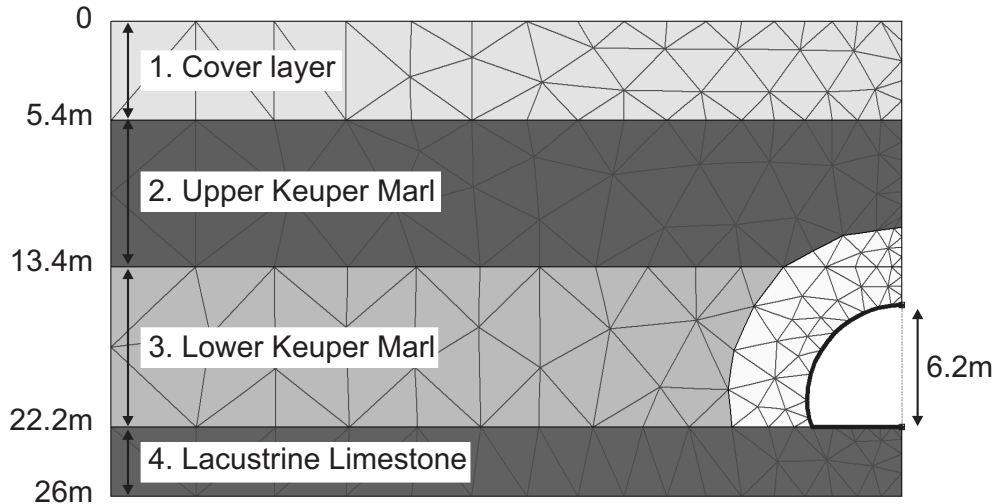


Figure 5.8: 2D FE-mesh of Steinhaldenfeld tunnel

with the MC, the HS and the HS-Small Model<sup>4</sup> with parameters given in Tables 5.1 and 5.2. Please note that for the MC Model the stiffnesses for unloading-reloading have been considered as the ground was heavily overconsolidated. Because stiffness is stress level dependent and this is not accounted for by the MC Model, the values of  $E$  given in Table 5.1 have been adjusted to the stress level acting in the middle of the respective layers (compare Section 4.8.3). The values of  $E_{ur}^{ref}$  as used for the HS and the HS-Small Model (Table 5.2) are reference values and are thus different from the absolute stiffnesses of the MC Model. The shell elements have a normal stiffness of  $E_t A = 10.5GN$ , a flexural rigidity of  $E_t I = 26.78MNm^2$  and a unit weight of  $\gamma = 24kN/m^3$ .

**Surface settlements** Fig. 5.9 shows results of measured and computed settlement troughs by using the stress reduction method. The best fit for the settlement analysis was found for unloading factors of  $\beta = 0.28$ ,  $\beta = 0.36$  and  $\beta = 0.3$ , meaning a stress reduction of around 70% for this particular conventionally driven tunnel, which is well above the usual assumption of a stress reduction of 50% ( $\beta = 0.5$ ). The HS-Small Model gives the best prediction, but the measured settlement trough is still slightly steeper.

Fig. 5.10 shows similar results for the normalized settlement troughs using the same unloading factors of  $\beta = 0.28$  for all three constitutive models. The HS-Small Model still gives the best prediction but the HS-curve considerably improves. Using a smaller unloading factor of  $\beta = 0.28$  for the HS Model increases the steepness of its settlement curve, but it also has a considerable effect on the magnitude of settlements, giving  $S_{max} = 4.0cm$  instead of  $2.0cm$ . This dependency of the shape of the settlement trough on unloading factors is also observed for the MC Model. Like the HS Model its settlement curve is becoming slightly steeper, but this time the change of the magnitude of

<sup>4</sup>For the elemental stress-strain behavior of the HS- and the HS-Small models, the reader is referred to BENZ (2006).

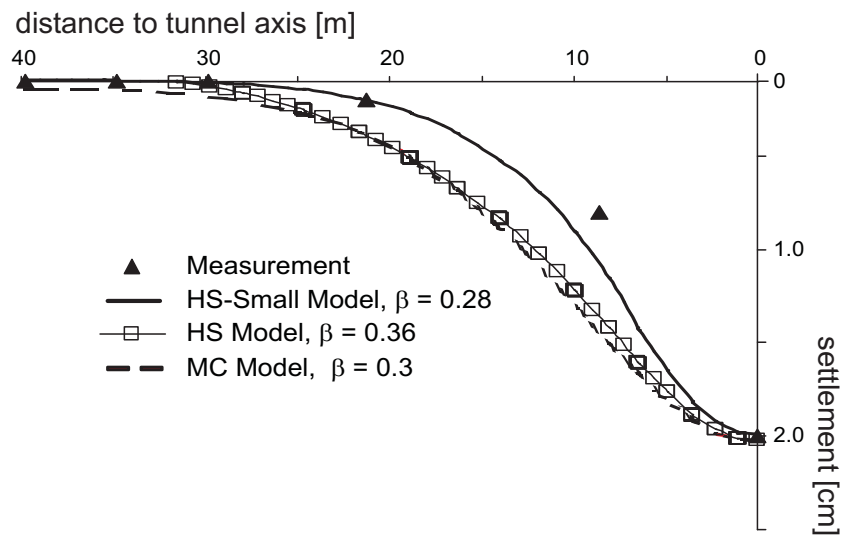


Figure 5.9: Settlement troughs from 2D analyses using the stress reduction method. The  $\beta$ -values are chosen such that 2D analyses match the measured settlement.  $K_0$  as indicated in Table 5.1.

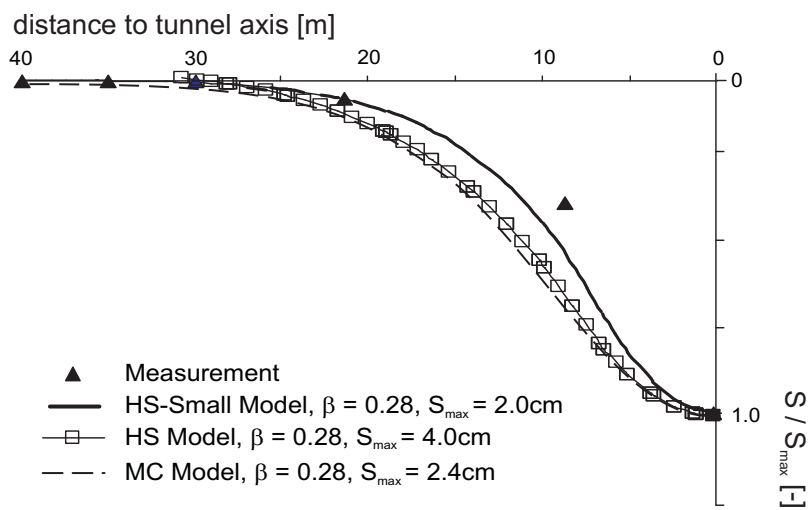


Figure 5.10: Normalized settlement troughs from 2D analyses with constant unloading factor

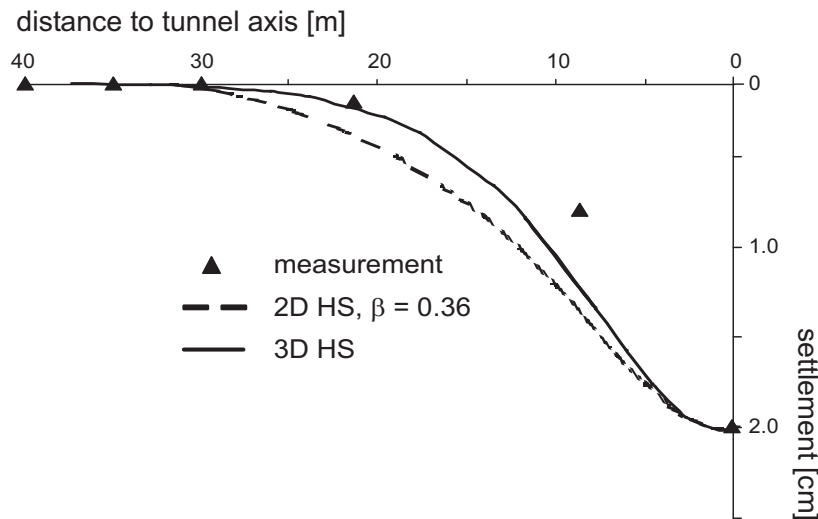


Figure 5.11: Comparison of surface settlements of 2D and 3D analyses

the settlement is somewhat smaller. Instead of the correct maximum settlement of  $2.0\text{cm}$  a value of  $S_{max} = 2.4\text{cm}$  is observed.

The effect that the measured settlement curve is more steep than the computed one has been discussed in Section 4.4.2. The statement by LEE and NG (2002) that 2D analyses in combination with large  $K_0$ -values tend to predict too wide settlement troughs when compared to 3D analyses was not observed in the studies of Section 4.4.2. In the present study, however, this effect is observed when comparing results of the HS Model from 2D and 3D analyses. Fig. 5.11 shows that the 3D analysis improves and gives a considerably steeper settlement trough, but it is believed that this is rather an effect of the non-constant 3D soil profile as well as the non-circular tunnel cross section being used in the present studies.

Moreover, the present results show that the use of the small-strain stiffness considerably improves results for the surface settlement trough, but the measured settlement curve still remains slightly steeper. Most probably this is related to the fact, that the material behavior of the Keuper Marl layers contains some anisotropy. However, this was not accounted for by the present studies and only isotropic constitutive models were applied to model the ground behavior. It is thus believed, that the additional consideration of the grounds anisotropy will further improve the results of the surface settlement trough.

**Structural forces** Fig. 5.12 shows results of structural forces of both 2D and 3D analyses using the HS Model. As three-dimensional structural forces oscillate within one ring of lining, maximum values from the front of a lining ring are plotted on the right side of the tunnel and rear-values are plotted on the left side of the tunnel. The 2D settlement analysis with  $\beta=0.36$  yields too low bending moments and normal forces almost by a

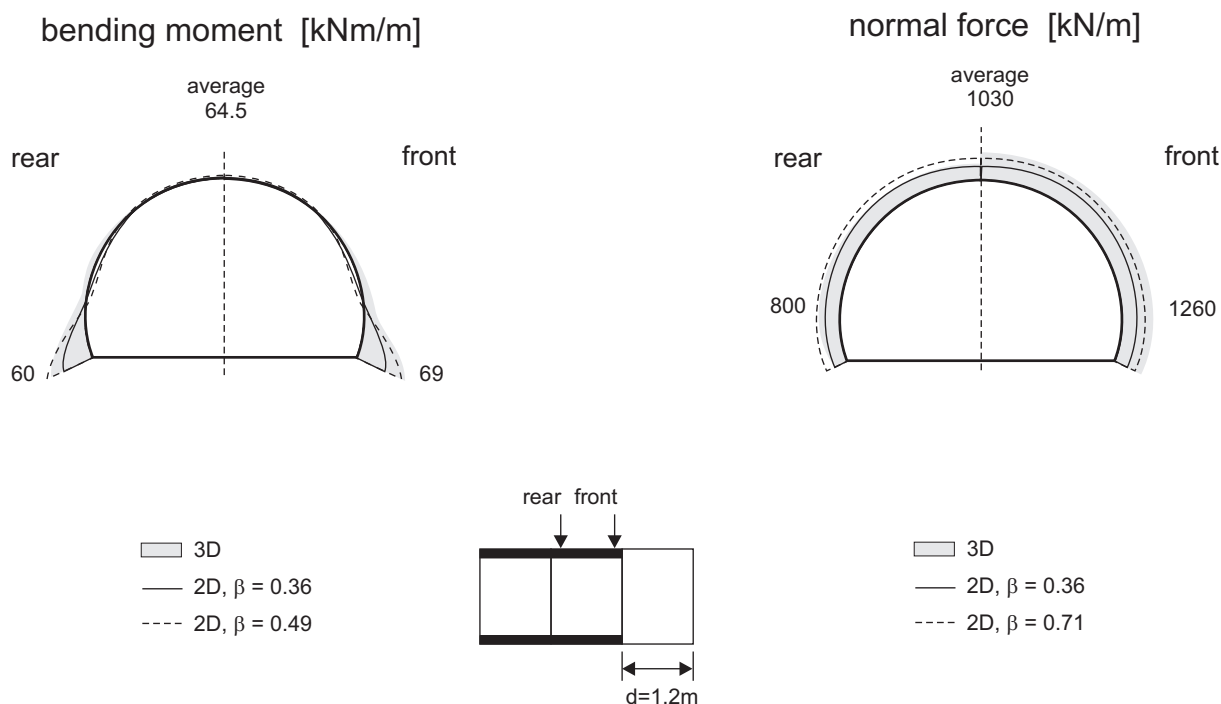


Figure 5.12: Comparison of structural forces of 2D and 3D analyses using the HS Model

factor of two. To match the average maximum 3D bending moment of 64.5 kNm/m a considerable higher unloading factor of 0.49 had to be applied and for the average maximum normal force of 1030kN/m an unloading factor of even 0.71 was necessary. The need for different unloading factors for surface settlements, bending moments and normal forces has been discussed in Section 4.8. The present analyses make it clear that for structural forces the required amount of stress reduction is significantly smaller than for surface settlements.

## 5.2 Second Heinenoord slurry shield tunnel

In 1996 the construction of the Second Heinenoord Tunnel was started as one of two pilot projects for bored tunnelling in the Netherlands. The tunnel consists of two tubes with an external diameter of 8.3m, passing underneath the river Oude Maas. Starting from the North Bank the TBM began excavating in February 1997. On the South Bank the machine was turned to drive the second tube and tunnel excavation was completed in June 1998. The total length of the tunnel is 1350m (one way), including a TBM driven part of 950m. The project was accompanied by an extensive monitoring programme, providing detailed measurements on both face and grout pressures as well as settlements and horizontal ground deformations. Fig. 5.13 illustrates the installation of strain gauges on both the inside and the outside of the tubing segments to measure structural forces. As measurements are important to validate numerical simulations, the present case study was

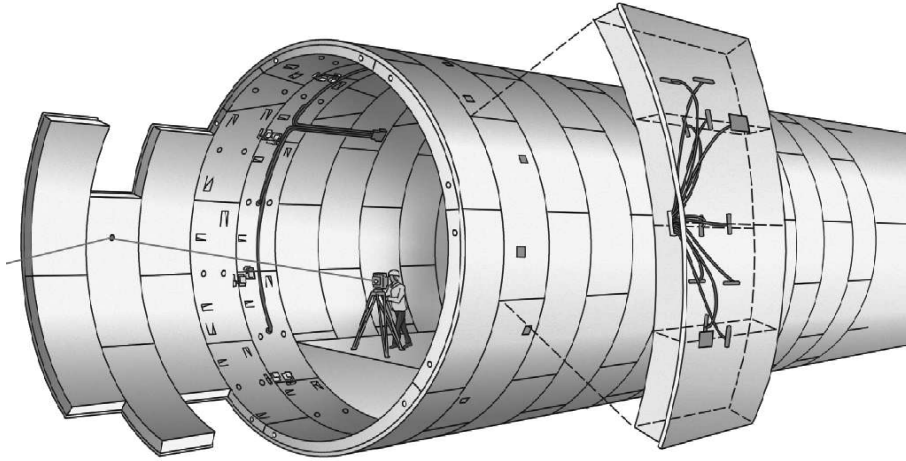


Figure 5.13: Measurement instrumentation of Heinenoord tunnel (BAKKER, 2000). Installation of strain gauges on tubing segments.

an ideal possibility to evaluate both constitutive models and installation procedures.

### 5.2.1 3D FE-analyses

Fig. 5.14 shows a three-dimensional mesh block, with a length of  $120m$ , a width of  $40m$  and a height of  $27.5m$  as used for the analyses of the Second Heinenoord tunnel. The ground water table is at  $1.5m$  below ground surface. The top ground layer is a fill underlain by two layers of sand and a subsequent sand-clay layer. All layers are assumed to behave drained. Mohr-Coulomb soil parameters as listed in Tab. 5.3 were available from the site report (BAKKER, 2000). For the 3D analyses only the HS Model (see Appendix A.2) was applied. Because the HS-Small Model (see Appendix A.3) was not yet operational in 3D, it was only considered in the 2D analyses (Section 5.2.2). Ground parameters of the HS and the HS-Small Models are listed in Tab. 5.4<sup>5</sup>.

The Poissons ratio  $\nu_{ur}$  for unloading/reloading and the stiffness exponent  $m$  have been assumed, considering that for many soils  $\nu_{ur} = 0.2$  and typically  $m = 1.0$  for a clay and  $m = 0.5$  for a sand. The stress dependent oedometer modulus  $E_{oed}^{ref}$  was calculated from the oedometer modulus in Tab. 5.3, considering the stresses acting in the middle of ground layers and using Eq. A.27 from Appendix A.2. For the first three layers it was assumed that  $E_{50}^{ref} \approx E_{oed}^{ref}$  as found for sands by (SCHANZ, 1998), for the clayey bottom layer it was assumed that  $E_{50}^{ref} \approx 2 \cdot E_{oed}^{ref}$  SCHANZ (1998). The stress dependent Youngs modulus  $E_{ur}^{ref}$  for unloading/reloading has been calculated from the secant modulus  $E_{50}^{ref}$  assuming a ratio of  $E_{ur}^{ref} / E_{50}^{ref} = 3$ . The parameters of the HS-Small Model were not directly available, but were estimated to be  $G_0^{ref} = 175MPa$  and  $\gamma_{0.7} = 5 \cdot 10^{-4}$ .

<sup>5</sup>For a full description of the HS- and the HS-Small models and their performance in drained and undrained triaxial tests, the reader is referred to BENZ (2006).

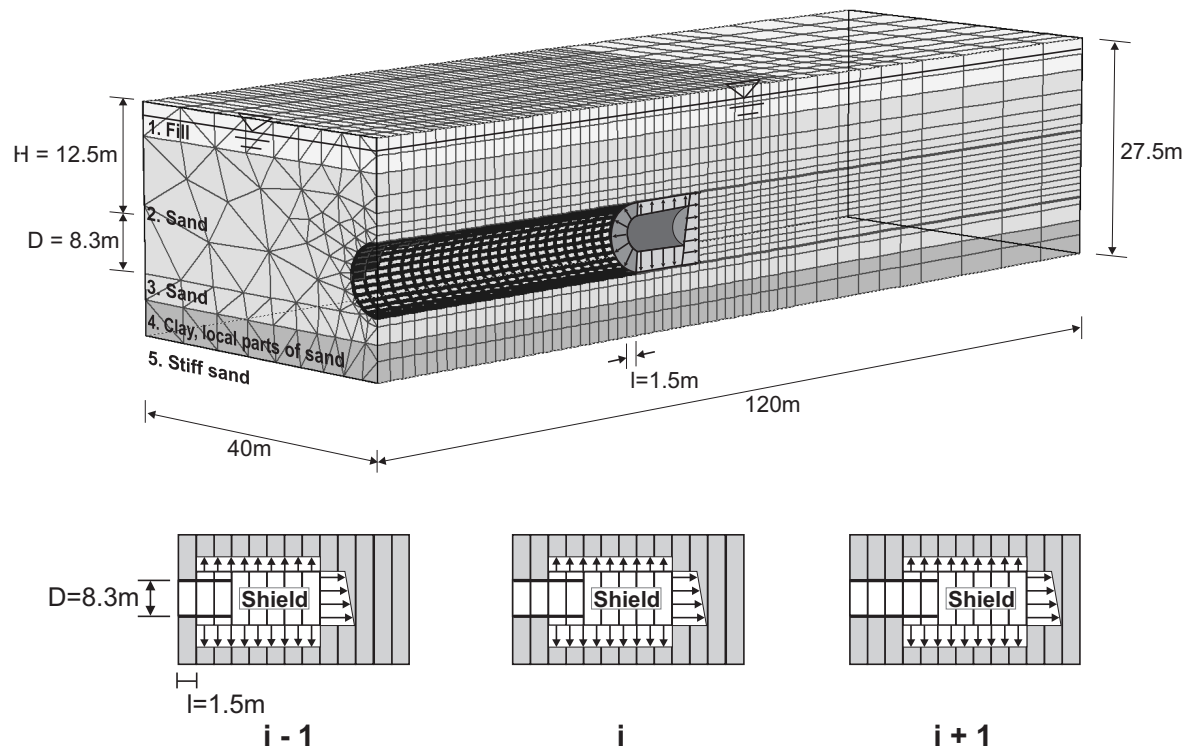


Figure 5.14: 3D FE-mesh of Heinenoord tunnel

The tunnel lining has been modelled linear elastically, using shell elements with a flexural rigidity of  $E_l I = 26.78 MNm^2$ , a normal stiffness of  $E_l A = 10.5 GN$  and a lining weight of  $\gamma = 24 kN/m^3$ . The flexural rigidity has been reduced to account for joints between segments. Following MUIR WOOD (1975) a reduction factor of four has been applied to the flexural rigidity of the tubings. The TBM and the shield was modelled according to the step-by-step pressure method (Section 4.5.2.2). The slurry at the face of the tunnel is simulated by an axial pressure, the shield is simulated by a radial pressure and the fresh grout in the tail void behind the shield is also simulated by a radial pressure.

All prescribed pressures increase hydrostatically with depth according to a unit weight of  $15 kN/m^3$  of the slurry and the grout. The face pressure of  $230 kPa$  at the tunnel crown was chosen according to measurements of the Heinenoord tunnelling project (BAKKER, 1999). The radial shield pressure was taken equal to the grout pressure of  $125 kPa$  at the crown. This pressure is applied along the shield and along two lining rings directly behind the shield, as shown in Fig. 5.14. Here a ground-lining gap is simulated by deactivating ground elements with a thickness of  $20 cm$  and a length of  $1.5 m$  according to the width of a lining ring. Within this gap the ground may deform until contact to the shield or the lining is made. Hence ground displacements were controlled not to exceed the ground-lining gap of  $20 cm$ . For subsequent lining rings, the grout is assumed



layer	$\gamma_{saturated}$ [kN/m <sup>3</sup> ]	$\nu$ [–]	$E_{oed}$ [MPa]	$c'$ [kPa]	$\varphi'$ [°]	$K_0$ [–]
1	17.2	0.34	8	3	27	0.58
2	20	0.3	40	0.01	35	0.47
3	20	0.3	120	0.01	35	0.47
4	20	0.32	48	7	31	0.55

Table 5.3: Heinenoord ground parameters of the MC-Model

layer	$\nu_{ur}$ [–]	$E_{oed}^{ref}$ [MPa]	$E_{50}^{ref}$ [MPa]	$E_{ur}^{ref}$ [MPa]	$G_0^{ref}$ [MPa]	$\gamma_{0.7}$ [%]	$m$ [–]	$OCR$ 1
1	0.2	14	14	42	52	$5 \cdot 10^{-4}$	0.5	1
2	0.2	35	35	105	175	$5 \cdot 10^{-4}$	0.5	1
3	0.2	35	35	105	175	$5 \cdot 10^{-4}$	0.5	1
4	0.2	7	12	35	88	$5 \cdot 10^{-4}$	0.9	1

Table 5.4: Additional ground parameters as used for the HS- (see Appendix A.2) and the HS-Small Model (see Appendix A.3).  $G_0^{ref}$  and  $\gamma_{0.7}$  are parameters used in the HS-Small model.

to be hardened and the radial pressure is switched off. Each time radial pressures are switched off, volume elements are activated to fill the gap, assuming linear elastic lining properties for the hardened grout.

To simulate the excavation and support sequence a step-by-step pressure approach as described in Section 4.5.2.2 and as indicated in Fig. 5.14 has been applied. In the present study a steady state solution of surface settlements was reached after 30 excavations of segmental lengths of  $l = 1.5m$ , resulting in a tunnel length of  $45m$ .

**Surface settlements** Fig. 5.15 shows results of the longitudinal settlement trough by the HS-Model and different grout pressures. Measured settlements appear to be well matched by a crown pressure of  $125kPa$ . The largest maximum settlement of  $3.25cm$  is obtained for a radial pressure of  $p_{crown} = 120kPa$  and a significantly smaller maximum settlement of  $2.0cm$  is obtained for a crown pressure of  $p = 130kPa$ . From these analyses it is obvious that settlements are extremely sensitive to grout pressures and in addition to the pressure boundary condition a limitation of tunnel convergence is needed. This limitation of tunnel convergence is the outer diameter of the TBM or the tunnel lining respectively as explained in Section 4.7. However, such a restriction was not implemented

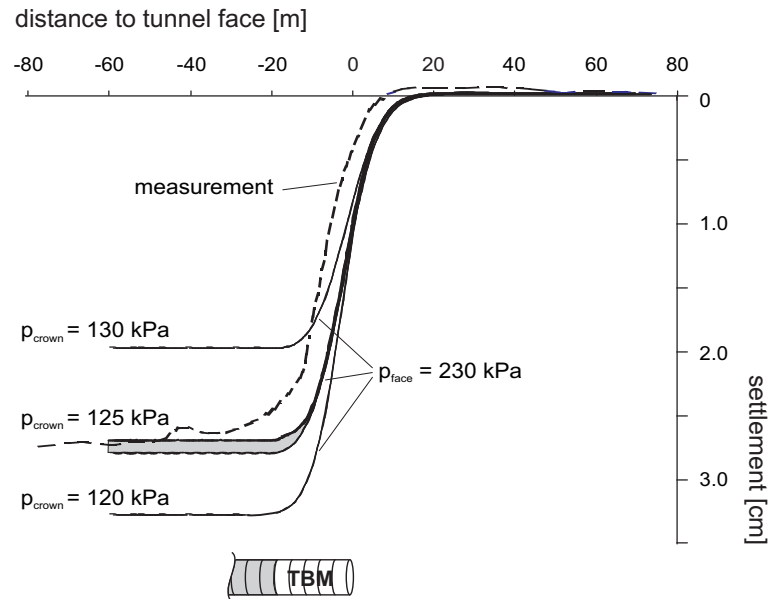


Figure 5.15: Longitudinal surface settlement troughs of different crown pressures

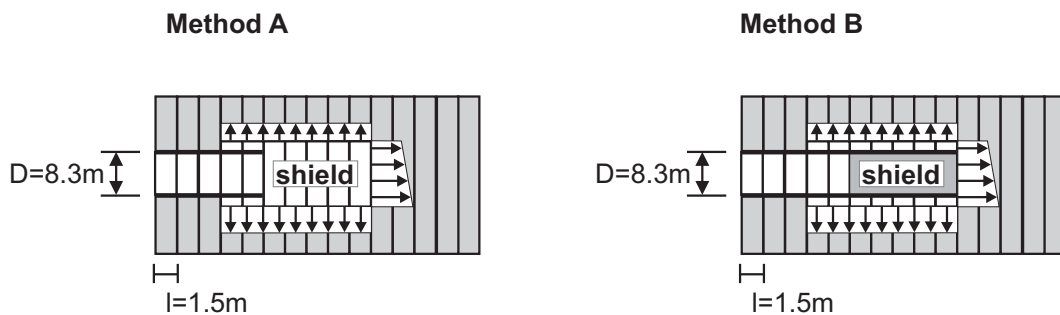


Figure 5.16: Modelling details of Method A and Method B

in the present analyses and a check was carried out after the analyses to find that for all analyses the maximum tunnel convergence was well below this restriction.

Please note that Fig. 5.15 shows two nearly coinciding settlement lines for the crown pressure of  $125\text{ kPa}$ , as two slightly different computations were carried out. Besides the standard analysis (Method A) as explained above, another analysis (Method B) has been carried out. In this B-analysis a shield has been simulated by shell elements, as shown in Fig. 5.16. Between shield and ground, volume elements of width  $20\text{ cm}$  were switched off, to simulate a gap as also used around the lining. Inside this gap radial pressures were applied both to the shield and to the ground. The difference between results from Method A and Method B is an extra settlement of only  $1\text{ mm}$  as indicated by the thin shaded zone in Fig. 5.15. It is also observed from Fig. 5.15 that the steepness of the longitudinal settlement curve is matched well, but compared to measurements the

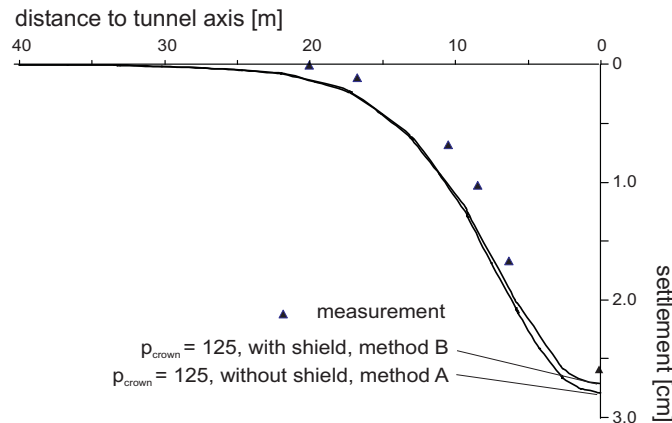


Figure 5.17: Transverse settlement troughs of Method A and Method B

calculated curve is shifted about  $10m$ .

Fig. 5.17 shows the computed cross-section of the settlement trough at a distance of  $4D$  behind the tunnel face. As explained earlier Method A and Method B give nearly the same settlement. Both settlement curves are slightly too flat when compared to the steepness of measured settlements. As will be shown in the following section, the steepness of the transverse settlement trough can be improved by using the HS-Small Model. For the three-dimensional analysis of Heinenoord, however, the HS-Small Model was not applied as the  $3D$  version was not yet available.

**Structural forces** Fig. 5.18 and 5.19 show results of  $3D$  bending moments and normal forces. The longitudinal distributions show results of both Method A and Method B. Both results of bending moments and normal forces indicate convergence towards a steady-state solution. The longitudinal distributions show a zigzagging pattern that matches the step-by-step installation of  $l = 1.2m$ .

The analyses with a shield appear to have slightly different values than the ones without a shield. The graphs indicate that due to structural forces in the shield (first five slices behind the tunnel face as indicated by the inserts of these figures) the distribution of the subsequent lining forces start with a value equal to the shield forces, whereas in the case of no shield they start with a value close to zero. In Method B forces are transferred from the shield to the lining as the interaction of shield and lining has been modelled fully rigid. In reality the outer shield diameter is somewhat smaller than the inner lining diameter, leaving some possibility for the shield to freely deform. One may thus argue that the simplification of full bound in the transverse section is not appropriate. However, this simplification can be accepted as it slightly increases the value of steady-state bending moments whereas at the same time normal forces are slightly decreased. The transverse distribution of bending moments, shown in Fig. 5.18, indicates relatively little difference between front and rear values of a lining ring. The maximum bending moment of about  $-25kNm/m$  is observed at the tunnel wall. The positive value

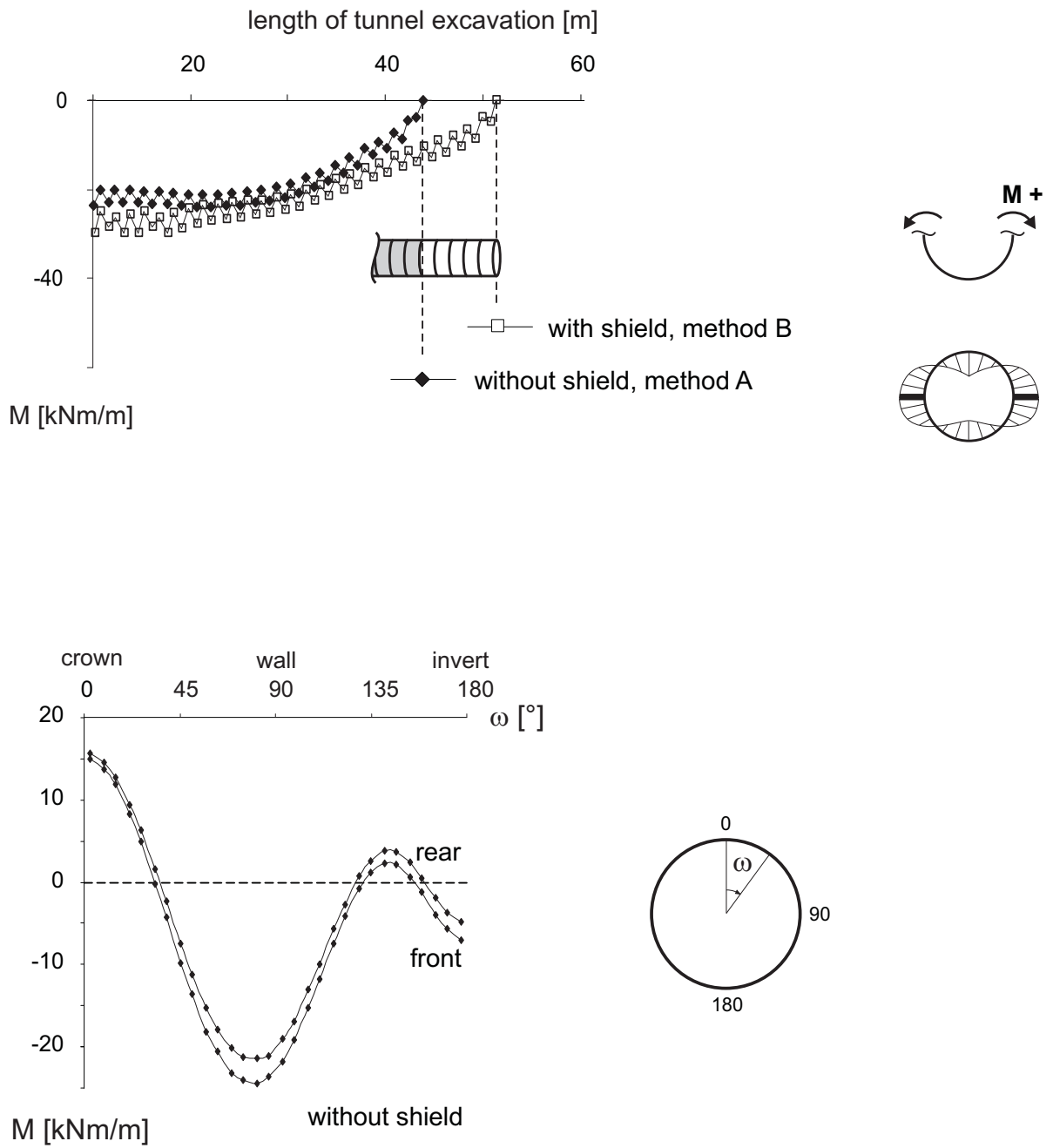


Figure 5.18: Bending moments from 3D analysis

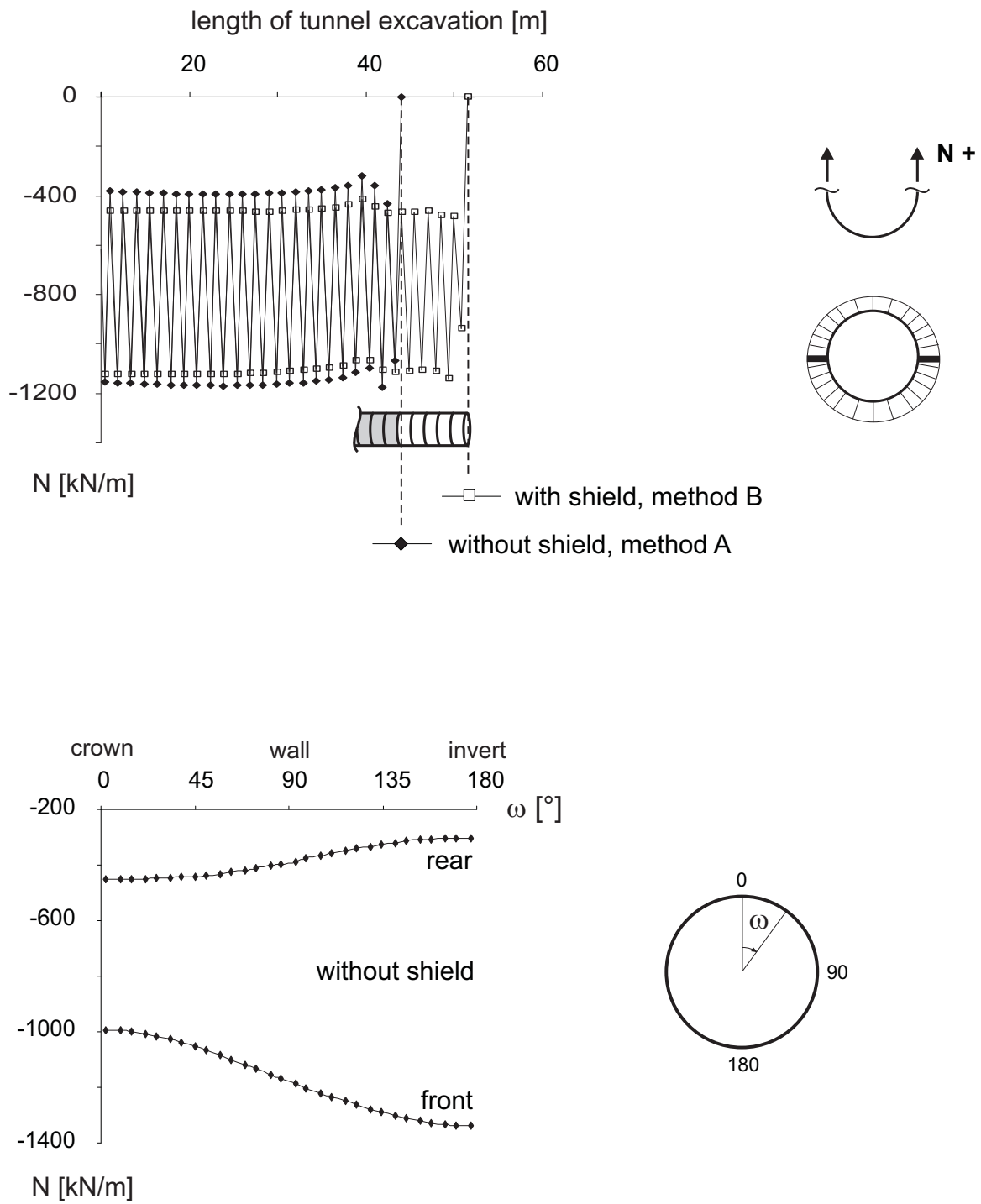


Figure 5.19: Normal forces from 3D analysis

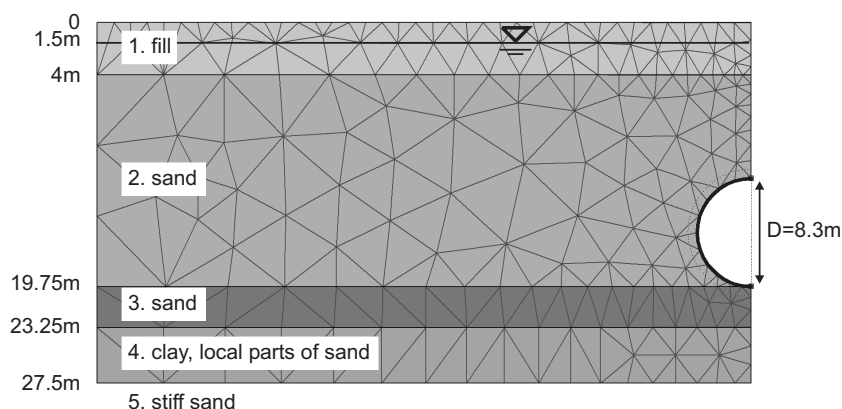


Figure 5.20: 2D FE-mesh of Heinenoord tunnel

indicates inward deflection of the lining. The difference between front and rear values of normal forces is significant, as shown in Fig. 5.19. It is interesting to note that the front normal force increases from the crown value of  $-1000kN/m$  down to a maximum at the invert of about  $-1400kN/m$ , whereas the rear normal force shows a reversed distribution decreasing from a crown value of about  $-450kN/m$  down to the invert normal force of about  $-300kN/m$ .

### 5.2.2 2D FE-analyses

Fig. 5.20 shows a two-dimensional FE-mesh of the Heinenoord tunnel. Again 6-noded triangular elements were used for the mesh with a width of  $40m$  and a height of  $27.5m$ . The soil parameters to model drained ground behavior with the MC, HS and the HS-Small Model are listed in Tables 5.3 and 5.4. Please note that for the MC Model the stiffnesses given in Table 5.3 are absolute stiffnesses which have been adjusted to the stress level acting in the middle of the respective layers (compare Section 4.8.3). The values of  $E_{ur}^{ref}$  as used for the HS and the HS-Small Model (Table 5.4) are reference values and are thus different from the absolute stiffnesses of the MC Model. Whereas the HS and the HS-Small Model automatically make distinction between primary loading and unloading-reloading stiffnesses, the MC Model uses a constant stiffness, no matter the loading history. In order to account to some extent for the unloading behavior in the MC Model, the layers underneath the tunnel have been assigned the unloading-reloading stiffness, whereas the layers on top were assigned the stiffness for primary loading. Besides the evaluation of the influence of constitutive models, the influence of different installation procedures for shield tunnels, namely the stress reduction method, the contraction method and the grout pressure method, was studied. In the latter method, the ground-lining interaction described in Section 4.7 was not yet implemented and therefore a slightly simplified approach was chosen. In order to model the Heinenoord shield tunnel only the grout pressure distribution was assigned to the excavated ground modelling no lining. Doing so, the results of ground displacements were still controlled not

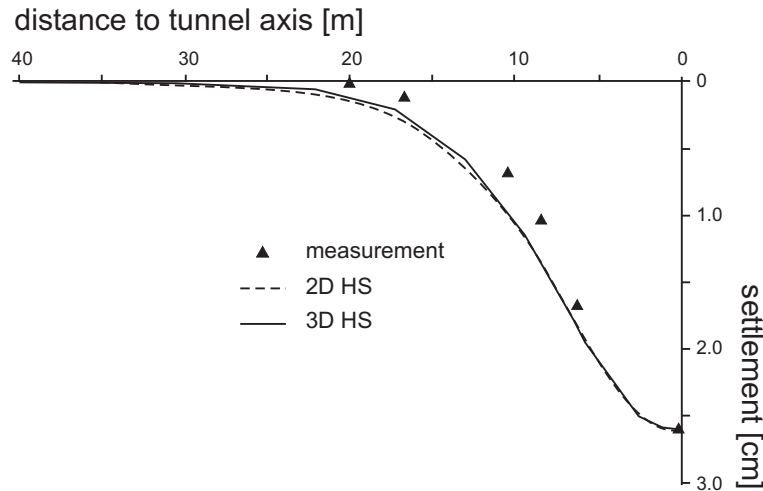


Figure 5.21: Comparison of 2D and 3D transverse surface settlement trough

to exceed the proposed ground lining gap of 20cm.

**Surface settlements** The results of the 2D grout pressure method are shown in Fig. 5.21. Although the 2D grout pressure method does not model a face pressure, results compare well to the 3D analysis of Heinenoord. This indicates that the face pressure of the 3D analysis does not much contribute to the development of surface settlements. Indeed, as discussed previously in Section 3.3, ground deformations due to shield tunnelling are predominantly determined by the process of tail void grouting, causing the largest deformations at the shield tail. If appropriate face pressures are assigned almost no deformations will occur around the tunnel heading.

Fig. 5.22 shows results of the transverse settlement trough of the grout pressure method using different constitutive models. The best agreement to measurements is obtained from the HS-Small Model with a crown grout pressure of 128.5kPa and a unit grout weight of  $\gamma = 15kN/m_3$ . Considering the initial total overburden stress of 225kPa, the present analysis renders a stress reduction of 43%, being slightly less than the stress reduction of 50% as proposed by MUIR WOOD (1975). The difference to the settlement trough of the MC and the HS Model is moderate, but slightly higher crown pressures of 135kPa and 133kPa respectively had to be applied to match the maximum settlement. Fig. 5.23 shows results of normalized transverse settlement troughs of different constitutive models, using the same crown pressure of 128.5kPa for all analyses. The results of maximum settlements as indicated in this figure, demonstrate the fact that ground displacements are very sensitive to a variation of the grout pressure, giving now significantly larger settlements of  $S_{max} = 4.2cm$  and  $S_{max} = 3.6cm$  for the MC and the HS Model respectively. Moreover, Fig. 5.23 demonstrates the large influence of a pressure variation on the steepness of the settlement curves. Whereas the steepness of the HS curve has not changed much, the steepness of the MC curve is heavily influenced, al-

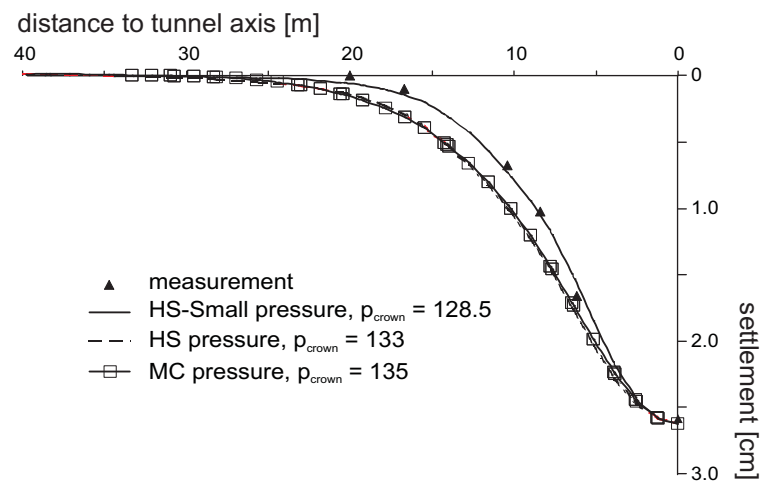


Figure 5.22: Transverse settlement trough using the grout pressure method and different constitutive models

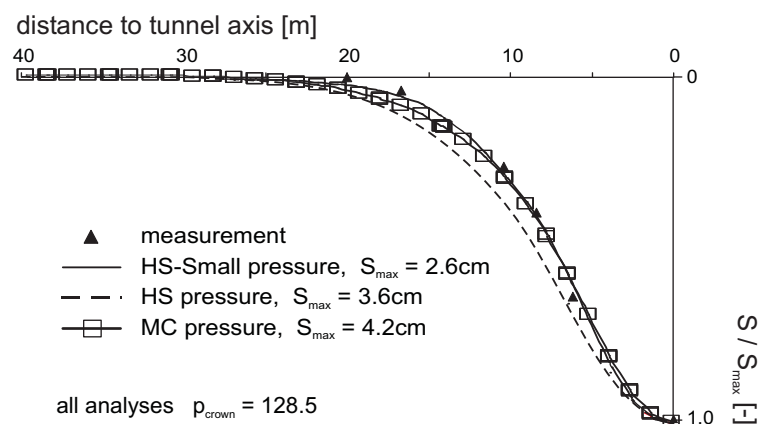


Figure 5.23: Normalized transverse settlement troughs of different constitutive models using the same crown pressure



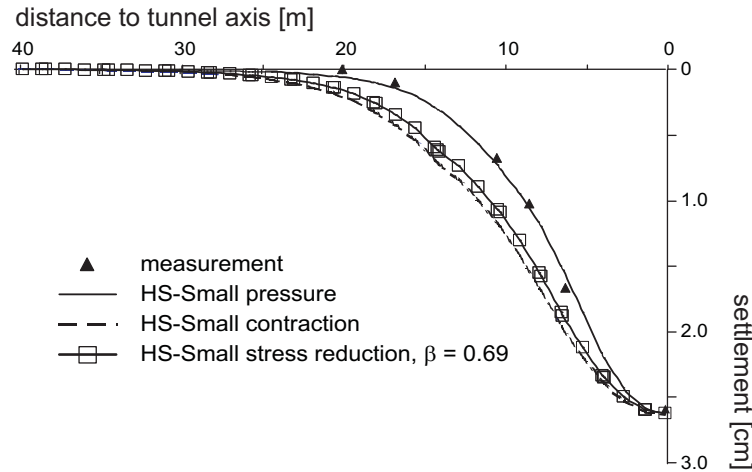


Figure 5.24: Transverse settlement troughs of different installation procedures

most matching now the solution of the HS-Small Model. The fact that the MC Model is giving a steeper normalized settlement curve than the HS Model may seem somewhat surprising. Most probably this is also related to the fact that the layers underneath the tunnel had been assigned the unloading-reloading stiffness of the ground. However, interrelations are complex and no definite explanation of this effect was found. But the clear statement shall be given here that by no means it is meant to recommend the use of the MC Model superior to the HS Model for tunnel analysis.

The fact that the shape of the settlement trough is first of all affected by the tunnel installation procedure is demonstrated by Fig. 5.24. Indeed, it is shown by this figure that the shape of the transverse settlement trough is more affected when applying different installation procedures rather than different constitutive models. Using the HS-Small Model the settlement trough of the stress reduction and the contraction method is far more flat than for the grout pressure method. Obviously numerical installation procedures are most important for the shape of the settlement trough.

**Installation procedures and tunnel deformation** Fig. 5.25 shows the influence of numerical installation procedures on the displacements around the tunnel lining. The tunnel convergence of both the grout pressure method and the stress reduction method is predominantly located at the tunnel crown whilst at the tunnel invert almost no convergence occurs. The relatively small tunnel uplift in the region between tunnel invert and tunnel wall is logical, as for the ground underneath the tunnel the much higher unloading-reloading stiffness of the HS-Small model is involved. The contraction method imposes far more tunnel uplift than observed for the grout pressure and the stress reduction methods, regardless of the high unloading-reloading stiffness being used. Moreover, the contraction method contains a circular tunnel shape whereas the other methods allow for a concentration of deformations at the tunnel crown.

Fig. 5.25 also shows the influence of the installation procedure on the shape of the

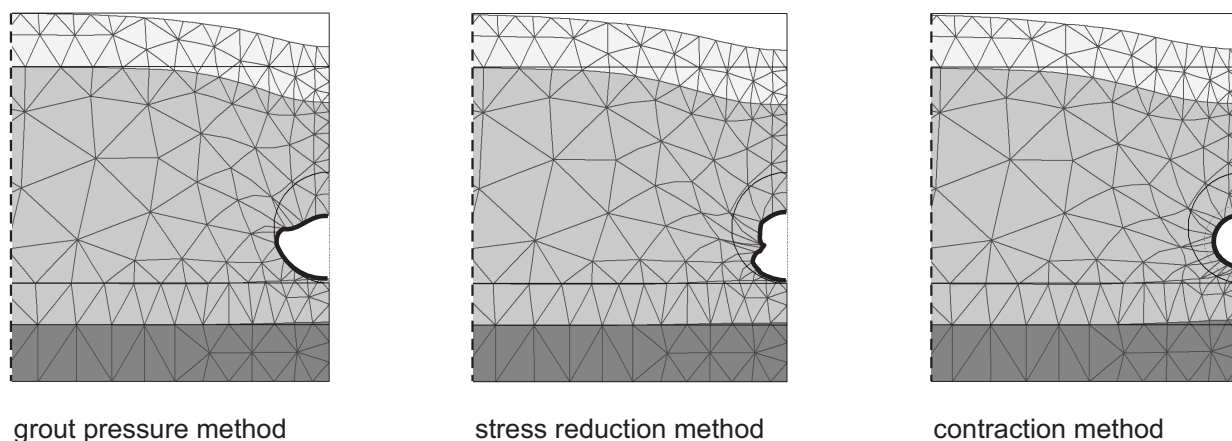


Figure 5.25: Deformed FE-mesh scaled up 100 times from different installation procedures using the HS-Small Model

surface settlement trough. Whilst the grout pressure method has the most localized crown convergence and therefore gives the steepest and narrowest settlement curve, the stress reduction and the tunnel contraction methods show considerably wider and more flat troughs.

The difference between the crown convergence of the grout pressure method and the stress reduction method is explained by Fig. 5.26. From the tunnel wall up to the tunnel crown the ground tends to deform into the tunnel and the resulting convergence is governed by the radial stress distributions of the methods. Fig. 5.26 shows the total radial initial stresses before construction of the tunnel and the reduced total radial stresses after construction of the tunnel of the grout pressure and the stress reduction methods respectively. The stress reduction method was carried out with  $\beta = 0.69$ , i.e. a stress reduction of 31%. As illustrated in Fig. 5.26, the stress reduction from total radial initial down to reduced total radial stresses applies only to the effective radial initial stresses. The pore water pressures  $u$  are not reduced.

Fig. 5.26 shows that in the region from the tunnel wall up to the tunnel crown, the grout pressure method renders the highest stress reduction with the maximum stress reduction at the crown. This explains why the grout pressure method gives the largest displacements at the tunnel crown. The stress reduction method on the contrary renders a uniformly distributed stress reduction and therefore tunnel contraction is less concentrated at the tunnel crown, giving as well some contraction at the tunnel wall.

**Horizontal ground movements** To validate both constitutive models and numerical installation procedures, horizontal displacements are considered. Inclinometer measurements and horizontal displacements of different constitutive models, using the grout pressure method are shown in Fig. 5.27. The HS-Small Model gives a better prediction than the MC and the HS Model, but in the region closest to the tunnel all models tend to give outward horizontal movements instead of inward measurements. No doubt, hor-

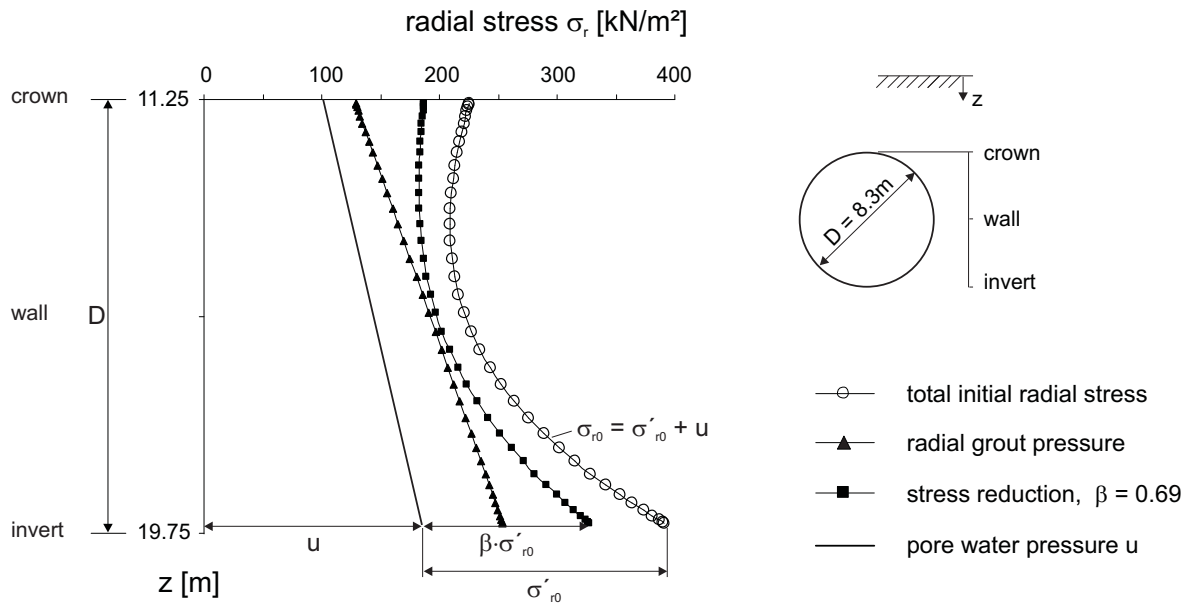


Figure 5.26: Difference in radial stresses from grout pressure and stress reduction methods of Heinenoord

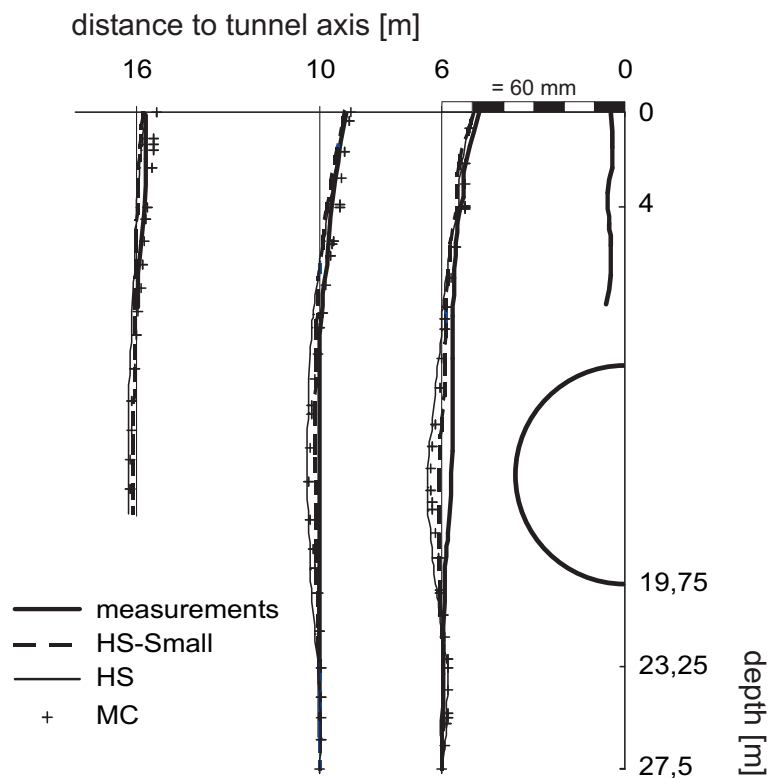


Figure 5.27: Horizontal ground movements scaled up 100 times of the grout pressure method using different constitutive models

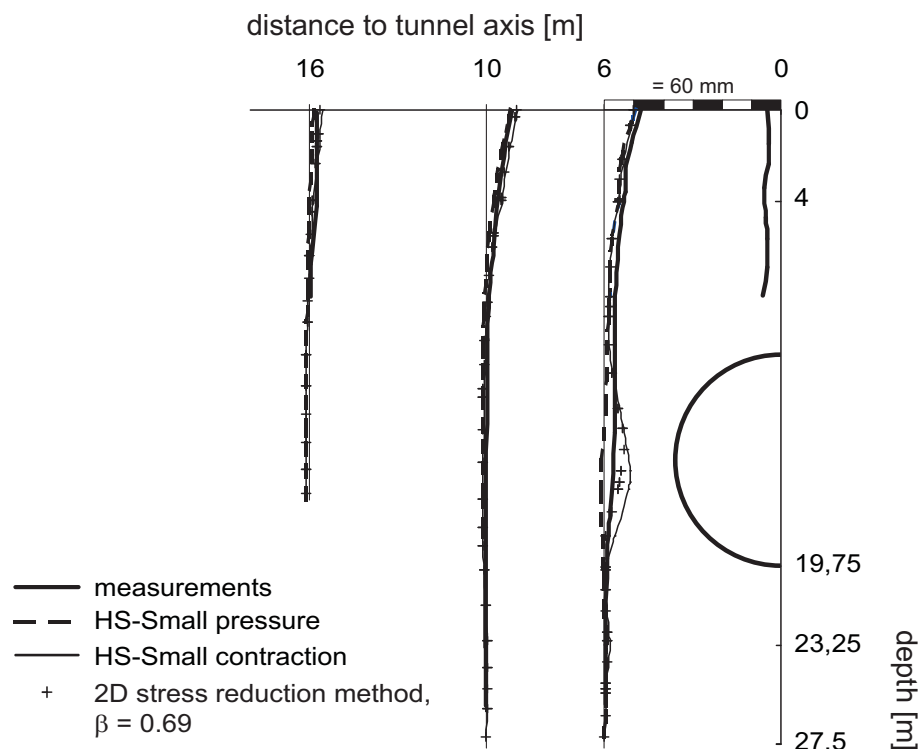


Figure 5.28: Horizontal ground movements scaled up 100 times of different installation procedures using the HS-Small Model

horizontal movements will strongly be influenced by the grouting pressure assigned and insufficient grouting may have lead to inward directed movements. However, applied grout pressures are difficult to measure and they remain uncertain. Fig. 5.28 shows horizontal displacements of different installation procedures. Using the HS-Small Model the stress reduction method predicts far too large inward horizontal displacements in the region closest to the tunnel, as well as the contraction method which predicts even more inward movement. For simulating horizontal displacements Fig. 5.27. and Fig. 5.28 show clearly that numerical installation procedures are more significant to the simulation of horizontal deformations than constitutive models. In the present case, the best prediction is obtained from the grout pressure method and the HS-small Model.

**Structural forces** Figs. 5.29 and show a comparison for bending moments and normal forces of the grout pressure method, the stress reduction method and the contraction method using the HS-Small model. For all methods the bending moments are relatively small. The contraction method gives the largest bending moment of around  $100kNm/m$  at the tunnel crown and wall, the stress reduction gives the smallest one, with around  $50kNm/m$  at the tunnel crown and wall. The grout pressure method is well in between the results of these two methods, giving crown and wall values of around  $75kNm/m$ . Higher and thus more important than bending moments are normal forces, giving a

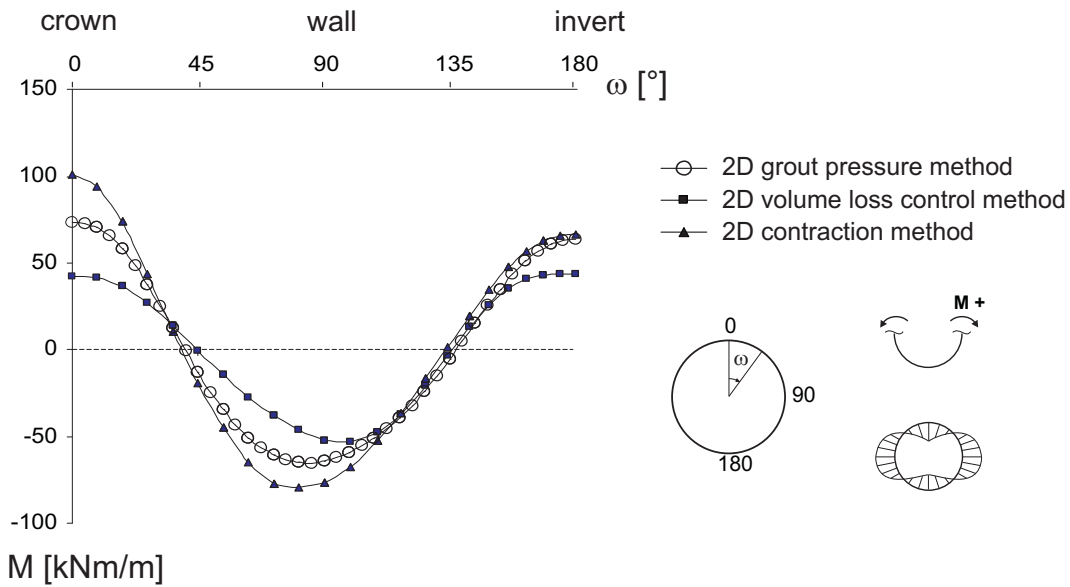


Figure 5.29: Comparison of bending moments from different 2D installation methods using the HS-Small model

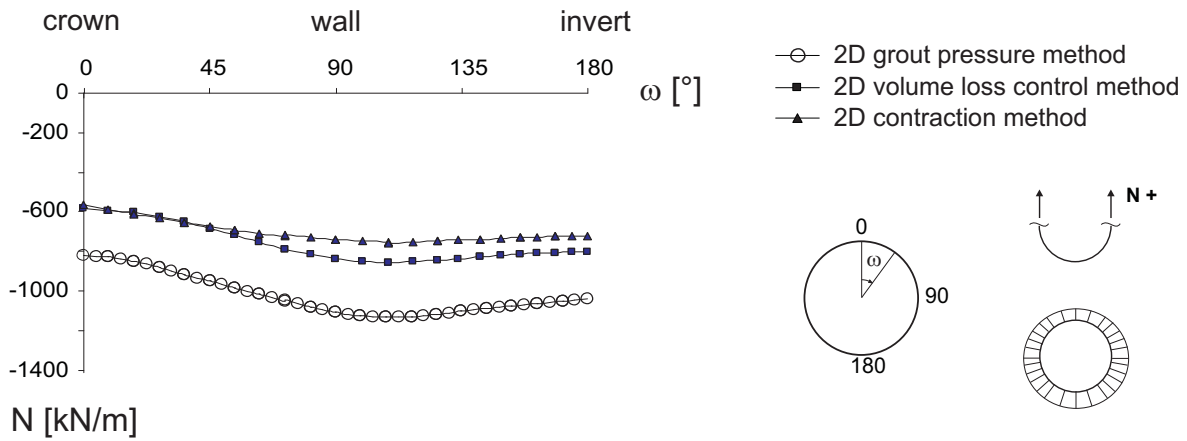


Figure 5.30: Comparison of normal forces from different 2D installation methods using the HS-Small model

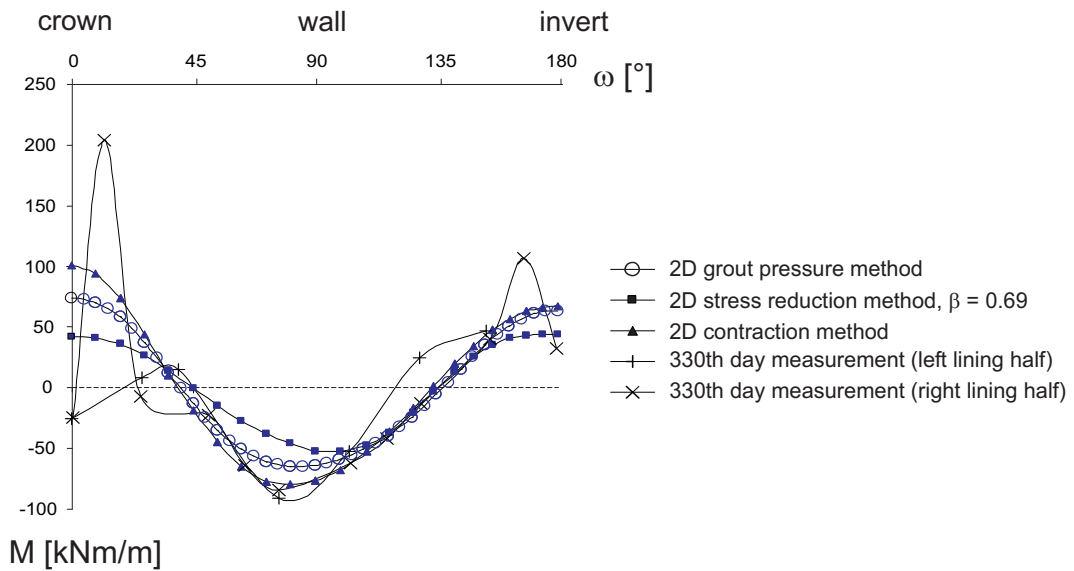
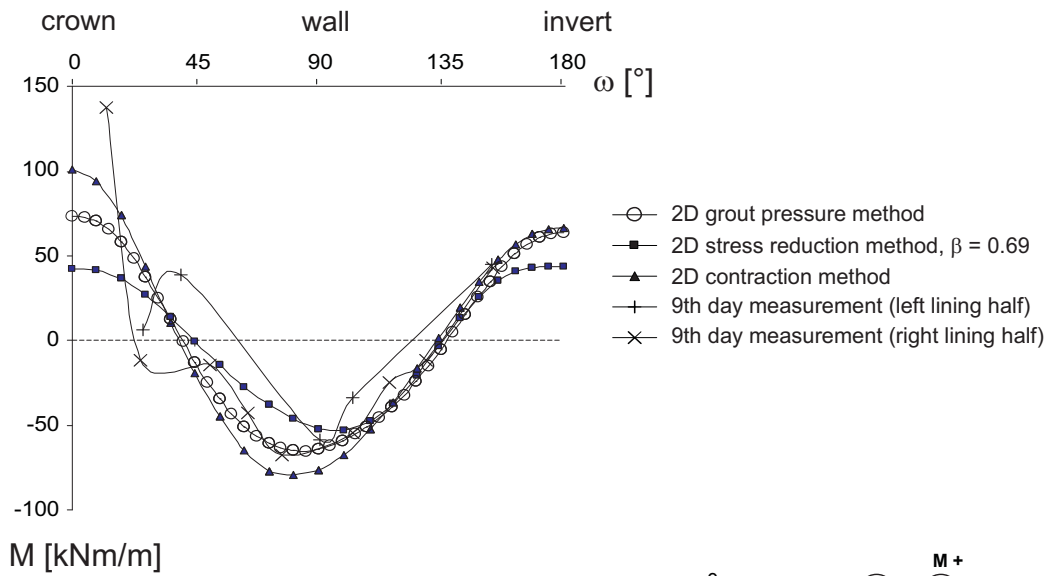


Figure 5.31: Comparison of computed and measured bending moments using the HS-Small model

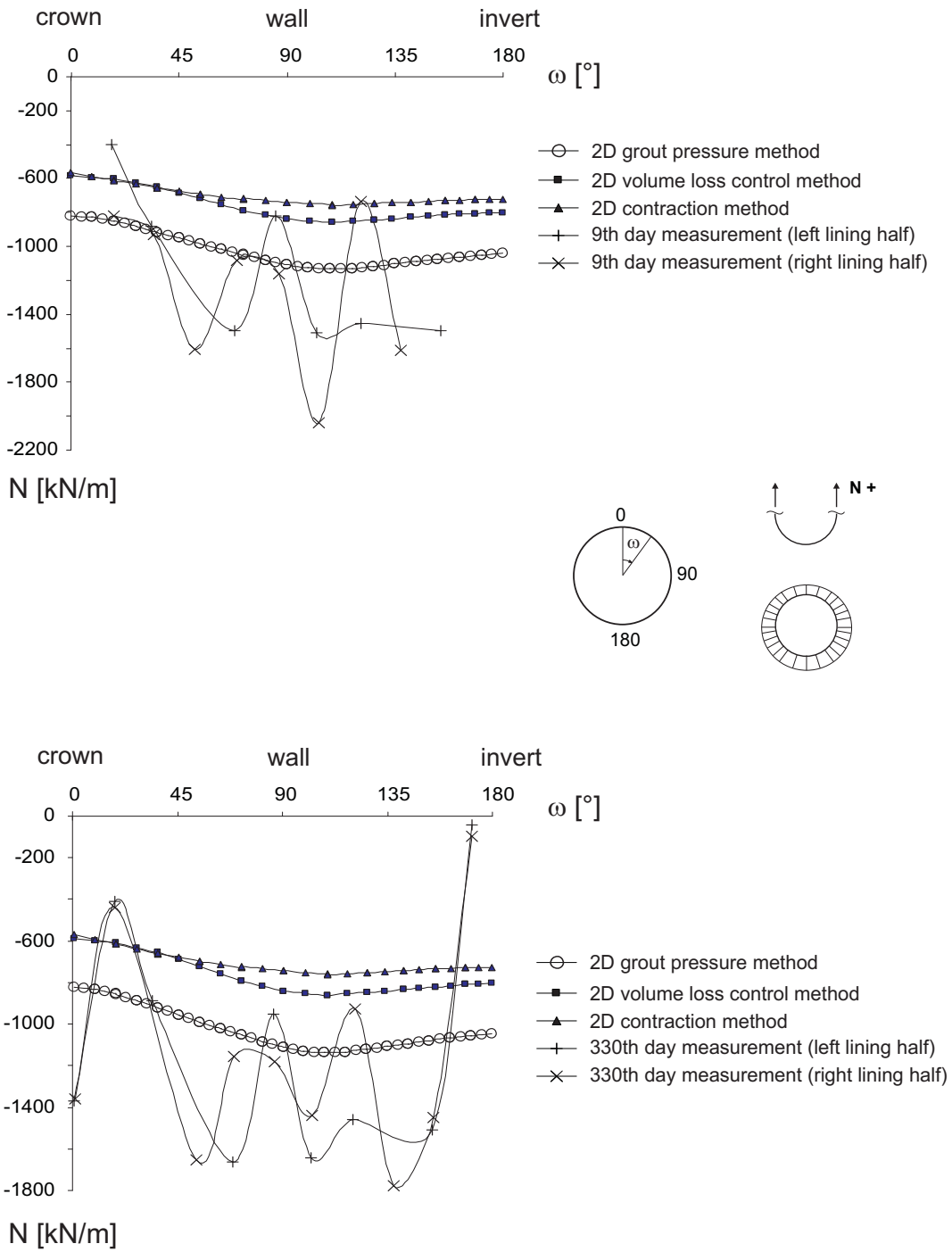


Figure 5.32: Comparison of computed and measured normal forces using the HS-Small model

crown value of around  $-600kN/m$  with very similar distributions for both the stress reduction and the contraction method. The grout pressure method gives considerably higher normal forces with a crown value of around  $-800kN/m$ .

In order to compute realistic values of bending moments and normal forces, it can not be expected that the stress reduction method and the contraction method give accurate solutions as they tend to predict ground movements incorrectly. This fact is also demonstrated by Figs. 5.31 and 5.32, by showing 2D bending moments of different installation methods and comparing them to measurements of Heinenoord. Please note that measurements of structural forces were taken after 9 days (upper figures) as well as after 330 days (lower figures). Both measurements of bending moments and normal forces show a slight increase from the first to the second measurement. Although measurements show a relatively high scatter both Figs. 5.31 and 5.32 show that measurements are best matched by the grout pressure method. In particular this is demonstrated for measured normal forces, being significantly higher than predicted by the stress reduction and the contraction method. The grout pressure method clearly improves, giving higher normal forces much closer to the measured ones.

No doubt, bending moments and normal forces in tunnel linings are difficult to measure and good quality data for validating magnitudes of structural forces are difficult to obtain. Nevertheless, the presented results of the grout pressure method indicate that this method gives better predictions than the stress reduction and the contraction method for both tunnel displacements and structural forces.





# Chapter 6

## Conclusions

### Introduction

The objective of this thesis was to analyze tunnel induced settlements and structural forces in linings, considering both elementary methods of analysis and the Finite Element Method. The most important conclusions will be given in the following sections, followed by some recommendations for further research.

### 6.1 On elementary design methods

For settlements, the empirical Gaussian settlement trough after PECK (1969) would seem to be the only method frequently used in engineering practice. However, the ground loss ratio  $GLR$  for an estimate of the trough depth remains uncertain. Proposals for estimating  $GLR$  on the basis of a stability number  $N$  exist, but such estimates show a relatively wide scatter. Nevertheless, the method seems to be well suited for an initial estimate of settlement profiles.

The concept of the ground response curve for loads on tunnel linings as initiated by FENNER (1938) and PACHER (1964) is still important for understanding the interaction between tunnel lining and ground. Analytical solutions of ground response curves are sometimes used in engineering practice for deep tunnels.

Analytical solutions to assess structural forces in linings are restricted by a number of crucial simplifications, such as circular cross sections and homogeneous elastic (or elastoplastic) ground. Therefore they might be used for preliminary tunnel design only. Nevertheless, they remain important as they can be taken to validate complex numerical methods.

Contrary to analytical solutions bedded lining computations can be applied to non-circular tunnel cross sections as well as to layered grounds and they are therefore frequently used in engineering practice, at least in some countries. This method has led to a significant advancement in tunnel design from the view point of soil mechanics. However, the method comprises a considerable simplification when replacing soil by springs.

Throughout the literature the fact that structural design models should generally account for a stress reduction of primary ground stresses is well noticed. However, magnitudes of stress reduction are hardly discussed. DUDDECK and ERDMANN (1982) distinguish between shallow tunnels, moderately deep tunnels and deep tunnels. For deep

tunnels they state that some stress reduction should generally be valid, but again magnitudes are not discussed. For shield tunnels it would seem that mostly full primary stresses are incorporated into structural design models, not accounting for effects of tunnel installation.

## 6.2 On the FEM

For 3D surface settlements and structural forces it has been shown that a considerable tunnel length needs to be excavated in order to arrive at the steady-state solution. Structural forces from 3D tunnel analyses appear to have a zigzagging pattern with high forces at the front of a lining ring and low forces at the rear of a lining ring. Bending moments tend to be relatively low. Instead normal forces are more important for tunnel design.

**Influence of  $K_0$ :** From a parametric study on the magnitude of the lateral earth pressure it was observed that both surface settlements and structural forces are heavily influenced by the value of  $K_0$ . For surface settlements much wider and shallower settlement troughs were computed for larger  $K_0$ .

The above observations hold both for two- and three-dimensional settlement analyses, which appear to show good agreement for settlements up to a value of  $K_0 \leq 1.25$ , at least as long as appropriate unloading factors are used in the 2D analyses. This is conform the findings of several other authors, but in contrast to the findings by LEE and NG (2002). For  $K_0 \geq 1.25$  both 2D and 3D analyses predicted unrealistic surface heave instead of settlement. It may therefore be concluded that an isotropic hardening model as used in the present studies, gives a reasonable prediction of settlements for approximately  $K_0 \leq 1.0$ . For  $K_0$  values being beyond one, however, an isotropic hardening model with elastic unloading behavior would not seem to be appropriate anymore.

Similar to surface settlements, structural forces are heavily influenced by a change of  $K_0$ . For  $K_0 \geq 1$  the bending moment at the tunnel wall changes from an outward deflection to an inward deflection. Results of 2D analyses of structural forces are generally well in between the values at the front and at the rear of a lining ring of three-dimensional normal forces. 2D analyses of bending moments reasonably match results from 3D analyses for the case of  $K_0 = 0.5$ . For  $K_0 > 0.5$  2D analyses of bending moments show some deviation from results of 3D analyses. However, this may be considered not so important as in comparison to normal forces magnitudes of bending moments appear to be relatively small.

**Unloading factor  $\beta$  for open face tunnelling:** 3D step-by-step modelling of tunnel excavation and support is straight forward, but still engineering time consuming. Therefore the 2D stress reduction method is frequently used. A parametric study on the magnitude of the unloading factor being used in the stress reduction method has been carried out by a calibration to results of 3D analyses. It has been shown that three different

unloading factors need to be considered in order to match surface settlements, bending moments and normal forces. For circular tunnels in homogeneous soil, independent of the round length, the settlements are well matched using unloading factors between 0.3 and 0.4. For bending moments approximately the same values are found, as long as the effective cohesion is below  $50kN/m^2$ . A conservative approach for structural forces would be to use  $\beta$ -values of at least 0.5-0.7 in soil. However, unloading factors are significantly influenced by the tunnel geometry and ground layering as well as the constitutive model being used. For practice it is therefore recommended to perform at least one full 3D analysis which may serve as a reference for unloading factors of further 2D analyses.

**Overconsolidation:** The importance of considering overconsolidation and related higher ground stiffness was demonstrated for the simulation of a conventionally driven open face tunnel. On adopting a degree of overconsolidation settlements were significantly smaller, but the trough itself was steeper. Moreover, it was shown that the HS-Small Model increases the steepness of the surface settlement curve.

**2D shield tunnelling:** 2D approximations of shield tunnels are either accomplished on the basis of the contraction method, the stress reduction method or the grout pressure method. It has been shown that the tunnel contraction method leads to unrealistic results of both ground deformations and lining forces. Instead the stress reduction method is more realistic. An advanced pressure approach for shield tunnels was proposed, being named the grout pressure method. This method adopts a different pressure distribution than the stress reduction method and it was found to give most realistic predictions for both vertical and horizontal ground deformations as well as structural forces.

The two-dimensional analyses carried out for a particular shield tunnel demonstrate that the shape of the surface settlement curve is predominantly influenced by the installation procedure, rather than by the constitutive model. Considering measured data of surface settlements and horizontal ground deformations it was observed that the best agreements for ground deformations was computed by the grout pressure method in combination with the use of the HS-Small Model. Moreover, a comparison to measurements showed that the grout pressure method results in the most realistic prediction of structural forces.

**3D shield tunnelling:** 3D shield tunnel analyses are still under debate, but the tendency is to use step-by-step pressure simulations. The simulation of a slurry shield tunnel by the step-by-step pressure method showed that these simulations are extremely sensitive to the magnitude of grout pressures. On the contrary, an alternative analysis to model as well the shield by stiff shell elements showed that almost no difference in surface settlement and structural forces occurred as compared to an analysis without a shield.

### 6.3 Recommendations for further research

**Grout pressure method** The results obtained from the presented case study of a slurry shield tunnel demonstrate the need to consider a simulation of grout pressures. The grout pressure method proposed in the present thesis suggests how the interaction of ground-grout-lining may be solved and it has been shown that realistic results for both ground deformations and lining forces are to be obtained from such an approach. However, it has been shown that this method is sensitive to the magnitude of grout pressures. Similar to the magnitude of the unloading factor in the stress reduction method the magnitude of the grout pressure remains an uncertain input parameter. Rather than estimating the magnitude of the grout pressure, the ground loss ratio may be considered as an alternative input parameter in the grout pressure method. Indeed, shield tunnelling is controlled in terms of ground loss and experience exists about the magnitude of such an input parameter.

The implementation of the grout pressure method would be an important tool for the use in future simulations of shield tunnels, both for slurry and EPB shields.

**Ground-surface structure interaction** The present thesis was intended to highlight some basic modelling approaches of FEM tunnel analyses for surface settlements and structural forces. In order to do so green field settlements were considered as a starting point. However, the FEM provides possibilities to model as well the interaction of tunnel induced ground deformations to existing surface and subsurface structures, which is an important topic of consideration in the period of planning a tunnel. Therefore the present approach may be extended to the FE-modelling of tunnel induced ground deformations with respect to existing structures on the basis of some case studies.

# Appendix A

## On constitutive models as used in this thesis

In order to discuss the influences of three different constitutive models on the results of FE-tunnel analysis (see Section 5) first of all the simple MC Model will shortly be described. Hereafter main features of two advanced models will be described, namely the Hardening-Soil (HS) and the Hardening-Soil-Small (HS-Small) Model. As the focus is on tunnelling settlements and lining forces, i.e. on ground deformation, emphasis will be placed on the formulation of the ground stiffness. For more details on the formulation of these two models the reader is referred to other publications.

### A.1 The Mohr-Coulomb Model

The MC Model is a *first order* approximation of soil behavior, being a linear elastic perfectly plastic constitutive law. It involves five input parameters, namely Young's modulus  $E$  and Poisson's ratio  $\nu$  for soil elasticity, effective shear parameters cohesion  $c'$  and angle of friction  $\varphi'$  for soil plasticity and  $\psi$  as an angle of dilatancy.

As shown in Fig. A.1a for primary loading the stress-strain behavior is modelled elastic with a constant stiffness up to a certain failure stress  $\sigma_f$ . Similarly unloading-reloading is modelled, adopting the same material response and stiffness as for primary loading. When the failure stress is reached, perfectly plastic deformation takes place, involving the development of irreversible strains. In order to evaluate whether or not plasticity takes place, yield functions are introduced. As shown in Fig. A.1b, for general states of stress soil failure can be represented as a fixed hexagonal yield surface in principal stress space. By extending Coulomb's friction law to general states of stress the equations of the hexagonal yield surface are obtained as

$$f_1 = 0 \quad \text{with} \quad f_1 = \frac{1}{2} \cdot |\sigma'_2 - \sigma'_3| - \frac{1}{2} \cdot (\sigma'_2 + \sigma'_3) \cdot \sin \varphi' - c' \cdot \cos \varphi' \leq 0 \quad (\text{A.1})$$

$$f_2 = 0 \quad \text{with} \quad f_2 = \frac{1}{2} \cdot |\sigma'_3 - \sigma'_1| - \frac{1}{2} \cdot (\sigma'_3 + \sigma'_1) \cdot \sin \varphi' - c' \cdot \cos \varphi' \leq 0 \quad (\text{A.2})$$

$$f_3 = 0 \quad \text{with} \quad f_3 = \frac{1}{2} \cdot |\sigma'_1 - \sigma'_2| - \frac{1}{2} \cdot (\sigma'_1 + \sigma'_2) \cdot \sin \varphi' - c' \cdot \cos \varphi' \leq 0 \quad (\text{A.3})$$

Please note that compression is considered positive. For stress states that are within this yield surface the MC Model responds linear elastic and all strains are reversible. Adopting Hooke's law in rate formulation the elastic stress-strain relationship is written as

$$\dot{\sigma}' = \mathbf{D}^e \dot{\varepsilon}^e, \quad (\text{A.4})$$

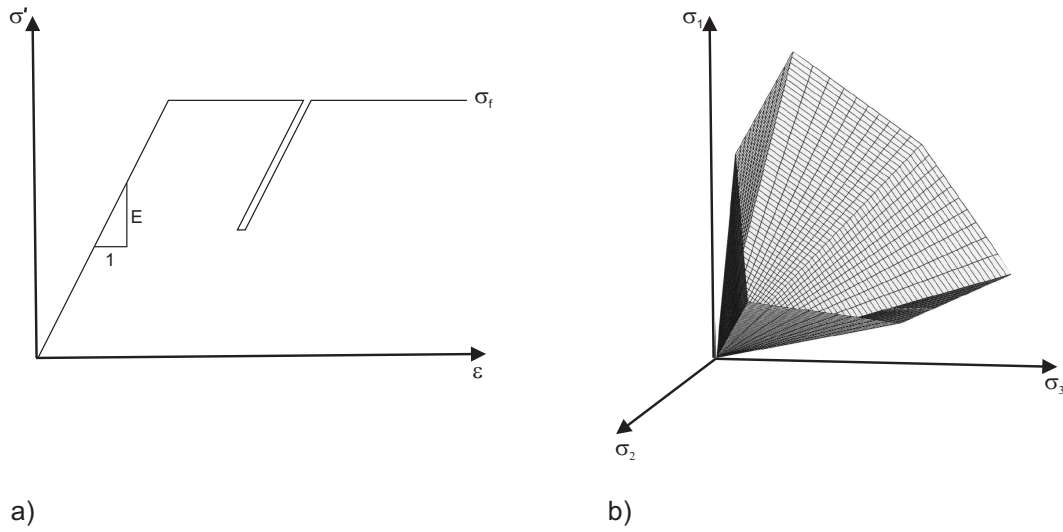


Figure A.1: Basic ideas of MC-Model: a) liner elastic perfectly plastic material behavior, b) yield surface in principal stress space with  $c' = 0$

where  $\dot{\sigma}$  is the stress rate,  $\dot{\epsilon}^e$  the corresponding elastic strain rate and  $\mathbf{D}^e$  is the elastic material stiffness matrix. The latter one is formulated using the two elastic material constants  $E$  and  $\nu$ . The formulation of perfect plasticity decomposes strain rates  $\dot{\epsilon}$  into an elastic and a plastic part

$$\dot{\epsilon} = \dot{\epsilon}^e + \dot{\epsilon}^p, \quad (\text{A.5})$$

where  $\dot{\epsilon}^p$  is the plastic strain rate. Combining Eqs. A.4 and A.5 yields

$$\dot{\sigma}' = \mathbf{D}^e(\dot{\epsilon} - \dot{\epsilon}^p). \quad (\text{A.6})$$

If associated plasticity is assumed, the plastic strain rates can then be formulated using the yield function introduced in Eqs. A.1 - A.3. Doing so, the plastic strain rates become vectors perpendicular to the surface of the yield function. However, the use of MC type of plastic potential functions would lead to a considerable overprediction of the angle of dilatancy. Therefore, in addition to yield functions, different plastic potential function  $g$  are employed. Using the plastic potential functions, non-associated plasticity is adopted and the plastic strain rates are formulated as

$$\dot{\epsilon}^p = \lambda_1 \frac{\partial g_1}{\partial \sigma'} + \lambda_2 \frac{\partial g_2}{\partial \sigma'} + \lambda_3 \frac{\partial g_3}{\partial \sigma'}, \quad (\text{A.7})$$

where  $\lambda_1$ ,  $\lambda_2$  and  $\lambda_3$  are plastic multipliers. The plastic potential functions are

$$g_1 = \frac{1}{2} \cdot |\sigma'_2 - \sigma'_3| - \frac{1}{2} \cdot (\sigma'_2 + \sigma'_3) \cdot \sin \psi \quad (\text{A.8})$$

$$g_2 = \frac{1}{2} \cdot |\sigma'_3 - \sigma'_1| - \frac{1}{2} \cdot (\sigma'_3 + \sigma'_1) \cdot \sin \psi \quad (\text{A.9})$$

$$g_3 = \frac{1}{2} \cdot |\sigma'_1 - \sigma'_2| - \frac{1}{2} \cdot (\sigma'_1 + \sigma'_2) \cdot \sin \psi \quad (\text{A.10})$$

The dilatancy angle  $\psi$  is used to model positive plastic volumetric strain increments (dilatancy) in case of plastic yielding. Using the consistency condition

$$\dot{f} = \frac{\partial f}{\partial \boldsymbol{\sigma}'} \dot{\boldsymbol{\sigma}}' = 0, \quad (\text{A.11})$$

and employing Eqs. A.6, A.7 and A.11, the plastic multipliers  $\lambda_1$ ,  $\lambda_2$  and  $\lambda_3$  are solved from the equation

$$\dot{f}_i = \frac{\partial f_i}{\partial \boldsymbol{\sigma}'} \mathbf{D}^e (\dot{\boldsymbol{\epsilon}} - \lambda_1 \frac{\partial g_1}{\partial \boldsymbol{\sigma}'} - \lambda_2 \frac{\partial g_2}{\partial \boldsymbol{\sigma}'} - \lambda_3 \frac{\partial g_3}{\partial \boldsymbol{\sigma}'}) = 0, \quad (\text{A.12})$$

where  $i$  runs from 1 to 3.

For more details on the formulation and implementation of the MC Model the reader is referred to SMITH and GRIFFITH (1982), VAN LANGEN and VERMEER (1990) and BRINKGREVE and VERMEER (2001).

## A.2 The Hardening-Soil Model

Similarly to the MC Model limiting states of stress are simulated by means of the effective shear parameters cohesion  $c'$ , friction angle  $\varphi'$  and the angle of dilatancy  $\psi$ . But pre-failure states of soil behavior are more accurately described by using three input stiffnesses: the triaxial loading stiffness  $E_{50}$ , the oedometer loading stiffness  $E_{oed}$  and the triaxial unloading stiffness  $E_{ur}$ . Compared to the MC Model the formulation of these stiffnesses is advanced, adopting a stress dependent formulation according to the ideas of OHDE (1951). In contrast to the constant MC formulation they increase/decrease with increasing/decreasing pressure. In the following basic features of the HS Model will be explained, adopting a standard drained triaxial test. Please note that compression is considered positive.

**Hyperbolic stress-strain relationship** When soil is subjected to primary deviatoric loading a decrease in stiffness is observed and irreversible plastic strains develop. For the special case of a drained triaxial test KONDNER (1963) was the first to formulate a hyperbolic relationship between the deviatoric stress  $q = \sigma_1 - \sigma_3$  and the axial strain  $\varepsilon_1$  and later a hyperbolic model was presented by DUNCAN and CHANG (1963). Although the HS Model by far supersedes the model presented by DUNCAN and CHANG one of its basic ideas is the hyperbolic formulation

$$\varepsilon_1 = \frac{q_a}{2 \cdot E_{50}} \cdot \frac{q}{q_a - q}, \quad (\text{A.13})$$

where  $q_a$  is the asymptotic failure stress as shown in Fig. A.2. This figure also shows the typical curve of a drained triaxial test with constant lateral pressure  $\sigma_3$ , assuming that under primary loading the behavior is distinctly nonlinear and hyperbolic up to a Mohr-Coulomb failure stress  $q_f$ . The asymptotic failure stress has the relation

$$q_a = \frac{q_f}{R_f} = (c \cdot \cot \varphi' + \sigma_3') \cdot \frac{2 \cdot \sin \varphi'}{R_f \cdot (1 - \sin \varphi')}, \quad (\text{A.14})$$



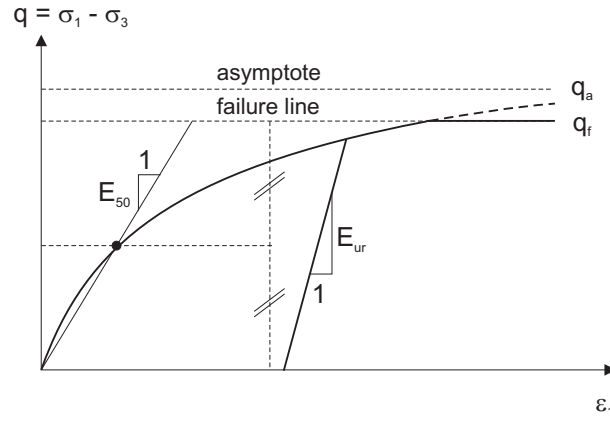


Figure A.2: Drained triaxial test: hyperbolic relationship for primary loading between deviatoric stress and axial strain

where  $R_f = 0.9$  for many soils. While the maximum stress is determined by the Mohr-Coulomb failure criterion, the hyperbolic part of the curve can be defined using a single secant modulus as additional input parameter. In the HS Model this is the stress dependent modulus  $E_{50}$ , as used in Eq. A.13, which is defined as

$$E_{50} = E_{50}^{ref} \cdot \left( \frac{c' \cdot \cot \varphi' + \sigma_3'}{c' \cdot \cot \varphi' + p^{ref}} \right)^m, \quad (\text{A.15})$$

where  $E_{50}^{ref}$  is a reference stiffness modulus, corresponding to the reference confining pressure  $p^{ref}$ . Following the ideas by OHDE (1951) the amount of stress dependency is governed by the exponent  $m$ , which can be measured both in oedometer tests and in triaxial tests. One tends to find values between 0.4 and 1.0. A value of 0.5 is typical for sands and clays tend to have  $m = 1.0$ .

In contrast to  $E_{50}$ , which determines the magnitude of both the elastic and the plastic strains,  $E_{ur}$  is a true elasticity modulus. In conjunction with a Poisson's ratio  $\nu_{ur}$  it determines the ground behavior under unloading and reloading; the indices  $ur$  stand for *unloading/reloading*. As the average primary loading modulus  $E_{50}$  the unloading modulus  $E_{ur}$  is stress-level dependent. For the HS Model it yields

$$E_{ur} = E_{ur}^{ref} \cdot \left( \frac{c' \cdot \cot \varphi' + \sigma_3'}{c' \cdot \cot \varphi' + p^{ref}} \right)^m, \quad (\text{A.16})$$

where  $E_{ur}^{ref}$  is the reference Young's modulus, corresponding to the reference confining pressure  $p^{ref}$ .

When comparing the hardening model to the previous elastic perfectly-plastic MC Model another significant difference is that plastic strains may already occur before the limit MC-failure stress is reached. This implies that the HS Model incorporates another yield surface, which is not fixed in principal stress space, but it may expand and soil hardening is simulated due to plastic straining. As shown in Fig. A.3a, distinction is

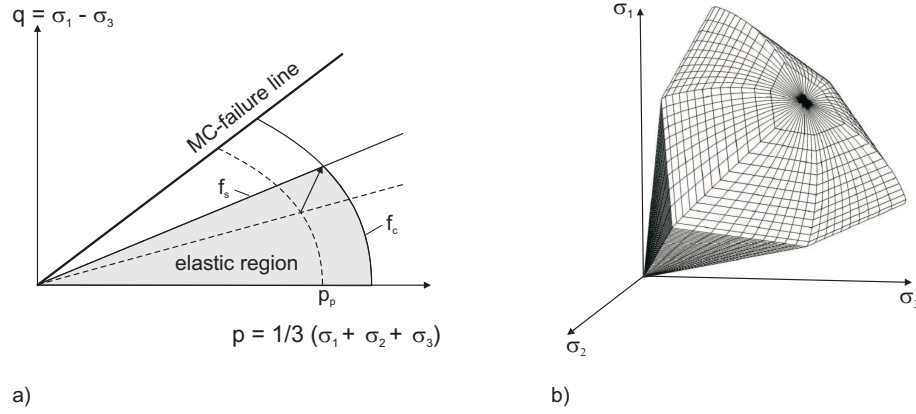


Figure A.3: Yield surface of the HS Model for  $c = 0$ : a) successive yield loci for shear hardening and compression hardening in p-q-space b) total yield contour in principal stress space

made between two types of hardening, namely shear hardening and compression hardening. For the shear hardening law a yield function  $f^s$  is introduced, which is a function of the triaxial loading stiffness  $E_{50}$  and for the compression hardening a yield function  $f^c$  is formulated, being governed by the oedometer loading stiffness  $E_{oed}$ . As also indicated in Fig. A.3a for unloading-reloading elastic soil behavior is assumed, adopting Hook's law with Young's modulus  $E_{ur}$ . Fig. A.3b shows the total contour of the HS yield surface in principal stress space.

**Yield function  $f_s$**  The yield function  $f_s$  adopted in the HS-Model has the formulation

$$f^s = \bar{f} - \gamma^p, \quad (\text{A.17})$$

where

$$\bar{f} = \frac{1}{E_{50}^{ref}} \cdot \left( \frac{c' \cdot \cot \varphi' + \sigma_3'}{c' \cdot \cot \varphi' + p^{ref}} \right)^m \cdot \frac{q}{1 - q/q_a} - \frac{2q}{E_{ur}^{ref}} \cdot \left( \frac{c' \cdot \cot \varphi' + \sigma_3'}{c' \cdot \cot \varphi' + p^{ref}} \right)^m \quad (\text{A.18})$$

is a function of stress and the hardening parameter

$$\kappa^s = \gamma^p = \varepsilon_1^p - \varepsilon_2^p - \varepsilon_3^p = 2 \cdot \varepsilon_1^p - \varepsilon_v^p \approx 2 \cdot \varepsilon_1^p \quad (\text{A.19})$$

is a function of plastic strains. Similar to the MC-Model the HS-Model adopts non-associated plasticity to determine the rates of plastic strain with the plastic potential

$$g^s = (3 - \sin \psi_m) \cdot q - 6 \cdot \sin \psi_m \cdot p, \quad (\text{A.20})$$

with  $p = 1/3 \cdot (\sigma_1 + \sigma_2 + \sigma_3)$ . The mobilized angle of dilatancy  $\psi_m$  is calculated according to the so-called stress-dilatancy equation of ROWE (1962)

$$\sin \psi_m = \frac{\sin \varphi_m - \sin \varphi_{cv}}{1 - \sin \varphi_m \cdot \sin \varphi_{cv}}, \quad (\text{A.21})$$

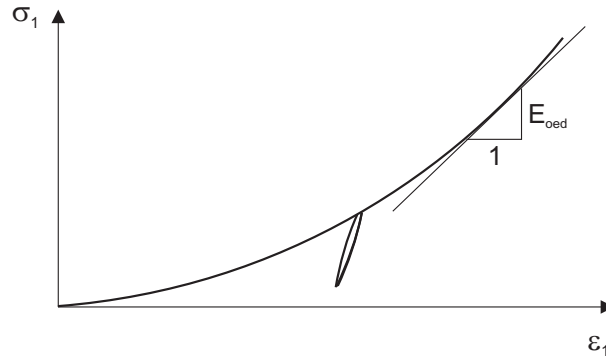


Figure A.4: Characteristic curve of an oedometer test

where the mobilized friction angle  $\varphi$  is governed by the equation

$$\sin \varphi_m = \frac{\sigma_1 - \sigma_3}{\sigma_1 + \sigma_3 + 2 \cdot c \cdot \cot \varphi} \quad (\text{A.22})$$

and the constant-volume angle  $\varphi_{cv}$  by the equation

$$\sin \varphi_{cv} = \frac{\sin \varphi - \sin \psi}{1 - \sin \varphi \cdot \sin \psi}. \quad (\text{A.23})$$

The dilatancy angle is thus positive as soon as  $\psi_m$  exceeds a constant-volume angle  $\varphi_{cv}$ . Considering dense materials contraction is excluded by taking  $\psi_m = 0$  for a mobilized friction angle  $\varphi_m < \varphi_{cv}$ .

**Yield function  $f_c$**  So far the model can be considered to be an elastoplastic reformulation of the model by DUNCAN and CHANG (1963) with an extension to shear hardening. Another extension of that early soil model is achieved by introducing compression hardening. The latter is formulated by means of cap-type yield surfaces, which makes the model both suitable for hard soils as well as very soft clays. The cap-type yield function has the formulation

$$f^c = \frac{q^2}{M^2} + (p + c \cdot \cot \varphi)^2 - (p_p + c \cdot \cot \varphi)^2 \quad (\text{A.24})$$

with

$$M = \frac{6 \cdot \sin \varphi}{3 - \sin \varphi}. \quad (\text{A.25})$$

The position and shape of the cap in stress space is governed by the isotropic preconsolidation pressure  $p_p$  as also indicated in Fig. A.3. The hardening law

$$\kappa^c = \varepsilon_v^{pc} = \frac{\beta}{1 - m} \left( \frac{p_p}{p^{ref}} \right)^{1-m} \quad (\text{A.26})$$

formulates the relation between the plastic volumetric cap-strain  $\varepsilon_v^{pc}$  and the preconsolidation stress  $p_p$ .  $p_{ref}$  is an isotropic reference pressure. The cap parameter  $\beta$  is not used as a direct input parameter. Instead the odometer stiffness  $E_{oed}$  is used as an input parameter which is linked to  $\beta$ . Fig. A.4 shows the typical characteristic curve of an oedometer test. In the HS Model the virgin oedometer stiffness obeys a stress dependency according to the formula

$$E_{oed} = E_{oed}^{ref} \cdot \left( \frac{c' \cdot \cot \varphi' + \sigma'_1}{c' \cdot \cot \varphi' + p^{ref}} \right)^m, \quad (\text{A.27})$$

where  $E_{oed}^{ref}$  is the reference Oedometer Modulus for the axial reference pressure  $p_{ref}$ . In the special case of  $m = 1$  one obtains a linear stress-dependency as usual for a clay. In addition to the moduli  $E_{50}$  and  $E_{ur}$ , the oedometer modulus  $E_{oed}$  is also an input modulus for the HS Model. Together with the parameters  $m, \nu_{ur}, c', \varphi'$  and the dilatancy angle  $\psi$ , there are a total of eight input parameters. To determine the rates of plastic volumetric strains associated plasticity, i.e.  $g^c = f^c$  is adopted.

**Plastic multipliers** The strain rates are decomposed into an elastic part  $\dot{\varepsilon}^e$  and into a plastic shear hardening part  $\dot{\varepsilon}^{ps}$  and/or volumetric hardening part  $\dot{\varepsilon}^{pc}$

$$\dot{\varepsilon} = \dot{\varepsilon}^e + \dot{\varepsilon}^{ps} + \dot{\varepsilon}^{pc} \quad (\text{A.28})$$

$$\dot{\varepsilon} = \mathbf{D}^{-1} \dot{\sigma} + \lambda^s \frac{\partial g^s}{\partial \sigma} + \lambda^c \frac{\partial g^c}{\partial \sigma} \quad (\text{A.29})$$

The plastic multipliers  $\lambda^s$  and  $\lambda^c$  are then solved from the consistency conditions  $\dot{f}^s = 0$  and  $\dot{f}^c = 0$ :

$$\dot{f}^s = \frac{\partial f^s}{\partial \sigma} \dot{\sigma} + \frac{\partial f^s}{\partial \kappa^s} \dot{\kappa}^s = \frac{\partial f^s}{\partial \sigma} \dot{\sigma} + \frac{\partial f^s}{\partial \kappa^s} \frac{\partial \kappa^s}{\partial \varepsilon^{ps}} \dot{\varepsilon}^{ps} = 0 \quad (\text{A.30})$$

$$\frac{\partial f^s}{\partial \sigma} \mathbf{D}^e \dot{\varepsilon} - \lambda^s \frac{\partial f^s}{\partial \sigma} \mathbf{D}^e \frac{\partial g^s}{\partial \sigma} + \lambda^s \frac{\partial f^s}{\partial \kappa^s} \frac{\partial \kappa^s}{\partial \varepsilon^{ps}} \frac{\partial g^s}{\partial \sigma} = 0 \quad (\text{A.31})$$

$$\Rightarrow \lambda^s = \frac{1}{H^s - d^s} \frac{\partial f^s}{\partial \sigma} \mathbf{D}^e \dot{\varepsilon} \quad (\text{A.32})$$

with the shear hardening modulus

$$H^s = \frac{\partial f^s}{\partial \kappa^s} \frac{\partial \kappa^s}{\partial \varepsilon^{ps}} \frac{\partial g^s}{\partial \sigma} \quad (\text{A.33})$$

and

$$d^s = \frac{\partial f^s}{\partial \sigma} \mathbf{D}^e \frac{\partial g^s}{\partial \sigma}, \quad (\text{A.34})$$

$$\dot{f}^c = \frac{\partial f^c}{\partial \boldsymbol{\sigma}} \dot{\boldsymbol{\sigma}} + \frac{\partial f^c}{\partial \boldsymbol{\kappa}^c} \dot{\boldsymbol{\kappa}}^c = \frac{\partial f^c}{\partial \boldsymbol{\sigma}} \dot{\boldsymbol{\sigma}} + \frac{\partial f^c}{\partial \boldsymbol{\kappa}^c} \frac{\partial \boldsymbol{\kappa}^s}{\partial \boldsymbol{\varepsilon}^{pc}} \dot{\boldsymbol{\varepsilon}}^{pc} = 0 \quad (\text{A.35})$$

$$\frac{\partial f^c}{\partial \boldsymbol{\sigma}} \mathbf{D}^e \dot{\boldsymbol{\varepsilon}} - \lambda^c \frac{\partial f^c}{\partial \boldsymbol{\sigma}} \mathbf{D}^e \frac{\partial g^c}{\partial \boldsymbol{\sigma}} + \lambda^c \frac{\partial f^c}{\partial \boldsymbol{\kappa}^c} \frac{\partial \boldsymbol{\kappa}^c}{\partial \boldsymbol{\varepsilon}^{pc}} \frac{\partial g^c}{\partial \boldsymbol{\sigma}} = 0 \quad (\text{A.36})$$

$$\Rightarrow \lambda^c = \frac{1}{H^c - d^c} \frac{\partial f^c}{\partial \boldsymbol{\sigma}} \mathbf{D}^e \dot{\boldsymbol{\varepsilon}} \quad (\text{A.37})$$

with the compression hardening modulus

$$H^c = \frac{\partial f^c}{\partial \boldsymbol{\kappa}^c} \frac{\partial \boldsymbol{\kappa}^c}{\partial \boldsymbol{\varepsilon}^{pc}} \frac{\partial g^c}{\partial \boldsymbol{\sigma}} \quad (\text{A.38})$$

and

$$d^c = \frac{\partial f^c}{\partial \boldsymbol{\sigma}} \mathbf{D}^e \frac{\partial g^c}{\partial \boldsymbol{\sigma}}, \quad (\text{A.39})$$

**Over Consolidation Ratio (OCR)** Another input parameter which is embedded in the HS Model is the Over Consolidation Ratio (compare Section 4.4.1). When using the HS Model to consider over consolidated grounds ( $OCR > 1$ ), initial stresses may be modelled according to Eq. 4.11. The elastic unloading from the maximum vertical overburden stress down to the actual initial stress implies that the actual stress state is not on the yield surface. Contrary to a normally consolidated initial stress state, with the actual stress state located directly on the HS-yield surface, the initial stress state of an overconsolidated ground is in the elastic region, shown in Fig. A.3. Due to the higher unloading-reloading stiffness  $E_{ur}$ , which is used to model the elastic region, overconsolidated grounds in the HS Model have an initially much stiffer response than normally consolidated grounds.

For more information on the formulation of yield functions and for a more detailed description of the implementation of the HS-Model, the reader is referred to SCHANZ (1998) and BRINKGREVE and VERMEER (2001).

### A.3 The HS-Small Model

The HS-Small Model constitutes an extension of the HS-Model. All model features described for the HS Model also hold true for the HS-Small Model. In addition to the HS Model, the HS-Small Model incorporates a formulation of the small strain stiffness. As displayed in Fig. A.5, small unloading-reloading stress-strain paths result in a considerably higher elasticity modulus  $E_0$ . In fact, maximum soil stiffness is observed at very low strain levels, e.g. strains smaller than  $10^{-5}$  (ATKINSON and SALLFORS, 1998). This effect is referred to as small strain stiffness.

The formulation of small strain stiffness in the HS-Small Model assumes that the decay of small strain stiffness is primarily related to either break up of bonding forces between

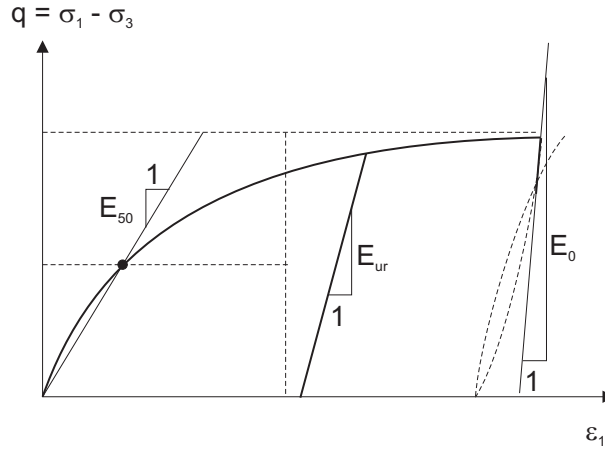


Figure A.5: HS-Small Model: extension of the HS Model incorporating small strain stiffness

soil particles or frictional particle forces exceeding their elastic limit. Thus, a drop of stiffness can be observed whenever inter-particle forces are reorganized and concentrated.

As shown in Fig. A.6, for strains higher than  $10^{-5}$  a rapid drop of small strain ground stiffness is measured, considering shear modulus  $G$ . The strain levels obtained here, are far below conventional laboratory testing, requiring special measuring devices such as dynamic methods or local strain gauges. To incorporate small strain stiffness effects into the HS Model a relatively simple expression for the small strain stiffness decay of the shear modulus, similar to the one suggested by SANTOS and CORREIA (2001), is adopted

$$G = \frac{G_0}{1 + 0.43 \cdot \frac{\gamma}{\gamma_{0.7}}}, \quad (\text{A.40})$$

where  $G$  is the actual shear modulus at shear strain  $\gamma$ ,  $G_0$  is the initial shear modulus and  $\gamma_{0.7}$  is the shear strain at which the initial shear modulus has reduced to  $0.7 \cdot G_0$ , as shown in Fig. A.6. For general states of stress the shear strain is expressed using the strain invariant

$$\gamma = \frac{1}{\sqrt{2}} \cdot \sqrt{(\varepsilon_1 - \varepsilon_2)^2 + (\varepsilon_2 - \varepsilon_3)^2 + (\varepsilon_3 - \varepsilon_1)^2}, \quad (\text{A.41})$$

which in the special case of triaxial loading reduces to  $\gamma = |\varepsilon_1 - \varepsilon_3|$ . While reducing the shear modulus with increasing shear strain, the Poisson's ratio  $\nu_{ur}$  is kept constant, such that the resulting bulk modulus is not a constant but is also reducing as a function of shear strain.

Conform the ideas by OHDE (1951) and the formulation of stiffnesses in the HS Model, the initial shear modulus  $G_0$  is pressure dependent according to the equation

$$G_0 = G_0^{ref} \cdot \left( \frac{c' \cdot \cot \varphi' + \sigma_3'}{c' \cdot \cot \varphi' + p_{ref}} \right)^m, \quad (\text{A.42})$$

The magnitude of  $G_0^{ref}$  is strongly correlated to the porosity of the soil. A typical correlation being used is  $G_0^{ref} = 450 \cdot \sqrt{p_{ref}}$  by BIAREZ and HICHER (1994).

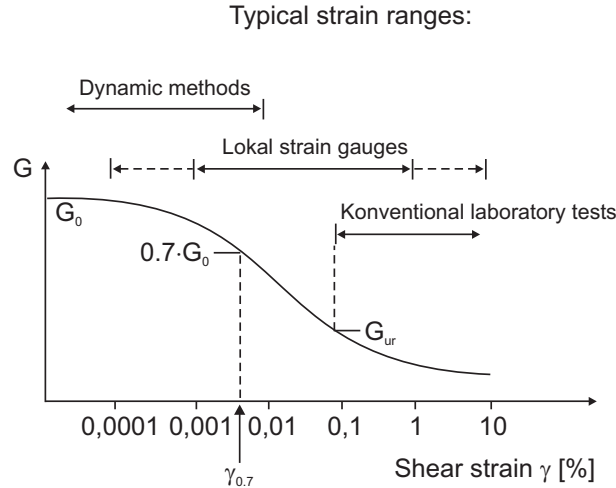


Figure A.6: Small strain stiffness curve for a particular soil adopting shear modulus

Fig. A.6 shows the stiffness degradation curve, reaching far into the plastic material behavior at larger strains. According to the formulation of the HS Model, stiffness degradation due to plastic straining is modelled by involving material hardening. Therefore, before reaching plastic material behavior, the formulation of the small strain stiffness curve is cut off at the unloading-reloading shear modulus  $G_{ur}$ , defined as

$$G_{ur} = \frac{E_{ur}}{2 \cdot (1 + \nu_{ur})}. \quad (\text{A.43})$$

The elastic constants  $E_{ur}$  and  $\nu_{ur}$  have already been introduced in the HS Model. Eq. A.43 indicates that  $G_{ur}$  is the shear modulus in complete deviatoric unloading as illustrated in Fig. A.5.

Besides the input parameters as introduced for the HS Model, there are a set of two additional input parameters for the HS-Small Model: the elastic small strain shear modulus  $G_0^{ref}$  at reference pressure  $p_{ref}$  and the threshold value  $\gamma_{0.7}$  in primary loading. A more detailed explanation of the HS-Small Model can be found in BENZ (2006).

# Bibliography

- T. I. ADDENBROOKE, D. M. POTTS, and A. M. PUZRIN. The influence of pre-failure soil stiffness on the numerical analysis of tunnel construction. *Géotechnique*, 47(3):693–712, 1997.
- H. AHRENS, E. LINDNER, and K.-H. LUX. Zur Dimensionierung von Tunnelausbauten nach den 'Empfehlungen zur Berechnung von Tunneln im Lockergestein (1980)'. *Die Bautechnik*, 8:260–273, 1982.
- J. H. ATKINSON and G. SALLFORS. Experimental determination of soil properties. In *10th Eur. Conference on Soil Mechanics*, number 3, pages 915–956, Florence, 1998.
- P. B. ATTEWELL and J. P. WOODMAN. Predicting the dynamics of ground settlement and its derivatives caused by tunnelling in soil. *Ground Engineering*, 15(8):13–22, 1982.
- P. B. ATTEWELL, J. YEATES, and A. R. SELBY. *Soil Movements Induced by Tunnelling and their Effects on Pipelines and Structures*. Blackie, Glasgow, 1986.
- C. E. AUGARDE, H. J. BURD, and G. T. HOULSBY. Some experience of modeling tunneling in soft ground using three-dimensional finite elements. In *4th European conference on Numerical Methods in Geotechnical Engineering*, pages 603–612, Udine, Italy, 1998.
- S. BABENDERERDE. *Underground Construction in Germany 2000*, chapter Verpressen der Schildschwanzfuge hinter einer Tunnelvortriebsmaschine mit Tübbingausbau, pages 113–116. STUVA, DAUB, 2000.
- S. BABENDERERDE and J. HOLZHÄUSER. *Taschenbuch für den Tunnelbau 2000*, volume 24, chapter Betriebszustand Druckluftstützung beim Hydroschild, pages 231–252. Glückauf, Essen, 2000.
- K. J. BAKKER. Monitoring the second heinenoord tunnel. Commission k100, report, Centre for Underground Consturction (COB), The Netherlands, 1999.
- K. J. BAKKER. *Soil Retaining Structures, Development of Models for Structural Analysis*. Phd thesis, Technical University of Delft, 2000.
- K. J. BATHE. *Finite Element Procedures in Engineering Analysis*. Prentice Hall, Englwodd Cliffs, 1982.
- M. BAUDENDISTEL. *Rock Mechanics*, chapter Zum Entwurf von Tunneln mit großem Ausbruchsquerschnitt, pages 75–100. Number Suppl. 8. 1979.



- T. BENZ. *Small-Strain Stiffness of Soils and its Numerical Consequences*. PhD thesis, Institute of Geotechnical Engineering, University of Stuttgart, Stuttgart, 2006.
- J. BIAREZ and P.-Y. HICHER. Elementary mechanics of soil behaviour. Technical report, Ecole Centrale de Paris, Cedex, France, 1994.
- L. BJERRUM. Engineering geology of norwegian normally-consolidated marine clays as related to settlements of buildings. *Seventh Rankine Lecture. Geotechnique*, 17:81–118, 1967.
- C. BLIEHM. *Advances in Geotechnical Engineering and Tunnelling*, chapter 3D Finite Element Berechnungen im Tunnelbau - 3D finite element calculation in tunnelling. Number 4. Logos, Berlin, 2001.
- R. B. J. BRINKGREVE and P. A. VERMEER. *PLAXIS Finite Element Code for Soil and Rock Analyses*. A. A. Balkema, Rotterdam, 2001.
- B. B. BROMS and H. BENNERMARK. Stability of clay at vertical openings. *ASCE Soil Mechanics and Foundations Division*, 93(SM1), 1967.
- E. T. BROWN, J. W. BRAY, B. LADANYI, and E. HOEK. Ground response curves for rock tunnels. *Journal of Geotechnical Engineering ASCE*, 109(1):15–39, 1983.
- A. BULL. Stresses in the linings of shield-driven tunnels. *ASCE Soil Mechanics and Foundations Division*, pages 1363–1394, 1944.
- W.-I. CHOU and A. BOBET. Predictions of ground deformations in shallow tunnels in clay. *Tunnelling and Underground Space Technology*, 17:3–19, 2002.
- G. W. CLOUGH and B. SCHMIDT. *Soft Clay Engineering*, chapter Design and performance of excavations and tunnels in soft clay, pages 569–634. Elsevier, 1981.
- E. J. CORDING and W. H. HANSMIRE. Displacements around soft ground tunnels - general report. In *5th Pan American Conference on Soil Mechanics and Foundation Engineering, Session IV*, pages 571–632, Buenos Aires, 1975. Balkema: Rotterdam.
- R. N. CRAIG and A. M. MUIR WOOD. A review of tunnel lining practice in the united kingdom. Supplem. 335, Transport and Road Research Laboratory, 1978.
- D. J. CURTIS. Correspondence on muir wood, a.m. : The circular tunnel in elastic ground. *Geotechnique*, 25(1):231–237, 1975.
- DGEG. Empfehlungen zur Berechnung von schildvorgetriebenen Tunneln. *Bautechnik*, 50(8):253–257, 1973.
- B. F. J. DIJK and F. J. KAALBERG. 3-d geotechnical model for the north/southline in amsterdam. In *4th European conference on Numerical Methods in Geotechnical Engineering*, pages 739–749, Udine, Italy, 1998.

- M. DOLEŽALOVÁ. Approaches to numerical modelling of ground movements due to shallow tunnelling. In *Proc. 2nd Int. Conf. on Soil Structure Interaction in Urban Civil Engineering*, pages 365–373, Zurich, 2002.
- H. DUDDECK. Zu den Berechnungsmethoden und zur Sicherheit von Tunnelbauten. *Bauingenieur*, 47(2):43–52, 1972.
- H. DUDDECK. Zu den Berechnungsmodellen für die Neue Österreichische Tunnelbauweise (NÖT). *Rock Mechanics*, (Suppl. 8):3–27, 1979.
- H. DUDDECK. Empfehlungen zur Berechnung von Tunneln im Lockergestein (1980). Released from Arbeitskreis Tunnelbau, DGEG. *Bautechnik*, 57(10):349–356, 1980.
- H. DUDDECK and J. ERDMANN. Structural design models for tunnels. *Tunnelling 82*, pages 83–91, 1982.
- J. M. DUNCAN and C.-Y. CHANG. Nonlinear analysis of stress and strain in soils. *Journal of the Soil Mechanics and Foundations Division ASCE*, (96, SM 5):1629–1653, 1963.
- M. R. DYER, M. T. HUTCHINSON, and N. EVANS. Sudden valley sewer: a case history. In R. J. Mair and R. N. Taylor, editors, *International Symposium on Geotechnical Aspects of Underground Construction in Soft Ground*, pages 671–676, London, 1996. Balkema.
- H. H. EINSTEIN. Improved desing of tunnel supports. *Cambridge, Mass.: Massachusetts Institute of Technology, Department of Civil Engineering*, 1 to 6, 1979-1980.
- H. H. EINSTEIN and C. W. SCHWARZ. Simplified analysis for tunnel supports. *Journal of the Geotechnical Engineering Division*, pages 499–517, 1979.
- K. ENGELBRETH. Correspondance on morgan, h.d.: A contribution to the analysis of stress in a circular tunnel. *Geotechnique*, 11(3):246 – 248, 1961.
- J. ERDMANN. *Vergleich ebener und Entwicklung räumlicher Berechnungsverfahren für Tunnel*. Bericht nr. 83-40, Institut für Statik, TU Braunschweig, 1983.
- R. FENNER. Untersuchung zur Erkenntnis des Gebirgsdrucks. *Glückauf*, 74(32):681–695, 1938.
- H. FLECK and S. SKLIVANOS. Statische Berechnung gebetteter Hohlräumeaussteifungen (Auskleidungen) bei Berücksichtigung einer tangentialern Bettungsmodulwirkung und Vergleich mit Ergnissen nach der Kontinuumstheorie. *Forschung Ing.-Wesen*, 44 (4):101–136, 1978.
- J. N. FRANZIUS, D. M. POTTS, and J. B. BURLAND. The influence of soil anisotropy and  $k_0$  on ground surface movements resulting from tunnel excavation. *Géotechnique*, 55 (3):189–199, 2005.

- R. J. GUEDES and C. SANTOS PEREIRA. The role of the soil  $k_0$  value in numerical analysis of shallow tunnels. In *Proc. Int. Symp. Geotechnical Aspects of Underground Construction in Soft Ground, IS-Tokyo '99*, pages 379–384, Tokyo, 2002.
- A. H. GUILLOUX, H. BISSONNAIS, J. ROBERT, and A. BERNARDET. Influence of the  $k_0$  coefficient on the design of tunnels in hard soils. In *Proc. of the World Tunnel Congress'98, Tunnels and Metropolises*, pages 367–392, Sao Paulo, Brazil, 1998. Rotterdam: Balkema.
- M. J. GUNN. The prediction of surface settlement profiles due to tunnelling. In G. T. Houlsby and A. N. Schofield, editors, *Predictive soil mechanics: Proceedings of the Wroth Memorial symposium*, pages 304–316, London, 1993. Thomas Telford.
- E. A. HANAFY and J. J. EMERY. Advancing face simulation of tunnel excavations and lining placement. *Underground Rock Engineering*, 22:119–125, 1980.
- F. HARTMANN. Elastizitätstheorie des ausgekleideten Tunnelhohlraumes und des eingebohrten kreisförmigen Rohres. *Strasse Brücke Tunnel*, 22(8, 9):209–215, 241–246, 1970.
- B. H. M. HEWETT and S. JOHANNESSEN. *Schild- und Druckluft-Tunnelbau*. Werner-Verlag, 1922.
- F. J. M. HOEFSLOOT and A. VERWEIJ. 4d grouting pressure model plaxis. In *5th Int. Symposium on Geotechnical Aspects of Underground Construction in Soft Ground*, pages 529–534, 2005.
- E.-D. HORNIG and R. F. BUCHMAIER. Verformungsverhalten vorbelasteter Tonböden. Forschungsbericht, Fachhochschule Stuttgart - Hochschule für Technik, Stuttgart, 2002.
- E.-D. HORNIG and R. F. BUCHMAIER. Laboratory and field tests investigating the stress strain behaviour of weathered Keuper Mudstone. In *Proc. of Int. Conf. on Problematic Soils*, volume 1, pages 389–396, Famagusta, N. Zypern, May 2005. Eastern Mediterranean University.
- ITA. Views on structural design models for tunnelling. *Advances in tunnelling technology and subsurface use*, 2(3):153–229, 1982.
- ITA. Guidelines for the design of tunnels. *Tunnelling and Underground Space Technology*, 3(3):237–249, 1988.
- T. KASPAR and G. MESCHKE. A 3d finite element simulation model for tbm tunnelling in soft ground. *Int. J. Numer. Anal. Meth. Geomech.*, 28:1441–1460, 2004.
- R. KATZENBACH. Entwicklungstendenzen beim Bau und der Berechnung oberflächennaher Tunnel in bebautem Stadtgebiet. Mitteilungen 24, Versuchsanstalt für Bodenmechanik und Grundbau, Technische Hochschule Darmstadt, November 1981.

- R. KATZENBACH and H. BRETH. Nonlinear 3d analysis for natm in frankfurt clay. In *10th Int. Conf. Soil Mech. and Found. Eng.*, volume 1, pages 315–318, Rotterdam, 1981. Balkema.
- D. KOLYMBAS. *Geotechnik-Tunnelbau und Tunnelmechanik*. Springer-Verlag, 1998. ISBN 3-540-62805-3.
- R. L. KONDNER. Hyperbolic stress-strain response: cohesive soils. *Journal of the Soil Mechanics and Foundations Division ASCE*, (89, SM 1):115–143, 1963.
- F. LAABMAYR and G. SWOBODA. Grundlagen und Entwicklung bei Entwurf und Berechnung im seichtliegenden Tunnel - Teil1. *Felsbau*, 4(3):138–143, 1986.
- G. T. K. LEE and C. W. W. NG. Three-dimensional analysis of ground settlements due to tunnelling: role of  $k_0$  and stiffness anisotropy. In *Proc. Int. Symp. on Geotechnical Aspects of Underground Construction in Soft Ground*, pages 617–622, Toulouse, 2002.
- K. M. LEE and R. K. ROWE. An analysis of three-dimensional ground movements: the thunder bay tunnel. *Canadian Geotechnical Journal*, 28:25–41, 1991.
- G. LOMBARDI. Zur Bemessung der Tunnelauskleidung mit Berücksichtigung des Bauvorganges. *Schweizerische Bauzeitung*, 89(32), 1971.
- S. R. MACKLIN. The prediction of volume loss due to tunnelling in overconsolidated clay based on heading geometry and stability number. *Ground Engineering*, 32(4):30–33, 1999.
- B. MAIDL, U. MAIDL, and N. RUSE. Erfahrung mit der FEM-Simulation im Rahmen des Prozesscontrollings beim Schildvortrieb. *Bauingenieur*, 80:337–342, 2005.
- R. J. MAIR. Settlement effects of bored tunnels. In *International Symposium on Geotechnical Aspects of Underground Construction in Soft Ground*, pages 43–53, London, 1996. Balkema.
- R. J. MAIR and R. N. TAYLOR. Bored tunnelling in the urban environment. In *14th international Conference on Soil Mechanics and Foundation Engineering*, pages 2353–2385, Hamburg, 1997. Balkema: Rotterdam.
- R. J. MAIR, R. N. TAYLOR, and BRACEGIRDLE. Subsurface settlement profiles above tunnels in clay. *Géotechnique*, 43(2):315–320, 1993.
- H. MEISSNER. Tunnelbau unter Tage - Empfehlungen des Arbeitskreises 1.6 Numerik in der Geotechnik. *Geotechnik*, 19(2):99–108, 1996.
- S. MÖLLER. Institutsbericht, Institute of Geotechnical Engineering, University of Stuttgart, Stuttgart, 2006.

- S. MÖLLER, T. LEHMANN, and E. ROGOWSKI. Dreidimensionale Finite-Element-Berechnung der Setzungsmulde am Beispiel des Steinhaldenfeldtunnels in Stuttgart. In *Kolloquium Bauen in Boden und Fels*, pages 275–282, TAE, Ostfildern, 2004.
- L. MÜLLER-SALZBURG. *Der Felsbau*, chapter Dritter Band: Tunnelbau. Ferdinand Enke Verlag, Stuttgart, 1978.
- Z.-C. MOH, D. H. JU, and R. N. HWANG. Ground movements around tunnels in soft ground. In R. J. Mair and R. N. Taylor, editors, *International Symposium on Geotechnical Aspects of Underground Construction in Soft Ground*, pages 725–730, London, 1996. Balkema.
- H. D. MORGAN. A contribution to the analysis of stress in a circular tunnel. *Geotechnique*, 11(3):37–46, 1971.
- A. M. MUIR WOOD. The circular tunnel in elastic ground. *Geotechnique*, 25(1):115–127, 1975.
- B. M. NEW and M. P. O'REILLY. Tunnelling induced ground movements; predicting their magnitude and effects. In *4th International Conference on Ground Movements and Structures*, volume 1, pages 671–697, Cardiff, 1991. Pentech Press.
- J. OHDE. *Grundbaumechanik*. Bd. III. Hütte, 1951.
- M. P. O'REILLY and B. M. NEW. Settlements above tunnels in the united kingdom - their magnitude and prediction. *Tunnelling 82*, pages 173–181, 1982.
- F. PACHER. Deformationsmessungen im Versuchsstollen als Mittel zur Erforschung des Gebirgsverhaltens und zur Bemessung des Ausbaues. *Felsmechanik und Ing. Geologie*, Suppl. I:49–161, 1964.
- R. B. PECK. Deep excavations and tunneling in soft ground. In *7th int. Conference on Soil Mechanics and Foundation Engineering*, pages 225–290. Sociedad Mexican de Mecanica de Suelos, A. C., 1969.
- R. B. PECK, A. J. HENDRON, and B. MOHRAZ. State of the art of soft-ground tunnelling. In *Proceedings of the 1st North American Rapid Excavation and Tunnelling Conference*, volume 1, pages 260–286, Illinois, 1972.
- W. J. RANKIN. Ground movements resulting from urban tunnelling: prediction and effects. In *Conference on Engineering Geology of Underground Movements*, pages 79–92, Nottingham BGS, 1988.
- E. ROGOWSKI. Personal communication, Landesamt für Geologie, Rohstoffe und Bergbau Baden-Württemberg, 2004.
- P. W. ROWE. The stress-dilatancy relation for static equilibrium of an assembly of particles in contact. In *Proceedings of the Royal Society of London*, volume 62 of A, *Mathematical and Physical Sciences*, pages 500–527, 1962.

- R. K. ROWE, J. R. BOOKER, and N. P. BALAAM. Application of the initial stress method to soil structure interaction. *International Journal of Numerical Methods in Engineering*, 12:873–880, 1978.
- R. K. ROWE, K. Y. LO, and G. J. KACK. A method of estimating surface settlement above tunnels constructed in soft ground. *Canadian Geotechnical Journal*, 20:11–22, 1983.
- L. ROZSA. Die Bemessung kreisförmiger Tunnelwandungen aus präfabrizierten Stahlbetonelementen nach dem Verfahren der Grenzbelastungen. *Bauingenieur*, 38(11): 434–441, 1963.
- N. M. RUSE. *Räumliche Betrachtung der Standsicherheit der Ortsbrust beim Tunnelvortrieb*. PhD thesis, Institute of Geotechnical Engineering, University of Stuttgart, Stuttgart, 2004.
- J. A. SANTOS and A. G. CORREIA. Reference threshold shear strain of soils. its application to obtain an unique strain-dependent shear modulus curve for soil. In *15th International Conference on Soil Mechanics and Geotechnical Engineering*, volume 1, pages 267–270, Istanbul, Turkey, 2001.
- K. SATTLER. Die neue Österreichische Tunnelbauweise, Teil ii: Statische Wirkungsweise und Bemessung. *Bauingenieur*, 40(8):297–301, 1965.
- T. SCHANZ. Zur Modellierung des mechanischen Verhaltens von Reibungsmaterialien. *Mitteilungen Heft 45*, Institut of Geotechnical Engineering, University of Stuttgart, Stuttgart, 1998.
- K. SCHIKORA and T. FINK. Berechnungsmethoden moderner bergmännischer Bauweisen beim U-Bahn-Bau. *Bauingenieur*, 57:193–198, 1982.
- H. SCHMID. *Statische Probleme des Tunnel- und Druckstollenbaus*. Berlin, 1926.
- B. SCHMIDT. Discussion of earth pressure at rest related to stress history. *Canadian Geotechnical Journal*, 4(4):239–242, 1966.
- B. F. SCHMIDT. *Settlements and ground movements associated with tunnelling in soils*. Phd thesis, University of Illinois, Urbana, 1969.
- H. SCHULZE and H. DUDDECK. Statische Berechnung schildvorgetriebener Tunnel. In *Festschrift Beton- und Monierbau AG 1889-1964*, pages 87–114, Düsseldorf, 1964a.
- H. SCHULZE and H. DUDDECK. Stresses in shield driven tunnels. *Beton und Stahlbetonbau*, (8):169–175, 1964b.
- H. F. SCHWEIGER. *Ein Beitrag zur Anwendung der Finite-Elemente-Methode in der Geotechnik*. Mitteilungsheft, Technische Universität Graz, Institut für Bodenmechanik und Grundbau, Graz, 1995.

- I. M. SMITH and D. V. GRIFFITH. *Programming the Finite Element Method*. J. Wiley & Sons, Chisester, UK, 2 edition, 1982.
- G. SWOBODA, W. MERTZ, and A. SCHMID. Three dimensional models to simulate tunnel excavation. In *Proc. Int. Symp. Numerical Methods Geomechanics (NUMOG III)*, pages 277–318, Niagara Falls, Canada, 1989.
- A. M. TALMON and A. BEZUIJEN. Grouting the tail void of bored tunnels: the role of hardening and consolidation of grouts. In *5th Int. Symposium on Geotechnical Aspects of Underground Construction in Soft Ground*, pages 319–325, 2005.
- A. O. URIEL and C. SAGASETA. General report: Discussion session 9: Selection of design parameters for underground construction. In *12th International Conference on Soil Mechanics and Foundation Engineering*, volume 4, pages 2521–2551, Rio de Janeiro, 1989. Balkema.
- H. VAN LANGEN and P. A. VERMEER. Automatic step size correction for non-associated plasticity problems. *International Journal for Numerical Methods in Engineering*, 29:579–598, 1990.
- P. A. VERMEER. Bodenmechanik. In *Vorlesungsunterlagen Geotechnik II*. Institut für Geotechnik, Universität Stuttgart, 2000.
- P. A. VERMEER and R. BRINKGREVE. *PLAXIS Version 5 Manual*. Rotterdam, a. a. balkema edition, 1993.
- P. A. VERMEER, T. MARCHER, and N. RUSE. On the ground response curve. *Felsbau*, 20(6):19–24, 2002.
- H. WAGNER, J. ARNOLD, and S. MÜLLER. Tunnelbau in plastischem Lockergestein mit variabler Überhöhung und kontrolliertem Sohlschluss. *Geotechnik*, 3(3):120–126, 1980.
- R. WINDELS. Kreisring im elastischen Kontinuum. *Der Bauingenieur*, 42(12):429–439, 1967.
- E. WINKLER. *Die Lehre von der Elasticitaet und Festigkeit*, volume 1. Theil. Verlag v. H. Dominicus, Prag, 1867.
- W. WINKLER. Anwendung der Federanalogie bei der statischen Berechnung von kreisförmigen Tunnelprofilen. *Schweizerische Bauzeitung*, 88(44):991–993, 1970.
- W. WITTKÉ. *Rock Mechanics*. Springer-Verlag, Berlin, 1984.
- O. C. ZIENKIEWICZ and R. L. TAYLOR. *The Finite Element Method*. McGraw Hill, London, 4 edition, 1991.

## Curriculum Vitae

Name: Sven Möller

Date of birth: 30th of September 1975

Place of birth: Berlin, (West) Germany

Nationality: German

Marital Status: Married, two children

Education: 09/82-07/92  
Free Waldorf School Rengoldshausen/Überlingen  
08/92-01/93  
The Toronto Waldorf School, Canada  
02/93-07/95  
Free Waldorf School Rengoldshausen/Überlingen

Civil service: 07/95-01/97  
Civil service at "Freunde der Erziehungskunst Rudolf Steiners e.V.", Germans teacher at School No. 625, St. Petersburg, Russia

Studies: 04/97-07/01  
Civil Engineering, University of Stuttgart  
Specialization in: Geotechnical engineering, structural engineering and construction operation

Professional Occupation: 08/01-11/01  
Graduate assistant at the Institute of Geotechnical Engineering, University of Stuttgart since 11/01  
Assistant Lecturer at the Institute of Geotechnical Engineering, University of Stuttgart



## Mitteilungen des Instituts für Geotechnik

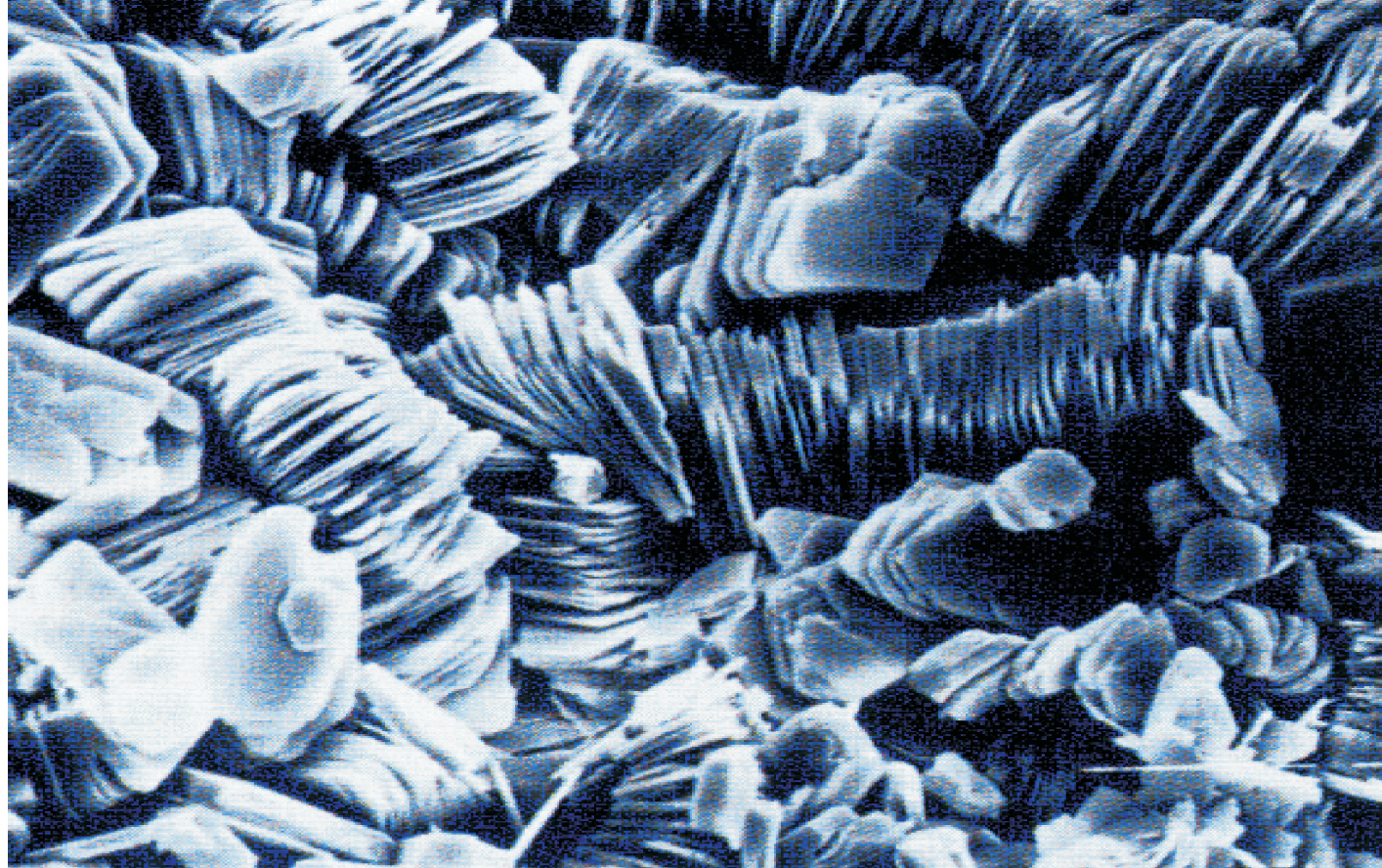
- Nr. 01 Thamm, B. R. (1974) Anfangssetzungen und Anfangsporenwasserüberdrücke eines normalverdichteten wasser-gesättigten Tones.  
€ 5,11
- Nr. 02 Gußmann, P. (1975) Einheitliche Berechnung von Grundbruch und Böschungsbruch.  
€ 2,56
- Nr. 03 Feeser, V. (1975) Die Bedeutung des Kalziumkarbonats für die bodenphysikalischen Eigenschaften vom Löß.  
**Vergriffen**
- Nr. 04 Du Thin, K. (1976) Standsicherheit von Böschungen: Programm-Dokumentation.  
**Vergriffen**
- Nr. 05 Smoltczyk, U. / (1976) Messungen an Schleusen in der UDSSR.  
Pertschi, O. / Schleusennorm der UDSSR (SN 30365).  
Hilmer, K.  
**Vergriffen**
- Nr. 06 Hilmer, K. (1976) Erddruck auf Schleusen-kammerwände.  
€ 9,20
- Nr. 07 Laumans, Q. (1977) Verhalten einer ebenen, in Sand eingespannten Wand bei nichtlinearen Stoffeigenschaften des Bodens.  
€ 9,20
- Nr. 08 Lächler, W. (1977) Beitrag zum Problem der Teilflächenpressung bei Beton am Beispiel der Pfahlkopfanschlüsse.  
**Vergriffen**
- Nr. 09 Spotka, H. (1977) Einfluß der Bodenverdichtung mittels Oberflächenrüttelgeräten auf den Erddruck einer Stützwand bei Sand.  
**Vergriffen**
- Nr. 10 Schad, H. (1979) Nichtlineare Stoffgleichungen für Böden und ihre Verwendung bei der numerischen Analyse von Grundbauaufgaben.  
**Vergriffen**
- Nr. 11 Ulrich, G. (1980) Verschiebungs- und kraftgesteuerte Platten-druckversuche auf konsolidierenden Böden.  
Gußmann, P. Zum Modellgesetz der Konsolidation.  
€ 10,23
- Nr. 12 Salden, D. (1980) Der Einfluß der Sohlenform auf die Traglast von Fundamenten.  
€ 12,78

- Nr. 13 Seeger, H. (1980) Beitrag zur Ermittlung des horizontalen Bettungsmoduls von Böden durch Seitendruckversuche im Bohrloch.  
€ 12,78
- Nr. 14 Schmidt, H.H. (1981) Beitrag zur Ermittlung des Erddrucks auf Stützwände bei nachgiebigem Baugrund.  
€ 12,78
- Nr. 15 Smolczyk, U. / Schweikert, O. (1981) Vorstudie über bauliche Alternativen für Durchgangsstraßen in Siedlungen.  
€ 6,14
- Nr. 16 Malcharek, K. / Smolczyk, U. (1981) Vergleich nationaler Richtlinien für die Berechnung von Fundamenten.  
€ 7,67
- Nr. 17 Gruhle, H.D. (1981) Das Verhalten des Baugrundes unter Einwirkung vertikal gezogener Ankerplatten als räumliches Problem des Erdwiderstandes.  
**Vergriffen**
- Nr. 18 Kobler, W. (1982) Untersuchungen über Böschungs- und Grundbruch bei begrenzten Lastflächen.  
€ 12,78
- Nr. 19 Lutz, W. (1983) Tragfähigkeit des geschlitzten Baugrunds neben Linienlasten.  
€ 12,78
- Nr. 20 Smolczyk, U. (1983) Studienunterlagen Bodenmechanik und Grundbau; überarbeitete Ausgabe 1983.  
€ 20,45
- Nr. 21 Schweikert, O. (1984) Der Einfluß des Böschungswinkels auf die Berechnung des aktiven Erddrucks.  
€ 10,23
- Nr. 22 Vogt, N. (1984) Erdwiderstandsermittlung bei monotonen und wiederholten Wandbewegungen in Sand.  
**Vergriffen**
- Nr. 23 Buchmaier, R. (1985) Zur Berechnung von Konsolidationsproblemen bei nichtlinearem Stoffverhalten.  
€ 12,78
- Nr. 24 Schad, H. (1985) Möglichkeiten der Böschungssicherung bei kleinen Baugruben.  
Smolczyk, U. /  
Schad, H. /  
Zoller, P.  
Sonderkonstruktionen der Böschungssicherung.  
€ 17,90
- Nr. 25 Gußmann, P. (1986) Die Methode der Kinematischen Elemente.  
€ 10,23

- Nr. 26 Steinmann, B. (1985) Zum Verhalten bindiger Böden bei monotoner einaxialer Beanspruchung.  
**Vergriffen**
- Nr. 27 Lee, S.D. (1987) Untersuchungen zur Standsicherheit von Schlitzn im Sand neben Einzelfundamenten.  
**Vergriffen**
- Nr. 28 Kolb, H. (1988) Ermittlung der Sohlreibung von Gründungskörpern unter horizontalem kinematischen Zwang.  
€ 12,78
- Nr. 29 Ochmann, H. (1988) Ebene Grenzzustände von Erdböschungen im stochastischen Sicherheitskonzept.  
€ 12,78
- Nr. 30 Breinlinger, F. (1989) Bodenmechanische Stoffgleichungen bei großen Deformationen sowie Be- und Entlastungsvorgängen.  
€ 15,34
- Nr. 31 Smoltczyk, U. / Breinlinger, F. / Schad, H. / Wittlinger, M. (1989) Beitrag zur Bemessung von Tunneln in offener Bauweise.  
€ 12,78
- Nr. 32 Gußmann, P. / Schanz, T. / Smoltczyk, U. / Willand, E. (1990) Beiträge zur Anwendung der KEM (Erddruck, Grundbuch, Standsicherheit von Böschungen)  
**Vergriffen**
- Nr. 33 Gruhle, H.D. (1990) Der räumliche Erdwiderstand vor überwiegend horizontal belasteten Ankerplatten.  
**Vergriffen**
- Nr. 34 Henne, J. (1995) Zur Bewehrung von verformten Bodenschichten durch Einsatz zugfester Geokunststoffe.  
€ 15,34
- Nr. 35 Wittlinger, M. (1994) Ebene Verformungsuntersuchungen zur Weckung des Erdwiderstandes bindiger Böden.  
€ 15,34
- Nr. 36 Schad, H. (1992) Zeit- und geschwindigkeitsabhängiges Materialverhalten in der Geotechnik – Experimentelle Erfassung und numerische Analyse.  
€ 15,34
- Nr. 37 Belz, I. (1992) Zur Ermittlung dynamischer Bodenkennwerte in situ aus der Systemantwort des Erregers.  
€ 15,34

- Nr. 38 Ma, J. (1994) Untersuchungen zur Standsicherheit der durch Stützscheiben stabilisierten Böschungen. € 15,34
- Nr. 39 Smoltczyk, U. (1994) Sonderheft: 25 Jahre Lehre und Forschung in der Geotechnik. € 15,34
- Nr. 40 Rilling, B. (1994) Untersuchungen zur Grenztragfähigkeit bindiger Schüttstoffe am Beispiel von Lößlehm. € 17,90
- Nr. 41 Vermeer, P.A. (1996) Deponiebau und Geotechnik. € 17,90
- Nr. 42 Vermeer, P.A. (1997) Baugruben in Locker- und Festgestein. € 17,90
- Nr. 43 Brinkmann, C. (1998) Untersuchungen zum Verhalten von Dichtungsübergängen im Staudambau. € 17,90
- Nr. 44 Fiechter-Scharr, I. (1998) Beeinflussung von Erdbaustoffen durch Beimischen eines organophilen Bentonits. € 17,90
- Nr. 45 Schanz, T. (1998) Zur Modellierung des mechanischen Verhaltens von Reibungsmaterialien. € 17,90
- Nr. 46 Akinrogunde, A.E. (1999) Propagation of Cement Grout in Rock Discontinuities Under Injection Conditions. € 17,90
- Nr. 47 Vogt-Breyer, C. (1999) Experimentelle und numerische Untersuchungen zum Tragverhalten und zur Bemessung horizontaler Schraubanker. € 17,90
- Nr. 48 Vermeer, P.A. (1999) Neue Entwicklungen in der Geotechnik. € 17,90
- Nr. 49 Marcher, T. (2002) Resultate eines Versuchsprogramms an Beaucaire-Mergel. € 17,90
- Nr. 50 Marcher, T. (2003) Nichtlokale Modellierung der Entfestigung dichter Sande und steifer Tone. € 17,90
- Nr. 51 Ruse, N.M. (2004) Räumliche Betrachtung der Standsicherheit der Ortsbrust beim Tunnelvortrieb. € 17,90
- Nr. 52 Beutinger, P.H. (2005) Ein geotechnischer Beitrag zur Standsicherheit mobiler Baumaschinen. € 17,90

- Nr. 53 Wehnert, M. (2006) Ein Beitrag zur drainierten und undrainierten Analyse in der Geotechnik. € 17,90
- Nr. 54 Möller, S.C. (2006) Tunnel induced settlements and structural forces in linings. € 17,90



Universität Stuttgart

Sven Möller

2006 - Mitteilung 54

ISBN-10: 3-921837-54-5

ISBN-13: 978-3-921837-54-2